THE UNIVERSITY
of EDINBURGH

This thesis has been submitted in fulfilment of the requirements for a postgraduate degree (e.g. PhD, MPhil, DClinPsychol) at the University of Edinburgh. Please note the following terms and conditions of use:

This work is protected by copyright and other intellectual property rights, which are retained by the thesis author, unless otherwise stated.
A copy can be downloaded for personal non-commercial research or study, without prior permission or charge.
This thesis cannot be reproduced or quoted extensively from without first obtaining permission in writing from the author.
The content must not be changed in any way or sold commercially in any format or medium without the formal permission of the author.
When referring to this work, full bibliographic details including the author, title, awarding institution and date of the thesis must be given.

A NOVEL ROLE FOR SOX2 IN THE DEVELOPMENT OF THE ZEBRAFISH EPITHALAMUS

Sofia Pavlou

A thesis submitted for the degree of Doctor of Philosophy

The University of Edinburgh

2013

Στους γονείς μου

Declaration

I declare that this thesis has been composed by me, the work described is my own and contributions by others are clearly indicated. This work has not been submitted for any other degree or professional qualification except as specified.

Sofia Pavlou
May 2013

Abstract

The *sex determining region Y-box 2* (*sox2*) gene is one of the most important transcription factors during development, particularly the development of the central nervous system (CNS). It is expressed in embryonic stem cells and later in neural stem cells, where it modulates their maintenance and differentiation. In humans, heterozygous mutations are associated with eye malformations, including anophthalmia and severe microphthalmia. Also, a subset of patients has extra-ocular phenotypes, such as hearing loss, seizures and pituitary hypoplasia. Although the roles of *sox2* in embryonic stem cells and eye development are well studied, the function of sox2 in brain development and disease is still elusive. The aim of this project was to characterize a novel role for sox2 in the development of zebrafish epithalamus, which was identified from an *in silico* screen previously performed in our laboratory.

The zebrafish epithalamus, located in the dorsal diencephalon, consists of three main structures: the pineal gland, the parapineal organ and the habenular nuclei. The pineal gland, also known as epiphysis, is a photoreceptive (in zebrafish) and neuroendocrine organ that detects light and rhythmically produces melatonin in order to regulate the circadian rhythms. The parapineal organ is located to the left side of the pineal gland and is important for the elaboration of the asymmetries observed between the left and right habenular nuclei. Finally, the bilateral habenulae are part of the dorsal diencephalic conduction system that links the forebrain with the mid- and hindbrain. The left and right habenulae show both molecular and neuroanatomical asymmetries, including differences in neuropil organization, in levels of gene expression and in the morphology and connectivity of their neurons' projections. The relatively simple architecture of the pineal gland and the asymmetric character of the habenulae provide a useful tool for studying cell-fate determination, cell migration and establishment of brain asymmetries.

In this study, we used zebrafish as a model to dissect the novel functions of *sox2* in the development of the epithalamus. We showed that sox2 works synergistically with Notch pathway to negatively regulate neurogenesis within the pineal gland. The pineal gland consists of only two cell types: the photoreceptors and the projection neurons.

Previous studies showed that the Notch and BMP pathways are important for the proper specification of these cells. Here, we show that sox2 normally inhibits the photoreceptor cell fate, whereas it has no effect on the number of projection neurons. Therefore, sox2 complements Notch and BMP pathways in cell-fate determination within the pineal gland.

In addition, downregulation of sox2 results in abnormal parapineal organ development and disruption of the asymmetric architecture of the habenulae. A subset of *sox2* morphant embryos develops right-sided parapineal organs, which is consistent with abnormal bilateral expression of the Nodal gene, *pitx2* (*paired-like homeodomain transcription factor 2*). Also, timelapse experiments showed that migration of the parapineal cells is defective, resulting in scattered cells. The aberrant parapineal development leads to disorganization of the habenular nuclei, as shown by the abnormal neuropil arrangement and the expression of the asymmetric marker *kctd12.1* (*potassium channel tetramerisation domain containing 12.1*).

Acknowledgements

First of all, I would like to thank all my supervisors. A huge thank you to Richard Baldock for accepting me into his group, even though I am really bad with programming, and for being so supportive and approachable. I hope you enjoyed hearing about my little fish for a change! Also, many thanks to Veronica van Heyningen for her invaluable help, starting from a bench in her lab to comments, support and suggestions about the work. It was an honour working with both of you. Last, but definitely not least I would like to thank my big boss: Pedro Coutinho. I don't think I can find the right words to thank you. My PhD would have not been the same without you... I was lucky to have a friend as my supervisor! Obrigado meu amigo (is this correct?)!!!

I would also like to thank all the people that provided us with reagents and fish. In particular, many thanks to Dr. David C. Klein, Dr. Patrick Blader, Prof. Marnie Halpern and Dr. Benjamin Feldman for kindly sending us plasmids to generate probes. Also, Dr. Elise Cau, Prof. Steve Wilson, Dr. Martin Gering and Nadine Borel for sending us fish.

Of course, my life in the unit was easier due to the help and support of many people! So thanks to everyone in E2 and C2 labs and in West Wing office! Special thanks to Katy Astell and Milica Gakovic for helping, especially at the beginning of the project, and of course for providing me with such a nice western blot!! Many thanks to DJ Kleinjan, Patricia Yeyati, Anne Seawright, Anna Klingseisen and Shalini Jadeja for all their help with protocols, reagents, antibodies (lots of antibodies!) and for so kindly sharing their expertise with me! Extra thanks to Shalini for actually reading my thesis (at least that's what she said! Just kidding! Thank you). I would also like to thank Matt Pearson and Paul Perry for all their help with imaging, as well as Kerry Taylor for sharing her "secrets" about timelapses! Also, many thanks to Alyson Ross for teaching me how to section and to Richard Mort for the many hours he spent trying to teach me statistics!

Working with fish is great and fun, but it requires countless hours in the wet, warm and humid fish room! Shipra Bhatia, David Sexton, Keith Erskine and of course

Pedro (along with many less-frequent fish-people) made all those hours enjoyable and pleasant! Thank you all!

Saganaki! Thanks for everything! Kai sta dika sou!

And although people in Edinburgh are very nice and supportive, I wouldn't be happy without MY people back home! Sorry for writing this in Greek but they deserve it!

Μπορεί να είμαι μακρυά, μπορεί να μην σας βλέπω όσο θα ήθελα, αλλά είστε πάντα μέσα στην καρδιά μου. Ό,τι κι αν πω θα είναι λίγο! Δεν θα κατάφερνα τίποτα χωρίς εσάς. Μάμα και παπά (κυρία Κούλλα και κύριε Χριστόφορε) ευχαριστώ που με κάνατε τόσο τέλεια!! Δεν σας το λέω συχνά, αλλά φαντάζομαι πως το ξέρετε: σας χρωστάω τα πάντα. Ευχαριστώ.

Ανδρονικούλα μου, έκαμα την αρχή αλλά περιμένω κι εγώ να διαβάσω το όνομά μου στο δικό σου "βιβλίο" μια μέρα! Σ΄αγαπώ πολύ! Άτε ετοίμασε την Monopoly να παίξουμε! Κυρία Σοφία και κυρία Ντίνα (άτε να βάλλω Κωνσταντίνα) ευχαριστώ! Ξέρετε εσείς το γιατί…

Νικολούλι μου!! Ευχαριστώ για τα μηνύματα που μου κρατούσαν συντροφιά στις ατέλειωτες ώρες γραψίματος, καθώς και για την δύναμη και θετική ενέργεια που προσπαθούσες να μου μεταδώσεις! Φιλενάδε! Κωστάκη! Είσαι μια λεεεέρα! Καφέ και…..μπιρίμπα σε μισή ώρα; Ευχαριστώ!

Thank you all!

Table of contents

List of Figures

List of Tables

Abbreviations

(f)MRI	(functional) magnetic resonance imaging
AI	asymmetry index
BCIP	5-Bromo-4-chloro-3-indolyl phosphate
bHLH	basic helix-loop-helix
BMP	bone morphogenetic protein
BrdU	5-bromo-2'-deoxyuridine
BRE	BMP-responsive element
BSA	bovine serum albumin
$CaCl_2$	calcium chloride
cDNA	complementary deoxyribonucleic acid
ChIP	chromatin immunoprecipitation
CNS	central nervous system
DAPI	4',6-Diamidino-2-Phenylindole, Dihydrochloride
DAPT	*N*-[(3,5-Difluorophenyl)acetyl]-L-alanyl-2-phenyl]glycine-1, 1-dimethylethyl ester
DBS	deep brain stimulation
dH_2O	distilled water
DIG	digoxigenin
DMSO	dimethyl sulfoxide
DNA	deoxyribonucleic acid
DNase (I)	deoxyribonuclease (I)
dNTPs	deoxyribonucleotide triphosphate
dorsomorphin	6-[4-(2-Piperidin-1-ylethoxy)phenyl]-3-pyridin-4-ylpyrazolo [1,5-a]pyrimidine
dpc	days postcoitum
dpf	days post fertilization
DSPS	delayed sleep phase syndrome
ECR	evolutionary conserved region

EDTA	ethylenediaminetetraacetic acid
EdU	5-ethynyl-2'-deoxyuridine
EGTA	ethylene glycol-bis(2-aminoethylether)-N,N,N′,N′-tetraacetic acid
EMSA	electrophoretic mobility shift assay
EtOH	ethanol
FACS	fluorescence activated cell sorting
fby	*from beyond* (*tbx2b* mutant)
gDNA	genomic deoxyribonucleic acid
HCl	hydrochloric acid
HEPES	4-(2-Hydroxyethyl)piperazine-1-ethanesulfonic acid
HMG	high mobility group
hpf	hours post fertilization
IgG	immunoglobulin G
IPN	interpeduncular nucleus
kb	kilobase
KCl	potassium chloride
KOH	potassium hydroxide
LiCl	lithium chloride
LPM	lateral plate mesoderm
M	molar
mbl	*masterblind* (*axin1* mutant)
MeOH	methanol
mg	milligram
$MgCl_2$	magnesium chloride
$MgSO_4$	magnesium sulphate
ml	millilitre
mm	millimeter
mM	millimolar
mRNA	messenger ribonucleic acid
MWU test	Mann-Whitney U test with Bonferrroni correction

NaCl	sodium chloride
NBT	nitro-blue tetrazolium chloride
ng	nanogram
Nicd	Notch intracellular domain
NP-40	nonyl phenoxypolyethoxylethanol
^{o}C	degree Celsius
OPT	optical projection tomography
PBS	phosphate buffered saline
PBT	phosphate buffered saline with 0.1% Tween20
PCR	polymerase chain reaction
PFA	paraformaldehyde
pg	picogram
PTU	1-Phenyl-2-thiourea
qRT-PCR	quantitative real-time polymerase chain reaction
REM	rapid eye movement
RGC	retinal ganglion cell
RNA	ribonucleic acid
RNase	ribonuclease
rpm	revolutions per minute
RT	reverse transcription
SAD	seasonal affective disorder
SDS	sodium dodecyl sulfate
sox2-MO	morpholino directed against sox2 (2)
sox2-MO1	morpholino directed against sox2 (1)
sox2-MO2	morpholino directed against sox2 (2)
sox2MO	sox2 morphants
ss	somites stage
SSC	saline sodium citrate
TAE	buffer solution containing Tris base, acetic acid and EDTA
TALEN	Transcription activator-like effector nucleases

TE buffer	buffer solution containing Tris and EDTA
TILLING	Targeting induced local lesions in genomes
Tris	tris(hydroxymethyl)aminomethane
tRNA	transfer ribonucleic acid
TUNEL	terminal deoxynucleotidyl transferase dUTP nick end labeling
UAS	upstream activating sequence
UTR	untranslated region
Wilcoxon test	Wilcoxon paired signed-rank test
µg	microgram
µl	microlitre
µM	micromolar
μm^3	cubic micrometer

Genes

Short name	**Full name**
(MZ,LZ)*oep*	(maternal-zygotic, late-zygotic) *one-eyed pinhead*
aanat2	*arylalkylamine N-acetyltransferase*
abp1	*amiloride binding protein 1 (amine oxidase (copper-containing))*
adcyap1a	*adenylate cyclase activating polypeptide 1a*
ascl1a	*achaete-scute complex-like 1a*
asic1c	*acid-sensing (proton-gated) ion channel 1c*
bmp(2a)	*bone morphogenetic protein (2a)*
bmpr1aa	*bone morphogenetic protein receptor, type 1aa*
cadps2	*Ca2+-dependent activator protein for secretion 2*
ccnd1	*cyclin D1*
cdh2	*cadherin2*
crx	*cone-rod homeobox*
cxcr4b	*chemokine (C-X-C motif), receptor 4b*
dachd	*dachshund d*
dl(a,b,d)	*delta(A,B,D)*

elavl3	*ELAV(embryonic lethal, abnormal vision, Drosophila)-like 3 (Hu antigen C)*
etv1	*ets variant gene 1*
fezf2	*FEZ family zinc finger 2*
fgf(4,8a)	*fibroblast growth factor (4,8a)*
fgfr4	*fibroblast growth factor receptor 4*
flh	*floating head*
foxd3	*forkhead box D3*
foxh1	*forkhead box H1*
fsi	*frequent-situs-inversus*
GFAP	*glial fibrillary acidic protein*
gfi1ab	*growth factor independent 1ab*
GFP	*green fluorescent protein*
her(2,4.1,15.1)	*hairy and enhancer of split related (2,4.1,15.1)*
HSP	*heat shock protein*
hsp70l	*heat shock cognate 70-kd protein, like*
IL(1,2,18)	*interleukin (1,2,18)*
irbp	*interphotoreceptor retinoid-binding protein*
isl1	*islet1*
kctd(8,12.1,12.2)	*potassium channel tetramerisation domain containing (8,12.1,12.2)*
lft(1,2)	*lefty(1,2)*
lhx3	*LIM homeobox 3*
mab21l1	*mab-21-like-1*
mib	*mind bomb*
myca	*myelocytomatosis oncogene a*
ndr2	*nodal-related 2*
neurod	*neurogenic differentiation*
neurog1	*neurogenin 1*
nog3	*noggin 3*
nr1d1	*nuclear receptor subfamily 1, group d, member 1*

nrp1a	*neuropilin 1a*
onecutl	*one cut domain, family member, like*
otx(2,5)	*orthodenticle homolog (2,5)*
pax6(a,b)	*paired box gene 6(a,b)*
pcdh10(a,b)	*protocadherin 10*
per3	*period homolog 3 (Drosophila)*
pitx2	*paired-like homeodomain transcription factor 2*
pou4f(1,3)	*POU domain, class 4, transcription factor (1,3)*
pou5f1	*POU domain, class 5, transcription factor 1*
rx2	*retinal homeobox gene 2*
samsn1b	*SAM domain, SH3 domain and nuclear localization signals, 1b*
six(3b,7)	*sine oculis homeobox homolog (3b,7)*
sox2	*SRY-box containing gene 2*
sox6	*SRY-box containing gene 6*
spaw	*southpaw*
spon1b	*spondin 1b*
tbx2b	*T-box 2b*
tshz1	*teashirt family zinc finger 1*

Chapter 1. Introduction

“ ‘Εν οἶδα ὅτι οὐδὲν οἶδα”

“All I know is that I know nothing”

Socrates, 470-399 BC

1.1 Zebrafish: an excellent genetic model

In order to understand the mechanisms underlying normal development and disease of complex organs, such as the brain, rigorous experimental procedures are required. To achieve this, scientists use a variety of animal models of different complexity, such as worms (*Caenorhabditis elegans*), flies (*Drosophila melanogaster*), rodents (*Mus musculus*, *Rattus norvegicus*) and primates (*Pan troglodytes*, *Macaca mulatta*). During the last few decades, zebrafish (*Danio rerio*) have been increasingly used and proving to be an excellent genetic model for studying vertebrate development and disease, due to their numerous advantages.

1.1.1 Advantages of zebrafish

Zebrafish are tropical freshwater fish that normally inhabit vegetation-rich waters in India, Nepal, Bhutan and Bangladesh (reviewed in Spence et al., 2008). Their small size (adults are about 3-4 cm long), along with the fact that they are inexpensive, makes them suitable even for small laboratories with limited space. Another advantage is their high fecundity, with each female capable of producing hundreds of eggs per clutch every week. Also, zebrafish embryos develop rapidly and *ex-utero* enabling constant monitoring of cell divisions, cell movements and even the development of organs. By 5 days post fertilization (dpf) most organs, including brain, heart, liver, pancreas and kidneys, are fully developed and functional and approximately 12 weeks post fertilization, zebrafish are able to mate and produce new offspring (reviewed in Spence et al., 2008; Renninger et al., 2011; Rinkwitz et al., 2011). Moreover, embryos are optically translucent and pigmentation can easily be prevented by raising them in 1-Phenyl-2-thiourea (PTU), a chemical that prevents melanin synthesis. A number of mutants that lack pigmentation, such as *albino* or *casper* fish, are also available. Their transparency, along with their small size, provides a great advantage for high-resolution *in vivo* imaging of individual cells, structures or even whole organs (reviewed in Renninger et al., 2011; Rinkwitz et al., 2011).

An important requirement for a genetic model is a sequenced and well-annotated genome. Although the zebrafish genome is not completely annotated, it is one of the

best-characterized genomes. This is important for both forward and reverse genetics. In forward genetics approaches, scientists introduce random mutations into the genome and screen for phenotypic effects. An annotated genome is then required to map the mutation and identify the gene(s) responsible for the phenotypes. Zebrafish allow large-scale screens and the function of hundred of genes involved in embryonic development has been identified using forward genetics in zebrafish (reviewed in Beretta et al., 2012). In contrast, reverse genetics can be used to identify the function of a particular gene of interest. By disrupting its expression, we can understand how a specific gene controls normal development, as well as how mutations in this gene can lead to diseases.

The ease of genetic manipulations of zebrafish provides an invaluable tool for reverse genetics. Knockdown of a gene of interest can easily be achieved by microinjections of morpholino antisense oligonucleotides (morpholinos). These molecules are short oligonucleotides, in which morpholine rings replace the ribose-phosphate backbones. This modification makes them more stable and resistant to nucleases. Morpholinos are typically complementary to the region adjacent or containing the translation start site of the targeted mRNA sequence and therefore bind to the transcripts and block their translation (translation blocking morpholinos). Alternatively, morpholinos can be designed to target splice sites, resulting in aberrant splicing of the targeted mRNA and non-functional protein products (splice blocking morpholinos) (Nasevicius and Ekker, 2000; reviewed in Renninger et al., 2011). Although morpholinos result in a reliable downregulation of the targeted gene, other techniques including TILLING (Targeting Induced Local Lesions In Genomes), zinc finger nucleases and TALEN (transcription activator-like effector nucleases) can also be used to generate (null) mutants if required (Bedell et al., 2012; Cade et al., 2012; reviewed in Renninger et al., 2011).

Due to their transparency, zebrafish are an excellent system, in which to express fluorescent proteins. This allows the visualization of organs, cells and even axons in real time and throughout development and even into adulthood, if non-pigmented fish are used. Various techniques have been developed that led to the generation of many transgenic lines that recapitulate the full or partial expression of several genes (reviewed

in Renninger et al., 2011; Rinkwitz et al., 2011). Conditional mutants are also available, in which ectopic expression of a particular gene is stimulated by heat-shock (reviewed in Teh et al., 2005). Additionally, transgenic lines can be used to facilitate laser ablations, photoactivations or the identification of mutants that affect a particular process (reviewed in Renninger et al., 2011).

In addition to development, zebrafish are used in other scientific fields, such as oncology, behaviour studies, degeneration, toxicology and environmental studies.

1.1.2 Zebrafish epithalamus: a model for brain development

The development of the vertebrate brain involves the reiterative use of spatiotemporally controlled processes, such as cell proliferation, differentiation and migration. Therefore, understanding how a relatively simple brain structure develops and which pathways and gene networks are involved will provide invaluable insights into the development of a complete and functional brain. The zebrafish epithalamus is proving to be an excellent model for brain development. It is found in the dorsal diencephalon and contains three main structures: the pineal gland, the parapineal organ and the habenular nuclei (**Figure 1.1**).

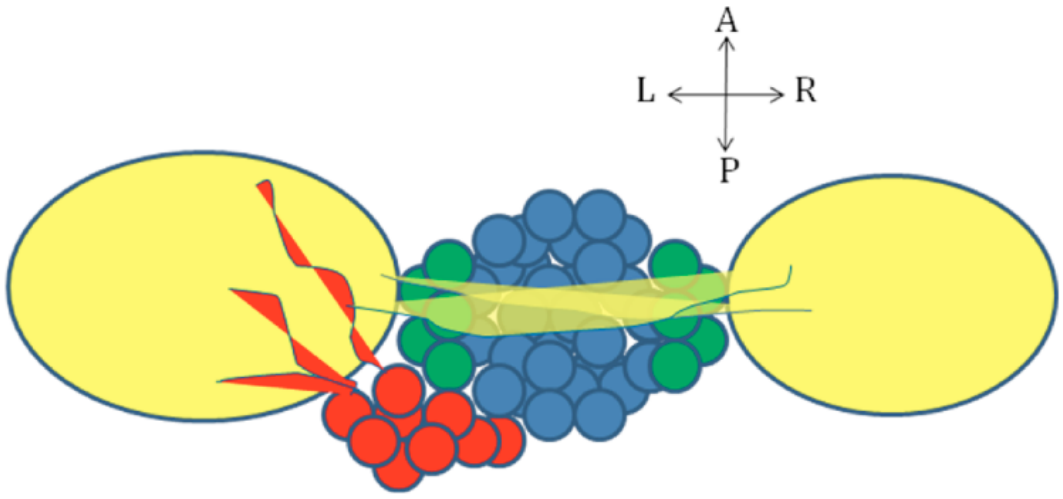

Figure 1.1 The zebrafish epithalamus. The pineal gland is found in the middle of the dorsal diencephalon and consists of the pineal photoreceptors (blue) and projection neurons (green). The habenulae (yellow) are bilateral structures that interact through the

habenular commissure (yellow lines connecting the two habenulae). The parapineal organ (red) is found on the left side of the brain and specifically innervates the left habenula. Notably, the left and right habenulae differ in size, number of neuropil, gene expression and connectivity. Dorsal view, anterior (A), posterior (P), left (L) and right (R).

A number of the main processes that are required for the development of a functional human brain and the mechanisms that control them are also involved in the development of the zebrafish epithalamus (discussed in detail in section **1.3**). For example, the Notch pathway and proneural genes control the timing of neurogenesis both during early brain development (by controlling which neural progenitor cells will continue to divide and which will start differentiating) and during the development of the pineal gland. In addition, the pineal gland consists of only two cell types: the photoreceptors and the projection neurons. Therefore, by understanding how this relatively simple structure is specified, we hope to get an insight into how the many different types of neurons found within the human brain are specified. Although Notch and bone morphogenetic protein (BMP) pathways have important roles in cell-fate determination within the pineal gland, further research is required to understand the complete mechanism that controls specification. Moreover, parapineal cells originate from the anterior part of the pineal anlage and their proper function requires their migration to the left side of the brain. Understanding the mechanisms that control their migration will provide insights into the mechanisms that control migration of neurons elsewhere in the brain. Finally, the zebrafish epithalamus exhibits asymmetries both at neuroanatomical and functional level and it can, therefore, be used to study how brain asymmetries are established.

In addition to being an excellent and relatively simple model to study vertebrate brain development and disease, the zebrafish epithalamus comprises the pineal gland and the habenular nuclei. These structures are highly conserved among vertebrates and have been associated with a wide range of physiological and behavioural functions, such as circadian rhythms and sleep, spatial learning and attention, responses to aversive stimuli, as well as psychotic disorders, including schizophrenia and depression (discussed in detail in sections **1.2.1.1-1.2.1.4** and **1.2.3.1**). Despite the importance of the

epithalamus, very little is known about its development, function and disease. However, over the last few decades, research on the zebrafish epithalamus has shed some light on how the structures develop and an increasing number of researchers are using zebrafish to decipher how these structures control such a plethora of functions.

1.2 The epithalamus: function and evolution

The epithalamus is a neuroanatomically distinct part of the diencephalon, found above (hence "epi") the thalamus. It contains the pineal gland (also known as the epiphysis), in some species the parapineal organ (discussed in section **1.2.2**), the habenular nuclei, the habenular commissure (that interconnects the habenulae) and a membranous evagination of unknown function called the saccus dorsalis. The organization of the epithalamus varies between species, but in general the pineal gland is found in the midline, flanked by the bilateral habenular nuclei. In addition, the parapineal (if present) is usually placed asymmetrically on one side of the brain and, together with the pineal gland, forms the pineal complex (reviewed in Concha and Wilson, 2001).

1.2.1 Pineal gland

The pineal gland is a very small, but highly conserved, neuroendocrine structure, found in all vertebrate species examined. In an average adult human, the pineal gland is 1-5 mm in width, 3-5 mm in height and 3-5 mm in thickness and weighs approximately 100-180 mg. Its main function is to convert light/dark information from the environment into neurohormonal messages, particularly the rhythmical production of melatonin (*N*-acetyl-5-methoxytryptamine). Melatonin, which is synthesized and released into the blood during the night, is a hormone involved in the regulation of circadian rhythms (reviewed in Macchi and Bruce, 2004; Karasek, 2007; Stehle et al., 2011).

In non-mammalian species, the pineal gland is both photoreceptive and neuroendocrine. Therefore, direct photic inputs perceived by pineal photoreceptors are used to regulate melatonin synthesis (reviewed in Mano and Fukada, 2007; Stehle et al., 2011). In addition, non-mammalian pineal glands contain endogenous circadian clocks (also known as pacemakers or oscillators), as well as entrainment mechanisms that

synchronize the rhythmic production of melatonin with light/dark information received from the environment. This is illustrated by *in vitro* experiments in zebrafish (Cahill, 1996) and chicks (Deguchi, 1979; Binkley et al., 1978). For example, in cultured zebrafish pineal glands melatonin is rhythmically released under complete darkness for up to 5 days, with maximum production in periods that correspond to night and minimum production during the subjective days (Cahill, 1996). Also, exposure to light during a subjective night period leads to acute suppression of melatonin production and resets the circadian rhythms to opposite phases (Cahill, 1996).

In contrast, mammalian pineal glands have lost their photoreceptive properties. As a consequence, light/dark information is perceived by melanopsin-positive retinal ganglion cells (RGCs) in the eye and then transmitted through the retinohypothalamic tract to the suprachiasmatic nucleus. This information is used to entrain the master circadian pacemaker found in the suprachiasmatic nucleus. The pacemaker generates and sends (over a neural pathway) circadian signals to the pineal gland. Finally, the pineal gland uses these signals to rhythmically produce melatonin (reviewed in Karasek, 2007; Falcón et al., 2010; Stehle et al., 2011).

Unlike the many differences in the regulation of melatonin synthesis, the biochemical pathway used is highly conserved among vertebrates. In particular, pinealocytes (pineal gland cells) use the amino acid tryptophan as a substrate to generate firstly serotonin and finally melatonin, through a series of biochemical reactions (**Figure 1.2**). Serotonin levels are high during the day and low during the night, while melatonin levels are low during the day and high during the night. This increase in melatonin production during the night reflects an increase in the expression of arylkylamine N-acetyltransferase (AANAT), which is the rate-limiting enzyme (reviewed in Macchi and Bruce, 2004; Falcón et al., 2010; Stehle et al., 2011).

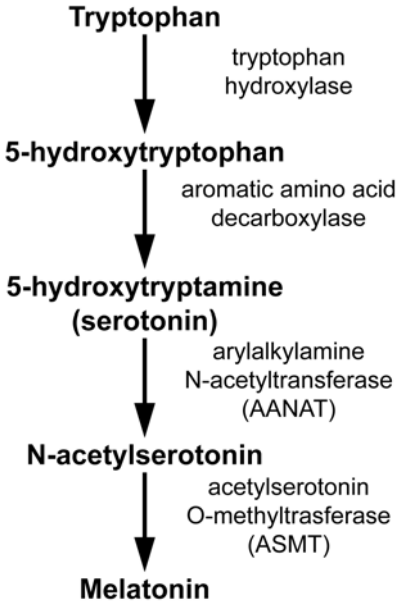

Figure 1.2 Melatonin synthesis pathway. Pinealocytes use tryptophan as a substrate to generate melatonin, through a series of biochemical reactions.

The pineal gland and its main product melatonin have several functions, including the regulation of circadian rhythms, antioxidant protection and the regulation of the immune system. As a consequence, dysfunction of the pineal gland can lead to sleep disturbances and increased susceptibility to diseases. Interestingly, melatonin levels reduce with age, suggesting a possible role for pineal gland and melatonin in the process of aging. Some of these functions are discussed in sections **1.2.1.1-1.2.1.4**.

1.2.1.1 Circadian rhythms and sleep regulation

One of the most important functions of melatonin, and therefore the pineal gland, is the regulation of circadian rhythms, which in turn regulate sleep. In mammals, circadian rhythms are generated by the biological clock in the suprachiasmatic nucleus and are responsible for the differences in several physiological (e.g. body temperature) and behaviour (e.g. sleepiness) functions, observed between day and night. Several lines of evidence suggest a link between melatonin/pineal gland and regulation of circadian functions, such as sleep.

First, melatonin functions, at least in part, as an endogenous synchronizer in mammals. This is illustrated by the phase shifts observed in circadian functions, such as sleep and thermoregulation, after administration of exogenous melatonin (Deacon and J Arendt, 1995; Kräuchi et al., 1997). In fact, administration of melatonin can be used to eliminate jet lag symptoms: in nine out of ten individuals, exogenous melatonin was able to decrease the effects of jet lag (Herxheimer and Petrie, 2002). Moreover, exogenous melatonin can entrain the biological clock of completely blind patients (Lockley et al., 2000; Sack et al., 2000).

In addition to its roles in entraining the biological clock, melatonin has soporific properties. The onset of melatonin production (which normally occurs approximately 2 hours before bedtime) is thought to be the hormonal signal that induces sleep (Lavie, 1997). Administration of melatonin in healthy subjects during the day or early evening (when endogenous levels are low) leads to increased sleepiness, fatigue and sleep efficiency, and decreased sleep latency, the time needed from full wakefulness to sleep (Dollins et al., 1993; Nave et al., 1996; Hughes and Badia, 1997). Notably, melatonin intake during the night (when endogenous levels are high) has minimal effects in most cases (James et al., 1987; Stone et al., 2000). In addition, exogenous melatonin results in a decrease in body temperature, which is also observed at the onset of sleep (Dollins et al., 1993; Nave et al., 1996; Hughes and Badia, 1997). In contrast, suppression of melatonin production during the night (by exposure to bright light) results in increased body temperature (Cagnacci et al., 1993; Strassman et al., 1991). Therefore, melatonin may promote sleep by controlling thermoregulatory mechanisms.

Despite the lack of systematic research, preliminary data suggest a moderate increase in sleep and mood disturbances in pinealectomized patients, due to the low levels of melatonin after-surgery. In some of these cases, administration of melatonin was able to minimize the defects (Etzioni et al., 1996; Lehmann et al., 1996; Jan et al., 2001). Also, exogenous melatonin can treat patients with delayed sleep phase syndrome (DSPS). DSPS is a circadian rhythm disorder that is characterized by delayed sleep onset (Dahlitz et al., 1991; Nagtegaal et al., 1998). It is associated with polymorphisms in the clock gene *period homolog 3 (Drosophila)* (*PER3*) (Archer et al., 2003; Ebisawa

et al., 2001), as well as the *AANAT* gene that encodes an enzyme crucial for melatonin synthesis (**Figure 1.2**) (Hohjoh et al., 2003).

1.2.1.2 Aging and age-related diseases

Over the last decades, several studies demonstrate a link between dysfunction of the pineal gland, aging and age-related diseases. First of all, the amount of melatonin produced by the pineal gland decreases gradually with age. As a result, in elderly individuals the levels of melatonin are almost identical during the night and day (Touitou et al., 1981, 1984; Waldhauser et al., 1988; Magri et al., 1997). This age-related decrease in melatonin production may explain a number of the age-related diseases.

One of the most common complains of elderly people is sleep disturbance. The inability of the pineal gland to produce sufficient melatonin during the night may, therefore, be responsible for the increased incidents of sleep defects in elderly people. In agreement with this, melatonin administration can minimize these symptoms in most cases (Lyseng-Williamson, 2012).

Moreover, aging is associated with increased susceptibility to diseases, due to impairments of the immune system. In rodents, suppression of melatonin leads to decreased spleen and thymus activity, as well as decreased antibody response to T-dependent antigens (Scalabrino et al., 1979; Maestroni et al., 1986; Cernysiov et al., 2010). These defects can be rescued by melatonin administration (Cernysiov et al., 2010). Also, several data suggest a link between melatonin and the regulation of immune system in humans. For example:

a) Melatonin receptors are found in many lymphoid organs and lymphocytes (Lopez-Gonzalez et al., 1992).
b) Endogenous melatonin is thought to have a role in the regulation of the *interleukin 1* (*IL1*) family of genes, which are known to regulate immune and inflammatory responses (Morrey et al., 1994).

c) Chronic administration of melatonin leads to increased activity of T-helper cells and elevated levels of interleukin 2 (IL2). IL2 is a protein important for the proliferation of B and T lymphocytes (Garcia-Mauriño et al., 1997).

In addition to its immune properties, melatonin provides antioxidant protection. According to the free radical theory of aging, cells and organs are damaged and thus unable to properly function, partly as a result of increased levels of highly toxic free radicals with age (Harman, 1956). Notably, free radicals are thought to be involved in the pathogenesis of many age-related diseases, such as Alzheimer's disease, cataract, Parkinson's disease and atherosclerosis. Melatonin, which is a highly diffusible molecule, provides antioxidant protection from such radicals and in addition stimulates antioxidative enzymes (Hardeland et al., 1995). It should be noted that melatonin is the only antioxidant known to substantially decrease with age. Thus, the progressive impairment of the pineal gland to produce sufficient melatonin may be one of the factors that contribute to the process of aging.

1.2.1.3 Cancer

Aging is also associated with an increased risk of neoplastic diseases. Several *in vivo* and *in vitro* studies in animals and humans demonstrate that melatonin has oncostatic properties. Thus, the reduction in melatonin levels observed with age may contribute to the increase in cancer incidents.

Pinealectomized hamsters or rats show accelerated growth of several types of neoplasias (e.g. transplanted melanoma, transplantable leukemia and mammary tumours) and these effects can be rescued by administration of melatonin (Rodin, 1963; Lapin and Frowein, 1981; Tamarkin et al., 1981; Shah et al., 1984). Also, melatonin exhibits antiproliferative effects against many different cancer cell lines, including the human MCF-7 breast cancer line (Hill et al., 1992). Moreover, several studies showed reduced levels of circulating melatonin in patients with certain types of cancer and in many cases melatonin administration can slow down tumor progression (Bartsch et al., 1981, 1985; Lissoni et al., 1986, 1992; Khoory and Stemme, 1988). In addition, melatonin (via its antioxidant properties) can protect skin cells from UV-mediated damage (Gonzalez et

al., 1991). One of the most important advantages of the use of melatonin as a treatment is that it has no or little side effects, unlike other cancer treatments.

1.2.1.4 Seasonal reproduction

In most animals, the pineal gland is involved in regulating seasonal reproduction. Depending on the season, the length of the day (photoperiod) and subsequently the duration of melatonin secretion, varies: short nights during summer reflect short duration of melatonin production, while during the long nights of winter melatonin is produced for a longer period. Therefore, seasonal light/dark information is translated into hormonal changes (different duration of melatonin production). This difference in melatonin production regulates seasonal changes in several behavioural and physiological functions (e.g. reproduction, metabolism) in seasonal species (Lincoln et al., 1981; Piezzi et al., 1984; McConnell, 1986; Paydar-Ravandi and Meier, 1989; reviewed in Revel et al., 2009). In humans, seasonal changes in reproduction and behaviour are less obvious. However, there is an increase in the incidents of depressive behaviours in humans during winter, followed by a spontaneous spring-summer remission (Rosenthal et al., 1984). This seasonal change in behaviour is known as seasonal affective disorder (SAD) and although sufficient data are not present, SAD could be associated with seasonal changes in melatonin production by the pineal gland.

1.2.2 Parapineal organ

Unlike the highly conserved pineal gland, the parapineal organ is a less evolutionarily conserved organ (**Figure 1.3**). It has been described in most lamprey species (with one exception, the *Mordacia mordax*), some teleosts (including *Danio rerio*), the bowfin *Amia calva*, the coelacanth *Latemeria chalumnae* and some reptiles (known as parietal eye). Although in all species examined, the parapineal organ has at least some photoreceptive properties, the role of this structure is still unclear. Interestingly, the parapineal organ shows asymmetric connectivity as it mostly projects to the left habenula and in some species it is also asymmetrically positioned. It can therefore be used to better understand how asymmetric brain development and

connectivity are established (reviewed in Concha and Wilson, 2001; Bianco and Wilson, 2009).

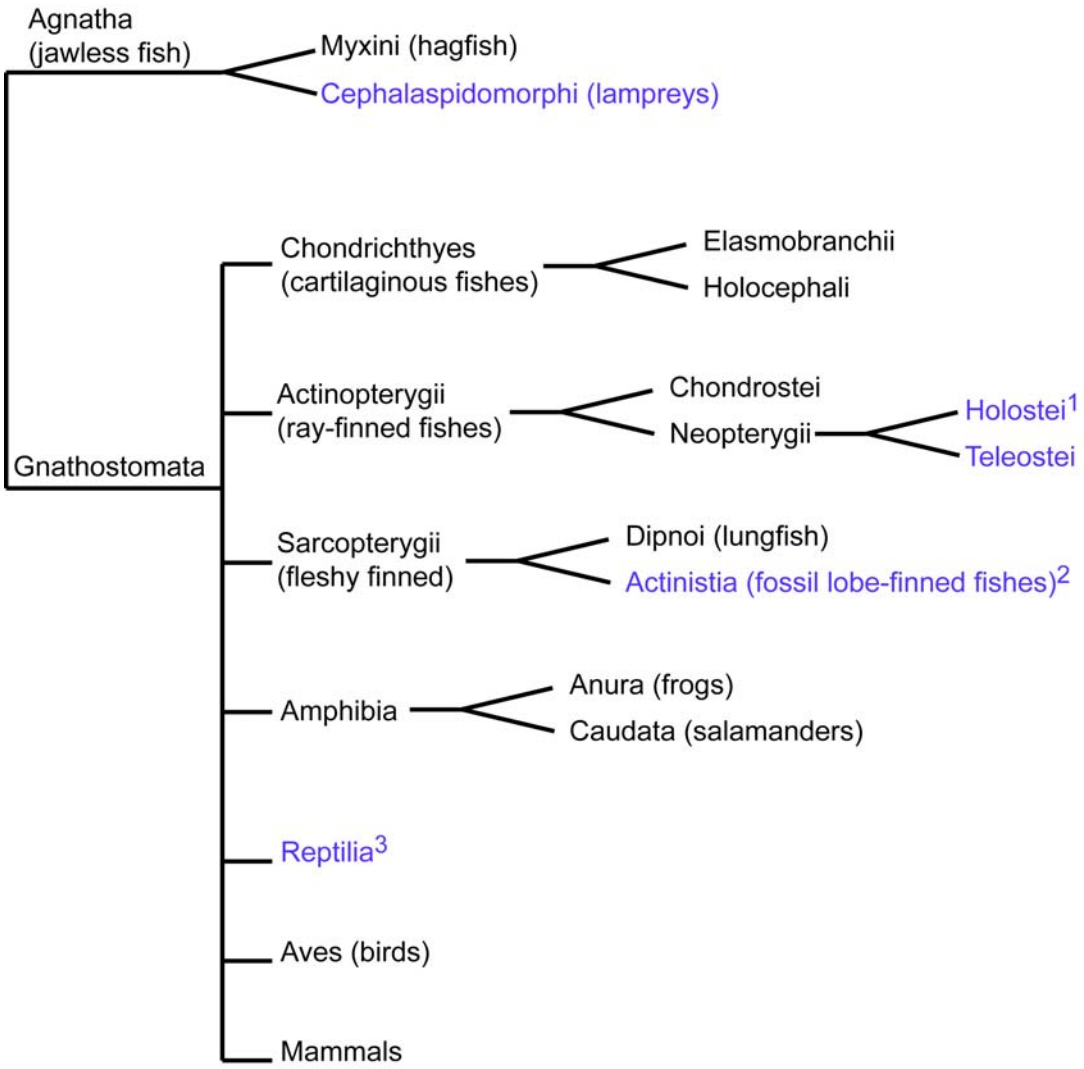

Figure 1.3 The evolution of the parapineal organ across vertebrates. The parapineal organ is not highly conserved as it is found only in some species (purple), including lampreys, teleosts and some reptiles.

[1] Within the Holostei infraclass, a parapineal organ has been described only in *Avia calva*

[2] A parapineal organ has also been reported in *Latimeria chalumnae* that belongs to the Actinistia subclass.

[3] Within the Reptilia class, a parietal eye (which is homologous to the parapineal gland) has been described in sphenodon and in some lizards that live in higher temperate latitudes.

In zebrafish, the parapineal organ is found on the left side of brain in approximately 95% of individuals (**Figure 1.1**) (Concha et al., 2000). It expresses the photoreceptive molecule opsin, as well as arylalkylamine N-acetyltransferase (aanat2), an enzyme important for melatonin biosynthesis (Gothilf et al., 1999; Concha et al., 2000; Gamse et al., 2002). In addition, parapineal cells extend axons that specifically innervate the left habenula (Concha et al., 2003). In zebrafish, laterality of the parapineal organ is closely linked with laterality of habenular asymmetries. Therefore, a possible role for the parapineal organ is to control the laterality of asymmetries between the left and right habenulae (discussed in detail in section **1.3.4.3**). However, whether the parapineal organ has additional (physiological or behavioural) functions is still elusive. In their review, Snelson and Gamse (2009) suggest that embryos with early-ablated parapineal organs are viable and therefore behavioural tests may provide some clues about its adult function.

Although no behavioural tests have been performed in fry or adult zebrafish with absent parapineal organs, several studies showed differences in the behaviour of fish with normal left-sided or reversed right-sided parapineal organs (Barth et al., 2005; Facchin et al., 2009; Dadda et al., 2010). For example, both fry and adult fish with reversed parapineal organs exhibit reversal of eye preference in the mirror-viewing test (Barth et al., 2005; Dadda et al., 2010). Also, *frequent-situs-inversus* (*fsi*) adult fish with normal parapineal organs (and normal laterality of the viscera) tend to use their right eye when approaching a target and if presented with two identical targets, they prefer the one on the right. In contrast, *fsi* mutants with reversed parapineal organs (as well as reversed visceral organs) tend to approach the target with their left eye and prefer to bite the left-sided target (Barth et al., 2005). Moreover, fry with reversed parapineal organs, e.g. *southpaw* (*spaw*) morphants or fish with spontaneous reversal of the parapineal, show a delay in the onset of swimming, as well as a reduction in their exploratory behaviour and average swimming speed, when compared with control siblings with left-sided parapineal organs (Facchin et al., 2009). It is important to note that not all asymmetric behaviours are affected in fish with reversed parapineal organs (Barth et al., 2005; Facchin et al., 2009; Dadda et al., 2010). For example, fry with both left- and right-sided

parapineal organs tend to turn right, when startled by sudden darkness (Barth et al., 2005). Therefore, laterality of the parapineal organ is important for at least some lateralized behaviours. Notably, *fsi* mutants, *spaw* morphants and fish with spontaneous reversal of the parapineal organ (that were used in the behavioural tests) tend to have reversal of the habenular asymmetries. Thus, the differences in lateralized behaviours may be caused by the abnormal laterality of the habenulae and not the parapineal organ *per se*.

1.2.3 Habenular nuclei

The bilateral habenulae are part of the evolutionarily conserved dorsal diencephalic conduction system that links the forebrain with the mid- and hindbrain. Inputs from the forebrain are transferred mainly through the stria medullaris to the habenular nuclei, which in turn send efferent axons through the fasciculus retroflexus to targets in the midbrain and hindbrain (reviewed in Klemm, 2004; Lecourtier and Kelly, 2007; Bianco and Wilson, 2009; Hikosaka, 2010; Okamoto et al., 2012; Shelton et al., 2012; Beretta et al., 2012).

In mammals and lizards, the habenulae are subdivided into medial and lateral sub-nuclei, each of which receives inputs from and sends outputs to different targets. The medial habenulae predominantly receive inputs from the septum and project to the interpeduncular nucleus (IPN) in the midbrain (Herkenham and Nauta, 1977, 1979). The IPN subsequently projects to other areas in the brain, including the raphe nuclei and the ventral tegmental area (Groenewegen et al., 1986). The efferent axons from the habenulae to the IPN comprise the core of the fasciculus retroflexus (also called the habenulo-interpeduncular tract) and this connection is highly conserved among vertebrates. In contrast, the lateral habenulae exhibit a broader and less conserved connectivity. They receive inputs from the basal ganglia and several limbic regions of the forebrain (Parent et al., 2001; Greatrex and Phillipson, 1982; Herkenham and Nauta, 1977; Araki et al., 1984). The lateral habenulae also receive circadian (light/environmental) information from the suprachiasmatic nucleus and RGCs (demonstrated in rodents) (Buijs, 1978; Hattar et al., 2006; Qu et al., 1996). Many of

these connections are reciprocal, for example the lateral habenula both receives and sends information to the lateral hypothalamic area. However, the major targets of the lateral habenulae are the serotonin-releasing median and dorsal raphe, as well as the dopamine-releasing ventral tegmental area and the substantia nigra (Herkenham and Nauta, 1979; Wang and Aghajanian, 1977; Araki et al., 1988; Aghajanian and Wang, 1977). The different afferent and efferent connections between the medial and lateral habenulae underlie the difference in their functions.

The fish and amphibian habenulae are subdivided into dorsal and ventral sub-nuclei. Several lines of evidence suggest that the zebrafish dorsal and ventral habenulae are homologous to the mammalian medial and lateral sub-nuclei, respectively. For example, *protocadherin 10* (*Pcdh10*) is expressed in the lateral (but not the medial) habenulae in adult mice and rats and similarly the zebrafish orthologs *pcdh10a* and *pcdh10b* are expressed in the zebrafish ventral (but not dorsal) habenulae (Amo et al., 2010). Moreover, a combination of labelling techniques revealed that the dorsal habenulae mostly innervate the IPN, whereas the ventral habenulae innervate the dorsal part of the median raphe (Aizawa et al., 2005; Gamse et al., 2005; Kuan et al., 2007; Aizawa et al., 2007; Bianco et al., 2008; Amo et al., 2010). This is analogous to the mammalian system, where the medial habenulae innervate the IPN and the lateral habenulae innervate the median raphe (among other targets).

Despite the many similarities between the dorsal/medial and ventral/lateral habenulae in zebrafish/mammals, some differences do exist. For example, in zebrafish, the ventral habenula can be distinguished based on the expression of *amiloride binding protein 1 (amine oxidase (copper-containing))* (*abp1*), previously known as *diamine oxidase* (*dao*), a gene that is expressed specifically in these sub-nuclei from approximately 4 dpf until adulthood. However, this gene is not expressed in the rat habenulae (Amo et al., 2010). Also, the main afferent connections of the larval zebrafish habenulae are with neurons of the eminentia thalami that will give rise to the entopeduncular nucleus (Hendricks and Jesuthasan, 2007). Although, the study (Hendricks and Jesuthasan, 2007) was performed before the characterization of the zebrafish dorsal and ventral habenulae (Amo et al., 2010), the eminentia thalami afferent

projections appear to terminate in the dorsal habenulae (based on their position); further investigation is required to confirm this. Since the entopeduncular nucleus projects into the lateral habenulae in mammals, afferent projections may differ between zebrafish and mammalian species.

Most of the scientific research in zebrafish focuses on the dorsal and not the ventral habenulae. Therefore, for simplicity from hereon I will refer to the zebrafish dorsal habenula as the habenula. Also, the zebrafish dorsal habenulae are further divided into dorsal medial and dorsal lateral sub-divisions. I will refer to these sub-divisions as medial and lateral habenulae, respectively, but they should not be confused with the mammalian medial and lateral sub-nuclei.

1.2.3.1 Habenular function

Due to the wide variety of afferent and efferent connections, habenulae (especially the lateral habenulae) are involved in the transmission of many neurotransmitters, including serotonin, dopamine, norandrenaline and acetylcholine. In fact, stimulation of the lateral habenulae in rats inhibits the activity of serotonin (Stern et al., 1979; Wang and Aghajanian, 1977) and dopamine neurons (Christoph et al., 1986; Ji and Shepard, 2007) and increases the release of norandrenaline (Kalén et al., 1989; Cenci et al., 1992) and acetylcholine (Nilsson et al., 1990). Consistent with their key role in the transmission of neurotransmitters, the habenulae are associated with many different types of behaviours, such as sleep regulation, reward-based decision-making, responses to an aversive stimulus, stress/fear/anxiety responses and cognition (learning, memory and attention). They have also been associated with a number of psychiatric disorders, such as depression, schizophrenia and drug-induced psychosis (discussed in detail in sections **1.2.3.1.1-1.2.3.1.6**).

The majority of habenular functions are associated with the lateral habenular sub-nuclei. This is partly due to the fact than in mammals the medial habenulae are found deeper in the brain and are smaller than the lateral habenulae. As a consequence, in most functional magnetic resonance imaging (fMRI) studies, the medial habenulae are

not resolvable. Also, the lack of suitable technology for the definite separation of the lateral and medial habenulae in mammals makes it extremely difficult to manipulate them independently. Therefore, most lesion experiments involve the impairment of both lateral and medial habenulae. However, in zebrafish the dorsal habenulae (which are homologous to the mammalian medial habenulae) are large and easily accessible, enabling their manipulation. Also, transgenic lines are available that allow a definite separation between the dorsal and the ventral habenulae, and even the dorsal medial and dorsal lateral sub-divisions (reviewed in Jesuthasan, 2012; Okamoto et al., 2012). Zebrafish are, therefore, proving to be an invaluable tool to further explore the functions of the habenulae (for example, experiments using zebrafish demonstrated a link between the habenulae and fear/anxiety, discussed in section **1.2.3.1.4**).

1.2.3.1.1 Sleep regulation and circadian functions

Several lines of evidence demonstrate an association between the habenulae and aspects of sleep. Firstly, the habenulae play an important role in rapid eye movement (REM) sleep. For example, in cats, there is a significant increase in the levels of glucose usage in the habenulae during REM (Lydic et al., 1991). Also, electrical stimulation of the cat lateral habenula disrupts the sleep pattern of the animal (decreased REM and increased non-REM sleep) (Goldstein, 1983). Similarly, after transection of the fasciculus retroflexus (the main habenular output tract), rats spend less time in REM sleep and exhibit reduced muscle atonia, which is a component of REM sleep (Haun et al., 1992; Valjakka et al., 1998). Transplantation of fetal habenular cells into these rats (near the IPN) can partly restore their sleep patterns (Haun et al., 1992).

Further evidence demonstrating the role of the habenulae in sleep regulation come from the fact that neural activity is increased in the habenulae during drug-induced general anesthesia in rats (it is thought that similar mechanisms control both sleep and anesthesia) (Herkenham, 1981; Abulafia et al., 2009), as well as in hibernating squirrels (Kilduff et al., 1990). In addition, medial habenular neurons are able to produce interleukin 18 (interferon-gamma-inducing factor) (IL18), a protein known to promote sleep (Sugama et al., 2002).

Moreover, the habenulae are involved in circadian functions and in some species, habenular cells are able to produce melatonin (Sato et al., 1991). Also, habenular neurons respond to retinal illumination and their firing rates show circadian rhythmicity in rats (H Zhao and Rusak, 2005). Notably, neurons in both the lateral and medial habenulae showed higher baseline firing during the day than the night, *in vivo*, and lateral habenular neurons maintained their rhythmicity *in vitro* (in slice preparations) for 48 hours (H Zhao and Rusak, 2005). As mentioned above, the habenulae receive afferent projections from the suprachiasmatic nucleus and the RGCs (Buijs, 1978; Hattar et al., 2006; Qu et al., 1996) and therefore they may have roles in converting light/dark information and circadian rhythms into behavioural functions, such as sleep.

1.2.3.1.2 Motor activity and reward-based decision-making

Habenulae are also linked with motor behaviours and reward-based decision-making. For example, rats with habenular lesions are hyperactive with increased exploratory and locomotor activity (Lee and Huang, 1988), possibly due to the increased activity of dopamine neurons. In contrast, electrical stimulation of the lateral habenulae inhibits the activity of dopamine neurons in the ventral tegmental area and the substantia nigra (two of the main targets of lateral habenulae) (Christoph et al., 1986; Ji and Shepard, 2007). It is therefore thought that normal activity of the habenulae, especially the lateral habenulae, negatively regulates dopamine neurons and consequently promotes suppression of motor activity (reviewed in Klemm, 2004; Bianco and Wilson, 2009; Hikosaka, 2010).

Another function of the habenulae linked with dopaminergic activity is the control of reward-based decision-making. It is thought that dopamine neurons provide teaching signals during reinforcement learning, i.e. learning from the consequences of a specific action. Particularly, dopamine neurons are stimulated by a larger-than-expected reward and inhibited by a smaller-than-expected reward. Therefore, if an action is advantageous and thus receives larger-than-expected reward, dopamine is released, which in turn promotes that specific action. In contrast, following an action that gives a

smaller-than-expected reward, dopamine neurons are inhibited resulting in suppression of that specific action (reviewed in Hikosaka, 2010).

The habenulae seem to provide instructions to dopamine neurons regarding negative reward-related signals. This is illustrated by experiments where macaque monkeys were performing visual saccade tasks with positionally-based rewards. In these experiments, the lateral habenulae were activated by visual stimuli that were linked with an absent or small reward and inhibited by stimuli indicating a (larger) reward (Matsumoto and Hikosaka, 2009). Additionally, fMRI on human subjects, performing a motion-prediction task, showed that the habenulae are activated upon unexpected negative feedback or the absence of expected positive feedback (which is analogous to absent/small reward) (Ullsperger and Von Cramon, 2003). Therefore, a simplified model suggests that habenulae are involved in reinforcement learning by inhibiting dopamine neurons when an action gives smaller-than-expected reward.

1.2.3.1.3 Pain processing and aversive response

The fact that habenulae have both afferent and efferent connections with structures involved in pain modulation (such as the lateral hypothalamus, nucleus accumbens, basal ganglia and raphe nuclei) (Herkenham and Nauta, 1977, 1979) suggests a role for the habenulae in pain processing. In agreement with this, lateral habenular neurons respond to painful stimuli (Benabid and Jeaugey, 1989) and neuronal activity of the lateral habenulae (as marked by positive c-fos staining) is increased in experimental pain (Smith et al., 1997; Lehner et al., 2004). Also, electrical stimulation of the habenulae or injections of morphine into the habenulae induce analgesia (inability to feel pain) in rat models with tonic pain (S. R. Cohen and Melzack, 1986, 1985).

In addition to pain, the habenulae are associated with aversive stimuli that are not necessarily painful. This is best illustrated by the results from a standard Pavlovian-conditioning experiment performed in macaque monkeys (Matsumoto and Hikosaka, 2009). The experiment consisted of two blocks of trials: the “appetitive” and the “aversive”. During the test, the activity of lateral habenular neurons was recorded. Three symbols were shown on a screen. Each symbol was indicative of the probability (100%,

50% or 0%) of receiving juice (reward in appetitive block) or air puff (punishment in aversive block). Interestingly, the lateral habenulae were strongly activated by the "worst" possible outcome (symbols that indicated 0% probability of receiving juice in the appetitive block or 100% possibility of receiving air push in the aversive block). Contrarily, the lateral habenulae were inhibited by the "best" possible outcome (100% probability of receiving juice or 0% probability of receiving air push). Moreover, the lateral habenular neurons were activated by punishment itself and inhibited by reward, especially when these were not expected. Based on their results, the authors suggest that the lateral habenulae have the potential to control both reward-seeking and punishment-avoiding behaviours, possibly by controlling the downstream serotonergic and dopaminergic systems (Matsumoto and Hikosaka, 2009).

1.2.3.1.4 Stress, Fear, Anxiety

The repetitive exposure to aversive stimuli (painful or not) is stressful and can lead to fear and anxiety. The lateral habenular neurons are activated by stress-induced stimuli, such as continuous aversive stimuli, open field exposure and physical constraint. Also, the medial habenulae are associated with neuroendocrine and immunological responses to stressful stimuli. Notably, heat shock proteins (HSPs, proteins whose expression is increased under stress-conditions, especially heat) are expressed in the medial habenulae (among other brain areas) in response to heat-induced stress (Blake et al., 1990; Li et al., 1992). Moreover, although IL18 is expressed in the medial habenulae of unstressed (non-restrained) rats, its expression is increased in response to acute or chronic stress (Sugama et al., 2002).

In addition, animals with habenular lesions are less able to respond to aversive stimuli, especially under stressful conditions. Thornton and Bradbury (1989) demonstrated this by performing active avoidance learning experiments in rats. Rats with control lesions or habenular lesions were placed in a box, where light and sound stimuli (warning signals) were followed by an aversive stimulus (electric shock). The authors were measuring the period of time the animals needed to respond to the signals and jump out of the box (on a platform free of electric shock). Control rats responded

faster than habenular-lesioned animals, under normal conditions, although the difference in time was not statistically significant. Their results suggest that even rats with impaired habenulae are able to learn and avoid an aversive stimulus. However, under stressful conditions (higher shock intensity and shorter intervals between each shock) habenular-lesioned rats were impaired to respond to both the warning (light and sound) and the aversive (electric shock) stimuli. Moreover, the increased effort required to avoid/escape the aversive stimuli decreased the response of habenular-lesioned rats. Rats with habenular lesions could not response to the stimuli when the platform was higher (17 cm above the floor of the box as opposed to 4 cm in the previous experiments) and therefore more effort was required. Together the data suggest that the habenulae are involved in avoidance learning (behavioural responses to avoid aversive stimuli), especially under stressful conditions (Thornton and Bradbury, 1989).

Stress, fear and anxiety are three closely related concepts that can lead to each other. Considering the association between habenulae and stress, it is not surprising that several studies demonstrate a link between the habenulae and fear/anxiety. Rats with damaged fasciculus retroflexus (the main habenular efferent projection tract) appear more anxious, as indicated by the increased plasma levels of corticosterone and their behavioural responses in elevated plus-maze and open-field tasks, in relation to control animals (Murphy et al., 1996). Moreover, larval and adult zebrafish with impaired habenular function exhibit increased fear and anxiety (Lee et al., 2010; Agetsuma et al., 2010). In particular, fish were subject to a standard avoidance learning task: they were placed in a tank, where a red light (warning signal) on one side of the tank was coupled with electric shock (aversive stimulus) on the same side. Fish were assessed for their ability to avoid the aversive stimulus by moving to the other side of the tank. Instead of swimming away from the source of the electric shock, zebrafish with impaired habenulae showed a persistent freezing and startling, indicative of increased fear and anxiety. Therefore, habenulae may normally function by suppressing the choice of freezing and promoting escaping, in response to stress/fear/anxiety (Lee et al., 2010; Agetsuma et al., 2010).

1.2.3.1.5 Cognition: learning, memory and attention

The habenulae have also been implicated in cognitive functions, such as learning, memory and attention. The first evidence supporting the involvement of the habenulae in cognition comes from experiments with rats, performing a classical Morris water maze test (Villarreal et al., 2002). In this test, rats are placed in a pool of water, which contains a platform hidden a few centimetres below the surface of the water. Once placed in the pool, rats start searching for an escape route. On subsequent trials, unimpaired rats are able to find the platform much faster, as a result of spatial learning and memory. Aged and memory-impaired rats showed reduced metabolic activity in the lateral habenula after training in a Morris water maze, in relation to young and unimpaired rats. In fact, greater habenular metabolic activity was correlated with better performance in Morris water maze (Villarreal et al., 2002). However, although these results suggest a correlation between habenular activity and spatial learning and memory, the role of habenulae in these processes is better demonstrated by lesion experiments. Notably, rats with habenular lesions were impaired in both acquisition (learning) and retrieval (memory) of the Morris water maze test (Lecourtier et al., 2004), suggesting that normal function of the habenulae is required for optimum spatial learning and memory.

In addition to spatial learning and memory, habenulae seem to be associated with attention. In 1980s, Thornton and Evans performed forced swimming tests (with a rope as an escaping route) in rats with habenular lesions. They found that lesioned-animals were less likely to climb the rope and therefore escape (Thornton and Evans, 1982). These results led to the hypothesis that habenular lesions may lead to attention defects. To confirm this, Lecourtier and Kelly (2005) performed a 5-Choice-Serial-Reaction-Time Test, which is a well-accepted test for attention. Rats with habenular lesions showed increased premature responding (indicative of increased impulsive behaviour), as well as a progressive decrease in choice accuracy.

1.2.3.1.6 Psychiatric disorders

In addition to normal functions and behaviours, the habenulae are also associated with a number of psychiatric disorders, including depression, schizophrenia and drug-induced psychosis.

First of all, data from several studies (using both animal models and human patients) demonstrate a link between habenular activity and depression. Notably, hyperactivity of the habenular neurons correlates with increased depressive behaviours. For instance, in three different rat models of depression, neuronal activity in the habenulae and the IPN (main target of the medial habenulae) was elevated (Caldecott-Hazard et al., 1988; Shumake et al., 2003). Interestingly, habenular lesions in these rats led to reduction in depressive behaviours (Yang et al., 2008), whereas treatment with antidepressant drugs reduced both habenular activity and depressive behaviours (Caldecott-Hazard et al., 1988). Moreover, patients with depression showed increased habenular blood flow when depressive relapses were induced by depletion of tryptophan (tryptophan is required for serotonin synthesis and low levels of serotonin are associated with depression) (Morris et al., 1999). Finally, magnetic resonance imaging (MRI) in patients with depression or bipolar disorder revealed that patients had significantly smaller habenular volume when compared to control subjects (Savitz et al., 2011).

Furthermore, depression is associated with a number of functions and/or behaviours that are modulated by the habenulae. For example, reduced motor activity is often used as an indication of depression in animal models (Caldecott-Hazard et al., 1988). As discussed above, increased habenular activity is associated with reduced dopamine levels that can lead to suppression of motor activity. Moreover, both depression and aberrant habenular function are associated with low levels of serotonin (Yang et al., 2008), as well as circadian rhythm and sleep disturbances.

All the data described above suggest, but do not prove, a direct link between habenular function and depression. However, Sartorius et al. (2010) were able to treat a patient with therapy-resistant depression by deep brain stimulation (DBS) of the lateral habenulae. Similarly, DBS of the lateral habenula in rat models of depression significantly improved the depressive behaviours (Meng et al., 2011). DBS is a surgical

technique, where a DBS pacemaker is implanted in specific brain regions and used to electrically modulate brain activity in small areas of the brain. DBS has been effectively used to treat several disorders including Parkinson's disease, chronic pain, dystonia and tremor (reviewed in Kringelbach et al., 2010). Therefore, these results provide a direct link between aberrant habenular function and increased depressive behaviours both in animal models and human patients.

In addition to depression, a number of studies demonstrate a correlation between habenular dysfunction and schizophrenia. Firstly, an increased incidence of epithalamic (both the habenulae and the pineal gland) calcification is observed in schizophrenic patients in relation to control subjects (Caputo et al., 1998). Also, influenza A virus, which is associated with increased risk of schizophrenia, selectively attacks the habenulae, thalamic midline and monoaminergic brainstem neurons, when introduced via the olfactory bulbs in mice (Mori et al., 1999). Finally, habenular activity is abnormal in patients with schizophrenia, as demonstrated by fMRI studies (Shepard et al., 2006). In particular, patient and control subjects were performing a difficult mental test, followed by positive (when answers were correct) or negative (when they made errors) feedback. Interestingly, the habenular nuclei were activated in response to negative feedback in healthy subjects, but not in patients suffering from schizophrenia. In addition, schizophrenic patients were unable to improve on repeating the test whereas control subjects showed a significant improvement. These results suggest that dysfunction of the habenular nuclei in patients with schizophrenia decreases their ability to respond to negative feedback and learn from their errors. Importantly, the inability to learn from errors is one of the most characteristic defects associated with schizophrenia (Shepard et al., 2006).

Continuous and excessive intake of addictive drugs, such as amphetamine and cocaine, can lead to paranoia, delusions, hallucinations, mania and other symptoms that are also observed in patients with paranoid schizophrenia. Experiments in rats demonstrate that continuous administration of drugs (including amphetamine and cocaine) results in strong and highly specific degeneration of lateral habenular axons at the sheath of fasciculus retroflexus (Ellison, 1992; Carlson et al., 2000). In contrast,

constant nicotine administration leads to degeneration of medial habenular neurons projecting through the core of the fasciculus retroflexus (Carlson et al., 2000, 2001). Moreover, nicotine receptors that mediate withdrawal responses are concentrated in the medial habenulae and the IPN (Salas et al., 2009). Together these findings raise the possibility that in humans, continuous intake of drugs may lead to dysfunction of the habenulae, which in turn may lead to drug-induced psychosis or symptoms associated with drug withdrawal.

1.2.3.2 Evolution of asymmetric architecture of the habenulae

The habenulae, along with their afferent (stria medullaris) and efferent (fasciculus retroflexus) connections, are highly conserved throughout the vertebrate lineage. They are found in all vertebrate species examined, from the lamprey (one of the evolutionarily oldest vertebrates) to fish, amphibians, reptiles, birds and mammals, including humans. However, as evolution proceeded the habenulae acquired more afferent and efferent connections and the whole system became more complex (reviewed in Concha and Wilson, 2001).

One of the most striking characteristics of the habenulae is their asymmetric architecture. In fact, asymmetries in size, cytoarchitecture, connectivity, gene expression and/or neurochemistry between the left and right habenular nuclei have been described in a wide range of vertebrate species (summarized in **Figure 1.4**) (reviewed in Harris et al., 1996; Concha and Wilson, 2001). However, the laterality of asymmetries differs between the different classes of vertebrates. For example, hagfish, lamprey and the majority of non-teleost actinopterygian fishes have enlarged right habenulae, whereas Chondrichthyes, frogs and reptiles have a larger left habenula. In addition, variability in the asymmetric architecture of the habenulae is observed even within the same group of animals. For example, within the Teleostei infraclass of fishes the habenulae can be:

a) Symmetric in the majority of species examined, e.g. *Pantodon buchholzi*, *Clupea harengus*, *Fundulus heteroclitus*, *Carassius auratus*, *Coris julis* etc.
b) Asymmetric with enlarged left habenula, e.g. *Anguilla anguilla*, *Oncorhynchus kisutch* and *Danio rerio*.

c) Asymmetric with enlarged right habenula e.g. *Oncorhynchus mykiss*, *Osmerus eperlanus* and *Cyclothone acclinidens*.

In contrast to the lower vertebrates, the left and right habenular nuclei appear symmetric in most mammalian species examined, with the following exceptions (reviewed in Harris et al., 1996; Concha and Wilson, 2001):

a) In developing and mature albino rats, the left medial habenula is slightly but significantly larger than the right one.
b) In developing and mature albino mice, the right lateral habenula is larger than the left one.
c) Neuronal organization is asymmetric in macrosmatic mole, since a row of dark cells is only detected in the left habenula.

Further and more detailed analysis is required to investigate whether subtle differences in size, organization, gene expression and connectivity between the left and right habenulae are present in other mammalian species.

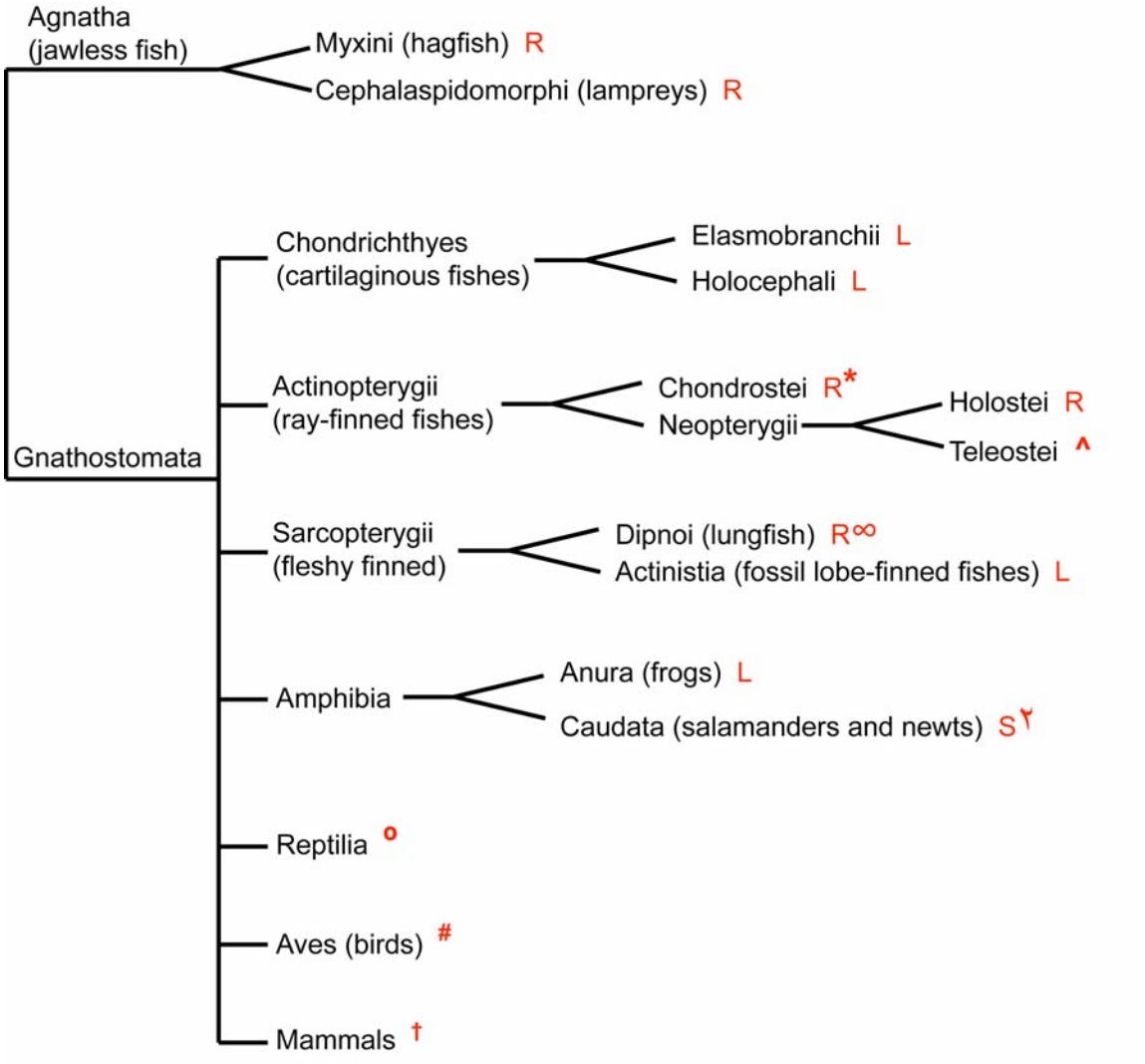

Figure 1.4 The evolution of habenular asymmetries across vertebrates. The left and right habenulae often differ in size and/or cytoarchitecture. The laterality of these asymmetries varies between the different classes of vertebrates and some variability is present even within the same class of animals.
R = right habenula is enlarged, L = left habenula is enlarged, S = habenulae are symmetric, * except *Polyodon spathula* where the left habenula is enlarged, ^ most teleostei species have symmetric habenulae, but *Anguilla anguilla*, *Oncorhynchus kisutch* and *Danio rerio* have an enlarged left habenula and *Oncorhynchus mykiss*, Osmerus eperlanus and *Cyclothone acclinidens* have an enlarged right habenula, ∞ except *Neoceratodus forsteri* where habenulae appear symmetric, ٢ in the newt *Triturus cristatus* left and right habenulae are similar in size but differ in their cytoarchitecture, ° habenulae are symmetric in turtles, ophidians, crocodiles and some lizards, but an enlarged left habenula is found in *Uta stansburiana*, # sex-dependent asymmetry, since the right habenula is enlarged in male but not female chicks, † symmetric in most mammalian species but with some exceptions: enlarged left habenula in albino rats, enlarged right habenula in albino mice and asymmetric cytoarchitecture in the mole *Talpa europaea*.

1.3 Development of the zebrafish epithalamus

1.3.1 Specification of the pineal complex

As discussed above, the zebrafish pineal complex consists of the pineal gland and the left-sided parapineal organ. Both structures are generated from the same pool of pineal complex precursors. Understanding how these two different cell types (pineal and parapineal cells) are specified from a common pool of precursors, may provide some insights into the mechanisms that control specification of the many different types of neurons found in the human brain.

The presumptive pineal complex can be visualized very early during development by the expression of *floating head* (*flh*). From approximately the 80-90% epiboly stage, *flh* is expressed in two groups of cells on either side of the neural plate. These *flh* domains fuse together at the midline of the dorsal diencephalon to form the pineal anlage, at about 8 somite stage (ss) (Masai et al., 1997). By 14 ss, the first differentiated cells, within the *flh*-positive domain, start expressing *islet1* (*isl1*), a gene expressed by neurons after their final mitotic division and before their full maturation (Ericson et al., 1992; Masai et al., 1997). Expression of *flh* persists throughout embryonic, larval and adult stages (Liang et al., 2000).

Currently two pathways have been implicated in the restriction of *flh*, and therefore pineal complex, in the middle of the dorsal diencephalon. First, proper activity of the Wnt signaling pathway positions the pineal gland along the anteroposterior axis (Heisenberg et al., 1996; Masai et al., 1997). The *masterblind* (*mbl*) mutants carry a mutation that result in an amino-acid substitution within the glycogen synthase kinase 3 (Gsk3) binding domain of axin 1 (axin1). This mutation leads to reduction of axin1 and therefore overactivation of the Wnt signaling pathway (Heisenberg et al., 2001). As a consequence, *flh* expression and thus pineal anlage are expanded into the anterior forebrain in *mbl* mutants (Heisenberg et al., 1996; Masai et al., 1997). In contrast, a proper bone morphogenic protein (BMP) gradient is required for the positioning of the *flh*-positive pineal anlage along the dorsoventral axis. In particular, if BMPs are overexpressed, *flh* is not induced. Contrarily, if BMP gradient is lowered, *flh* is expressed more ventrally in relation to control embryos (Barth et al., 1999).

In addition to *flh*, the transcription factor *T-box 2b* (*tbx2b*) is also expressed in the presumptive pineal complex. Particularly, from about 6 ss *tbx2b* is expressed in two bilateral domains, similarly to *flh*, and by 10 ss a single *tbx2b* expression domain is detected in the middle of the dorsal diencephalon (Snelson et al., 2008a). Although the expression domains of *flh* and *tbx2b* are largely overlapping, some cells express only one of the two genes (Snelson et al., 2008a).

As mentioned above, both pineal and parapineal cells originate from the same pool of precursors that is defined by the expression of *flh* and *tbx2b*. This was first illustrated by fate mapping experiments using photoactivation of caged fluorescein in *Tg(-1.6flh:gap43-EGFP)u1* transgenic embryos (I will refer to this line as *Tg(flh:GFP)* from hereon) (Concha et al., 2003). Photoactivation within the left or right side of the anterior *flh* domain labelled both pineal and parapineal cells. In contrast, photoactivation within the posterior *flh* domain only labelled pineal cells. In addition, ablation of cells from the left or right side of the anterior presumptive pineal complex at 22-24 hour post fertilization (hpf) resulted in fewer parapineal cells, whereas bilateral ablation resulted in fewer pineal cells and completely absent parapineal cells (Concha et al., 2003). These results suggest that the anterior part of the presumptive pineal complex contains precursors that give rise to both pineal and parapineal cells, whereas precursors found in the posterior will only generate pineal cells.

The mechanism that defines whether cells will adopt a pineal or a parapineal fate is still elusive. However, analysis of mutant embryos with disrupted *flh* or *tbx2b*, suggest that the two genes are important for the development of the pineal and parapineal organ, respectively. Specifically, neurogenesis within the pineal gland ends prematurely in *flh* mutants, resulting in fewer *isl1*-positive cells (Masai et al., 1997). The specification of parapineal cells though is normal in *flh* mutants, although positioning of the parapineal organ is randomized (discussed in section **1.3.4.3**) (Gamse et al., 2002; Snelson et al., 2008b). In contrast, the *tbx2b*-null mutants (*from beyond - fby* mutants) have normal pineal glands, but fewer and mispositioned parapineal cells (Snelson et al., 2008a). Also, double *flh*;*fby* mutants show additive effects: smaller pineal and parapineal organs (Snelson et al., 2008b).

As mentioned above, a subset of cells within the presumptive pineal complex expressed *tbx2b* but not *flh* and therefore one hypothesis is that those cells will adopt a parapineal fate, whereas the remaining cells that express *flh* will adopt a pineal fate (Snelson et al., 2008b). A more detailed fate mapping is necessary to confirm this hypothesis.

A second mechanism that can explain the differential fate of cells originating from the same pineal complex precursors came from the study of Snelson et al. (2008b). In this study, birth-dating experiments, using 5-bromo-2'-deoxyuridine (BrdU), showed differences in the timing of pineal and parapineal neurogenesis. Both pineal and parapineal cells had maximum BrdU incorporation when embryos were treated for 30 minutes at 15 ss. After this stage, most parapineal cells stop dividing. However, a second smaller peak of BrdU incorporation was observed in the pineal cells at 24 hpf. Thus, although pineal and parapineal cells start dividing at the same time (with maximum cell division rate at 15 ss), parapineal-cell division stops before pineal-cell division (Snelson et al., 2008b).

Based on the phenotypes of *flh* and *fby* mutants and the differential timing of neurogenesis, Snelson et al. (2008b) proposed the following model. The pineal complex precursors are defined by the expression of *flh* and *tbx2b* before the 15 ss and start dividing to give rise to pineal complex cells. At this stage, cells that express *tbx2b* (but not *flh*) will adopt a parapineal cell fate, whereas the remaining cells will adopt a pineal cell fate. A second wave of cell division will only give rise to pineal cells. This second phase of cell division depends on the activity of *flh*, since in *flh* mutants neurogenesis stops after the 18 ss (Masai et al., 1997; Snelson et al., 2008b).

In an independent study, Cau and colleagues (2008) also showed that cell division marked by BrdU incorporation in pineal cells peaks at approximately 15 ss, but they did not detect a second wave of cell divisions at 24 hpf. The two groups used different methodologies, which could explain the differences in their results. For example, Snelson et al. (2008b) performed a 30-minute BrdU treatment on *Tg(foxd3:GFP)zf15* embryos (that have GFP expression in both pineal and parapineal cells) and assessed the number of cells co-labelled with BrdU and GFP at 4 dpf. In

contrast, Cau et al. (2008) treated embryos with BrdU for 2 hours and 20 minutes and evaluated the number of BrdU-positive cells at 48 hpf. Also, Cau and colleagues used different reporter transgenic lines: *Tg(aanat2:EGFP)y8* and *Tg(elavl3:EGFP)knu3* that label the photoreceptors and projection neurons, respectively.

1.3.2 Neurogenesis within the pineal gland

The vertebrate brain contains many different types of neurons that are organized into many structures, each of which has specific functions. The mechanisms that control the main processes necessary for early brain development, such as neurogenesis, differentiation, migration, establishment of connections, are reiteratively used to generate a functional and mature brain. Therefore, understanding how these mechanisms work in a small and relatively simple structure, such as the pineal gland, will give invaluable insights about the development of the complete brain.

During early CNS development, the activity of basic helix-loop-helix (bHLH) transcription factors (collectively known as proneural genes), BMP and Notch pathways (among other genes and pathways) is crucial for proper neurogenesis. In particular, the BMP pathway has key roles during early neural tissue induction (reviewed in Wolpert et al., 2002). In addition, the synergistic activity of proneural genes, such as *achaete-scute complex homolog 1 (Drosophila)* (*Ascl1*, previously known as *Mash1*) and Neurogenins, and neurogenic genes such as Notch and *delta* genes, controls the timing of cell birth and differentiation, via a process called lateral inhibition. Activation of the Notch pathway in a particular cell leads to downregulation of proneural genes in that cell and therefore that specific cell will maintain its progenitor identity. In contrast, its neighboring cells, with inactive Notch, will upregulate the expression of proneural genes. Cells with high levels of proneural genes will start expressing other bHLH transcription factors required for neuronal differentiation, such as members of the *neurogenic differentiation* (*Neurod*) family of genes (reviewed in Bertrand et al., 2002; Wolpert et al., 2002; Sanes et al., 2011).

In addition to controlling neurogenesis, the same pathways are involved in specification of neurons. Secreted molecules, called morphogens, generate gradients

along the dorsoventral (sonic hedgehog, Wnts and BMPs) and the anteroposterior (fibroblast growth factors (FGFs), Wnts and retinoic acid) axes of the neural tube and provide positional information to the precursor cells. Depending on its position, each neural precursor expresses a different set of bHLH (proneural and neuronal-differentiation genes) and homeodomain transcription factors (prepattern genes) that control the number and identity of the neurons that will be generated. Prepattern genes are downstream of morphogens and upstream of bHLH transcription factors and are thought to be the link between patterning and neurogenesis within the neural tube (Gómez-Skarmeta et al., 2003).

The activity of these genes and pathways has also been demonstrated to be important for the proper neurogenesis and cell-fate determination within the pineal gland in zebrafish. In particular, *flh* and bHLH transcription factors (discussed in **1.3.2.1**), as well as the Notch pathway (discussed in **1.3.2.2**) and the BMP pathway (discussed in **1.3.2.3**), are required for the proper neurogenesis within the pineal gland. In addition, Notch and BMP pathways are important for the proper cell-fate determination within the pineal gland (discussed in section **1.3.3**). Despite the large amount of data available, the complete network that controls these processes is still unknown.

1.3.2.1 The *flh* and bHLH activity

As discussed in section **1.3.1**, the presumptive pineal gland expresses *flh*, which is necessary for the proper neurogenesis within the pineal gland (Masai et al., 1997). The mechanism, by which *flh* controls neurogenesis, is not fully understood. However, data suggest that *flh* functions (at least in part) as a prepattern gene, since its expression is restricted by the activity of Wnt and BMP morphogens and it controls the expression of bHLH transcription factors (Cau and Wilson, 2003).

Three bHLH transcription factors are expressed within the pineal gland anlage: *achaete-scute complex-like 1a (Drosophila)* (*ascl1a*), *neurogenin 1* (*neurog1*) and *neurod* (Masai et al., 1997; Cau and Wilson, 2003). Notably, these transcription factors have differences in their spatiotemporal expression. Expression of *ascl1a* is observed throughout the diencephalon from 6 ss and becomes restricted to the presumptive pineal

gland from about 8 ss (Masai et al., 1997; Cau and Wilson, 2003). In contrast, *neurog1* is expressed at low levels in a few cells in the posterior end of the pineal gland from 12 ss onwards. Finally, *neurod* is expressed in a subset of pineal cells from 18 ss, consistent with previous studies suggesting that expression of members of the *Neurod* family of genes follows the expression of the proneural genes and controls differentiation of neuronal progenitors (Cau and Wilson, 2003 and reviewed in Bertrand et al., 2002).

In *flh* mutants, *ascl1a* is expressed normally up to 14 ss, but is downregulated by 18 ss (Masai et al., 1997; Cau and Wilson, 2003). Furthermore, *neurog1* and *neurod* expression is severely reduced or absent in the majority of *flh* mutants (Cau and Wilson, 2003). Thus, *flh* activity is required for the maintenance of *ascl1a* expression and the initiation of *neurog1* and *neurod* expression.

The proneural genes *ascl1a* and *neurog1* are in turn essential for proper neurogenesis within the pineal gland anlage (Masai et al., 1997; Cau and Wilson, 2003). Downregulation of *ascl1a* using morpholinos results in a small but significant decrease in the number of *isl1* epiphysial neurons. In contrast, downregulation of *neurog1*, either in *neurog1* morphants or *neurog1* mutants, does not affect the number of *isl1*-positive neurons within the pineal gland. Interestingly, disruption of both *ascl1a* and *neurog1* simultaneously, results in severely reduced or absent epiphysial *isl1* expression. The two genes do not regulate each other since expression of *ascl1a* is normal in *neurog1* morphants and *vice versa*. Also, *ascl1a* and *ascl1a*/*neurog1* morphants have normal *flh* expression, suggesting that the two genes work downstream of *flh*. However, expression of *neurod* (the third proneural gene expressed within the pineal gland anlage) is severely reduced in *ascl1a*/*neurog1* double morphants. Together the data suggest that *ascl1a* and *neurog1* are expressed independently of each other and have redundant roles in controlling neurogenesis within the presumptive pineal gland, downstream of the prepattern gene *flh* and upstream the proneural gene *neurod* (Cau and Wilson, 2003).

In addition to regulating the expression of proneural genes, *flh* controls the expression of other genes that are also involved in the modulation of neurogenesis and/or cell-fate determination. This was shown by comparing the expression profiles of

genes expressed within the epiphysis between *flh* mutant and *ascl1a*/*neurog1* double morphant embryos (Cau and Wilson, 2003).

For example, *flh* regulates the expression of *deltaA* (*dla*) and *deltaD* (*dld*) through an *ascl1a*-independent pathway. Three Notch ligands are expressed within the pineal gland: *deltaB* (*dlb*) and *dld* are expressed specifically in the laterally located projection neurons, whereas *dla* is expressed throughout the pineal gland (Cau and Wilson, 2003; Cau et al., 2008). Expression of the *delta* genes is absent at 14 ss and reduced at 24 ss in *ascl1a* morphants, normal in *neurog1* morphants and completely absent even at later stages (up to 24 ss) in *ascl1a*/*neurog1* double morphants. In *flh* mutants, though, *dla* and *dld* (but not *dlb*) expression is severely reduced even at 14 ss, when *ascl1a* expression is normal (Cau and Wilson, 2003).

flh controls not only the expression of *delta* genes, but also the expression of the homeodomain transcription factor *orthodenticle homolog 5* (*otx5*). At early stages (up to 28 hpf), *otx5* is co-expressed with *flh* and *aanat2* within the pineal gland. From about 48 hpf, a group of *otx5*-positive cells is also detected in the left side of the pineal gland and corresponds to the migrating parapineal cells (Gamse et al., 2002). *otx5* activity is required for the proper expression of genes that are regulated by circadian rhythms, including *aanat2, nuclear receptor subfamily 1, group d, member 1* (*nr1d1,* previously known as *reverbα*) and *interphotoreceptor retinoid-binding protein* (*irbp*), but is dispensable for the expression of non-cycling genes, such as *retinal homeobox gene 2* (*rx2*), *cone-rod homeobox* (*crx*), *flh* and *otx5* itself (Gamse et al., 2002). Similar to *delta* genes, *otx5* is reduced in *ascl1a* morphants, unaffected in *neurog1* morphants and further reduced or absent in *ascl1a*/*neurog1* double morphants and *flh* mutants (Cau and Wilson, 2003). Since *ascl1a* is expressed normally up to 14 ss in *flh* mutants, the data suggest that *flh* controls early expression of *otx5* (as well as *dla* and *dld*) through an *ascl1a*-independent pathway (Cau and Wilson, 2003). In addition, *flh* expression is normal at early stages (14 ss), but is downregulated at 24 ss in *flh* mutants, suggesting that *flh* is a self-regulating gene. Since *flh* expression is normal in *ascl1a* and *ascl1a/neurog1* morphants, *flh* regulates itself independently of *ascl1a* and *neurog1* (Cau and Wilson, 2003).

1.3.2.2 The Notch pathway

In addition to *flh* and bHLH transcription factors, the Notch pathway is another important modulator of the pineal development and in particular of neurogenesis within the pineal anlage.

The Notch pathway is a short-range signaling mechanism, with multiple roles during development. It modulates the timing of neurogenesis, as well as cell-fate decisions, during embryogenesis and acts at different developmental stages even within the same tissue (reviewed in Bray, 2006; Cau and Blader, 2009). Although some differences are observed between different species, the general framework of Notch pathway (**Figure 1.5**) is highly conserved from simple organisms such as *Caenorhabditis elegans* to mammals, including humans (reviewed in Bray, 2006; Kovall, 2008).

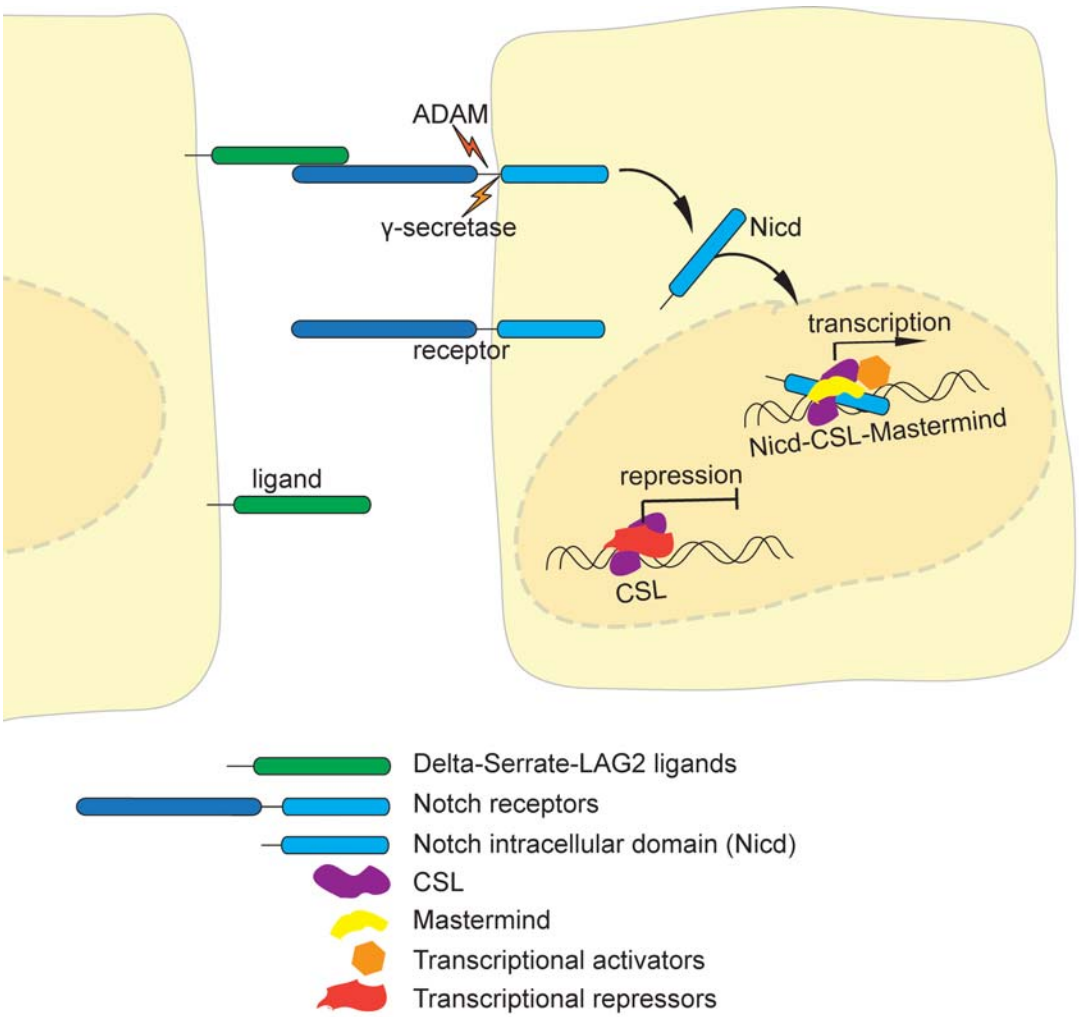

Figure 1.5 The Notch pathway. Notch receptors and Delta/Serrate/LAG-2 ligands are transmembrane proteins with long extracellular domains. Binding of a ligand to the extracellular domain of a Notch receptor in a neighboring cell triggers two proteolytic cleavage events. During the first cleavage, members of the ADAM-family (a disintegrin and metalloprotease family) remove the majority of the receptor's extracellular domain. The second cleavage is catalysed by the γ-secretase complex and releases the Notch intracellular domain (Nicd). The Nicd is then translocated into the nucleus, where it forms a trimeric complex with CSL, a DNA-binding transcription factor, and Mastermind, a transcriptional co-activator. The Nicd-CSL-Mastermind complex activates transcription by recruiting transcriptional activators, such as histone acetyl transferases and chromatin-remodelling complexes. Kinases and the nuclear ubiquitin ligase F-box and WD-40 domain protein 7 (Fbxw7, previously known as SEL10) are also recruited and trigger quick degradation of the Nicd. In the absence of the Nicd, the activation complex is dissociated and transcription stops. The CSL transcription factor interacts with co-repressors to ensure that Notch target genes are repressed until the initiation of a new cycle.

During development, expression of Notch ligands is dynamic to ensure differential activity of the pathway. However, in some cases neighboring cells have similar levels of ligands and therefore differential transcription cannot solely predict in which cells the Notch pathway will be activated. In addition, Notch receptors are often expressed in broad domains within tissues, although cleavage of the Nicd only occurs in a subset of cells expressing Notch receptors. In such cases, activation of the pathway is achieved via post-transcriptional modifications of the Notch ligands and receptors. Two E3 ubiquitin ligases have been involved in the activation of Notch ligands: Neuralized and Mind bomb (Mib) (reviewed in Bray, 2006). Interestingly, zebrafish embryos with a mutation in *mib* have neurogenic phenotypes as a consequence of reduced Notch signalling. These embryos have increased expression of *delta* genes and their phenotypes can be rescued by injections of mRNA encoding the active intracellular domain of *notch5*, suggesting that mib-mediated ubiquitylation of Notch ligands is necessary for them to effectively activate Notch in neighboring cells (Itoh et al., 2003). In addition, glycosylation and proteolytic processing of Notch receptors can influence the activity of the receptors, whereas ubiquitylation and endocytic trafficking control the amount of receptors available in a particular cell and thus the level of Notch pathway activation (reviewed in Bray, 2006).

Although the expression patterns of Notch receptors have not been determined in the zebrafish epithalamus, three Notch ligands (*dla*, *dlb*, *dld*) are expressed within the pineal anlage (discussed in section **1.3.2.1**) (Cau and Wilson, 2003; Cau et al., 2008). Moreover, three *hairy and enhancer of split related* (*her*) genes: *her2*, *her4.1* and *her15.1*, which are known Notch targets, are expressed in the developing epithalamus and their expression is lost in embryos treated with DAPT, a γ-secretase inhibitor known to downregulate Notch activity (Quillien et al., 2011). The fact that Notch ligands, as well as Notch targets, are expressed within the pineal gland suggests that Notch signalling is involved in pineal gland development.

Cau and colleagues (2008) demonstrated that the Notch pathway controls neurogenesis within the pineal gland by inhibiting the neuronal fate. Particularly, neurogenesis, as judged by the number of isl1-positive cells, is increased in *mib* mutants

and embryos treated with DAPT at early stages (9 hpf, 12 hpf and 14 hpf). However, treatment with DAPT at or after 16 hpf does not affect neurogenesis, suggesting that Notch activity is required during early development of the pineal gland to negatively regulate neurogenesis. Although the number of *flh*-positive pineal precursors is unaffected, *ascl1a* and *neurog1* expressions are increased in embryos with compromised Notch activity. Therefore, the data propose that Notch works downstream of *flh* to inhibit epiphysial neurogenesis, by negatively regulating the expression of the proneural genes *ascl1a* and *neurog1* (Cau et al., 2008).

1.3.2.3 The BMP pathway

As mentioned above, the BMP pathway is involved in pineal neurogenesis. BMPs, which are members of the transforming growth factor-β (TGFβ) superfamily of proteins, were first identified due to their ability to induce ectopic cartilage and bone development in rodents (Urist, 1965). However, studies in the last 50 years demonstrated that BMPs have much broader range of function. They are required during various biological processes, such as cell proliferation, differentiation and migration, morphogenesis, apoptosis and development of multiple organs, including the skeleton.

BMP pathway (**Figure 1.6**) is also crucial during the development of CNS, where it fulfils multiple roles from early neural cell-fate decisions through neural crest formation and patterning of the spinal cord to embryonic and postnatal development of the brain (reviewed in Liu and Niswander, 2005). However, neural specification and brain development are complex and fine-tuned processes and thus BMP signaling integrates with other pathways including the FGF, Wnt and Notch pathways, to ensure their proper regulation.

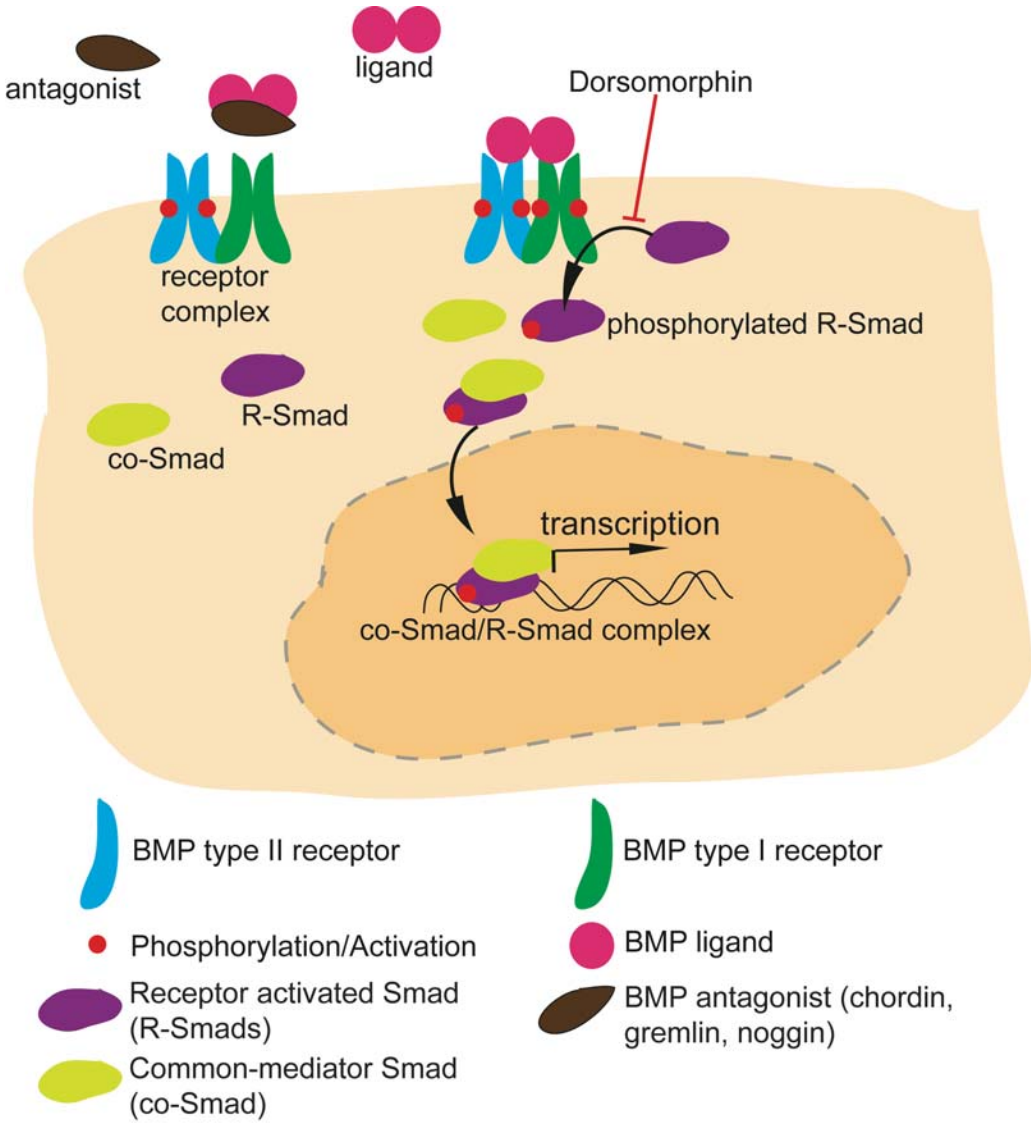

Figure 1.6 The BMP pathway. Full-length BMP ligands are inactive and their activation requires dimerization of the proteins, followed by proteolytic cleavage. The active BMP dimers are then secreted, forming a gradient of ligands. Activation of the canonical BMP pathway is achieved by binding of a ligand to a transmembrane BMP receptor complex, which consists of two type I and two type II receptors. Type II receptors are constitutively active and upon ligand binding, they phosphorylate and activate type I receptors. Subsequently, type I receptors phosphorylate receptor-activated Smad proteins (R-Smads), which in turn bind to Smad4, a common-mediator Smad (co-Smad). The R-Smad/co-Smad complex is translocated into the nucleus, where it interacts with other transcriptional co-activators to regulate transcription of BMP target genes. BMP antagonists bind to activated BMP ligands and block their binding to the BMP receptor complex. Dorsomorphin is a small-molecule inhibitor that selectively inhibits BMP type I receptors and therefore inhibits phosphorylation of R-Smads.

Due to the diverse range of BMP functions, the pathway is tightly modulated at multiple levels. For example, activation of the BMP pathway promotes the transcription of its own extracellular antagonists, including chordin, gremlin and noggin proteins. These antagonists bind to active BMP ligands and inhibit their binding to BMP receptors. Moreover, intracellular antagonists, for instance inhibitory Smads, decrease the efficiency of R-Smads binding to the activated type I receptors. In addition, ligand binding to BMP receptors can activate Smad-independent pathways, including the mitogen-activated protein kinase (MAPK) pathway (reviewed in Ducy and Karsenty, 2000; Liu and Niswander, 2005; Kondo, 2007).

BMP signaling has key roles during the development of the zebrafish epithalamus. This is illustrated by the fact that components of the BMP pathway are expressed within the presumptive epithalamus. Expression of *bone morphogenetic protein 2a* (*bmp2a*) gene, which encodes a BMP ligand, is first detected within the pineal anlage at approximately 14 hpf and increases as development proceeds. From about 16 hpf, the pathway is active, as determined by binding an antibody against phosphorylated Smad1/5/8 (Quillien et al., 2011). Also, a number of R-smads, as well as the co-smad *smad4*, are expressed within a broad domain of the developing brain that includes the presumptive epithalamus (http://zfin.org/). In addition, *Tg(BmpRE-AAVmlp:EGFP)mw29* (refer to as (*Tg(BRE:GFP)*) transgenic embryos have GFP expression within the developing pineal gland. In these transgenics, GFP expression is under the control of the BMP response element (BRE) and recapitulates the activity of BMP signaling (Collery and Link, 2011).

Quillien et al. (2011) demonstrated that disruption of BMP pathway during early pineal gland development affects neurogenesis. Downregulation of BMP signaling was achieved by heat-shock treatment of *Tg(hsp70l:dnHsa.BMPR1A-CFP)ups4* transgenic embryos. These embryos carry a transgene that, upon heat-shock activation, encodes a dominant-negative form of *bone morphogenetic protein receptor, type 1aa* (*bmpr1aa*) that lacks the intracellular kinase domain and thus is unable to phosphorylate R-smads. Activation of the transgene, and as a result downregulation of BMP pathway, at 9 or 12 hpf results in a reduced number of isl1-positive epiphysial neurons. In contrast, heat-

shock from 14 to 22 hpf does not affect the number of neurons produced. Birth-dating experiments (using BrdU) revealed that upon early reduction of BMP activity (heat-shock at 12 hpf), pineal progenitors exit their proliferative state prematurely. Downregulation of BMP at 16 hpf, on the other hand, does not affect the number of BrdU-positive cells. Altogether, the data suggest that BMP activity is required during early development of the pineal gland (up to 12 hpf) for the proper proliferation of progenitor cells (Quillien et al., 2011).

1.3.3 Cell-fate determination within the pineal gland

The zebrafish pineal gland is a relatively simple structure with only two cell types: photoreceptors and projection neurons (**Figure 1.1**). Both cell types are generated from the same pool of *flh*-positive pineal precursors and express *isl1* (Masai et al., 1997).

In zebrafish, the pineal photoreceptors are found in the middle of the dorsal diencephalon. They were first identified as a group of cells positive for zpr-1 (previously known as FRet43), an antibody that recognizes a membrane-associate protein, which is also expressed in the double-cone class of retinal photoreceptors (Larison and Bremiller, 1990; Masai et al., 1997). These cells also express the photoreceptive molecule opsin, confirming that they are true photoreceptors (Masai et al., 1997). Pineal photoreceptors also expressed *aanat2*, suggesting that they are able to produce melatonin.

Projection neurons are found laterally to the medial photoreceptors and extend long axons towards the ventral diencephalon, thus their name (Masai et al., 1997). They can be distinguished using a number of markers, including *paired box gene 6* (*pax6*), tubulin, *one cut domain, family member, like* (*onecutl*, previously known as *onecut*), *LIM homeobox 3* (*lhx3*) and *ELAV (embryonic lethal, abnormal vision, Drosophila)-like 3 (Hu antigen C)* (*elavl3*, previously known as *HuC*) (Masai et al., 1997; Glasgow et al., 1997; Cau and Wilson, 2003; Cau et al., 2008).

Cau et al. (2008) proposed that the best markers for pineal photoreceptors and projection neurons are *aanat2* and *elavl3*, respectively. The transgenic reporters for these genes: *Tg(aanat2:EGFP)y8* (refer to as *Tg(aanat2:GFP)*) and *Tg(elavl3:EGFP)knu3*

(refer to as *Tg(elavl3:GFP)*) are able to label the majority of isl1-positive neurons within the epiphysis, while zpr-1 and *lhx3* only label approximately one third of the total number of isl1 neurons. The fact that not all photoreceptors and projection neurons are positive for zpr-1 and *lhx3*, respectively, suggests that there are, at least, two subtypes for each cell type within the pineal gland, according to their molecular properties. More detailed analysis is required to accurately characterize all the subtypes of pineal cells.

Birth-dating experiments demonstrated that both cell types are born at the same time. Particularly, BrdU treatment before or at 18 hpf labelled the majority of photoreceptors and projection neurons, whereas in embryos treated after 20.5 hpf most pineal cells were BrdU negative. By comparing the BrdU incorporation curves for photoreceptors and projection neurons, Cau and colleagues (2008) showed that both cell types are born during the same time window. These results, along with the fact that *flh*-positive pineal precursors can give rise to both photoreceptors and projection neurons, raised the question of how these two cell types are specified.

Although *flh* and subsequently *ascl1a* and *neurog1* are required for neurogenesis within the pineal gland, they have no roles in cell-fate determination. Disruption of these genes, results in reduced number of both photoreceptors and projection neurons (Masai et al., 1997; Cau and Wilson, 2003). In contrast, Notch (discussed in **1.3.3.1**) and BMP (discussed in **1.3.3.2**) pathways are important for the specification of projection neurons and photoreceptors, respectively. In addition, recent data suggest that the two pathways interact to control projection neuron cell fate (discussed in **1.3.3.3**).

1.3.3.1 The Notch pathway and the projection neuron fate

Cau et al. (2008) were the first to propose a role for the Notch pathway in pineal cell-fate determination. The Notch pathway has been associated with cell-fate decisions both in invertebrates and vertebrates. The pathway is often involved in binary decisions, where it promotes one cell fate and inhibits the other. However, recent data, including the data from the zebrafish pineal gland, suggest that cell-fate determination controlled by Notch is achieved via a more complicated mechanism (Cau and Blader, 2009).

As mention above, two Notch ligands, *dlb* and *dld*, are specifically expressed in the projection neurons, whereas *dla* is expressed throughout the pineal gland (Cau and Wilson, 2003; Cau et al., 2008). The differential expression of Notch ligands suggests a role for Notch in the specification of pineal cells, in addition to neurogenesis. Interestingly, downregulation of Notch, either genetically (*mib* mutants) or chemically (DAPT treatment), results in increased number of projection neurons, without affecting the number of photoreceptors (Cau et al., 2008). In contrast, downregulation of *dla* and/or *dld* results in increased number of projection neurons and decreased number of photoreceptors (Cau et al., 2008). Therefore, although disruption of Notch activity only affects the number of projection neurons, downregulation of the *delta* genes leads to production of more projection neurons at the expense of the photoreceptors (Cau et al., 2008).

In addition to its role in inhibiting projection neuron fate, Notch is also required to resolve mixed identity in a subset of pineal cells. In control embryos, the majority of pineal cells express either *aanat2* (photoreceptors) or *elavl3* (projection neurons) and only about 4% of cells express both markers, at 48 hpf. This suggests that at least a subset of neurons have mixed identities at this stage. In *mib* mutants and in embryos treated with DAPT at 16 hpf, approximately 12% and 14%, respectively, of pineal cells co-express *aanat2* and *elavl3*, at 48 hpf. Therefore, Notch is important for the resolution of mixed identities of pineal cells (Cau et al., 2008).

1.3.3.2 The BMP pathway and photoreceptor fate

As discussed in section **1.3.2.3**, downregulation of BMP, using the transgenic line *Tg(hsp70l:dnHsa.BMPR1A-CFP)ups4*, during early development of the pineal gland (up to 12 hpf) results in a reduced number of isl1-positive neurons. This decrease in neurogenesis affects the number of both photoreceptors and projection neurons, as judged by the reduced number of cells expressing GFP in *Tg(aanat2:GFP)* and *Tg(elavl3:GFP)*, respectively (Quillien et al., 2011).

Heat-shock of *Tg(hsp70l:dnHsa.BMPR1A-CFP)ups4* embryos after 14 hpf, does not affect neurogenesis. However, the number of photoreceptors is significantly reduced,

whereas the number of projection neurons is unaffected. This phenotype is not due to increased apoptosis of photoreceptors, since there is no difference in the expression of the apoptosis marker activated-caspase 3 between control and embryos with reduced BMP. Also, the reduced number of photoreceptors is not due to abnormal proliferation of cells that will adopt a photoreceptor fate, as the number of photoreceptors that are labelled with BrdU is similar between control embryos and *Tg(hsp70l:dnHsa.BMPR1A-CFP)ups4* embryos heat-shocked at 16 hpf. Embryos with reduced function of *smad5* or *bmp2a* (via morpholino microinjections) exhibit a similar phenotype: reduced number of photoreceptors neurons, but normal number of isl1-positive cells and projection neurons. Moreover, transplantation experiments demonstrate that cells with impaired BMP activity are less efficient in adopting the photoreceptor fate than wildtype cells. In summary, the data suggest that activity of the canonical smad-dependent BMP pathway (through *bmp2a* and *smad5* activity) is required, in a cell-autonomous fashion, for the pineal progenitor cells to adopt a photoreceptors fate (Quillien et al., 2011).

Furthermore, overactivation of the BMP pathway, achieved by heat-shock treatment of *Tg(hsp70l:bmp2b)fr13* at 16 and 18 hpf, leads to increased neurogenesis, as judged by the number of isl1-positive cells. The extra neurons generated are photoreceptors, while the number of projection neurons is unaffected. This suggests that BMP activity is sufficient to force cells into adopting a photoreceptor identity (Quillien et al., 2011).

1.3.3.3 Interactions between Notch and BMP pathways

Two pathways have been shown to be involved in the specification of pineal cells: BMP promotes photoreceptors, whereas Notch inhibits the projection neurons (Cau et al., 2008; Quillien et al., 2011). Quillien et al. (2011) demonstrated that the two pathways interact with each other to ensure coordination of their activities.

As discussed above, downregulation of Notch leads to an increased number of projection neurons, while overactivation of BMP results in an increased number of photoreceptors. Interestingly, simultaneous downregulation of Notch and upregulation of BMP leads to an additive phenotype: increased number of both photoreceptors and

projection neurons. These findings suggest that disruption of Notch pathway does not affect BMP ability to promote the photoreceptor program (Quillien et al., 2011).

In contrast, BMP plays a role in the Notch-controlled inhibition of projection neurons. Downregulation of BMP (using *bmp2a* morpholinos) does not alter the number of projection neurons, whereas ectopic activation of Notch pathway significantly reduces the number of projection neurons. Intriguingly, microinjections with *bmp2a* morpholinos are able to partially rescue the number of projection neurons generated in embryos with compromised Notch activity. Transplantation experiments, as well as investigation of the expression profiles of Notch targets in embryos with reduced BMP activity, suggests that the BMP pathway is cell-autonomously required for the activation of Notch targets (Quillien et al., 2011).

1.3.4 The architecture of epithalamic asymmetries: parapineal organ and habenular nuclei

The zebrafish epithalamus is also of great interest because of its asymmetric architecture. Within the epithalamus, the parapineal organ is found on the left side of the brain in the majority of embryos and specifically innervates the left habenula. The habenular nuclei are bilateral structures, but differences in size, number of neuropils, gene expression and connectivity of their projection are observed between the left and the right habenulae. Several studies propose that the laterality of parapineal organ is closely coordinated with the laterality of habenular asymmetries.

1.3.4.1 Zebrafish parapineal organ: development and molecular markers

From approximately 28 hpf, a group of parapineal cells forms a cluster at the anterior part of the pineal gland and starts migrating towards the left. Timelapse experiments show that parapineal migration consists of at least two phases. During the first phase, parapineal cells move leftwards, away from the midline, followed by a posterior-ventral-medial movement (Concha et al., 2003). The first parapineal efferent projections are observed from approximately 50 hpf and they extend towards the left, where they branch and cover a significant fraction of the left habenula (Concha et al., 2000, 2003).

Parapineal cells can be distinguished using a number of markers that usually label the whole pineal complex (i.e. pineal gland and parapineal organ). They were first identified as a group of left-sided cells labelled by anti-isl1/2 and anti-opsin antibodies (although only approximately 15% of embryos had one or two opsin-positive cells) (Concha et al., 2000). *otx5* is also expressed within the pineal complex and the parapineal organ can easily be recognized from about 48 hpf (Gamse et al., 2002). In addition, the melatonin enzyme *aanat2* is expressed only in the mature parapineal cells, since *aanat2* expression is detected from about 80 hpf on the left side of the pineal gland (Gamse et al., 2002). The fact that parapineal cells express genes involved in photoreception (opsin) and melatonin biosynthesis (*aanat2*) suggests that the zebrafish parapineal organ is photoreceptive and able to produce melatonin. However, further investigation is required to confirm this.

Parapineal cells can also be visualized using two transgenic lines: *Tg(flh:GFP)* and *Tg(foxd3:GFP)zf15* (refer to as *Tg(foxd3:GFP)*). *Tg(flh:GFP)* embryos have strong GFP expression in the presumptive pineal gland throughout its development and also in the migrating parapineal cells from 28 to 40 hpf. The parapineal GFP expression is then gradually downregulated and is not detected after 65 hpf. Therefore, *flh* is expressed within the parapineal cells before and at the start of their migration, but is downregulated as cells migrate away from the pineal gland (Concha et al., 2003). The transgenic line *Tg(foxd3:GFP)* also drives GFP expression within the pineal gland, recapitulating the expression of *forkhead box D3* (*foxd3*) (Gilmour et al., 2002). Interestingly, *Tg(foxd3:GFP)* embryos have GFP expression only in mature parapineal cells, that is parapineal cells that have already moved away from the pineal gland (Concha et al., 2003). Therefore, *Tg(flh:GFP);Tg(foxd3:GFP)* double transgenic embryos enable the visualization of parapineal cells at all stages and are often used for ablation and timelapse experiments.

In contrast to opsin, *isl1*, *flh* and *foxd3*, which are expressed in both pineal and parapineal cells, *growth factor independent 1ab* (*gfi1ab*, previously known as *gfi1.2*) is currently the only known gene to be expressed specifically within the parapineal organ (Dufourcq et al., 2004). Unfortunately, there are no available transgenic lines for *gfi1ab*

that drive GFP expression within the parapineal organ. The transgenic line *Et(krt4:EGFP)sqet11* (refer to as *Tg(ET11:GFP)*) expresses GFP in parapineal, but not pineal cells. This line was generated using an enhanced trap system and contains two insertions within an intron of *kalirin, RhoGEF kinase b* (*kalrnb*) (Choo et al., 2006, http://plover.imcb.a-star.edu.sg/webpages/ET11.html). However, *Tg(ET11:GFP)* embryos have GFP expression in other parts of the brain, as well as the mouth, throat and skin (http://plover.imcb.a-star.edu.sg/webpages/ET11.html and personal observation). Therefore, it is difficult to distinguish a small structure such as the parapineal organ without counterstaining the embryos with an additional marker. The generation of a transgenic line with specific expression in the parapineal organ would be a useful tool for studying parapineal organ development and migration, as well as for the identification of new genes involved in the process.

1.3.4.2 Zebrafish habenular nuclei: development, connectivity and molecular markers

The habenular nuclei are also part of the epithalamus (**Figure 1.1**). Although the habenulae are bilateral structures (found on each side of the pineal complex), difference in size, cytoarchitecture, gene expression and connectivity are observed between the left and right nucleus.

As discussed in section **1.2.3**, the zebrafish habenulae are sub-divided into dorsal and ventral sub-nuclei. However, most of the data described below were collected before the identification of the ventral habenulae (Amo et al., 2010) and therefore referred to the dorsal habenulae. For simplicity, I will refer to dorsal habenulae as the habenulae.

Fate-mapping experiments demonstrated that habenular progenitors are found adjacent to the pineal complex progenitors. In particular, photoactivation of caged fluorescein in cells expressing GFP in *Tg(flh:GFP)* does not significantly label the habenular nuclei, while photoactivation of cells in the left or right side of the epithalamus, directly ventral to the *flh*-positive domain, always labels the ipsilateral habenula. Therefore, habenular precursors are found bilaterally and immediately ventral to the pineal complex precursors (Concha et al., 2003).

The zebrafish habenular nuclei display striking asymmetries both at neuroanatomical and molecular level. At 4 dpf, the left habenula is about 18% larger than the right (Gamse et al., 2003). In addition, the left habenula has more extensive neuropil-labelling than the right, especially at the medial and dorsal part of the nucleus, as judged by immunolabeling for acetylated α-tubulin (Concha et al., 2000). This difference in neuropil size is first observed at about 70 hpf and becomes more prominent as development proceeds. The increase in neuropil size in the left habenula coincides both in time and space with the efferent parapineal projections, suggesting that interactions between the left habenula and the parapineal projections may influence the asymmetric architecture of the habenulae. In fact, parapineal projections enter the left habenula at approximately 72 hpf and start branching extensively to cover the medial and dorsal part of the nucleus, which displays the increased neuropil staining (Concha et al., 2003).

A number of genes are expressed within the habenulae and can be categorized into three groups depending on their expression profiles. The first group contains genes that are largely symmetrically expressed in both the left and right habenula (although usually the left expression domain is slightly larger than the right, possibly as a result of the larger left habenula). The second group consists of genes that are asymmetrically expressed, with broader expression domain in the left than the right habenula. Genes of the third category are also asymmetrically expressed, but more intense staining is observed in the right habenula when compared to the left habenula (**Table 1.1**). In addition to these categories, the *POU domain, class 4, transcription factor 1* (*pou4f1*, previously known as *brn3a*) gene is symmetrically expressed during embryonic and larval stages, but is asymmetric in adulthood, with higher expression in the right habenula than the left (Aizawa et al., 2005). The *elavl3* gene is also expressed in habenular neurons. At early stages more *elavl3*-positive cells are expressed in the left habenula than the right, but by approximately 72 hpf *elavl3* expression appears symmetric (Aizawa et al., 2007).

Table 1.1 Genes expressed within the habenular nuclei.

Expression	Gene	Full name	Reference
1) Symmetric Left ≈ Right	*spon1b*	*spondin 1b*	Gamse et al., 2003
	cadps2	*Ca2+-dependent activator protein for secretion 2*	Gamse et al., 2003
	etv1	*ets variant gene 1*	Roussigné and Blader, 2006
2) Asymmetric Left > Right	*asic1c*	*acid-sensing (proton-gated) ion channel 1c*	Concha et al., 2003
	adcyap1a	*adenylate cyclase activating polypeptide 1a*	Amo et al., 2010
	nrp1a	*neuropilin 1a*	Kuan et al., 2007
	kctd12.1 (*leftover*)	*potassium channel tetramerisation domain containing 12.1*	Gamse et al., 2003
3) Asymmetric Left < Right	*kctd12.2* (*right on*)	*potassium channel tetramerisation domain containing 12.2*	Gamse et al., 2005
	kctd8 (*dexter*)	*potassium channel tetramerisation domain containing 8*	Gamse et al., 2005

1.3.4.2.1 Habenular sub-divisions: medial and lateral sub-nuclei

The zebrafish habenulae are sub-divided into medial and lateral sub-nuclei that exhibit differences in their size and relative ratios between the left and right habenulae. In adults, the two sub-nuclei can be easily distinguished based on the expression pattern of *pou4f1* and *kctd12.1*, respectively. Particularly, the medial sub-nucleus expresses *pou4f1* and is larger in size on the right when compared to the left habenula, while the lateral sub-nucleus expresses *kctd12.1* and is larger on the left than the right habenula (**Figure 1.7**) (Aizawa et al., 2005).

In contrast to the largely exclusive *pou4f1* and *kctd12.1* expression domains in adults, the expression profiles of all the known genes within the habenula are extensively overlapping (with some differences) in embryonic and larval stages. It is therefore extremely difficult to distinguish the medial and lateral sub-nuclei based on gene expression. In fact, depending on the expression patterns of only the three *kctd* genes, Gamse et al. (2005) identified six sub-domains that differ in their relative size and position along the dorsoventral and anteroposterior axis within the left and right habenulae. This suggests that many more sub-types of neurons are present according to their molecular properties. A detailed mapping of the expression profiles of all the genes

expressed within the habenulae is therefore necessary in order to characterize all the different sub-types of habenular neurons.

Nevertheless, the medial and lateral sub-nuclei can be distinguished, in embryonic and larval stages, based on the distribution of neuronal somata (Doll et al., 2011; Taylor et al., 2011). During late development the two sub-nuclei shift places: the sub-nucleus found in the lateral part of the larval habenulae shifts dorsally and medially to become the adult medial sub-nucleus and *vice versa*. Therefore, medial and lateral sub-nuclei refer to their position in adulthood, which is opposite of their position in embryonic/larval stages (**Figure 1.7**). Consistent with the adult expression, *kctd12.1* is the only gene that is selectively expressed in the lateral sub-nuclei in embryonic stages and can be used as a marker. In contrast, *pou4f1* or *kctd12.2* are found predominantly in the medial sub-nuclei, although some expression is present in the left lateral sub-nuclei. Therefore, even thought the genes do not provide a perfect distinction of the two sub-nuclei, they are often used as an indication.

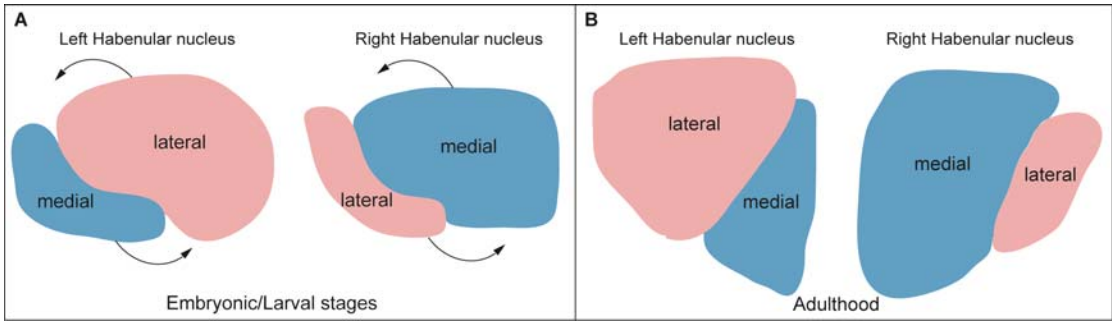

Figure 1.7 Architecture of the zebrafish habenulae. The habenulae are sub-divided into medial (blue) and lateral (pink) subnuclei. The size of the two sub-nuclei differs between the left and right habenulae. **A**) During embryonic and larval stages, the medial sub-nucleus is found at the outer-most part of the habenulae, while the lateral sub-nucleus is found towards the middle. As development proceeds, the two sub-nuclei change places. **B**) In the adult habenulae, the lateral sub-nucleus is found at the outer-most region, whereas the medial is found towards the middle. The sub-nuclei are named based on their position in adults.

1.3.4.2.2 Habenular axons: differences in their connectivity and morphology

In addition to differences in size, cytoarchitecture and gene expression, the left and right habenulae differ in their connectivity. As discussed in section **1.2.3**, the main target of the zebrafish habenulae is the IPN. Interestingly, the left and right habenular nuclei project axons towards different parts of the IPN (along the dorsoventral axis). This was first demonstrated by Aizawa et al. (2005) and confirmed by a number of other studies (Gamse et al., 2005; Kuan et al., 2007; Aizawa et al., 2007; Bianco et al., 2008). Particularly, anterograde axonal tracing using lipophilic dyes revealed that axons from the left habenula predominantly innervate the dorsal IPN (with only a few axons innervating the ventral IPN), whereas right-sided habenular axons specifically innervate the ventral IPN, in both adults and larvae (Aizawa et al., 2005, 2007; Bianco et al., 2008). Controversially, authors from two other publications found that left habenular neurons innervate both the dorsal and ventral IPN, whereas right-sided neurons only innervate the ventral region of the IPN (Gamse et al., 2005; Kuan et al., 2007). The groups used different methodologies that could explain the differences in their results.

Interestingly, the asymmetric innervation of axons along the dorsoventral axis of the IPN reflects left-right asymmetries within the habenulae. In particular, the large medial sub-nucleus found on the right habenula, along with the smaller medial sub-nucleus on the left side, innervates the ventral and intermediate IPN. In contrast, neurons located in the lateral sub-nuclei (larger in the left than the right habenulae) specifically innervate the dorsal IPN (Aizawa et al., 2005).

Although RNA transcripts, as detected by whole mount *in situ* hybridization, are only detected in the habenular nuclei, the proteins encoded by them (detected by whole mount immunofluorescence) are translocated through the fasciculus retroflexus to the synaptic terminals in the IPN. From about 2 dpf, differences in the expression of kctd12.1 are observed between the left and right fasciculus retroflexus: the left fasciculus retroflexus is more intensely labeled than the right (Gamse et al., 2005). This comes in agreement with the fact that more cells (and therefore more axons) express kctd12.1 in the left when compared to the right habenula. Between 3 and 4 dpf,

habenular axons reach the IPN and establish their connections along the dorsoventral axis (Kuan et al., 2007).

In summary, the left-right differences in sub-types of nuclei within the habenulae are translated into axonal innervation asymmetries along the dorsoventral axis of the midbrain target IPN.

In addition to the differential innervation of the IPN along the dorsoventral axis, axons from the left and right habenular nuclei display differences in their terminal arbors. Using focal electroporation, Bianco et al. (2008) were able to label individual habenular axons. They showed that neurons from both the left and right habenulae show a stereotypical unipolar morphology, with dendritic arbors that branch within the habenular neuropil area and a single axon that remains unbranched and extends (within the fasciculus retroflexus) towards the IPN. Within the IPN individual axons cross the midline multiple times and establish synapses on both the left and right side of the IPN. However, closer examination of the habenular axons revealed that they could be grouped into two sub-types according to their terminal arbors. The first sub-type, called the L-typical arbors, display extensive branching, they extend over a considerable dorsoventral depth and there is a great proportion of axon density towards the centre of the IPN (the branches extend both dorsally and medially). In contrast, R-typical arbors (the second sub-type) have fewer branches that concentrate in the periphery of the IPN and are flattened. Moreover, L-typical arbors terminate in the dorsal IPN, while R-typical arbors are found in the ventral IPN. Although the neuronal somata of both sub-types are found in both the left and right habenulae, their proportion significantly differs. The majority of L-typical arbors originate in the left habenula, whereas most R-typical arbors come from the right habenula. Thus, axons from the left habenula have a L-typical arbor morphology and project to the dorsal IPN and axons from the right habenula display an R-typical character and terminate in the ventral IPN (Bianco et al., 2008).

1.3.4.3 Laterality of the parapineal organ is coupled with laterality of habenular asymmetries

Several lines of evidence suggest that the proper laterality of parapineal migration is crucial for the proper asymmetric architecture of the habenulae. First, as discussed above, efferent projections from the parapineal organ specifically innervate the left habenula. These parapineal projections coincide both in time and space with the elaboration of neuropil in the left habenula (Concha et al., 2003). Moreover, analysis of mutant embryos with randomized parapineal migration (summarized in **Table 1.2**) showed that in most cases the habenula adjacent to the parapineal organ adopts a left-side character (Gamse et al., 2003).

In addition, laser-induced ablation of the parapineal cells, before their migration to the left (between 22-32 hpf), leads to right isomerism of the habenula: the larger domains of *kctd12.1* expression and neuropil formation in the left are reduced to levels similar to the right habenula (Concha et al., 2003; Gamse et al., 2003; Bianco et al., 2008). Moreover, in parapineal-ablated embryos the majority of left-sided habenular neurons innervate the ventral IPN, but not the dorsal IPN, a characteristic of right-sided neurons (Gamse et al., 2005; Kuan et al., 2007; Bianco et al., 2008). Also, left-sided habenular neurons, in parapineal-ablated embryos, elaborate arbors that are similar to R-typical arbors, although some differences persist (Bianco et al., 2008). A similar habenular phenotype (right isomerism) is observed in mutant embryos, in which parapineal cells fail to migrate and a parapineal organ is detected in the midline (*fibroblast growth factor 8a* (*fgf8a)* and *tbx2b* mutants) (Snelson et al., 2008a; Regan et al., 2009). Although the differences between the left and right habenulae are reduced, some variation is maintained suggesting that parapineal organ is not solely responsible for the habenular asymmetries (Concha et al., 2003; Gamse et al., 2003; Bianco et al., 2008).

1.3.5 Establishment of epithalamic asymmetries and laterality

Asymmetries can be assigned into three groups by analyzing their occurrence at a population-level: fluctuating asymmetry, antisymmetry and directional asymmetry

(Van Valen, 1962). Fluctuating asymmetries arise when an organism fails to follow the precise path of development. Antisymmetry, also called random asymmetry, refers to the situation where asymmetry normally exists within individuals, but laterality is random at a population level. In directional asymmetry a character is greater in one specific side in the majority of individuals within a population.

Zebrafish epithalamic asymmetries belong to the group of directional asymmetry, since in approximately 95% of individuals the direction of asymmetry is the same (the parapineal organ and the larger habenular nucleus are on the left side) (Concha et al., 2000). There are two possible ways for establishing directional asymmetry (reviewed in Concha et al., 2009). First, both asymmetry and laterality are controlled simultaneously by a common mechanism. In such a case, if the mechanism is disrupted both asymmetry and laterality will be affected and thus the organism will develop symmetrically. The other possibility is that one mechanism establishes asymmetry, followed by the action of a second mechanism that controls laterality. If the mechanism that controls asymmetry is disrupted, the organism will develop symmetrically, whereas disruption of the laterality mechanism will generate antisymmetry (random asymmetry). Currently, the data are in favor of the second possibility, where the FGF signaling controls the initiation of asymmetry and the Nodal pathway controls laterality (**Figure 1.8**).

1.3.5.1 Break of symmetry: FGF pathway and *tbx2b*

Currently, the data suggest that epithalamic asymmetries are established via a two-step mechanism. The first step involves the break of symmetry, whereas the second step controls laterality. Regan and colleagues (2009) demonstrated that FGF signaling plays a key role in the establishment of asymmetry.

fgf8a is expressed bilaterally within the epithalamus in an area immediately anterior to the presumptive pineal complex, whereas *fibroblast growth factor receptor 4* (*fgfr4*) is expressed in parapineal cells (also in a subset of pineal cells) (Regan et al., 2009). When *fgf8a* is disrupted either genetically ($fgf8a^{ti282a}$, previously known as *acerebellar* or *ace* mutants) or chemically (using SU5402) parapineal cells fail to

migrate towards the left side of the brain and subsequently the habenulae appear symmetric. Exogenous Fgf8 in *ace* mutants can rescue the lateralized migration of parapineal cells. However, the parapineal organ usually migrated leftwards in rescued *ace* mutants, even when the Fgf8-loaded beads were transplanted on the right side or at the midline (Regan et al., 2009). Therefore, although *fgf8a* is necessary for initiating the asymmetric migration of the parapineal, it does not control its laterality.

In addition to FGF signaling, *tbx2b* is also required for the generation of epithalamic asymmetries by controlling the specification of parapineal cells. The *fby* mutation results in a premature stop codon that eliminates *tbx2b* function. In *fby* mutants, as well as in two different *tbx2b* morphants, fewer parapineal cells are specified (3±2 *gfi1ab*-positive cells in *fby* compared to 10±1 cells in controls) and these cells fail to form a coherent structure and migrate towards the left (Snelson et al., 2008a). The authors hypothesized that parapineal migration may depend on the correct number of parapineal cells to form a coherent and polarized structure. However, ablation of approximately 5 parapineal cells before their migration in control embryos, does not affect their migration or the final position of the parapineal organ (Snelson et al., 2008a). Therefore, *tbx2b* activity not only controls the correct number of parapineal cells, but also provides them with properties essential for their migration.

1.3.5.2 Control of laterality: Nodal pathway

Although disruption of Fgf signaling or *tbx2b* expression results in symmetric development of the epithalamus, disruption of Nodal does not affect asymmetry *per se*. Instead, in embryos with bilateral or absent epithalamic Nodal, parapineal placement and habenular asymmetries are randomized (**Table 1.2**). Interestingly, asymmetric activation of Nodal (due to Kupffer's vesicle function) is observed very early during development in the lateral plate mesoderm (LPM) and is required for the proper laterality of the viscera.

In fact, the first known break of symmetry in zebrafish takes place within the Kupffer's vesicle. Dorsal forerunner cells are organized into the Kupffer's vesicle, where they protrude motile monocilia (Essner et al., 2005). By injecting fluorescent

beads into the Kupffer's vesicle, Essner and colleagues (2005) demonstrated that these cilia are able to generate a directional leftward flow. This leftward flow persists until 10-12 ss, when the asymmetric expression of *spaw* is first observed. *spaw* is a Nodal-related gene, which is asymmetrically expressed in the posterior part of the left LPM from 10-12 ss and its expression spreads anteriorly as development proceeds (Long et al., 2003). This is consistent with a model in which the leftward movement of the cilia within the Kupffer's vesicle generates a Nodal flow in the left LPM that travels from the posterior to the anterior (**Figure 1.8**). Shortly after the onset of *spaw* expression (at about 17-22 ss), four other Nodal-related genes are expressed within the left LPM: the Nodal ligand *nodal-related 2* (*ndr2*, previously known as *cyclops* or *cyc*), the antagonists *lefty1* (*lft1*) and *lefty2* (*lft2*), and the downstream effector of the pathway *paired-like homeodomain transcription factor 2* (*pitx2*) (Long et al., 2003). *spaw* is required for the proper unilateral activation of all these genes: in *spaw* morphants, expression of *ndr2*, *lft1*, *lft2* and *pitx2* is absent in the LPM. The absence of Nodal activity in *spaw* morphants leads to randomization of their visceral organs. Intriguingly, *spaw* morphants exhibit randomization of diencephalic asymmetries, even though the gene is not expressed in the diencephalon (Long et al., 2003).

In contrast to *spaw*, the Nodal pathway genes *ndr2*, *lft1* and *pitx2* are transiently expressed in the diencephalon between 18 ss to 24 hpf. The expression domain of these genes overlaps with the expression of *flh*, a marker for the presumptive pineal complex. However, the Nodal genes are only expressed in the left side of the brain and their expression extends more ventrally into a *flh*-negative domain (Liang et al., 2000; Concha et al., 2000). Since parapineal precursors are found in the anterior part of the *flh*-positive domain and habenular progenitors are found immediately ventral (discussed in sections **1.3.1** and **1.3.4.2**, respectively), both types of precursors could be influenced by Nodal activity (Concha et al., 2003).

In embryos with abnormal bilateral or absent epithalamic Nodal activity, the position of the parapineal organ, along with the laterality of habenular asymmetries, becomes randomized: 50% of embryos have left-sided parapineal organs and a larger left habenula and 50% of embryos have right-sided parapineal and a larger right

habenula. Mutant and/or morphant embryos and their defects are summarized in **Table 1.2**. Also, in the majority of mutants, disruption of Nodal activity in the LPM is coupled with disrupted Nodal in the diencephalon, suggesting that a crosstalk between the LPM and the diencephalon exists to ensure coordination of asymmetries within the body and brain (**Table 1.2**). Interestingly, although *spaw* is not expressed in the diencephalon, in *spaw* morphants expression of *ndr2*, *lft1* and *pitx2* in the diencephalon is absent (Long et al., 2003). Therefore, unilateral expression of *spaw* in the left LPM is essential for the subsequent activation of Nodal pathway in the left diencephalon.

Although *ndr2*, *lft1* and *pitx2* are expressed unilaterally within the diencephalon, other components of the Nodal pathway, including the EGF-CFC cofactor *one-eyed pinhead* (*oep*) and the downstream effector *forkhead box H1* (*foxh1*, previously known as *schmalspur* or *sur*) are bilaterally expressed (Liang et al., 2000; Concha et al., 2000). The bilateral expression of these genes, along with the fact that some mutants exhibit bilateral activation of Nodal in the diencephalon, suggests that both sides are competent in activating Nodal. In this context, the mechanism by which unilateral Nodal in the diencephalon is established may involve left-sided activation or right-sided repression or both.

A model involving an initial bilateral repression of Nodal in the diencephalon was first introduced by Concha et al. (2000). Mutants with complete loss of oep activity (maternal-zygotic *oep*, MZ*oep*) have bilateral *pitx2* expression in the diencephalon. In contrast, diencephalic *pitx2* is absent in *LZoep* (late-zygotic *oep* mutants), in which exogenous oep rescues early Nodal activity, but late-zygotic activity is still compromised (Liang et al., 2000; Concha et al., 2000). Based on these results, Concha et al. (2000) proposed a model in which early Nodal activity is required to bilaterally repress *pitx2* in the diencephalon, whereas late Nodal activity removes the left-sided repression and thus promotes the expression of *pitx2* in the left diencephalon. However, MZ*oep* mutants have neural tube defects and fail to form an intact midline. In fact, a number of mutants with bilateral Nodal activity in the diencephalon have midline defects (summarized in **Table 1.2**). Also, physical ablation of the midline leads to bilateral activation of Nodal pathway (Concha et al., 2000). Therefore, it is unclear

whether the bilateral activation of Nodal in MZ*oep* embryos is due to their inability to bilaterally repress epithalamic Nodal or due to midline defects that in turn disrupt the restriction of epithalamic Nodal to the left.

Further support for the initial repression of Nodal in the diencephalon came from two independent studies in 2009. First, simultaneous disruption of *sine oculis homeobox homolog 3b* (*six3b*) and *sine oculis homeobox homolog 7* (*six7*), two homeodomain transcription factors that are bilaterally expressed in the epithalamus, leads to bilateral activation of Nodal in the diencephalon without affecting its activity in the LPM (Inbal et al., 2007). Also, *mbl* mutants show a similar phenotype: normal expression of Nodal genes in the LPM and bilateral activation of Nodal in the diencephalon (Carl et al., 2007). *mbl* embryos carry mutation in *axin1* gene, which encodes a negative regulator of the Wnt signaling (Heisenberg et al., 2001). Thus, Wnt signaling is important for the early bilateral repression of Nodal in the diencephalon, possibly by controlling the levels of *six3b* and *six7* expression (**Figure 1.8**) (Carl et al., 2007; Inbal et al., 2007).

Once the bilateral repression of Nodal in the epithalamus is established, the left-sided repression is removed leading to asymmetric expression of *ndr2*, *lft1* and *pitx2*. Activity of *spaw* in the left LPM is necessary for this alleviation of repression in the left-side of the brain (Long et al., 2003). However, the exact mechanism by which *spaw* influences Nodal de-repression is still unknown.

The unilateral activation of Nodal in the epithalamus subsequently influences the leftward migration of the parapineal organ and the establishment of asymmetries between the left and right habenulae. Since disruption of Nodal leads to randomization of these asymmetries rather than isomerism (**Table 1.2**), Nodal is important for the proper laterality of asymmetries but is not essential for the asymmetries *per se*.

Table 1.2 Mutants and morphants with disrupted epithalamic asymmetries.

Mutant or morphant (MO)	Midline formation	Nodal in LPM	Heart looping	Diencephalic Nodal	Parapineal migration	Habenular asymmetry	Reference
ntla$^{b160/b195/ts260}$	Defective	Bilateral	Random	Bilateral	Random	Random	1-6
flh^{n1}	Defective	Bilateral	Random	Bilateral	Random	Random	3, 5-7
MZ*oep*$^{tz57/m134}$	Defective	?	?	Bilateral *	?	?	1-2
LZ*oep*$^{tz57/m134}$	Normal	Absent	Random	Absent	Random	Random	1-5, 7-9
foxh1$^{m768/ty68b}$	Controversial°	Absent	Random	Absent	Random	Random	1, 3
spaw-MO	Normal	Absent	Random or no heart looping	Absent	Random	Random	6, 9, 10
ndr2$^{m294/tf219}$	Defective	Normal	Normal	Bilateral	Random	Random	1-3
sox32^{ta56} or MO (*casanova*)	Normal	Bilateral	Bilateral hearts	Bilateral #	Random	Random	2, 5, 11, 12
six3b^{vu87};*six7*-MO	Normal	Normal	Normal	Bilateral	Random	Random	13
axin1^{tm213} (*mbl*)	Normal	Normal ‡	?	Bilateral	Delayed	Right isomerism	10
fgf8a^{ti282a} or MO	Normal	Controversial ◊	Random or no heart looping	Controversial◊	No migration	Right isomerism	14-15
tbx2b^{c144} (*fby*)	?	Normal	Normal	Normal	No migration	Right isomerism	16
mib^{ta52b}	?	?	?	Bilateral †	?	Left isomerism	17

References: 1) Concha et al., 2000; 2) Liang et al., 2000, 3) Bisgrove et al., 2000; 4) Concha et al., 2003; 5) Gamse et al., 2003; 6) Long et al., 2003; 7) Gamse et al., 2002; 8) Aizawa et al., 2005; 9) Gamse et al., 2005; 10) Carl et al., 2007; 11) Wang and Yost, 2008; 12) Alexander et al., 1999; 13) Inbal et al., 2007; 14) Regan et al., 2009; 15) Albertson and Yelick, 2005; 16) Snelson et al., 2008a; 17) Aizawa et al., 2007.

? Not reported

* Reduced but bilateral *pitx2* and *ndr2* expression was reported in 1. Reduced bilateral *ndr2* expression, reduced bilateral or absent expression of *pitx2* and absent expression of *lft1* was reported in 2.

° No midline defects were reported in 1, where as 2 reported midline defects.

According to 2, the majority of embryos have bilateral expression of *ndr2*, *pitx2* and *lft1* in the diencephalon, but a significant subset of embryos has right-sided expression of these genes.

‡ Mutation in axin1 gene leads to overactivation of the Wnt pathway. Overactivation of Wnt via LiCl treatment at early stages (80% epiboly) does not affect Nodal pathway in the LPM (similar to axin1 mutants). However, LiCl treatment between 12-14 ss leads to bilateral activation of Nodal in both the LPM and diencephalon, in a subset of embryos.

◊ Two studies present different data. Authors in 14 showed that Nodal is normal in both the diencephalon (left-sided *pitx2* expression in 90% of embryos) and LPM (left-sided *spaw* expression in 97% of embryos). In contrast, authors in 15 showed that diencephalic *pitx2* expression is normal (29% of embryos), bilateral (38%) or absent (33%) and *spaw* in the LPM is normal (61%), reversed (16%) or bilateral (15%).

† Diencephalic *pitx2* expression was normal in 52% of embryos, bilateral in 36%, absent in 8% and right-sided in 4%.

1.3.5.3 Interactions between asymmetry and laterality

Although directional asymmetries within the zebrafish epithalamus are established in a two-step fashion, recent studies suggest that the two mechanisms interact (**Figure 1.8**). The first evidence for the interaction between the asymmetry (FGF signaling) and the laterality (Nodal pathway) mechanisms came from the study of Regan et al. (2009).

In this study, Regan and colleagues (2009) showed that although *fgf8a* is bilaterally expressed within the epithalamus, subtle differences in the levels of *fgf8a* between the left and right side of the brain are evident. Specifically, at 22 ss *fgf8a* expression on the right is higher than on the left, but by 28 hpf the majority of embryos have higher *fgf8a* expression on the left. This change in the asymmetric expression of *fgf8a* coincides with the initiation of parapineal migration. Notably, in embryos with absent diencephalic Nodal (*spaw* morphants and LZ*oep* mutants), the levels of *fgf8a*

expression are similar to wildtype siblings, but the small differences between the left and right side are diminished (Regan et al., 2009). Therefore, left-side Nodal activity is important for the asymmetric expression of *fgf8a*.

In addition, exogenous Fgf8 can specify the direction of parapineal migration in *fgf8a*^{ti282a} embryos with bilateral (*ntla* mutants) or absent (*spaw* morphants) Nodal. In particular, following injections of Fgf8 beads in *fgf8a*^{ti282a}/*ntla* or *fgf8a*^{ti282a}/*spaw* embryos, parapineal cells migrate towards the source of Fgf8 (Regan et al., 2009). Therefore in the absence of a directional bias from Nodal, Fgf signaling is able to direct parapineal migration.

Although studies of Nodal mutants propose a model in which Nodal is only important for the laterality of epithalamic asymmetries, more recent data suggest that it also controls asymmetry (Roussigné et al., 2009). Timing of neurogenesis differs between the left and right habenulae and correlates with the types of neurons generated (Aizawa et al., 2007). Birth-dating experiments revealed that most neurons born between 24 and 36 hpf will adopt a lateral character, whereas most medial neurons are born after 48 hpf. Also, during the first phase of neurogenesis most neurons are generated in the left habenula (Aizawa et al., 2007).

This difference in the timing of neurogenesis between the left and right habenulae was confirmed by the early expression of *chemokine (C-X-C motif), receptor 4b* (*cxcr4b*), a gene expressed in habenular precursors and/or newly born neurons (Roussigné et al., 2009). At 28 hpf, *cxcr4b* is only detected in the left habenula. However, at 32 and 36 hpf *cxcr4b* is expressed in both habenulae, but more cells are positive in the left when compared to the right habenula. In addition, quantification of *elavl3*-positive neurons confirms that at 36-38 hpf more neurons are present in the left than the right habenula. This early difference in number of neurons is independent of the parapineal, since it is not affected by parapineal ablation (Roussigné et al., 2009).

Interestingly, perturbation of epithalamic Nodal activity disrupts the asymmetric neurogenesis of habenular neurons. In particular, absence of Nodal in the epithalamus (*spaw* morphants and SB431542 treatment from 10 hpf), bilateral Nodal activity (*ntla* morphants) or randomization of Nodal (achieved by raising embryos at 22^{o}C) leads to

significant reduction in the asymmetric neurogenesis within the habenulae (Roussigné et al., 2009). Therefore, Nodal signaling is important for the establishment of early asymmetric habenular neurogenesis.

These findings suggest that Nodal might control laterality of parapineal migration by controlling expression of *fgf8a*. Since parapineal cells are chemoattracted to *fgf8a*, left-right differences in its expression could account for the direction of migration. In Nodal mutants, *fgf8a* is largely symmetric and therefore laterality becomes stochastic. Since ablation of the parapineal organ leads to reduction of habenular asymmetries, the parapineal organ might be responsible for the elaboration of the initial asymmetries established by Nodal activity.

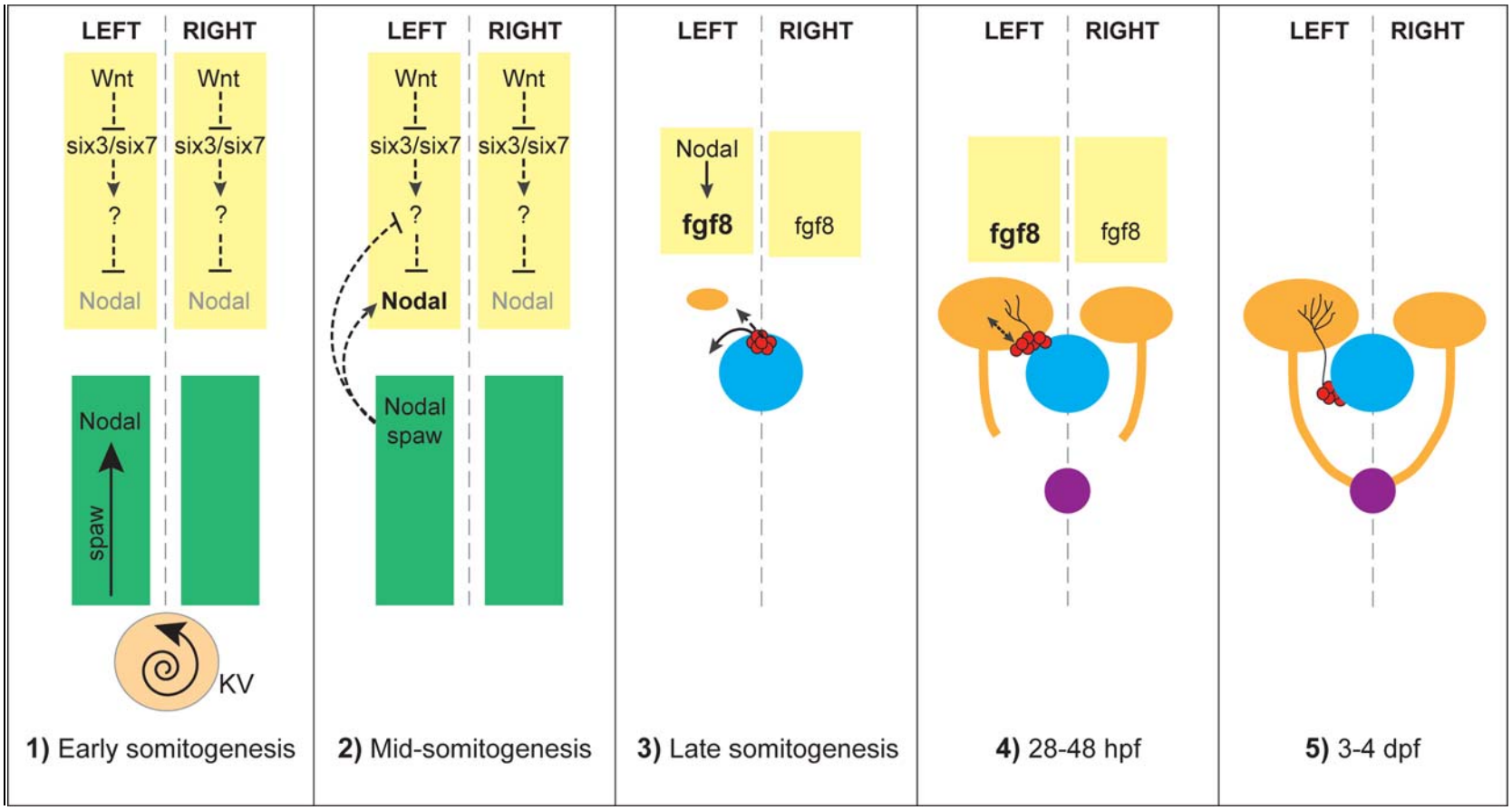
LEFT
RIGHT
Wnt
six3/six7
?
Nodal
Nodal
spaw
KV
1) Early somitogenesis
Nodal
spaw
2) Mid-somitogenesis
fgf8
3) Late somitogenesis
4) 28-48 hpf
5) 3-4 dpf

Figure 1.8 The model for the establishment of epithalamic asymmetries. 1) A group of approximately 20-30 dorsal forerunner cells are organized in a spherical structure called the Kupffer's vesicle (KV) in the tailbud. Cells within the Kupffer's vesicle have motile monocilia and generate a leftward fluid flow. This fluid flow is necessary for the asymmetric expression of the Nodal gene *spaw* in the left LPM (green columns). *spaw* expression extends from the posterior to the anterior part of the LPM as development proceeds. Shortly after the expression of *spaw* in the LPM, other Nodal genes (*ndr2*, *lft1*, *lft2* and *pitx2*) are asymmetrically expressed in the left LPM. In parallel, activity of Wnt pathway in the diencephalon (yellow columns) controls the expression of *six3b* and *six7* genes that in turn (directly or indirectly) suppress bilateral Nodal activity in the brain. **2**) The unilateral expression of Nodal genes in the LPM is necessary to alleviate left-sided Nodal repression in the diencephalon. For the specific left-sided removal of Nodal repression in the epithalamus, an intact midline (dashed grey line) is also required. Although *spaw* is thought to play a critical role in the derepression of left-sided diencephalic Nodal, the mechanism by which this is achieved is still elusive. **3**) Within the diencephalon, the left-sided Nodal activity upregulates *fgf8a* expression on the left side and controls the early asymmetric neurogenesis of the habenular neurons (orange). **4**) Parapineal cells (red) are specified in the presence of *tbx2b*, form a coherent structure at the anterior part of the pineal gland (blue) and start migrating leftwards, towards the upregulated *fgf8a*. Interactions between the left-sided parapineal organ and the left habenula are important for the elaboration of the asymmetric architecture between the left and right habenulae. **5**) Finally, the left and right habenulae establish asymmetric connections to the IPN (purple).

1.4 *SRY (sex determining region Y)-box containing gene 2* (*sox2*): a key developmental regulator

In this project, we identified and characterized a novel role for *sox2* in the development of zebrafish epithalamus (discussed in **Chapters 3-5**). Notably, downregulation of *sox2* results in abnormal development of all three epithalamic structures: the pineal gland, the parapineal organ and the habenular nuclei. *sox2* controls the development of these structures by modulating a variety of developmental processes, including proliferation and differentiation of pineal cells, specification and migration of parapineal cells and establishment of habenular asymmetries. This is not surprising, since several studies demonstrate that *sox2* is a key developmental regulator that controls the expression of many other genes, including other transcription factors. Therefore, depending on the context and developmental time, *sox2* has distinct functions.

SOX2 is an intronless gene, found on the long arm of chromosome 3 (3q26.3-q27). It encodes a 317 amino acid transcription factor and belongs to the *Sox* family of genes. Sox proteins are characterized by the presence of the highly conserved high mobility group (HMG)-box domain. Based on their protein sequence homology, Sox proteins are subdivided into eight groups (SoxA-H). The SoxB group is further divided into SoxB1 and SoxB2 subgroups. Sox2 belongs to the SoxB1 subgroup, along with Sox1 and Sox3 (reviewed in Kamachi et al., 2000; Pevny and Placzek, 2005; Kiefer, 2007; Lefebvre et al., 2007; Tziaferi et al., 2008).

Sox2 contains three domains: an N-terminal domain of unknown function, the 69 amino acid DNA-binding HMG-box domain and a transcriptional activation domain at the C-terminus (reviewed in Kamachi et al., 2000; Hever et al., 2006; Tziaferi et al., 2008). The HMG-box domain binds to the minor groove of the DNA, with some sequence specificity, and bends the DNA at a flexible angle (between 30º and 110º). This DNA bending widens the minor groove and facilitates interactions of Sox2 with other partner proteins. Since HMG-box binds DNA with low affinity, Sox2 interactions with other proteins stabilize its binding. In addition, the partner proteins are thought to confer a spatiotemporal specificity to the Sox2-mediated transcriptional regulation. Particularly, depending on the cell-type and developmental stage, different Sox2 partner proteins are expressed and therefore different protein complexes are assembled to control the expression of specific Sox2 targets. For example, Sox2 physically interacts with *POU domain, class 5, transcription factor 1* (*Pou5f1*, previously known as Oct3/4) in embryonic stem cells and embryonic carcinoma cells to activate stem cell-specific genes, including *fibroblast growth factor 4* (*Fgf4*) and *Sox2* itself (Yuan et al., 1995; Tomioka et al., 2002). In contrast, Sox2 partners with Pax6 to activate δ-crystallin, during lens development (Kamachi et al., 2001).

As mention above, Sox2 also contains a transactivation domain that accommodates a serine-rich region at the C-terminus. *In vitro* studies, using fusion proteins containing the DNA-binding domain of Gal4 and various regions of the Sox2 protein, demonstrate that the last ~100 amino acids of Sox2 are necessary for transactivation (Nowling et al., 2000). Interestingly, although SoxB1 (Sox1-3) and

SoxB2 (Sox14 and Sox21) proteins share more than 90% similarity in the HMG-box, their C-terminal domains are different. In fact, the C-terminal domain of SoxB2 proteins acts as a transrepression domain. Although, most studies suggest that Sox2 acts as a transcriptional activator, recent data suggest that depending on the context, it can also act as a repressor. For example, Cavallaro et al. (2008) showed that overexpression of *Sox2* in differentiated astroglial cells leads to downregulation of *glial fibrillary acidic protein* (*GFAP*). By performing luciferase reporter experiments, they were also able to demonstrate that overexpression of Sox2 leads to repression of a regulatory element found upstream of the *GFAP* promoter. In addition, Sox2 physically interacts with the *GFAP* upstream region both *in vitro* and *in vivo*, as shown by electrophoretic mobility shift assay (EMSA) and chromatin immunoprecipitation (ChIP), respectively. Therefore, these findings suggest that Sox2 (at least in part) directly represses *GFAP* expression (Cavallaro et al., 2008).

Sox2 is a highly conserved protein throughout the vertebrate lineage (**Figure 1.9**). In fact, the human SOX2 shares 96% identity at the amino acid level with the mouse Sox2 and 87% with the zebrafish sox2. Notably, the HMG-box domain is highly conserved even in invertebrates (**Figure 1.10**): the human SOX2 HMG-box shares 88% identity with the drosophila Dichaete (ortholog of SOX2).

```
human      MYNMMETELKPPGPQQTSGGG--GGNSTAAAAGGNQKNSPDRVKRPMNAFMVWSRGQRRK
mouse      MYNMMETELKPPGPQQASGGGGGGGNATAAATGGNQKNSPDRVKRPMNAFMVWSRGQRRK
chicken    MYNMMETELKPPAPQQTSGGGTGNSNS----AANNQKNSPDRVKRPMNAFMVWSRGQRRK
frog       MYNMMETDLKPPAPQQASGGNSNSG------SNNQSKNSPDRVKRPMNAFMVWSRGQRRK
zebrafish  MYNMMETELKPPAPQPNTGGTGNT-----NSSGNNQKNSPDRIKRPMNAFMVWSRGQRRK
           *******:****.**  :**           :  :.******:*****************

human      MAQENPKMHNSEISKRLGAEWKLLSETEKRPFIDEAKRLRALHMKEHPDYKYRPRRKTKT
mouse      MAQENPKMHNSEISKRLGAEWKLLSETEKRPFIDEAKRLRALHMKEHPDYKYRPRRKTKT
chicken    MAQENPKMHNSEISKRLGAEWKLLSEAEKRPFIDEAKRLRALHMKEHPDYKYRPRRKTKT
frog       MAQENPKMHNSEISKRLGAEWKLLSEAEKRPFIDEAKRLRALHMKEHPDYKYRPRRKTKT
zebrafish  MAQENPKMHNSEISKRLGAEWKLLSESEKRPFIDEAKRLRALHMKEHPDYKYRPRRKTKT
           *************************:**********************************

human      LMKKDKYTLPGGLLAPGGNSMASGVGVGAGLGAGVNQRMDSYAHMNGWSNGSYSMMQDQL
mouse      LMKKDKYTLPGGLLAPGGNSMASGVGVGAGLGAGVNQRMDSYAHMNGWSNGSYSMMQEQL
chicken    LMKKDKYTLPGGLLAPGTNTMTTGVGVGATLGAGVNQRMDSYAHMNGWTNGGYGMMQEQL
frog       LMKKDKYTLPGGLLAPGANPMTSGV--GASLGAGVNQRMDTYAHMNGWTNGGYGMMQEQL
zebrafish  LMKKDKYTLPGGLLAPGGNGMGAGVGVGAGLGAGVNQRMDSYAHMNGWTNGGYGMMQEQL
           ***************** * * :**  ** **********:*******:**.*.***:**
```

```
human      GYPQHPGLNAHGAAQMQPMHRYDVSALQYNSMTSSQTYMNGSPTYSMSYSQQGTPGMALG
mouse      GYPQHPGLNAHGAAQMQPMHRYDVSALQYNSMTSSQTYMNGSPTYSMSYSQQGTPGMALG
chicken    GYPQHPGLNAHNAAQMQPMHRYDVSALQYNSMTSSQTYMNGSPTYSMSYSQQGTPGMALG
frog       GYPQHPGLSAHNAPQMQPMHRYDVSALQYNSMSSSQTYMNGSPTYSMSYSQQGAPGMSLG
zebrafish GYPQHPSLNAHNTAQMQPMHRYDMSALQYNSMTNSQTYMNGSPTYSMSYSQQSTPGMTLG
           ******.*.** : *********:********:.******************.:***:**

human      SMGSVVKSEASSSPPVVTSSSHSRA-PCQAGDLRDMISMYLPGAEVPEPAAPSRLHMSQH
mouse      SMGSVVKSEASSSPPVVTSSSHSRA-PCQAGDLRDMISMYLPGAEVPEPAAPSRLHMAQH
chicken    SMGSVVKTESSSSPPVVTSSSHSRA-PCQAGDLRDMISMYLPGAEVPEPAAPSRLHMSQH
frog       SMGSVVKSESSSSPPVVTSSSHSRA-PCQAGDLRDMISMYLPGAEVPEPAAQSRLHMSQH
zebrafish SMGSVVKSESSSSPPVVTSSSHSRAGQCQTGDLRDMISMYLPGAEVQDQSAQSRLHMSQH
           *******:*:***************  **:**************** : :* *****:**

human      YQSGPVPGTAINGTLPLSHM
mouse      YQSGPVPGTAINGTLPLSHM
chicken    YQSAPVPGTAINGTLPLSHM
frog       YQSASVAGTAINGTLPLSHM
zebrafish YQSAPVPGTTINGTIPLSHM
           ***. * **:****:*****
```

Figure 1.9 SOX2 is a highly conserved protein. Alignment of the Sox2 amino acid sequence between human (*Homo sapiens*), mouse (*Mus musculus*), chicken (*Gallus gallus*), frog (*Xenopus tropicalis*) and zebrafish (*Danio rerio*). The HMG-box domain is highlighted in yellow. Only two amino acids (shown in red) differ between the human and the zebrafish HMG-box.
* indicates positions which have a single, fully conserved residue
: indicates conservation between groups of strongly similar properties
. indicates conservation between groups of weakly similar properties

```
human      VKRPMNAFMVWSRGQRRKMAQENPKMHNSEISKRLGAEWKLLSETEKRPFIDEAKRLRALHMKEHPDYK
mouse      VKRPMNAFMVWSRGQRRKMAQENPKMHNSEISKRLGAEWKLLSETEKRPFIDEAKRLRALHMKEHPDYK
chicken    VKRPMNAFMVWSRGQRRKMAQENPKMHNSEISKRLGAEWKLLSEAEKRPFIDEAKRLRALHMKEHPDYK
frog       VKRPMNAFMVWSRGQRRKMAQENPKMHNSEISKRLGAEWKLLSEAEKRPFIDEAKRLRALHMKEHPDYK
zebrafish IKRPMNAFMVWSRGQRRKMAQENPKMHNSEISKRLGAEWKLLSESEKRPFIDEAKRLRALHMKEHPDYK
fruitfly   IKRPMNAFMVWSRLQRRQIAKDNPKMHNSEISKRLGAEWKLLAESEKRPFIDEAKRLRALHMKEHPDYK
           :************ ***::*::********************:*:***********************
```

Figure 1.10 The HMG-box domain is highly conserved among vertebrates and invertebrates. Alignment of the Sox2 HMG-box domain between human (*Homo sapiens*), mouse (*Mus musculus*), chicken (*Gallus gallus*), frog (*Xenopus tropicalis*), zebrafish (*Danio rerio*) and fruitfly (*Drosophila melanogaster*). Amino acids that differ from the human HMG-box are shown in red.
* indicates positions which have a single, fully conserved residue
: indicates conservation between groups of strongly similar properties
. indicates conservation between groups of weakly similar properties

1.4.1 *Sox2* expression: insights into its function

In humans, *SOX2* is one of the first genes to be transcribed: RNA is detected from approximately 4-cell stage (Kimber et al., 2008; Shaw et al., 2012). During embryogenesis (between 4.5 and 9 weeks of development), *SOX2* is found throughout the CNS, including the presumptive hypothalamus, telencephalon, cerebellum, thalamus and eyes. In addition, *SOX2* is expressed in the nasal epithelium, the tracheoesophageal tract and the developing lungs, as well as the gut endoderm and the epithelium lining of the stomach's lumen. Moreover, *SOX2* RNA is detected by RT-PCR in both male (from 7 weeks) and female (from 10 weeks) gonads (Kelberman et al., 2008). It should be noted that human embryonic and fetal samples are sparse and thus the human SOX2 expression profile is based on a small number of biological replicates. Therefore, analysing its expression profile in animal models is necessary, in order to better understand how Sox2 functions.

The murine *Sox2* is also expressed very early during embryogenesis. It is first detected in some cells at the morula stage, at approximately 2.5 days post coitum (dpc) and its expression becomes more prominent within the inner cell mass during blastocyst stage (~3.5 dpc). As development proceeds, *Sox2* becomes restricted to the anterior part of the presumptive neuroectoderm, as well as the extraembryonic ectoderm. By 9.5 dpc, *Sox2* is expressed in the brain, neural tube, sensory placodes (otic and nasal placode), gut endoderm, branchial arches and germ cells (both male and female). Following differentiation of the neural tube, *Sox2* is found in the proliferating ventricular zone, but it is downregulated in the differentiated outer layers (Wood and Episkopou, 1999; Avilion et al., 2003; Ferri et al., 2004; Ellis et al., 2004). In adult brains, *Sox2* expression is maintained in some differentiated cells in the cortex, striatum and thalamus and in neurogenic regions, such as the periventricular ependyma, subependyma and hippocampus (Ferri et al., 2004; Ellis et al., 2004). Within the developing eye, *Sox2* is expressed in retinal neural progenitors and is downregulated with differentiation, with only exception being a small number of displaced amacrine cells (found in the retina ganglion cell layer) and Müller glial cells that maintain *Sox2* expression even after differentiation (Taranova et al., 2006).

Since *Sox2* is expressed in proliferating neural progenitors, Ellis and colleagues (2004) performed a clonogenic assay to test whether Sox2 is expressed in a subset or all of the neural stem cells. In this assay, disaggregated cells from both embryonic and adult nervous system were cultured under specific conditions and tested for their ability to proliferate (form colonies) and differentiate into neurons or glial cells (multipotential). Intriguingly, all multipotential colonies formed derived from Sox2-positive cells, suggesting that Sox2 is a universal marker for neural stem cells.

Similar to murine *Sox2*, chick *SOX2* is expressed throughout the neural tube during early development and is downregulated with differentiation. Interesting, *SOX2* is coexpressed with markers of proliferating but regionalized progenitor cells (such as PAX6 and PAX7), but is excluded from fully differentiated neurons (positive for Isl1 and β-tubulin type III). Labelling with BrdU confirmed that *SOX2* is expressed in proliferating cells of the chick spinal cord. Therefore, *SOX2* is expressed in proliferating cells of the CNS and is downregulated as they exit their final mitosis and start differentiating (Graham et al., 2003).

In zebrafish, *sox2* is first detected by RT-PCR at the 30% epiboly stage (Okuda et al., 2006). Whole mount *in situ* hybridization experiments at later stages revealed that *sox2* is expressed in the future ectoderm (shield stage) and then becomes restricted to regions of the presumptive neuroectoderm (75-80% epiboly stage). At this stage, *sox2* expression is strong in the presumptive forebrain, but weak in the presumptive spinal cord. As development proceeds, sox2 is found in distinct regions of the future brain, including the anterior margin of the neural plate, the presumptive retina and the hindbrain. By 25 ss, *sox2* is found throughout the brain, with strong expression in the retina, otic placode and cerebellum (Okuda et al., 2006). Expression of *sox2* is maintained in several regions along the entire length of the brain (such as the olfactory bulbs, the walls of telencephalic, diencephalic and rhombencephalic ventricles, the preoptic area and the optic tectum) during larval and juvenile stages (15-50 dpf) (Germanà et al., 2010). However, it becomes restricted to the olfactory bulbs and the telencephalic ventricle walls in adulthood (180 dpf, when the brain is fully mature) (Germanà et al., 2010). Within the developing retina, *sox2* is initially expressed in the

marginal zone (where proliferation takes place), consistent with the role of *sox2* in modulating proliferation. Following differentiation, *sox2* is expressed in a small number of amacrine cells (Pujic et al., 2006).

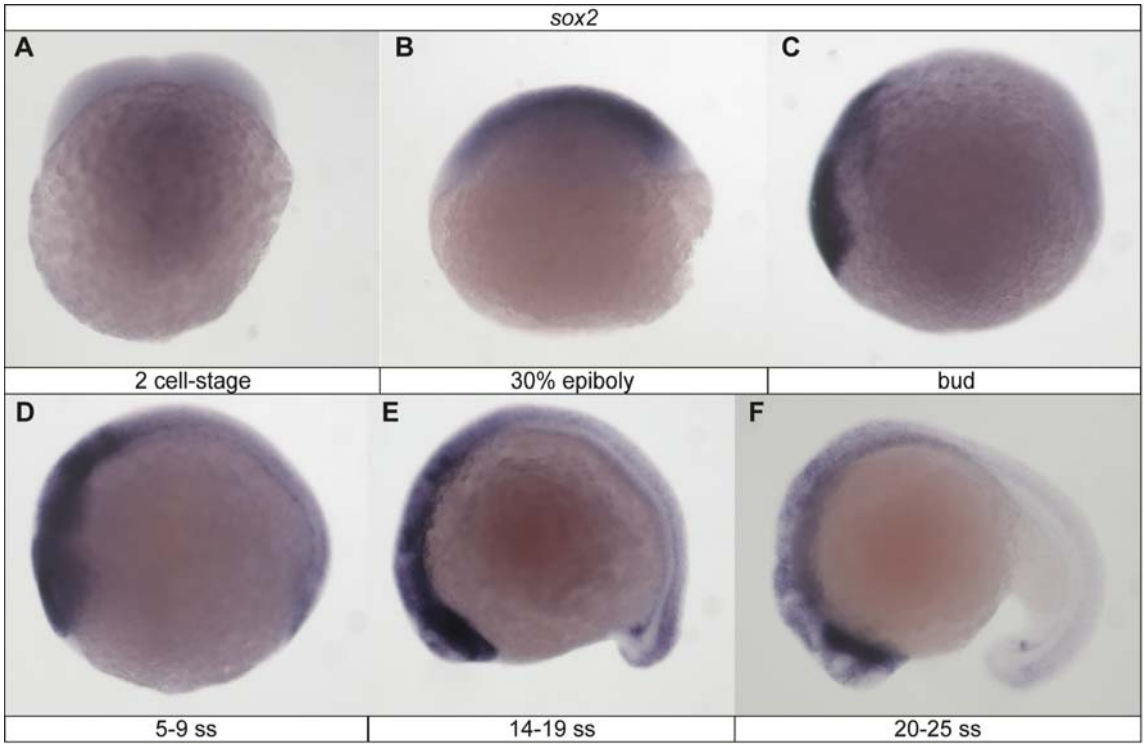

Figure 1.11 sox2 is expressed throughout the presumptive nervous system. (**A**) *sox2* expression is not detected at 2-cell stage. (**B-C**) *sox2* is expressed in the presumptive neural plate, at 30% epiboly and bud stage. (**D-F**) As development proceeds, *sox2* expression is strong at the anterior part of neural tissues, whereas expression at the posterior is weak. Whole mount in situ hybridizations, stages are shown at the bottom of each picture, adapted from Rauch et al. (2003).

In summary, *Sox2* is expressed from the earliest stages of development predominantly in proliferating neural stem/progenitor cells and is downregulated with differentiation. It is also expressed in neurogenic regions within the adult brains. Its expression in proliferating cells is consistent with its role in the maintenance of embryonic stem cells. Embryonic stem cells derive from the inner cell mass (which expresses *Sox2*) and can be cultured *in vitro* indefinitely (self-renewal property) and

differentiate into any cell type (pluripotency). Sox2, along with Pou5f1 and Nanog, is a key regulator for the maintenance of these properties of embryonic stem cells (reviewed in Chambers and Tomlinson, 2009). In addition, Takahashi and Yamanaka (2006) demonstrated that Sox2 is one of the four factors (along with Pou5f1, myelocytomatosis oncogene (Myc) and Kruppel-like factor 4 (gut)) that can induce pluripotent stem cells from mouse embryonic and adult fibroblast cultures.

1.4.2 Sox2 deficiency in humans and animal models

Consistent with its early expression, Sox2 has crucial roles during embryogenesis. This is illustrated by the plethora of phenotypic defects observed in humans and animal models with disrupted Sox2 expression.

Heterozygous (usually *de novo*) *SOX2* missense and nonsense mutations, as well as deletions and insertions, have been identified in a number of human patients (summarized in MRC Human Genetics Unit Leiden Open Variation Database (LOVD) at MRC IGMM, http://lsdb.hgu.mrc.ac.uk/variants.php?action=view_all). These mutations usually result in *SOX2* haploinsufficiency and are associated with a wide range of phenotypic defects. The most prominent defects are anophthalmia (complete absent of eyes) and/or microphthalmia (small eyes). A subset of patients has additional ocular defects, such as absent or hypoplastic optic nerves, colobomas and cataracts. *SOX2* mutations are also associated with extra-ocular defects, such as craniofacial dysmorphisms, genital abnormalities that are often linked with hypogonadotropic hypogonadism, global developmental delay, spastic diplegia, esophageal atresia and/or tracheoesophageal fistula, learning disabilities that vary from mild to severe, and seizures. In addition, several brain malformations have been identified in patients, including malformations of the hippocampus, hypothalamus, corpus callosum, and pituitary gland, as well as generalized reduction of white matter (Fantes et al., 2003; Zenteno et al., 2005; Hagstrom et al., 2005; Ragge et al., 2005; Faivre et al., 2006; Sisodiya et al., 2006; Williamson et al., 2006; Kelberman et al., 2006; Chassaing et al., 2007; Bakrania et al., 2007; Kelberman et al., 2008; Tziaferi et al., 2008; Schneider et al., 2009; Pedace et al., 2009; Reis et al., 2010). The plethora of the phenotypic defects

observed in patients carrying a single mutated copy of *SOX2*, as well as the fact that no homozygous mutation has been identified so far, highlights the importance of SOX2 during embryogenesis.

Although *SOX2* haploinsufficiency in humans results in such a variety of phenotypes, heterozygous *Sox2*-null mutant mice appear normal (albeit with a reduction in male fertility). In contrast, homozygous *Sox2*-null mice are normal at blastocyst stages, but die shortly after implantation. Notably, Avilion et al. (2003) suggest that *Sox2* function is necessary even before implantation, but the defects are masked due to the presence of maternally-derived Sox2 protein. In order to dissect the roles of *Sox2* in the nervous system, Ferri and colleagues (2004) generated compound heterozygous mice. These mice carry one *Sox2*-null allele and a second allele, where a regulatory element that drives expression in the dorsal telencephalon (Zappone et al., 2000) is deleted. In contrast to the heterozygous *Sox2*-null mice (in which approximately 50% of wildtype Sox2 protein is expected to be produced), compound heterozygous mice express only 25-30% of wildtype Sox2. This decrease in Sox2 levels leads to increased lethality (fewer than expected mice are born and their number declines as they age), growth retardation, slowed reactivity, neurological impairments due to increased neurodegeneration, epilepsy and “circling” behaviour (mice move in a circular pattern, normally indicative of a neurological disorder). In addition, adult compound heterozygotes have brain abnormalities, including reduced cortex, corpus callosum, anterior thalamus, dorsal striatum and septum, as well as enlargement of the lateral and third ventricle. Further analysis demonstrated that adult compound heterozygous mice have increased neurodegeneration, suggesting a role for Sox2 in the maintenance of neurons in adulthood. Also, neural precursor cells in adult neurogenic regions fail to proliferate and generate new neurons (Ferri et al., 2004). Altogether, these results suggest that correct levels of Sox2 are essential during both embryogenesis and adulthood.

Other than controlling brain development and function, Sox2 is also required for the proper development of eyes in a dose-dependent manner. In particular, the size of eyes negatively correlates with the amount of Sox2 protein present. Therefore, mice in

which Sox2 is completely ablated in the retina (conditional nulls) have smaller eyes in relation to *Sox2* hypomorphic/null compound heterozygous (which express less than 40% of wildtype Sox2 protein). The latter in turn have smaller eyes than wildtype mice. However, the eyes of heterozygous null-mice (expressing approximately 50% of wildtype protein) are indistinguishable from wildtype (Taranova et al., 2006).

Analysis of the hypomorphic and conditional-null eyes demonstrate that Sox2 is required for the proper proliferation and differentiation of retinal progenitor cells (Taranova et al., 2006). In particular, mutant eyes have fewer proliferating cells (as judged by BrdU incorporation), as well as fewer differentiated cells (as judged by the expression of neuronal markers). Moreover, adult hypomorphic mice have disrupted retinal cell lamination, demonstrated by the presence of rosette structures, and hypoplastic optic nerves, due to the absence of RGCs (which are the only cells to project outside the eye towards the optic nerve). Interestingly, RGCs are present (although mispositioned) in the developing eyes of embryos, but their axons fail to enter the optic nerve, as shown by anterograde labelling. These data, along with the increase in apoptosis observed in the *Sox2* hypomorphic retinas, suggest that although RGCs are specified, they are inappropriately localized, fail to project towards the optic nerve and as a results are eliminated via apoptosis. Thus, Sox2 is required for the proper specification and function of the RGCs (Taranova et al., 2006).

The disruption of *sox2* expression in zebrafish is achieved via morpholino injections, since there is no mutant line available. Similar to humans and other animal models, *sox2* deficiency in zebrafish results in abnormal eye development. Particularly, downregulation of *sox2* (using morpholinos) results in reduction in the number of parvalbumin-positive cells, a subtype of amacrine cells found in the RGC-layer. In contrast, the number of neuropeptide Y-positive cells (a further subtype of amacrine cells) is significantly increased in *sox2* morphants, suggesting a role for the gene in the specification of amacrine cells. Notably, the number of Müller glial cells and photoreceptor cones is unaffected. However, the size of the eyes and the number of RGCs of these embryos are not discussed (Pujic et al., 2006).

In addition, Millimaki et al. (2010) demonstrated a role for *sox2* in the maintenance and regeneration of hair cells within the inner ear. In particular, hair cells in *sox2* morphants develop slower than wildtype controls and are often disorganized. Moreover, downregulation of *sox2* results in increased cell death within the developing inner ear, suggesting that *sox2* is important for the maintenance of hair cells. Finally, following laser-ablation of hair cells in control embryos, support cells within the inner ear can transdifferentiate into hair cells to facilitate regeneration. However, *sox2* morphants show no signs of regeneration. Interestingly, although *sox2* is initially expressed throughout the developing otic placode, its expression is lost in mature hair cells but is maintained in support cells. Therefore, the maintenance of sox2 expression in support cells may provide them with developmental plasticity, so that they can transdifferentiate if necessary (Millimaki et al., 2010).

1.4.3 Experimental validation of computationally predicted sox2 developmental targets

The expression of developmental genes is tightly controlled in a spatiotemporal and quantitative manner. This is illustrated by the fact that in humans, haploinsufficiency often leads to abnormalities, malformations or disease. Therefore, important processes, like the development of the CNS, are highly regulated. This is achieved, at least partly, through transcriptional cascades. *sox2* is a key transcription factor, which controls the expression of many downstream developmental regulators, including other transcription factors, establishing a gene network. In order to understand the role of sox2 in development and disease is vital to identify and characterize the many interactions between the modules of this network. Many approaches can be used to identify downstream targets for a transcription factor. Previously in our laboratory, we used a combination of published ChIP data and an *in silico* screen that led to the prediction of new putative sox2 developmental targets (MRes thesis Pavlou, 2009). We then used the *sox2* morphants, along with whole mount *in situ* hybridization, to determine whether the expression pattern of the predicted genes is controlled by sox2.

1.4.3.1 Computational prediction of regulatory elements and sox2 targets

The *in silico* screen was performed prior to the start of my PhD project by P. Coutinho (HGU, Edinburgh) and myself as part of my MRes project (MRes thesis Pavlou, 2009). The strategy followed in order to predict developmental targets is summarized in **Figure 1.12**.

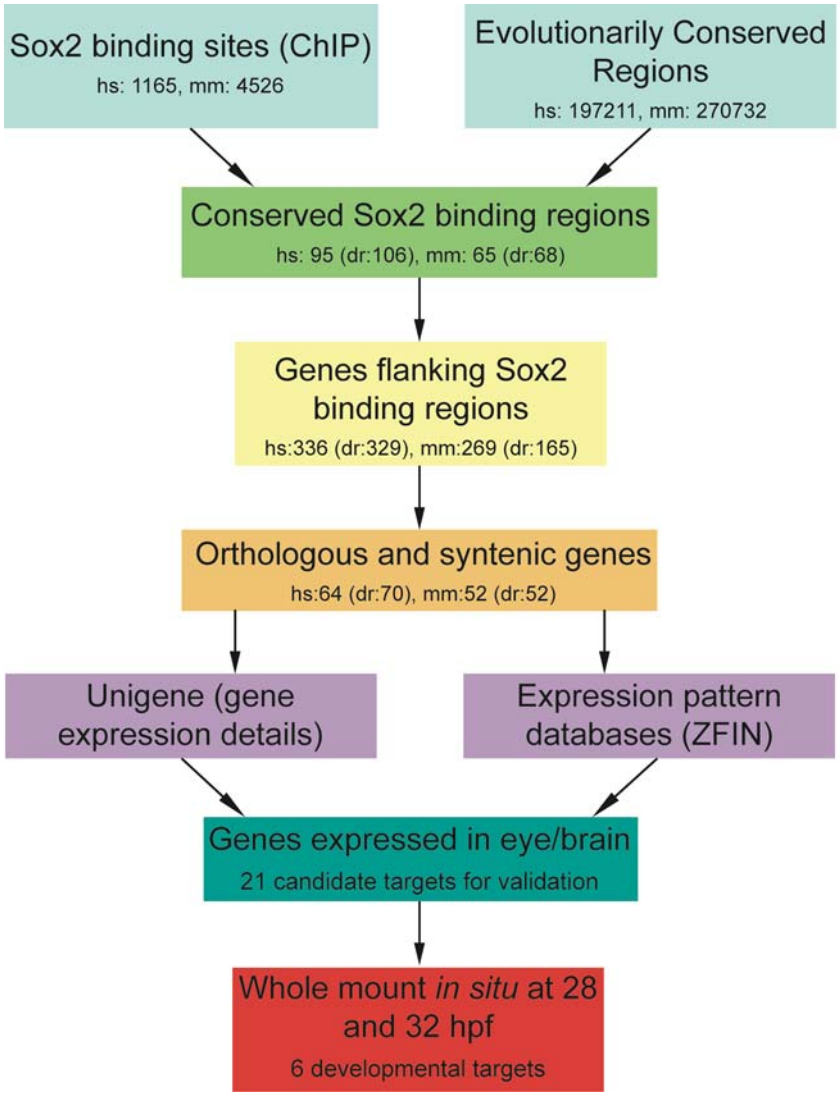

Figure 1.12 Flow diagram describing the *in silico* strategy followed to predict sox2 developmental targets. By comparing the previously published SOX2 and Sox2 binding regions with the evolutionarily conserved regions, we identified regions bound by SOX2/Sox2 that are evolutionarily conserved. These regions are our candidate regulatory elements. Two genes up- or downstream and any gene overlapping with the candidate regulatory elements were identified using perl scripts. From these genes, we

identified the ones that are othologous and in synteny between human-zebrafish and mouse-zebrafish. Finally, 21 genes expressed in brain and/or eyes were selected for validation using zebrafish. The expression of six genes was affected when sox2 was downregulated at 28 and 32 hpf. The number of binding sites or genes identified for each species are shown at the bottom of each box, hs = *Homo sapiens*, mm: *Mus musculus*, dr = *Danio rerio*.

In 2005, Boyer et al. identified 1165 regions bound by SOX2 in human embryonic stem cells, by combining ChIP with DNA microarrays. Later, Chen et al. (2008) identified 4526 regions bound by Sox2 in mouse embryonic stem cells by performing ChIP coupled with ultra-high throughput DNA sequencing. We used these data to predict regions bound by sox2 during development and the genes regulated by these regulatory regions.

Many biologically functional DNA sequences (such as genes and regulatory elements) are evolutionarily conserved due to natural selection (reviewed in Loots, 2008). Thus, we used the evolutionary conserved regions (100 bp long, at least 70% identity) between mouse/zebrafish and human/zebrafish from ECRbase (http://ecrbase.dcode.org/) to identify the Sox2 and SOX2 binding regions, respectively, that are evolutionarily conserved. These regions are candidate regulatory elements.

Regulatory regions can be upstream, downstream or within genes. Therefore, using PERL scripts (developed by P. Coutinho, MRC-HGU, Edinburgh), for each binding site, two genes upstream, two genes downstream and any genes overlapping with the candidate regulatory regions were selected as candidate sox2 developmental targets. Since we were planning to use zebrafish as an animal model to validate these targets, we selected the orthologous and syntenic genes between mouse/zebrafish and human/zebrafish. The result was 64 genes from the human data (that correspond to 70 zebrafish genes) and 52 genes from the mouse data. Using Unigene (http://www.ncbi.nlm.nih.gov/unigene) and the expression pattern database ZFIN (http://zfin.org/), 21 genes were selected for validation due to their specific expression in the brain and/or eyes (MRes thesis Pavlou, 2009).

1.4.3.2 Experimental validation of the computationally predicted sox2 targets

In order to validate the candidate developmental targets of sox2, we analyzed the expression profile of the target genes in control and *sox2* morphant siblings, at 28 and 32 hpf. Out of the 21 genes tested, 6 had disrupted expression when sox2 was downregulated at these stages (**Figure 1.13** and **Figure 1.14**) (MRes thesis Pavlou, 2009). The remaining 15 genes may also be regulated by sox2 at a different developmental stage or even in adulthood. Moreover, by whole mount *in situ* hybridization we can detect qualitative data, but not quantitative. Therefore, small changes in the level of expression of these genes are not analyzed.

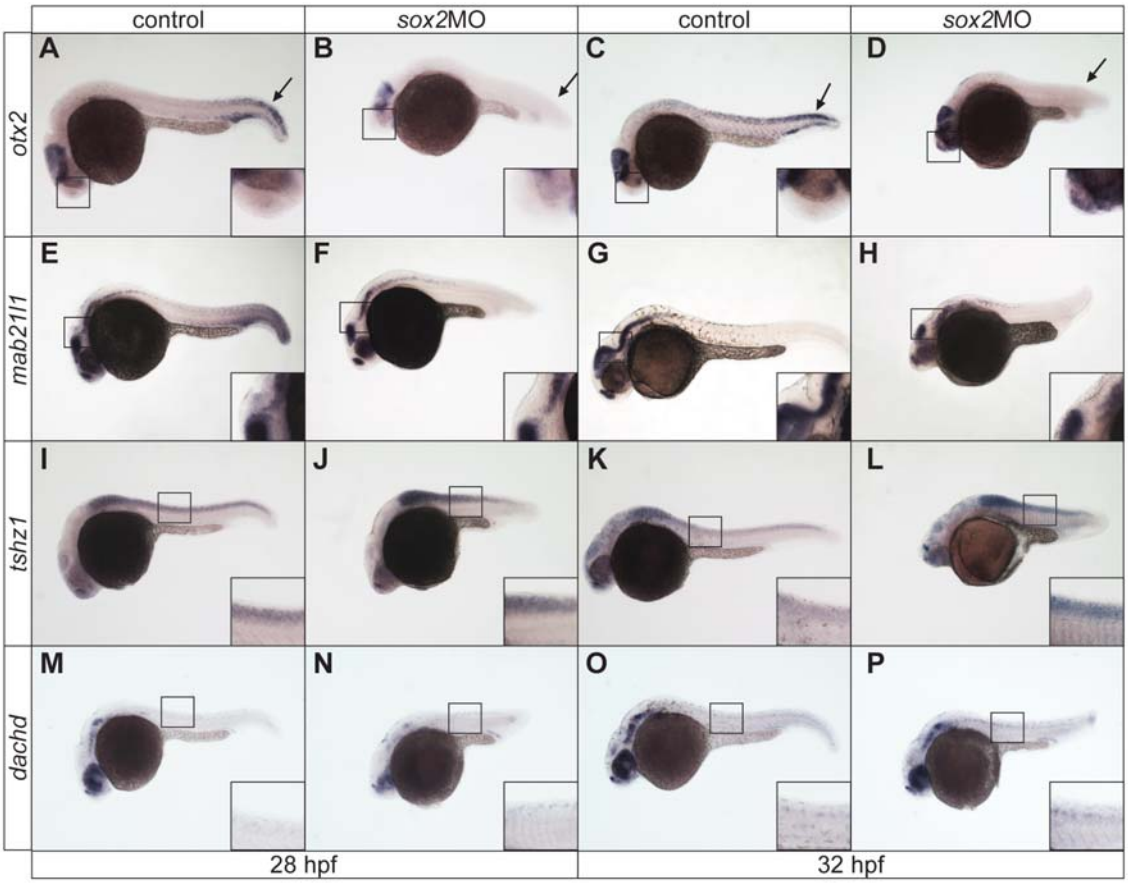

Figure 1.13 Disrupted expression of sox2 target genes in *sox2* morphants. (**A-D**) *otx2* is expressed in the midbrain and tail of control embryos. Downregulation of sox2 results in loss of the tail expression (arrows) and ectopic expression in the forebrain and eyes at 32 hpf. (**E-H**) *mab21l1* expression in the midbrain/hindbrain is disrupted in *sox2* morphants. (**I-L**) *tshz1* and (**M-P**) *dachd* expression in the neural tube is

abnormally maintained in the *sox2* morphants, when compared with control siblings. Lateral views of 28 (first and second columns) and 32 (third and fourth columns) hpf embryos, boxes in the right corner show the affected area in higher magnification.

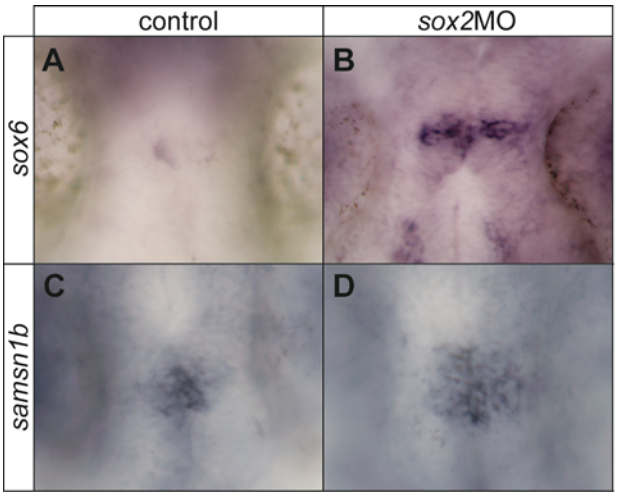

Figure 1.14 Downregulation of sox2 disrupts *sox6* and *samsn1b* expression in the epithalamus at 30 hpf. (**A**) *sox6* is normally expressed in a subset of cells within the epithalamus. (**B**) Downregulation of sox2 results in increased number of *sox6*-positive cells. (**C**) *samsn1b* is also expressed in the epithalamus and (**D**) its expression domain is broader in *sox2* morphants. Dorsal views of 30 hpf embryos, with anterior to the top.

In order to confirm that sox2 directly controls the expression of the 6 genes that had disrupted expression in the *sox2* morphants, we performed ChIP coupled with qPCR on chromatin extracts from 28 hpf whole embryos. As shown in **Figure 1.15**, 5 of the predicted regulatory regions are bound by sox2 at 28 hpf. The predicted enhancer for *samsn1b* does not show any significant enrichment for sox2 binding. However, the experiment was performed only at 28 hpf. Therefore, we cannot exclude the possibility that *samsn1b* predicted enhancer is bound by sox2 at different developmental stages or even in adulthood.

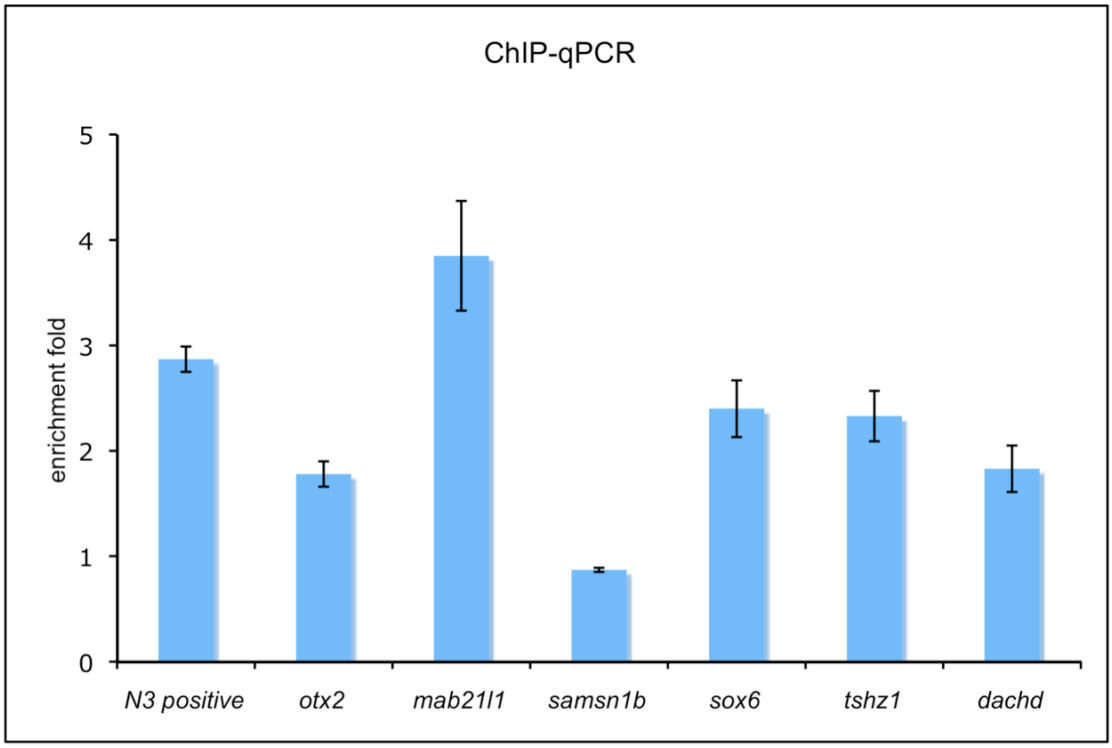

Figure 1.15 sox2 directly regulates 5 of the predicted genes at 28 hpf. Chromatin immunoprecipitation from 28 hpf zebrafish embryos, using antibodies against sox2 and control rabbit IgG, coupled with quantitative real-time PCR was used to investigate the binding of sox2 to the predicted binding regions for each gene. The x-axis names each enhancer by the gene that we predict is being regulated, the y-axis represents the fold-enrichment, after normalization. n=3, error bars represent ± standard error.

Interestingly, two of the predicted targets (*sox6* and *samsn1b*) were upregulated specifically in the epithalamus in *sox2* morphants when compared to control siblings (**Figure 1.14**). These results led to the hypothesis that sox2 has a role in the development of zebrafish epithalamus (discussed in **Chapters 3-5**). Therefore, by combining computational and "wet-lab" approaches, we were able not only to identify novel developmental targets for sox2, but also to identify a novel role for sox2 in development and possibly human disease.

1.5 Hypothesis and aims of the thesis

The development of a functional brain requires the reiterative use of cellular processes, such as proliferation, cell-fate determination and migration, in a spatiotemporally controlled manner. However, the pathways/mechanisms that control these processes are still elusive. The relatively simple zebrafish epithalamus is proving to be an excellent model to study brain development, since many of the main brain developmental processes also occur in the epithalamus. For example, different types of cells are generated from the same pool of progenitor cells, some cells migrate from their original place and asymmetries between the left and right sides of the epithalamus are observed. During the last years, our understanding about the development of the zebrafish epithalamus has increased dramatically. A number of genes and pathways have been shown to be involved, but their wiring is still obscure.

sox2 is one of the most important transcription factors during development, especially the development of the brain. A combination of computational predictions and experimental validations using zebrafish, previously performed in our laboratory, led to the hypothesis that sox2 is involved in the development of the zebrafish epithalamus. Therefore, the main aim of this project was to characterize these putative role(s) of sox2 in the development of the three main epithalamic structures: the pineal gland, the parapineal organ and the habenulae. To achieve this, we first established and characterized a zebrafish model with disrupted *sox2* expression (*sox2* morphants). In addition, we aimed to investigate the molecular networks mediated by sox2 and whether sox2 works in the same or independent pathways with other known mediators (such as Notch and BMP) during the development of the epithalamus.

By characterizing the molecular networks important for the development of the zebrafish epithalamus, we aim to obtain insights into how a functional vertebrate brain is developed. We also aim to understand how sox2 controls such a variety of functions. This in turn will provide us with a better understanding on how brain-related diseases arise and how we can treat and/or prevent them.

Chapter 2. Materials and Methods

“Της παιδείας οι μεν ρίζες πικρές, οι δε καρποί γλυκείς”

“The roots of education are bitter, but the fruit is sweet”

Aristotle, 384-322 BC

2.1 Zebrafish lines and maintenance

2.1.1 Fish lines

All wildtype and transgenic *Danio rerio* lines used in this study are listed in **Table 2.1**.

2.1.2 Fish maintenance

Adult zebrafish were maintained in Yamuna zebrafish facility (Human Genetics Unit, Institute of Genetics and Molecular Medicine, University of Edinburgh), at 28.5°C with a 14 hours light/10 hours dark cycle, according to the Zebrafish book (Westerfield, 2000). Embryos were raised in E3 medium (5 mM NaCl, 0.17 mM KCl, 0.33 mM $CaCl_2$, 0.33 mM $MgSO_4$ and 0.00001% methylene blue) at 28.5°C and staged according to Kimmel (1995). Stages are shown in somites stage (ss), hours post fertilization (hpf) or days post fertilization (dpf).

Table 2.1 List of zebrafish wildtype and transgenic lines used.

Short Name	Full Name	Description	Generated by	Reference
wildtype	Edinburgh (wildtype)	Out-crossed wildtype population (*WIK, TL, TU, Golden, AB*)	van Heyningen laboratory	n/a
Tg(pou4f3:GFP)	*Tg(pou4f3:GAP-GFP)s356t*	Reporter for RGCs and their axons	Baier laboratory	Xiao et al., 2005
Tg(elavl3:GFP)	*Tg(elavl3:EGFP)knu3*	Reporter for pineal projection neurons	Huh laboratory	Park et al., 2000
Tg(aanat2:GFP)	*Tg(aanat2:EGFP)y8*	Reporter for pineal photoreceptors	Dawid laboratory	Gothilf et al., 2002
Tg(flh:GFP)	*Tg(-1.6flh:gap43-EGFP)u1*	Reporter for pineal precursors	Wilson laboratory	Concha et al., 2003
Tg(hs:Gal4)	*Tg(hsp70l:Gal4)1.5kca4*	Heat-shock controlled Gal4 activator	Reugels and Campos-Ortega laboratory	Scheer et al., 2001
Tg(UAS:Notch-intra)	*Tg(UAS:myc-Notch1a-intra)kca3*	Ectopic expression of *Notch1a* intracellular domain, resulting in upregulation of Notch pathway	Reugels and Campos-Ortega laboratory	Scheer and Campos-Ortega, 1999
Tg(BRE:GFP)	*Tg(BmpRE-AAVmlp:EGFP)mw29*	BMP-activity reporter	Link laboratory	Collery and Link, 2011
Tg(foxd3:GFP)	*Tg(foxd3:GFP)zf15*	Pineal complex reporter	Nüsslein-Volhard laboratory	Gilmour et al., 2002
Tg(csl:venus)	*Tg(csl-venus)qmc61*	Notch-activity reporter	Gering laboratory	Unpublished

2.2 Microinjections of zebrafish embryos

Injection needles were generated by pulling borosilicate glass capillaries (Intrafil, 1 mm outside diameter X 0.8 mm inside diameter) using a micro-electrode puller (CFP), according to the manufacturer's instructions. Microinjections were performed using Picospritzer III injector (Intracel) and Nikon SMZ1000 stereomicroscope.

2.2.1 Antisense morpholino oligonucleotides (morpholinos)

Two *sox2* antisense morpholino oligonucleotides (*sox2*-MO1 and *sox2*-MO2) (Gene Tools, LLC), directed against the 5' sequence near the translation start site, were tested. Both morpholinos resulted in the same phenotype, although different severities, and *sox2*-MO2 was used throughout this study, unless stated. The morpholinos' sequences were:

sox2-MO1: CTCGGTTTCCATCATGTTATACATT

sox2-MO2: TCTTGAAAGTCTACCCCACCAGCCG

Morpholinos were dissolved in 63 µl dH_2O (RNase- and DNase-free) to make stock solutions of 4.7 nanomoles/µl. The stock solution was then diluted into an 1:16 solution, in injection buffer (5 mM HEPES; pH7.2, 0.2 M KCl, 2.5 mg/ml phenol red). *sox2*-MOs (3.5 ng) were injected at the 1-2 cells stage and the phenotype was consistent (approximately 95% of embryos) and fully penetrant.

2.2.2 messenger RNA (mRNA)

To address the specificity of the morpholinos, 25 pg of human *SOX2* mRNA was co-injected with *sox2* morpholino, at the 1-2 cell stage. The mRNA was transcribed *in vitro* using the mMessage mMachine kit T7 (Ambion), according to manufacturer's instructions. The plasmid containing human *SOX2* cDNA was obtained from D.A. Kleinjan (HGU, UK).

2.3 Heat-shock experiments

In order to upregulate Notch activity, we used heat-shock coupled with the Gal4:UAS system. *Tg(hs:Gal4)* fish were crossed with *Tg(UAS:Notch-intra)* and their offspring were heat-shocked to ubiquitously activate the intracellular domain of

Notch1a. For the heat-shock, embryos were transferred in Falcon tubes containing 40 ml E3 medium and incubated in a water bath for 30 minutes at 39^{o}C, as previously described (Aizawa et al., 2007). After treatment, embryos were returned to 28.5°C. In each experiment, 10-15 embryos were not treated as a control.

2.4 Polymerase Chain Reaction (PCR)

Each PCR was performed in a 25 µl reaction, consisting of approximately 100 ng DNA template, 10x PCR Rxn buffer without $MgCl_2$ (Invitrogen), 37.5 mM $MgCl_2$ (Invitrogen), 6.25 mM dNTPs (Invitrogen), 10 µM forward and 10 µM reverse primers (Sigma-Aldrich) and 1.25 units Taq (Invitrogen). dH_2O was used instead of DNA template as a negative control for all the primer sets. All primers were designed using Primer3 version 0.4.0 (http://frodo.wi.mit.edu/) and purchased from Sigma-Aldrich (http://www.sigmaaldrich.com/united-kingdom.html). Reactions were conducted in DNA Engine tetrad 2 thermal cycler (Bio-Rad) with the following cycle conditions:

Initial denaturation at 94°C for 5 minutes

Denaturation at 92°C for 1 minute

Annealing at 55°C for 1 minute

Extension at 72°C for 1 minute

Repeat denaturation, annealing and extension 34 more times

Final extension at 72°C for 5 minutes

Incubate at 4°C forever

All PCR products were run on 1% agarose gels in 1% TAE (with 1% TAE running buffer) with 1 kb molecular DNA size marker (Invitrogen).

2.5 Generation of cDNA library

2.5.1 RNA extraction from embryos

RNA extraction from 28 hpf dechorionated embryos was performed using the RNeasy kit (QIAGEN). Embryos were rinsed with dH_2O and their yolk was removed using a P200 pipette. Excess dH_2O was removed and embryos were homogenized in the lysis RLT buffer (350 µl RLT buffer, supplemented with 3.5 µl β-Mercaptoethanol). The lysate was centrifuged at 13000 rpm for 3 minutes and the supernatant was collected and

transferred into a new tube. One volume of 70% ethanol (350 µl) was then added and mixed by pipetting. The sample was then transferred to an RNeasy spin column and centrifuged for 15 seconds at 10000 rpm. The flow through was discarded and the column was washed using 700 µl of RW1 buffer, followed by 15 seconds centrifugation at 10000 rpm. The column was then transferred to a new collection tube and washed twice with 500 µl diluted RPE (100 RPE µl in 400 µl ethanol). The column was centrifuged once more at 13000 rpm for 1 minute to ensure that no ethanol is being carried over during the RNA elution. Finally, RNA was eluted from the column in 30 µl RNase-free water by centrifuging for 1 minute at 10000 rpm.

2.5.2 Reverse transcription with elimination of genomic DNA

Genomic DNA was eliminated and cDNA was synthesized using the QuantiTect Reverse Transcription Kit (QIAGEN). RNA concentration was measured using nanodrop ND-1000 (Thermo Scientific) and 1 µg RNA was mixed with 7x gDNA wipeout buffer and RNase-free water at 14 µl final volume. The sample was incubated for 2 minutes at 42°C and placed immediately on ice. A reverse transcription (RT) master mix was prepared on ice (1 µl reverse transcriptase, 4 µl RT buffer, 1 µl RT primer mix) and then the 14 µl RNA template was added to the master mix. Reverse transcription was performed by incubating the sample for 15 minutes at 42°C, followed by 3 minutes incubation at 95°C to inactivate the reverse transcriptase. The concentration of the cDNA was measured using nanodrop ND-1000 (Thermo-Scientific) and store at -20°C.

2.6 Amplification and linearization of plasmids

A number of antisense probes were generated from plasmids containing the gene of interest, obtained from various laboratories. In order to amplify the plasmids, we transformed them into DH5α competent cells (Invitrogen), according to manufacturer's instructions. Plasmids were then linearized with the appropriate restriction enzyme, at 37°C for 90 minutes (according to manufacturer's instructions). The antibiotics used for selection, as well as the restriction enzymes used to linearize each plasmid, are shown in **Table 2.2**.

Table 2.2 Antibiotics and restriction enzymes used to amplify and linearize plasmids.

Gene	Antibiotic Resistance	Enzyme	Provided by
aanat2	Ampicillin	EcoRI	Klein laboratory
fgf8a	Ampicillin	SalI	Feldman laboratory
gfi1ab	Ampicillin	NotI	Bladder laboratory
otx5	Ampicillin	NotI	Halpern laboratory
pitx2	Ampicillin	SpeI	Feldman laboratory

2.7 Whole mount *in situ* hybridization

The protocol used for the whole mount *in situ* hybridization experiments was adapted from Thisse (1993).

2.7.1 Synthesis of antisense RNA probe

In general, a cDNA library from 28 hpf (**Section 2.5**) was used to amplify regions of the genes of interest using standard PCR technique (**Section 2.4**). Primers are shown in **Table 2.3**. PCR products were then purified using the PureLink PCR purification kit (Invitrogen) and run on an agarose gel to confirm the presence of amplicons of the correct size. The *aanat2*, *fgf8a*, *gfi1ab*, *otx5* and *pitx2* probes were transcribed from linearized plasmids (**Section 2.6**) containing the full length or part of their cDNAs. RNA probes were synthesized and labelled with digoxigenin (DIG) by incubating the purified PCR products (or the linearized plasmids) with 10x T7 transcription buffer (Roche), 10x DIG RNA labelling mix (Roche), 40 units RNAse inhibitor (Promega) and 40 units T7 RNA polymerase (Roche) for 2 hours at 37°C (in 20 µl reactions). T7 polymerase was replaced by T3 polymerase (Roche) for the *gfi1ab* probe. The DNA template was digested by incubation with 10 units DNase I for 15 minutes at 37°C. The reaction was stopped and the RNA precipitated after 2-hour incubation on dry ice with 1 µl 0.5M EDTA; pH8, 2.5 µl 4M LiCl and 75 µl 100% EtOH. The resulting reaction was then centrifuged at 4°C for 30 minutes (13000 rpm). The pellet was washed with 70% EtOH, resuspended in 20 µl nuclease-free dH_2O and

stored in -20°C. A 1/4000 dilution in hybridization mix was used as working probe (1/1000 dilution for the probes generated from linearized plasmids).

Table 2.3 Primers used to make RNA probes for whole mount *in situ* hybridizations.

Name	Forward (5'-3')	Reverse (5'-3')
ascl1a	CGTAAACCAGCAGCAGTTCA	taagctttaatacgactcactatagggagaAGCGTCTCCACTTTGCTCAT
flh	CTAAACAGACGCCATGCAGA	taagctttaatacgactcactatagggagaTTCGCCAGTACTGCATCTTG
isl1	CGGCGCACATATTCACATAC	taagctttaatacgactcactatagggagaACGGACACGAACACATGAAA
kctd12.1	GTCGAGAATGAGCCAAAAGC	taagctttaatacgactcactatagggagaTCGGATGAAGCATTTGTTGA
pax6b	GAGCAAGATTCTGGGGAGGT	taagctttaatacgactcactatagggagaGCTCGGTATGTTATCGTTGG
samsn1b	TGTTCCCAGTCCATACGACA	taagctttaatacgactcactatagggagaGAGTCCAGCAGGTTTTCTGC
sox2	CTCGGGAAACAACCAGAAAA	taagctttaatacgactcactatagggagaTTCATATGCGCGTAGCTGTC
sox6	GACGCAGATCCCCATCAC	taagctttaatacgactcactatagggagaCTCGTCCTCAAAGTCCTCGT
tbx2b	ATTGCGGAGAAGAAAGACGA	taagctttaatacgactcactatagggagaAGCCAATAGATGTCCCATGC

2.7.2 Fixation and storage of the embryos

Manually dechorionated embryos were fixed in 4% PFA in PBS at 4°C overnight or for 30 min at room temperature, before being transferred in 100% methanol and stored at -20°C (for up to 3 months).

2.7.3 Permeabilization

Embryos were rehydrated by successive 5 minutes washes in 75%, 50% and 25% MeOH in PBS and four 5 minutes washes in 100% PBT (PBS supplemented with 0.1% Tween 20). The embryos were then digested in 10 μg/ml proteinase K; incubation time in proteinase K varies depending on the stage of the embryos and is shown in **Table 2.4**. They were then refixed in 4% PFA in PBS for 20 minutes at room temperature, followed by five 5 minutes washes in PBT.

Table .4 Time of proteinase K treatment for each developmental stage.

Stage of embryos	Period with proteinase K
somitogenesis (16-20 hpf)	5 minutes
24 hpf	10 minutes
28 hpf	13 minutes
32 hpf	13 minutes
48 hpf	17 minutes
3 dpf	20 minutes
4 dpf	25 minutes

2.7.4 Hybridization

Embryos were pre-hybridized in hybridization mix (50% formamide, 5x SSC, 0.1% Tween 20, 50 μg/ml Heparin, 500 μg/ml tRNA and citric acid to pH 6.0) for 2-5 hours at 65°C. Hybridization mix was replaced with the working probes (1/4000 dilution of probe in hybridization mix) and embryos were incubated overnight at 65°C.

2.7.5 Washes

The embryos were washed at 65°C briefly with 100% wash solution (50% formamide, 5x SSC, 0.1% Tween 20, citric acid to pH 6.0), followed by successive 15 minutes washes with 75%, 50% and 25% wash solution in 2x SSC, one 15 minutes wash with 2x SSC and two 30 minutes washes with 0.2x SSC. They were then washed for 10 minutes at room temperature with 75%, 50% and 25% 0.2x SSC in PBT. The last wash was with PBT at 65°C for 10 minutes to destroy any endogenous alkaline phosphatases.

2.7.6 Detection

The embryos were blocked in PBT supplemented with 2% sheep serum and 2 mg/ml BSA (bovine serum albumin) at room temperature for several hours and incubated overnight at 4°C in 1:5000 anti-DIG-AP-fab fragments (Roche). The antiserum was removed and the embryos were washed extensively with PBT (6 times for 15 minutes) at room temperature, followed by 3x 5 minutes washes with the staining buffer (100 mM Tris HCl; pH 9.5, 50 mM $MgCl_2$, 100 mM NaCl, 0.1% Tween 20). For the staining reaction, the embryos were incubated at room temperature in staining solution (50 mg/ml NBT, 50 mg/ml BCIP in staining buffer) and monitored with a microscope. To stop the reaction, staining solution was replaced by PBS containing 1 mM EDTA (3x 5 minutes washes).

2.7.7 Mounting embryos

Embryos were mounted by successive 5 minutes washes in 30%, 50% and 70% glycerol in PBT and stored at 4°C in the dark.

2.8 Drug treatments

2.8.1 Phenylthiourea (PTU)

PTU was used to inhibit pigmentation for better imaging of the embryos. Dechorionated embryos were transferred into E3 medium containing 0.003% PTU (Sigma), at 24 hpf and raised to the desired stage (Westerfield, 2000; Karlsson et al., 2001).

2.8.2 *N*-[(3,5-Difluorophenyl)acetyl]-L-alanyl-2-phenyl]glycine-1,1-dimethylethyl ester (DAPT)

DAPT was used to inhibit Notch signalling. Partially dechorionated embryos were transferred into E3 medium containing 100 μM DAPT (TOCRIS bioscience) and 1% DMSO (dimethyl sulfoxide) at 9 hpf, as previously described (Geling et al., 2002; Cau et al., 2008). Control embryos were incubated in E3 medium or E3 medium supplemented with 1% DMSO.

2.8.3 6-[4-(2-Piperidin-1-ylethoxy)phenyl]-3-pyridin-4-ylpyrazolo[1,5-a]pyrimidine (dorsomorphin)

Dorsomorphin was used to downregulate BMP activity. Partially dechorionated embryos were transferred in E3 medium complemented with 30, 40 or 50 μM dorsomorphin (Sigma, P5499) and 1% DMSO, as previously described (Chung et al., 2010; Collery and Link, 2011). Treatment was performed at about 6 hpf and embryos were left to develop to the desire stage. Control embryos were incubated in E3 medium or E3 medium containing 1% DMSO.

2.9 Whole mount immunofluorescence

Manually dechorionated embryos were fixed in 4% PFA in PBS overnight at 4°C or 30 minutes at room temperature, at the desired stage. They were then incubated in methanol overnight (or longer) at -20°C. Embryos were rehydrated by several washes in PBS supplemented with 0.1% Tween 20. They were then incubated in blocking solution (1% BSA, 0.1% Triton X-100, 0.05% DMSO and 2% sheep serum in PBS) for 1 hour at

4°C, followed by overnight incubation in primary antibodies at 4°C (dilutions of primary antibodies are shown in **Table 2.5**).

Table 2.5 Primary antibodies used for whole mount immunofluorescence.

Name	Host	Supplier, Catalog number	Dilution
anti-sox2	Rabbit	abcam, ab97959	1/200
anti-isl1	Mouse	DSHB, 39.4D5 (concentrated)	1/200
anti-myc	Goat	abcam, ab9132	1/400

Embryos were then washed extensively with PBS containing 0.1% Triton X-100 and incubated in 1/1000 dilution of Alexa Fluor conjugated secondary antibodies (Invitrogen) (**Table 2.6**) at 4°C.

Table 2.6 Secondary antibodies used for whole mount immunofluorescence.

Catalog number	Host and reactivity	Conjugated to Alexa Fluor
A11020	Goat anti-mouse	594 (red)
A11017	Goat anti-mouse	488 (green)
A31571	Donkey anti-mouse	647 (far red)
A21207	Donkey anti-rabbit	594 (red)
A11070	Goat anti-rabbit	488 (green)
A11055	Donkey anti-goat	488 (green)

Secondary antibodies were then removed and embryos washed in PBS supplemented with 0.1% Triton X-100 and stored in PBS at 4°C.

2.10 Whole mount phalloidin and DAPI labelling

Embryos were simultaneously fixed and permeabilized in PBS containing 4% PFA and 1% Tween 20, overnight at 4°C. They were then washed extensively in PBS complemented with 2% Triton X-100, followed by 1 hour incubation in blocking buffer (1% BSA, 0.1% Triton X-100, 0.05% DMSO and 2% sheep serum). Embryos were then incubated in 1/200 Alexa Fluor 594 Phalloidin (Invitrogen, A12381) and 1/200 DAPI (1mg/ml) in blocking solution for 2 days, at 4°C. They were washed in PBS containing 2% Triton X-100 and stored in PBS.

2.11 Chromatin Immunoprecipitation (ChIP) and quantitative real-time PCR (qRT-PCR)

Chromatin Immunoprecipitation (ChIP) was performed using a modified version of the protocol described in Boyer et al. (2005). In detail:

2.11.1 Fixation

Manually dechorionated embryos were rinsed with cold PBS. They were then homogenized in 10% fixation solution in PBS, followed by 15 minutes fixation at room temperature. Fixation solution consisted of 11% formaldehyde (Sigma), 0.1 M NaCl, 1 mM EDTA (pH 8), 0.05 mM EGTA (pH 8) and 50 mM HEPES (pH 8). Fixation was stopped by adding glycine to a final concentration of 140 mM, followed by 5 minutes incubation at room temperature. Homogenized embryos were then washed twice in PBS, by centrifugation at 1300 rpm for 5 minutes at 4°C.

2.11.2 Chromatin extraction

Homogenized-embryo pellet was resuspended in 5 ml ice-cold buffer 1 (50 mM HEPES/KOH; pH 7.6, 140 mM NaCl, 1 mM EDTA, 10% Glycerol, 0.5% NP-40, 0.25% Triton X-100 and 1x protease inhibitor cocktail) and incubated for 10 minutes at 4°C on a rocking platform. The mixture was then centrifuged at 1300 rpm for 5 minutes (4°C) and the pellet was resuspended in 5 ml ice-cold buffer 2 (200 mM NaCl, 1 mM EDTA, 0.5 mM EGTA, 10 mM Tris; pH 8, 1x protease inhibitor cocktail), followed by 10 minutes incubation at room temperature on a rocking platform. The mixture was centrifuged as above and pellet was resuspended in 3 ml buffer 3 (1 mM EDTA; pH 8, 0.5 mM EGTA pH 8, 10 mM Tris; pH 8, 0.1% SDS and 1x protease inhibitor cocktail).

2.11.3 Sonication

Chromatin was sonicated using MSE Soniprep 150, according to manufacturer's instructions. The sonicated chromatin was then run on a 0.7% agarose gel to determine the average length of the chromatin fragments. The desirable length of the sonicated chromatin was 1-2 kb.

2.11.4 Loading the antibodies to the beads

100 µl Dynabeads (Invitrogen) were washed 5 times for 4 minutes in blocking solution (5mg/ml BSA in PBS), at 4°C. The beads were then resuspended in 250 µl blocking solution and incubated with 10 µg of antibody for 4 hours at 4°C. The rabbit polyclonal antibody against sox2 (Abcam, ab15830) and the rabbit control IgG – ChIP Grade (Abcam, ab46540) were used.

2.11.5 Pre-clear chromatin

Chromatin was diluted 2.5 times in immunoprecipitation buffer (20 mM HEPES; pH 8, 0.1M NaCl, 2 mM EDTA, 0.1% sodium deoxycholate, 1% Triton X-100, 1 mg/ml BSA and protease inhibitor cocktail). The diluted chromatin was then incubated with 100 µl beads (washed like **2.11.4**) for at least 2 hours at 4°C to eliminate any non-specific binding of chromatin to the beads. 50 µl of sonicated chromatin was stored at -20°C and used later as an input control.

2.11.6 Immunoprecipitation and washes

The pre-cleared chromatin was added to the loaded beads and incubated at 4°C overnight. The beads were then washed 6 times for 4 minutes with modified RIPA buffer (50 mM HEPES; pH 7.6, 1 mM EDTA, 1% NP-40, 0.7% sodium deoxycholate and 0.5 M LiCl), followed by one wash in TE buffer supplemented with 50 mM NaCl. Finally, the beads were resuspended in 1 ml TE buffer.

2.11.7 Elution

Beads were resuspended in 210 µl of elution buffer (10 mM Tris; pH 8 and 1% SDS in dH_20) and incubated at 65°C for 30 minutes. Every 2 minutes, beads were gently and briefly mixed by vortexing. The 50 µl of sonicated chromatin (input control from **2.11.5**) were also treated in the same way. The beads were removed by centrifuging the samples twice for 1 minute at 1300 rpm. 200 µl TE, 40 µg proteinase K and 10 µl 5M NaCl were then added to the sample and incubated for 2 hours at 55°C, followed by overnight incubation at 65°C to reverse the cross-links.

2.11.8 DNA extraction

DNA was extracted by washing twice with phenol/chloroform and once with chloroform:isoamyl alcohol (24:1). The extracted DNA was then precipitated by adding 40 µg glycogen, 40 µl 3M sodium acetate and 800 µl ethanol, followed by incubation at -80°C for 30 minutes. Finally, DNA was pelleted and resuspended in 50 µl dH_2O.

2.11.9 qRT-PCR

qRT-PCR was performed using the SYBR Green Real-Time Master Mixes kit (Invitrogen), according to manufacturer's instructions. The primers used are shown in **Table 2.7**. DNA fragments bound by sox2 or IgG (control) were used as templates in two dilutions: 1/10 and 1/100. N3 enhancer was used as a positive control and a *fezf2* putative enhancer as a negative control. The relative occupancy values for sox2 and IgG were calculated by determining the immunoprecipitation efficiency (ratio of the amount of ChIP enriched DNA over that of the input) and normalized to the level observed at the negative *fezf2* region. The fold-enrichment was calculated by normalizing the relative occupancy for sox2 with the relative occupancy for IgG.

Table 2.7 Primers used for qRT-PCR.

Name	Forward (5'-3')	Reverse (5'-3')
N3	AAAGCTTTGCTTTCGCTGAC	TACGGAGGATGAGGGAAATG
otx2	GGTTACTTTTGTCCCTCTCCAA	ATGTGCACACAAGCCAGAAA
mab21l1	AAAATAATGGGGGCATCTCC	ACCGTCACCTTGAACTACCG
samsn1b	CCTCTTTTTCCTGCTGTTGC	TGGAGGGGAGATTTGAGATG
sox6	ATGCATCAGCTCACCACAAA	CCCCGTCTGACAGAGACAGT
tshz1	TGACAGGTGGGTTTTCACTG	GTTCTCGGTCTCTTCGCTGA
dachd	GAAATGGCTCATGCATCTCA	GGCAACAGCCACAGTGATTA
fezf2	AAAAACCCTCCGACCAGTTT	TAGGATCCGAGGGAGGTTCT

2.12 5-ethynyl-2'-deoxyuridine (EdU) labelling and Fluorescence Activated Cell Sorting (FACS) analysis

EdU labelling was performed using the Click-iT® EdU Alexa Fluor® 647 Flow Cytometry Assay Kit (A10202, Invitrogen), according to manufacturer's instructions. Although I performed the EdU incorporation and labelling of cells, E. Freyer (MRC-HGU, Edinburgh) performed the cell sorting and analysis.

2.12.1 EdU incorporation

Manually dechorionated embryos were placed in E3 medium supplemented with 400 μM EdU for 30 minutes at 48 hpf in dark.

2.12.2 Cell dissociation

The protocol for cell dissociation was adapted from (Covassin et al., 2006). Embryos were rinsed in calcium-free Ringer solution (116 mM NaCl, 2.9 mM KCl, 5 mM HEPES; pH 7.2) for 15 minutes and their yolks were removed using P200 pipette. The embryos were then transferred into 35 mm culture dish containing 5 ml trypsin: versene (1:1) and incubated for 1 hour at 28.5^{o}C, until the embryos were fully digested. Digestion was then stopped by adding $CaCl_2$ and fetal calf serum to the final concentration of 1 mM and 10%, respectively. The cells were passed through a mesh to remove any clumps. Finally, single cells were washed twice with 1% BSA in PBS by centrifugation at 2000 rpm for 5 minutes.

2.12.3 Fixation

Single cells were fixed in 4% PFA in PBS for 15 minutes at room temperature, protected from light and washed with 1% BSA in PBS by centrifugation at 2000 rpm for 5 minutes.

2.12.4 Permeabilization and EdU detection

Cells were permeabilized by washing them twice in 1x saponin-based permeabilization and wash reagent (Invitrogen). EdU was detected by incubating the cells in 0.5 ml Click-iT reaction cocktail (Invitrogen), followed by one wash in 1x saponin-based permeabilization and wash reagent. The cells were then resuspended in 0.5 ml 1x saponin-based permeabilization and wash reagent.

2.12.5 DNA content and cell-cycle distribution

Cell-cycle 405-blue was added to the cells, followed by 30-minutes incubation at room temperature. The cells were then pelleted and resuspended in 0.3 ml PBS.

2.12.6 Flow cytometry analysis

Flow cytometry analysis was performed by Elizabeth Freyer (MRC-HGU, Edinburgh) using a BD FACSArialI SORP (Becton Dickinson). BD FACSDiva software (Becton Dickinson, Version 6.1.2 was used for instrumental control and data analysis.

2.13 Immunofluorescence on sections

2.13.1 Fixation

Manually dechorionated embryos were fixed in 4% PFA in PBS overnight at 4°C and then incubated in methanol at -20°C overnight (or longer).

2.13.2 Washes and mounting

Embryos were transferred into 5ml glass dishes and washed twice in 100% ethanol for 5 minutes. They were then washed twice in histoclear (Thermo Scientific) for 10 minutes at room temperature, followed by one wash at 65°C. Embryos were then washed three times in molten wax for 10 minutes at 65°C. During the last wax treatment, embryos were orientated using forceps.

2.13.3 Sectioning

Sectioning of embryos was performed using the LEICA RM2235 microtome, according to manufacturer's instructions. Each section was 7 um thick and was placed on a positively charged glass slide (SuperFrost Plus, VWR). Multiple sections were placed on the same slide. Slides were left at room temperature overnight to dry and they were then incubated at 50°C overnight.

2.13.4 De-paraffinization and re-hydration

Slides carrying the specimens were washed 3x in xylene (Fisher Scientific) for 5 minutes, followed by two 5-minute washes in 100% ethanol. Specimens were then re-hydrated by successive 5-minute washes in 90%, 70%, 50% and 30% ethanol in dH_2O, followed by 3 washes in dH_2O.

2.13.5 Antigen retrieval, washes and blocking

Antigen retrieval was achieved by boiling the specimens in 1L citrate buffer (8.2 mM Trisodium citrate and 1.8 mM citric acid in dH_2O) for 15 minutes and then cooling to room temperature. Slides were washed twice in PBS (5 minutes), followed by one wash in dH_2O. The samples were then incubated in blocking buffer (2% sheep serum, 1% BSA, 0.1% Triton X-100, 0.05% Tween 20 in PBS) for one hour at room temperature.

2.13.6 Primary antibodies

Samples were incubated in 1/250 dilution of primary antibodies in blocking buffer overnight at 4°C. The rabbit polyclonal to sox2 (Abcam, ab97959) and the mouse monoclonal to isl1 (Developmental Studies Hybridoma Bank, 39.4D5) antibodies were used.

2.13.7 Washes and secondary antibodies

Slides were washed extensively in PBS supplemented with 0.05% Tween 20, before overnight incubation at 4°C in 1/500 dilution of Alexa Fluor conjugated secondary antibodies (Invitrogen) (**Table 2.5**).

2.13.8 Washes and mounting

Slides were washes extensively in PBS containing 0.05% Tween 20 and were mounted in Vectashield (Company) supplemented with 0.1 μl/ml DAPI.

2.14 Densitometric analysis of the western blot

Densitometric analysis of the western blot was achieved using the Gel Analyzer tool (Fiji). The relative density of sox2 bands was normalized to the relative density of the corresponding β-tubulin bands (loading control) in control, *sox2*-MO1 and *sox2*-MO2.

2.15 Image acquisition and analysis

2.15.1 Macroscope

Nikon AZ100 macroscope was used for colour-brightfield imaging of embryos. Image acquisition was performed using Micropublisher 5.0 (Qimaging) camera and IPLab software (Scanalytics). Image analysis was performed using Photoshop CS4 (Adobe).

2.15.2 Fluorescence microscope

Axioskop 2 fluorescence microscope (Carl Zeiss) with Plan neofluar objectives (Carl Zeiss) and triple-band filter set (Chroma technology, series 83000) were used for imaging fluorescence-stained sections of zebrafish. Coolsnap HQ^2 CCD camera (Photometrics) and in-house scripts written for IPLab (Scanalytics) were used for image acquisition. Image analysis was performed using Fiji.

2.15.3 Confocal microscope

A1R confocal imaging system (Nikon) was used for imaging live or fixed zebrafish embryos, which were stained with Alexa Fluorophores or were carrying transgenes encoding fluorescent proteins.

For timelapse experiments, live zebrafish embryos were anaesthetized using Tricaine and mounted in 0.8% low-melting Agarose in E3 medium containing Tricaine and 0.003% PTU. Motorized stage and perfect focus system were used to navigate between embryos during the experiment. Environmental control was maintained during imaging with a Solent Scientific incubation chamber incorporating temperature and humidified CO_2 control. Timelapse experiments were carried out for 60 hours and images were acquired every 40 minutes. Images were acquired using NIS-elements microscope imaging software (NIKON) and analyzed using the open source image-processing package Fiji and Volocity (PerkinElmer).

2.16 Quantifications and statistics

The open source image-processing package Fiji and Volocity (PerkinElmer) were used for the quantifications.

2.16.1 isl1 quantifications

Maximum projections of confocal images (or single sections for the eyes) were used to manually count the number of isl1-positive cells. Fiji was used as a platform.

2.16.2 Quantifications of GFP-positive cells

GFP expression is both nuclear and cytoplasmic and therefore counting single cells manually is very difficult. To facilitate counting, embryos were counterstained with isl1 (nuclear staining). Using Fiji as a platform and by navigating through the optical stacks, cells that were positive for both isl1 and GFP were counted.

2.16.3 Habenular neuropil volume quantification

Volume quantifications of the habenular neuropils were performed using Volocity (PerkinElmer). Confocal stacks were visualized using the 3D opacity mode and neuropils, as marked by phalloidin, were selected using the Intensity threshold tool in the Volocity measurement tab. This tool makes measurements for all the non-continuous objects, but only the volume (μm^3) of objects visually confirmed to be within the morphologically defined habenular borders were recorded. The asymmetry index (AI) was used as a measure of asymmetry between the left and right neuropils, as previously described (Roussigné et al., 2009). AI was calculated for each embryo as the difference between the volume of the right and left neuropils divided by their total volume:

AI = (vR-vL)/(vR+vL)

vR = volume of the Right neuropil

vL = volume of the Left neuropil

AI between -1 and 0 = Left neuropil is larger that the right

AI between 0 and 1 = Right neuropil is larger than the left

The average AI for each category, as well as the average volume of the left and right neuropils is shown.

2.16.4 Statistics

For isl1 and GFP quantifications, the average number of positive cells is shown. Error bars represent ± standard error. Standard error was calculated as standard deviation divided by the square root of the number of embryos analyzed.

To compare multiple groups of cell counts (more than two groups), a Kruskall-Wallis rank sum test was performed using R (http://www.r-project.org/). In all cases there was a statistically significant difference between groups (p-value < 0.001) (data not shown). Post-hoc pairwise comparisons were then performed using Mann-Whitney U test (MWU test) with Bonferroni correction (using R). If p-value ≤ 0.05, then there is a significant difference between the two datasets; p-values < 0.001 are referred as highly significant.

The non-parametric Wilcoxon paired signed-rank test (Wilcoxon test) was used for the habenular neuropil quantifications, since it allows comparisons of two matched samples. If p-value ≤ 0.05, then there is a significant difference between the two datasets; p-values < 0.001 are referred as highly significant. An online Wilcoxon test calculator was used: http://www.stattools.net/Wilcoxon_Pgm.php.

Chi-square test was performed (using R) in order to determine whether simultaneous downregulation of sox2 and Notch leads to additive effect on the number of isl1-, *aanat2*- or *elavl3*-positive cells. For this test, the observed and expected frequencies were calculated:

observed = sum of all cells counted for each group

expected = number of embryos * average number of cells for each group

To test our null hypothesis that “simultaneous downregulation of both sox2 and Notch results in additive effect on the number of cells”, we calculated the expected frequency of *sox2*MO/DAPT-treated embryos as the sum of the defects observed in the single downregulations (*sox2*MO + DAPT). As controls we used both untreated controls and DMSO-treated controls.

expected = number of embryos*[(*sox2*MO-control)+(DAPT-control)+control]

or = number of embryos*[(*sox2*MO/DMSO-DMSO)+(DAPT-DMSO)+DMSO]

Chi-square test was performed using the observed and expected frequencies of all six groups of embryos: 1) control, 2) DMSO-treated controls, 3) *sox2* morphants, 4) *sox2* morphants treated with DMSO, 5) DAPT-treated embryos and 6) *sox2* morphants treated with DAPT. However, chi-square test calculates whether the overall pattern of observed frequencies is significantly different from the expected frequencies. Therefore, when a significant p-value is observed, further tests are required to determine which group contributes to the difference. In the case of *aanat2*- and *elavl3*-positive cells, there was no significant difference according to the chi-square test. However, in the case of isl1-positive cells, there was a significant difference between the observed and expected frequencies and therefore the standardized residual was calculated for each group:

$$\text{Standardized Residual} = \frac{observed - \exp ected}{\sqrt{\exp ected}}$$

A group contributes to the significant chi-square statistics when its absolute standardized residual value is greater than 2.

2.17 Protein alignments

Sequences were retrieved from Protein Knowledgebase - UniProtKB (http://www.uniprot.org/, accessed in November 2012) and alignments were performed using Crystal Omega (1.1.0) – Multiple Sequence Alignment software (http://www.ebi.ac.uk/Tools/services/web/toolform.ebi?tool=clustalo, accessed in November 2012).

* indicates positions which have a single, fully conserved residue

: indicates conservation between groups of strongly similar properties - scoring > 0.5 in the Gonnet point accepted mutation (PAM) 250 matrix

. indicates conservation between groups of weakly similar properties - scoring =< 0.5 in the Gonnet PAM 250 matrix

Chapter 3. Establishment and characterization of the zebrafish *sox2* morphant animal model

"Γηράσκω δ' αἰεὶ πολλὰ διδασκόμενος"

"I grow old always learning many things"

Solon, 638-558 BC

3.1 Introduction

A common approach used to study the function(s) of a particular gene is to disrupt its expression in a model organism and evaluate the phenotypic effects. This approach is known as reverse genetics. Here, we used reverse genetics in zebrafish embryos in order to dissect the roles of sox2 in vertebrate development and disease. Since there is no zebrafish mutant line available, antisense morpholino oligonucleotides (refer to as morpholinos) were used to downregulate sox2.

3.2 sox2 is essential for zebrafish development

Two different morpholinos (*sox2*-MO1 and *sox2*-MO2) (**Figure 3.1**) were designed and purchased from Gene Tools (http://www.gene-tools.com/). Since *sox2* is an intronless gene, both morpholinos were directed against the 5' end of the gene. *sox2*-MO1 is complementary to the sequence flanking the translation start side, whereas *sox2*-MO2 is directed against the 5' untranslated region (5' UTR).

Figure 3.1 *sox2* morpholinos are directed against the 5' UTR (*sox2*-MO2) and the translation start side (*sox2*-MO1) of the zebrafish *sox2* sequence. DNA sequence alignment of the human (first row) and the zebrafish (second row) *sox2* near the translation start site. Although the coding sequence is similar between the human and the zebrafish, the 5' UTR differs significantly. Purple represents the 5' UTR, black represents the coding sequences, red shows the nucleotides that are not complementary to the morpholinos.

Microinjections with either morpholino resulted in the same phenotype, but with slightly different severities; *sox2*-MO1 results in a milder phenotype than the *sox2*-MO2 (**Figure 3.2**). Morphants have shorter anteroposterior body axis than control siblings. Their tails are curved and they often display cardiac edemas. Also, downregulation of sox2 results in microphthalmia (small eyes), which is one of the most common phenotypes observed in human patients that carry *SOX2* mutations

(http://lsdb.hgu.mrc.ac.uk/variants.php?action=search_all). In addition, disruption of sox2 levels in zebrafish is lethal, since morphants die at approximately 6 dpf.

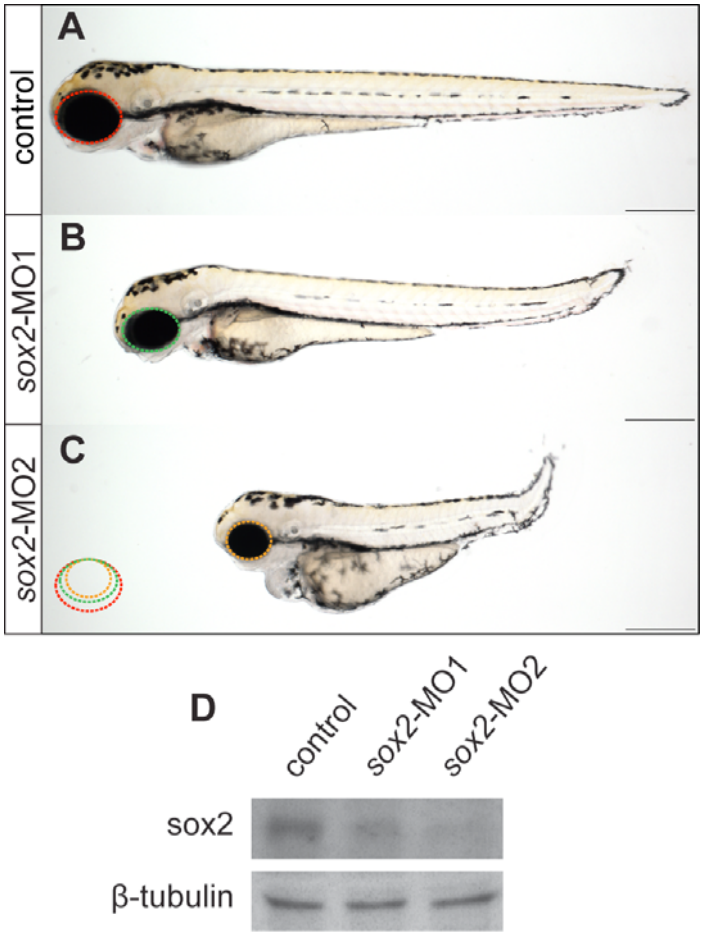

Figure 3.2 Downregulation of sox2 in zebrafish mimics the microphthalmia phenotype observed in human patients. (**A**) Lateral view of a control embryo at 3 dpf. Red circle surrounds the eye. (**B**) Microinjections with *sox2*-MO1 result in shorter body axis and smaller eyes (green circle) in relation to control embryos (red circle). (**C**) *sox2*-MO2 results in a more severe phenotype and it was used throughout the project. In the left corner of C, an overlay of the circles surrounding the eyes of control (red), *sox2*-MO1 (green) and *sox2*-MO2 (yellow) is shown, highlighting the progressive microphthalmia. (**D**) Western blot showing the level of sox2 in control embryos (first column), embryos injected with *sox2*-MO1 (second column) and *sox2*-MO2 (third column). β-tubulin was used as loading control. Western performed by M. Gakovic and K. Astell. Lateral view of 3 dpf live embryos with anterior to the left, scale bars = 250 μm.

Western blot analysis (performed by M. Gakovic and K. Astell) shows that microinjections with either morpholino result in decreased levels of sox2 protein (**Figure 3.2**). Densitometric analysis of the Western blot (using Gel analyzer tool in Fiji) suggests that *sox2*-MO1 results in 66% reduction, where as *sox2*-MO2 results in 80% reduction. The level of sox2 downregulation correlates with the severity of the phenotypes. Since *sox2*-MO2 is more efficient, we decided to use it throughout this study and I will refer to it as *sox2* morpholino (*sox2*-MO). Immunofluorescence, using a sox2 antibody, was also performed to confirm the reduction in sox2 protein levels. As shown in **Figure 3.3**, sox2 is almost completely lost in the eyes and the dorsal diencephalon in *sox2* morphants when compared to control siblings. Interestingly, *sox2* RNA levels are highly increased in *sox2* morphants, as shown by whole mount *in situ* hybridization (**Figure 3.4**). This suggests that the cells try to compensate for the reduction in sox2 protein levels by upregulating *sox2* transcription.

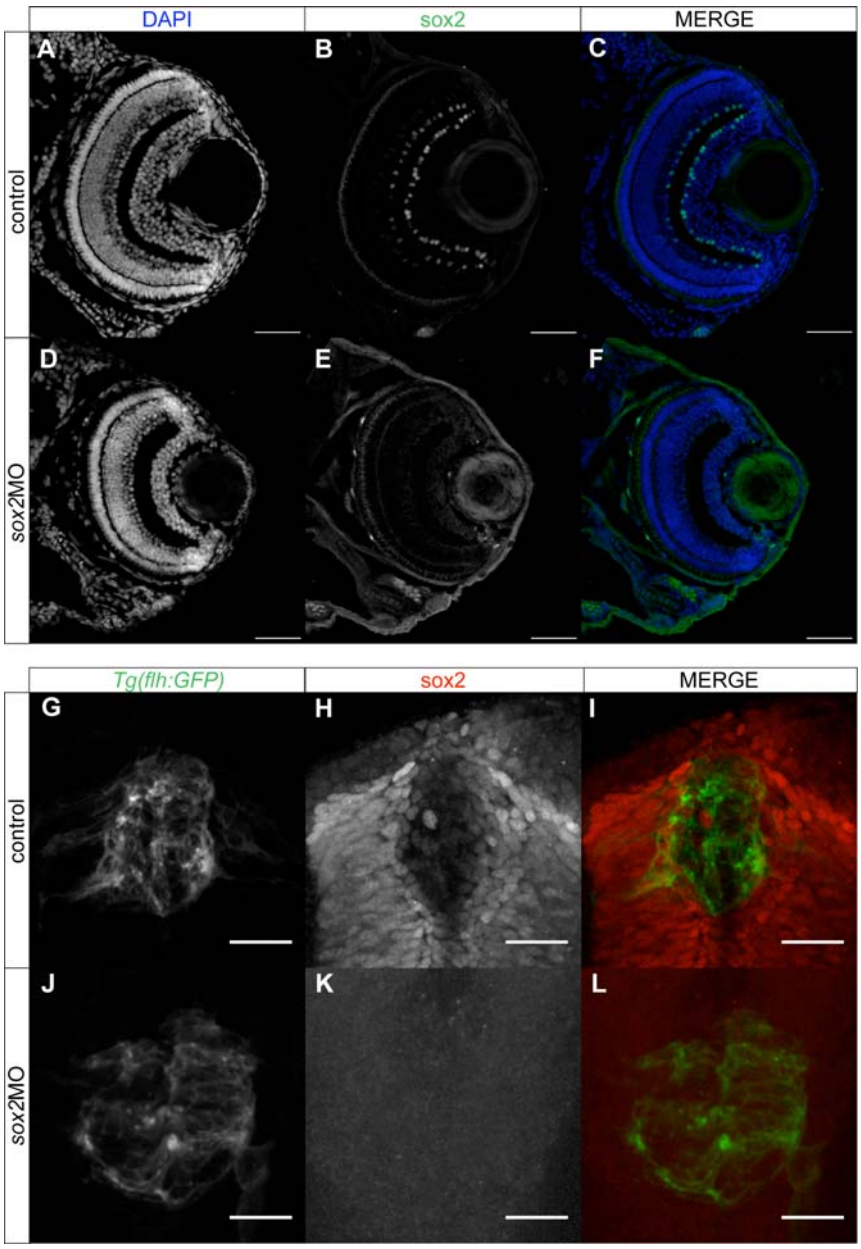

Figure 3.3 Microinjections of *sox2* morpholinos result in reduced sox2 protein levels. (**A-C**) sox2 (B, green in C) is expressed in a subset of amacrine cells and in some cells within the RGC-layer in control embryos. Sections were counterstained with DAPI (A, blue in C) to facilitate identification of cell layers. (**D-F**) In *sox2* morphants, sox2 (E) is completely absent within the eyes. (**G-I**) Whole mount immunofluorescence for sox2 (H, red in I) on *Tg(flh:GFP)* transgenic embryos (G, green in I) reveals that sox2 is expressed within the epithalamus but is excluded from the pineal gland. (**J-L**) No sox2 protein (K) is detected within the epithalamus in *sox2* morphants. (A-F) Frontal views of eye sections from 4 dpf embryos, scale bars = 50 µm (G-L) Maximum projection of confocal images, dorsal views with anterior to the top of 28 hpf embryos, scale bars = 25 µm.

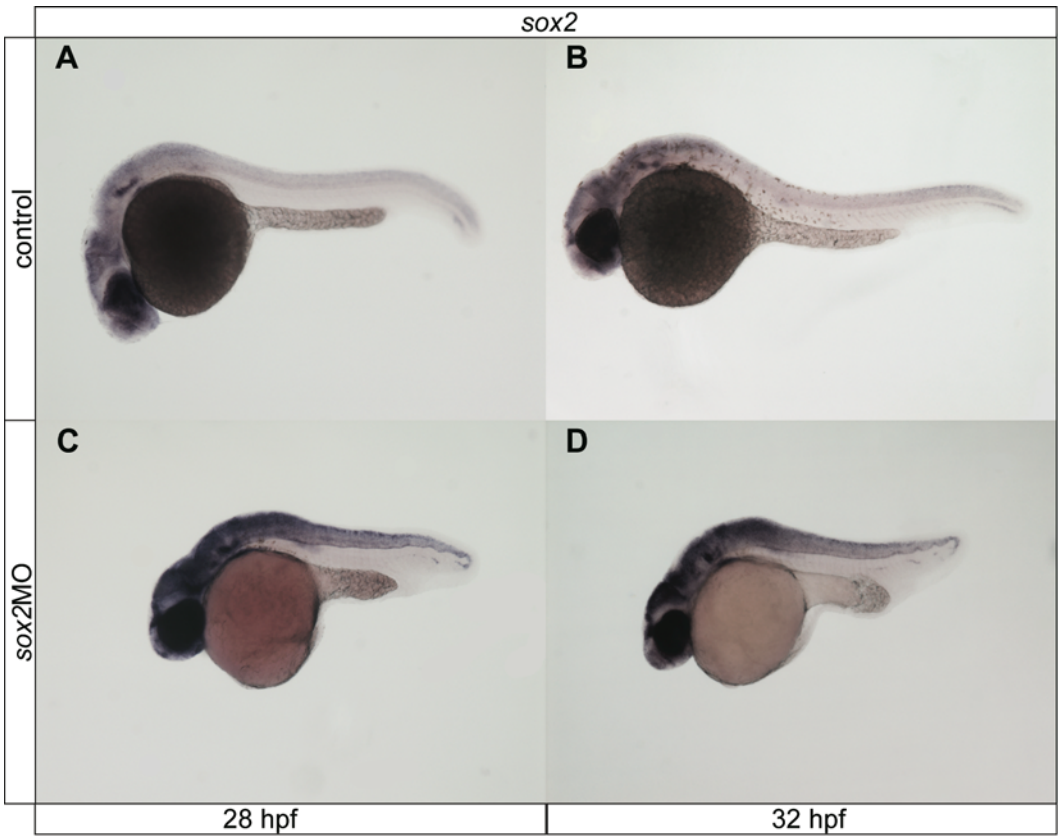

Figure 3.4 *sox2* transcription is upregulated in *sox2* morphants. (**A,B**) *sox2* is expressed in neuronal tissues at 28 and 32 hpf, as shown by whole mount *in situ* hybridization. (**C,D**) Morphant embryos have increased levels of *sox2* transcripts in relation to control siblings. Lateral views of 28 hpf (first column) and 32 hpf (second column) embryos.

In order to confirm the specificity of the phenotypes, rescue experiments were performed. The protein sequence of sox2 is evolutionarily conserved between zebrafish and humans (**Figure 1.9**). However, *sox2* morpholino (*sox2*-MO2) is directed against the 5' untranslated region (5' UTR), which significantly differs between the zebrafish and human genomes (**Figure 3.1**). This means that *sox2* morpholino can target and block translation of the zebrafish mRNA, but not of the human mRNA. Microinjections of human *SOX2* mRNA into *sox2* morphants were able to rescue the phenotypes (**Figure 3.5**), confirming that the phenotypic effects observed are specific to the downregulation

of sox2. Misexpression of human SOX2 does not result in any phenotype, as shown in **Figure 3.5**.

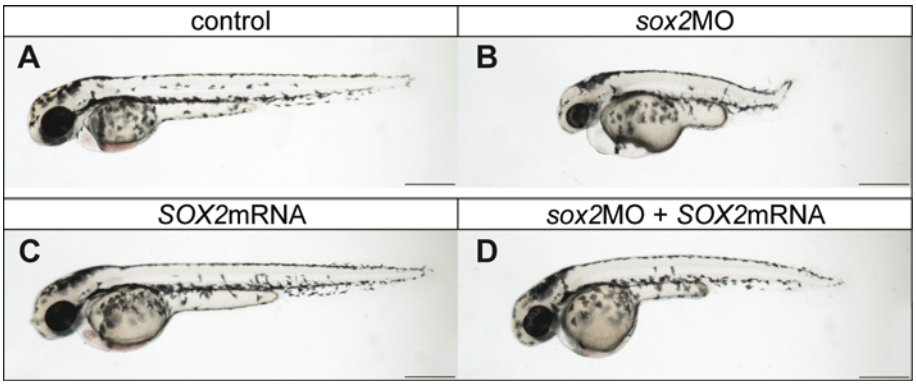

Figure 3.5 Microinjections with *SOX2* mRNA rescue the phenotypes caused by the *sox2* morpholinos. (**A**) Lateral view of control embryo at 52 hpf. (**B**) *sox2* morphants have small eyes and short body axis in relation to control siblings. (**C**) Microinjections with *SOX2* mRNA have no phenotypic effect. (**D**) mRNA injections into *sox2* morphants can rescue their short body axis and small eye phenotypes. Lateral views with anterior to the left of 52 hpf live embryos, scale bars = 250 μm.

3.3 Downregulation of sox2 results in ocular defects

In humans, *SOX2* haploinsufficiency leads to ocular defects, including anophthalmia, microphthalmia and optic nerve hypoplasia (summarized in http://lsdb.hgu.mrc.ac.uk/variants.php?action=search_all). Similarly, *Sox2*-hypomorphic mice exhibit microphthalmia, as well as hypoplastic optic nerves, possibly due to the reduced number of RGCs (Taranova et al., 2006). In addition, previous work on zebrafish *sox2* morphants demonstrated that downregulation of sox2 leads to reduced number of displaced amacrine cells (found in the RGC-layer) (Pujic et al., 2006). In order to better understand the ocular defects of *sox2* morphants, we performed immunostaining on eye sections at 3, 4 and 5 dpf.

In addition to the microphthalmia phenotype, *sox2* morphants have fewer RGCs and fewer amacrine cells (**Figure 3.6**). Eye sections were labeled using isl1 antibody and counterstained with DAPI. isl1 is expressed in the RGC-layer (in RGCs, as well as in some displaced amacrine cells) and in the inner nuclear layer (amacrine, bipolar and horizontal cells) (Perkins et al., 2005), whereas DAPI enables the identification of all

cell layers. At all stages analyzed, *sox2* morphants have a reduced number of cells within the RGC-layer (isl1-positive RGC and/or displaced amacrine cells) and reduced amacrine cells (isl1-positive cells at the inner-most edge of inner nuclear layer) (**Figure 3.6**). Interestingly, sox2 is co-expressed with isl1 in amacrine cells in the inner nuclear layer, as well as in a subset of cells in the outer-most edge of the RGC-layer (**Figure 3.6**). Further investigation is required to determine whether the sox2-positive cells within the RGC-layer are RGCs or amacrine cells.

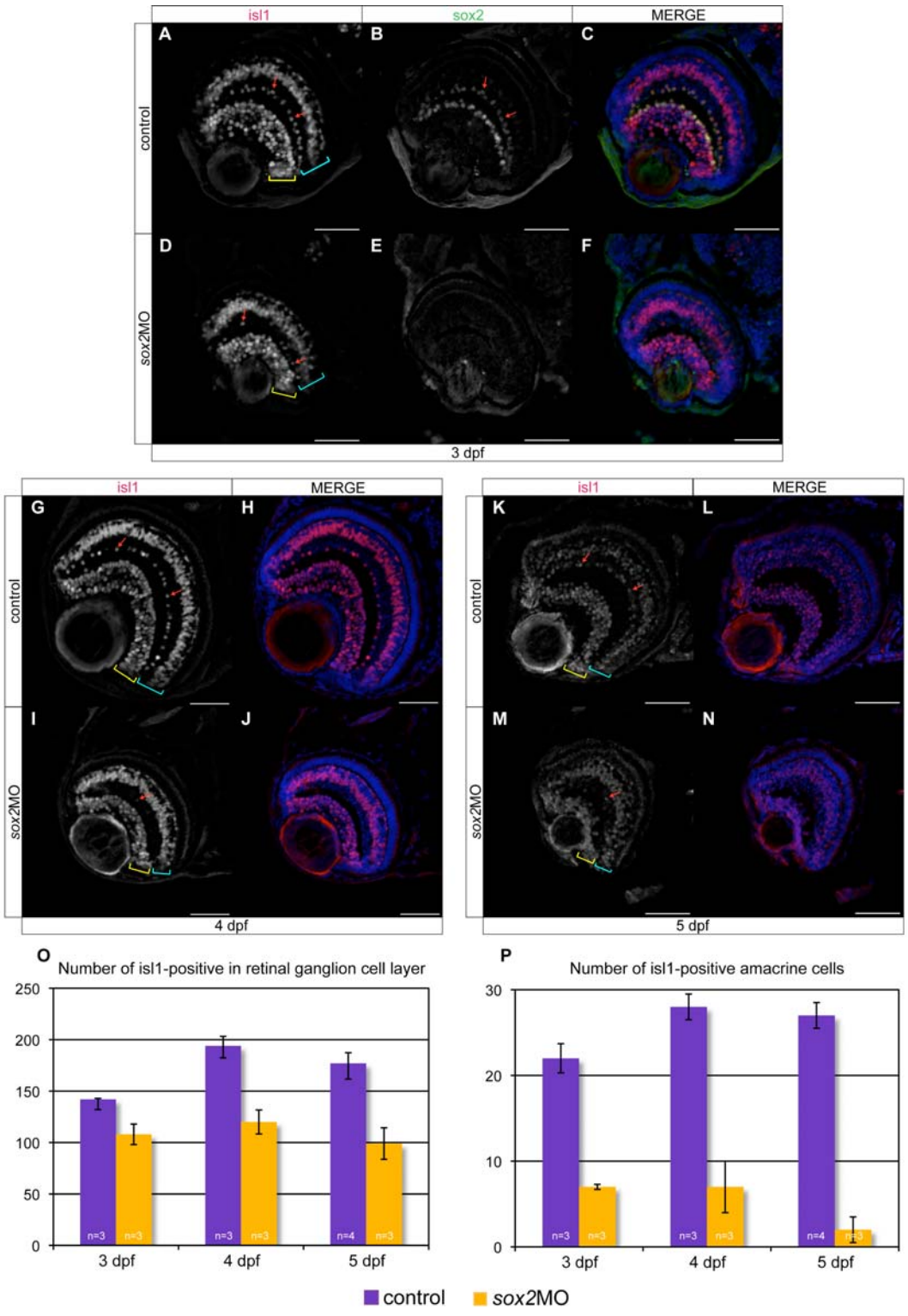

Figure 3.6 *sox2* morphants have ocular defects. (**A-C**) At 3 dpf, isl1 (A) is expressed in the RGC-layer (yellow bracket) and in a subset of cells within the inner nuclear layer

(blue bracket), including amacrine cells (red arrows). sox2 (B) is expressed in some cells within the RGC-layer and in amacrine cells (red arrows). Merged image is shown in C. (**D-F**) *sox2* morphants have fewer cells within the RGC-layer and fewer amacrine cells. sox2 expression (E) in the eye is almost completely absent. (**G-H**) isl1 is expressed in the same cells at 4 dpf. (**I-J**) *sox2* morphants have fewer RGCs and amacrine cells. (**K-N**) Similar to 3 and 4 dpf, downregulation of sox2 results in reduced cells within the RGC-layer and in fewer isl1-positive amacrine cells. (**O**) The average number of isl1-positive cells within the RGC-layer (RGCs and some displaced amacrine cells) in control (purple bars) and *sox2* morphants (orange bars). (**P**) The average number of isl1-positive amacrine cells (red arrows) in control (purple bars) and *sox2* morphants (orange bars). Immunofluorescence on eye sections, stages are shown at the bottom of each column, scale bars = 50 μm, error bars represent ± standard error, number of embryos is shown in each bar.

In *Sox2*-hypomorphic mice, reduction of RGCs leads to hypoplastic optic nerves (Taranova et al., 2006). In order to determine whether *sox2* morphants also have optic nerve defects, we used the transgenic embryos *Tg(pou4f3:GFP)* that express GFP in a subset of RGCs and their axons (Xiao et al., 2005). RGCs are the only retinal cells to project axons outside the eye. In fact, RGC axons grow towards the optic disc, where they exit the eye to form the optic nerve. In zebrafish, axons cross at the midline, forming the optic chiasm, in order to project to appropriate neurons in the controlateral hemisphere (reviewed in Inatani, 2005). The main target of the RGC axons is the optic tectum (superior colliculus in mammals). At 3 dpf, the first axons have already reached the optic tectum and started establishing connections within the entire tectal neuropil (**Figure 3.7**). However, in *sox2* morphants, although axons reach the optic tectum at 3 dpf, significantly fewer axon arbors are observed. By 5 dpf, axon arbors are observed in *sox2* morphants, but they accommodate a smaller area when compared to control siblings (**Figure 3.7**). In order to better understand the phenotype, we performed timelapse experiments (using the *Tg(pou4f3:GFP)* embryos) between 50 and 110 hpf. In addition to a small delay, axons in *sox2* morphants are misguided and often travel outside the optic tectum (**Figure 3.8** and **Movie S1-S2** in supplementary material). This defect suggests that axon guidance is defective in *sox2* morphants. However, further studies are necessary to confirm this hypothesis.

Altogether, the results suggest that *sox2* morphants, similarly to *Sox2*-hypomorphic mice, have ocular defects, including microphthalmia, reduced number of RGCs and amacrine cells, as well as optic nerve (optic tectum) defects. These results further support our hypothesis that zebrafish is an optimal model to dissect the functions of sox2 during vertebrate development.

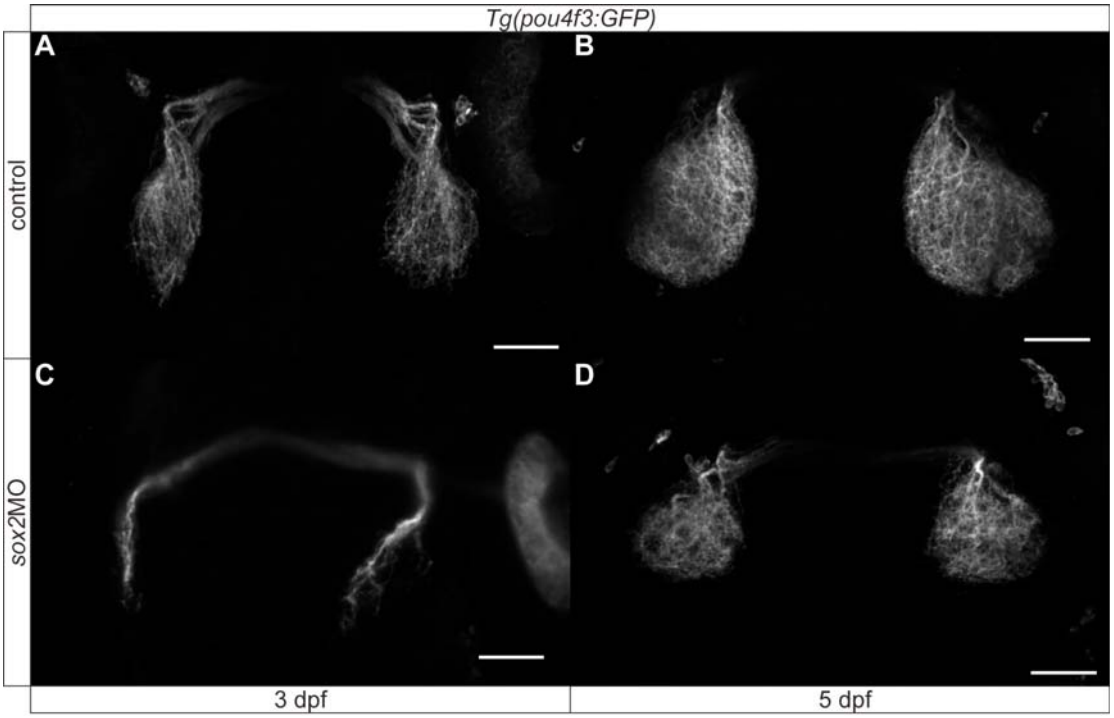

Figure 3.7 Downregulation of sox2 leads to abnormal RGC axon arborization at the optic tectum. (**A**) At 3 dpf, RGC axons reach the optic tectum and start establishing connections with the appropriate neurons. (**B**) By 5 dpf, RGC axon arbors occupy the entire tectal neuropil. (**C**) In *sox2* morphants, a delay in axon arborization is observed at 3 dpf. (**D**) By 5 dpf, axons establish connections within the optic tectum, but they occupy a smaller area in relation to control siblings. Dorsal views of *Tg(pou4f3:GFP)* embryos with anterior to the top, stages are shown at the bottom of each column, scale bars = 50 μm.

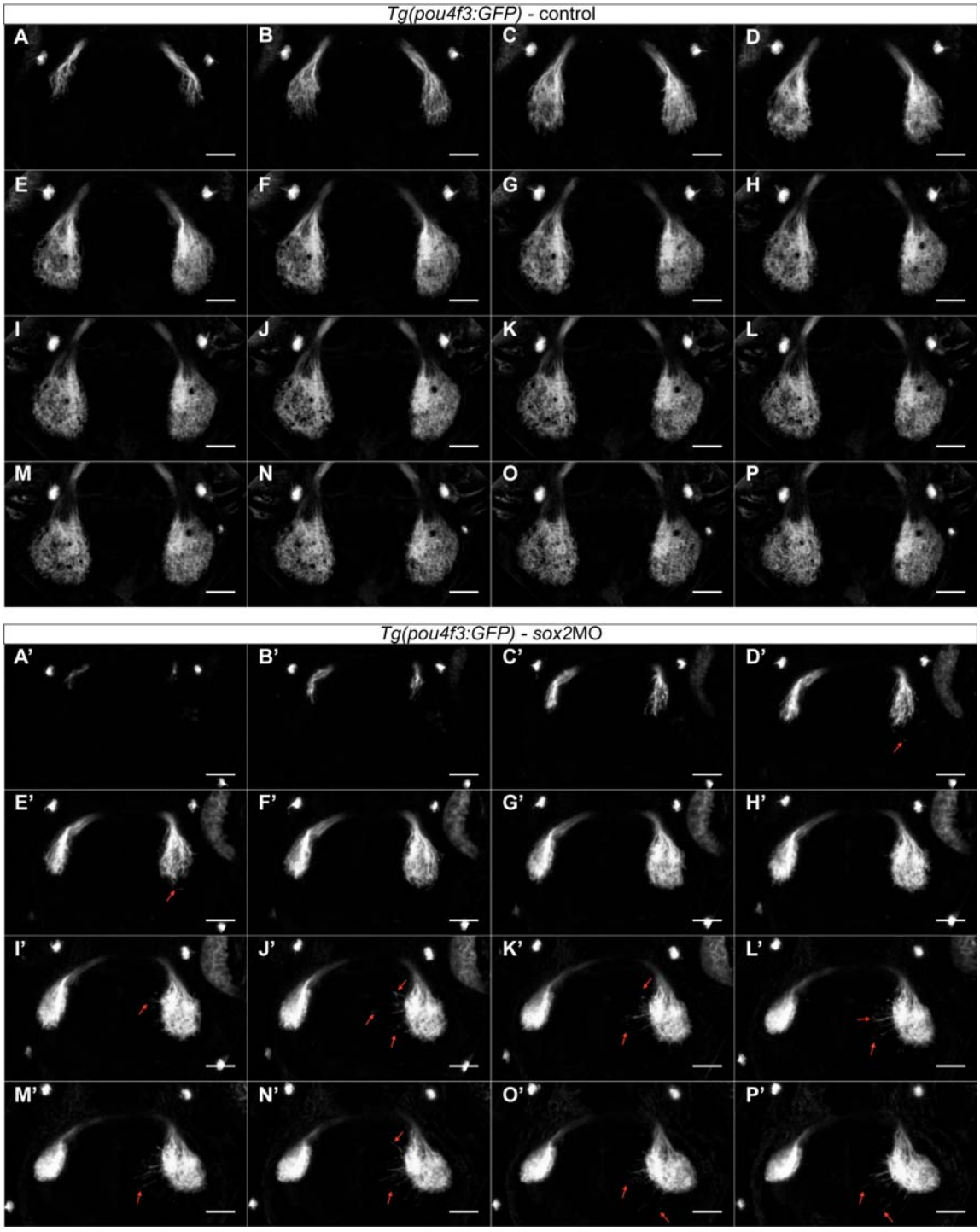

Figure 3.8 RGC axons are misguided in *sox2* morphants. Snapshots of timelapse confocal microscopy from approximately 50 hpf to 110 hpf. Images were acquired every 40 minutes, but here snapshots represent 240-minutes intervals. (**A-P**) From approximately 50 hpf, the RGC axons reach the optic tectum and start arborizing in the tectum. By the end of the timelapse (around 110 hpf) axon arbors occupy the entire

tectal neuropil. (**A'-P'**) In *sox2* morphants, a delay in the arborization is observed (compare A to C'). In addition, axon arbors occupy a smaller area within the optic tectum in relation to control embryos. Also, some axons (red arrows) exit the optic tectum suggesting an axon guidance defect. Dorsal views of *Tg(pou4f3:GFP)* embryos with anterior to the top, scale bars = 50 μm. Snapshots are from **Movie S1** (A-P) and **Movie S2** (A'-P') in supplementary material.

3.4 Downregulation of sox2 results in increased apoptosis and cell-cycle defects

The short anteroposterior body axis and small eyes observed in *sox2* morphants led us to hypothesize that downregulation of sox2 results in apoptotic and/or cell-cycle defects.

In order to investigate apoptosis in *sox2* morphants, we performed terminal deoxynucleotidyl transferase dUTP nick end labeling (TUNEL). TUNEL is a well-established assay that allows detection of fragmented DNA, a characteristic of apoptotic cells (Gavrieli et al., 1992). The TUNEL assay was performed as part of my MRes project (MRes thesis Pavlou, 2009). Downregulation of sox2 results in increased number of apoptotic cells in the lens, somites and neural tube at 28 hpf (data not shown). Later in development, at 32 hpf, the number of apoptotic cells is also increased in the fore-, mid- and hindbrain (**Figure 3.9**).

During development, surplus or damaged cells are eliminated by apoptosis (reviewed in Ravichandran, 2011; Wickman et al., 2012). This, along with the fact that correct levels of sox2 are important for the proper proliferation and differentiation of progenitor cells (Taranova et al., 2006), led us to hypothesize that the increased number of apoptotic cells is due to cell-cycle defects. In order to test this hypothesis, we performed whole mount *in situ* hybridization for two proliferation markers: *ccnd1* (*cyclin D1*) and *myca* (*myelocytomatosis oncogene a*) (MRes thesis Pavlou, 2009). Both genes are abnormally maintained in hindbrain and anterior neural tube in *sox2* morphants, in relation to control siblings (**Figure 3.9**). These results show that cell cycle is defective when sox2 is downregulated.

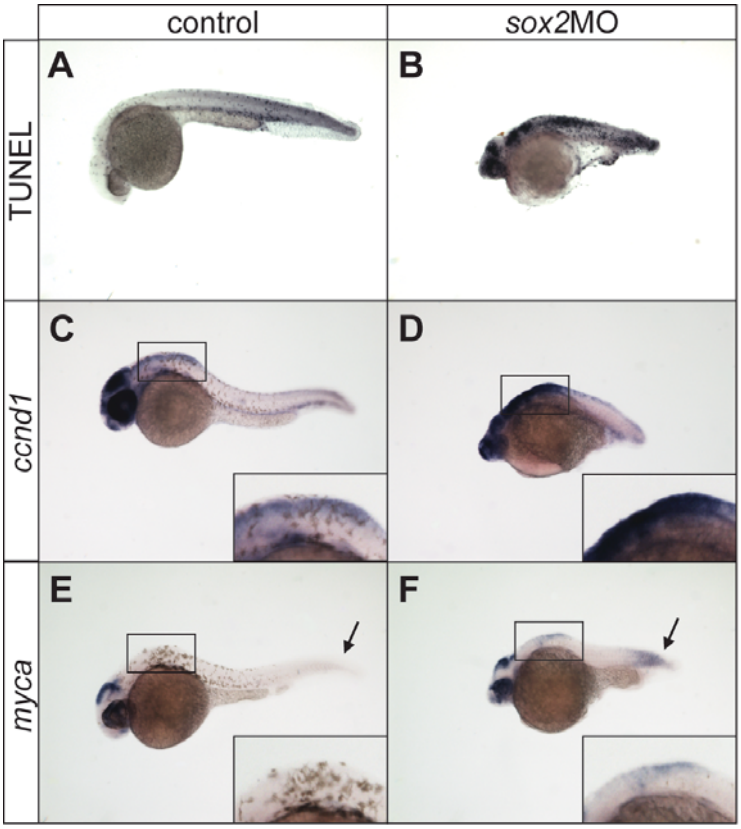

Figure 3.9 Downregulation of sox2 results in increased levels of apoptosis and impaired proliferation. (**A-B**) *sox2* morphants have increased levels of apoptosis in relation to control siblings, as shown by TUNEL assay. (**C-D**) The expression of the proliferative marker *ccnd1,* in the hindbrain, is abnormally maintained in *sox2* morphants when compared with control siblings. (**E-F**) Similarly, *myca*, another proliferative marker, is abnormally maintained in the hindbrain and tail (arrows) when sox2 is downregulated. Lateral view of 32 hpf embryos, boxes in the right corner show the hindbrain in higher magnification. Staining is seen in blue/purple, brown/black spots are pigmentation.

In order to better understand the cell-cycle defects, we performed EdU staining coupled with FACS analysis. EdU is a thymidine analogue that can integrate into the genome during DNA replication (Synthesis phase – S-phase) and is commonly used, in combination with FACS, to study the phases of cell cycle. After a 30-minutes treatment with EdU at 48 hpf, FACS analysis revealed that there is no significant difference in the percentage of cells in each phase (G0/G1 *versus* S *versus* G2/M) between the morphants and the control siblings (**Figure 3.10**). However, EdU signal in *sox2* morphants was less

intense in relation to control, suggesting that during the 30-minute incubation time, less EdU was incorporated in *sox2* morphants. This, along with the abnormal expression profiles of proliferation markers and the increased apoptosis observed in *sox2* morphants, demonstrates that downregulation of sox2 results in cell-cycle defects that in turn may result in increased apoptosis.

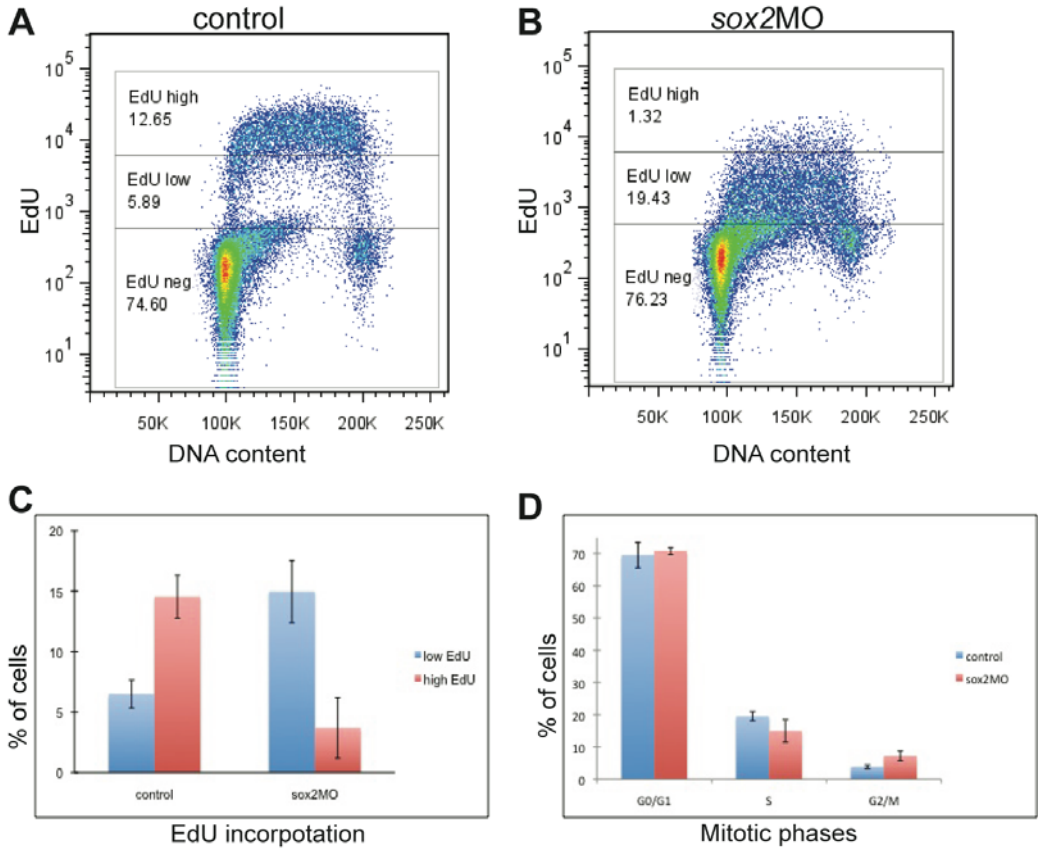

Figure 3.10 Downregulation of sox2 results in cell-cycle defects. (A-B) Flow cytometry analysis of EdU and DNA content at 48 hpf, after 30-minute EdU incubation, in control and *sox2* morphants. 'EdU high' indicates the percentage of cells where more EdU was incorporated into the genome when compared with 'EdU low'. In each sample 30000 cells were analyzed. (**C**) Average percentage of cells with low (blue bars) and high (red bars) EdU levels in control and *sox2* morphants. (**D**) Average distribution of cells in each mitotic phase. There is no significant difference in the percentage of cells in each phase between the control (blue bars) and *sox2* morphants (red bars). n=3, error bars represent ± standard error.

3.5 Conclusion

Embryos with compromised *sox2* expression have small anteroposterior axis, small eyes and die approximately 6 dpf. We also showed that *sox2* morphants have eye phenotypes that recapitulate the ones observed in human patients with *SOX2* mutations and in *Sox2*-hypomorphic mice. This suggests that the roles of sox2 are evolutionarily conserved and thus zebrafish can be used to dissect the roles of the gene during vertebrate development. In addition, *sox2* morphants have proliferation and apoptotic defects.

Chapter 4. sox2 modulates pineal neurogenesis and cell-fate determination

“Διπλοῦν ὁρῶσιν οἱ μαθόντες γράμματα”

“Those who know the letters see double [as much as those who don’t]”

Pythagoras, 570-495 BC

4.1 Introduction

The results from the sox2 screen (MRes thesis Pavlou, 2009) led us to hypothesize that sox2 has a role during the development of the zebrafish epithalamus. In agreement with our hypothesis, a patient carrying *SOX2* mutation has been reported to have a pineal cyst (Hagstrom et al., 2005) and a subset of *PAX6* patients has hypomorphic or completely absent pineal glands (Mitchell et al., 2003). Also, *pax6* is expressed in (at least some) pineal precursors and in projection neurons, one of the two cell types found in the pineal gland (Cau et al., 2008; Quillien et al., 2011). Since, *SOX2* and *PAX6* are known to work together in different aspects of development, we questioned whether sox2 is involved in the development of pineal gland.

4.2 sox2 is expressed in pineal precursors and is downregulated with differentiation

In order to gain a better insight into the role of *sox2* in the development of the pineal gland, we decided to examine the expression of sox2 within the epithalamus in more detail. The *Tg(flh:GFP)* transgenic line was used, which drives GFP expression in the presumptive pineal gland (Concha et al., 2003), in combination with whole mount immunofluorescence for sox2 and isl1. sox2 is expressed within the pineal anlage at 8 ss (**Figure 4.1** and **Movie S3** in supplementary material). From about 10 ss, pineal cells start expressing isl1, a gene expressed in pineal neurons after their final mitotic division (Masai et al., 1997). Within the post-mitotic isl1-positive cells, sox2 expression is downregulated (**Figure 4.1** and **Movie S4-S5** in supplementary material) and by 28 hpf sox2 is completely excluded from the fully differentiated pineal gland (**Figure 4.1** and **Movie S6** in supplementary material). Therefore, sox2 is expressed in pineal precursors during early development of the epithalamus and its expression is downregulated with neurogenesis. This comes in agreement with previous studies, which suggest that *sox2* is generally expressed in neuronal progenitor cells and is downregulated with differentiation (Avilion et al., 2003; Graham et al., 2003; Ferri et al., 2004; Ellis et al., 2004; Taranova et al., 2006).

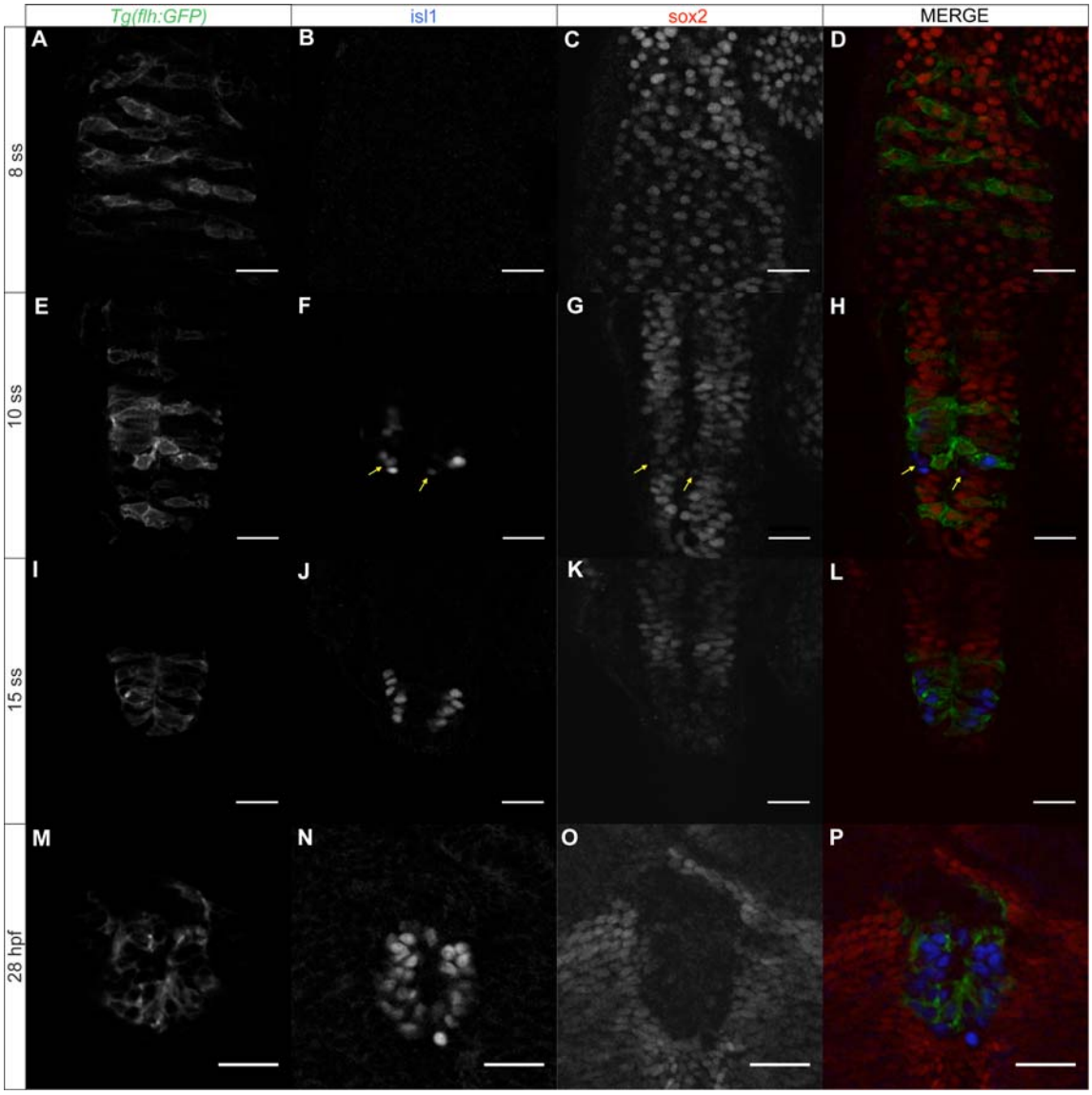

Figure 4.1 sox2 expression within the pineal gland anlage is downregulated with differentiation. (**A-D**) sox2 expression overlaps with expression of *flh*, a marker for pineal precursors, at 8 ss. (**E-L**) As pineal cells start differentiating, isl1 is upregulated where as sox2 is downregulated. Yellow arrows show cells that have both isl1 and sox2 expression at low levels. (**M-P**) sox2 is absent from the fully differentiated pineal cells. Optical sections from confocal microscopy (**Movie S3-S6** in supplementary materials show all the optical sections acquired), (A,E,I,M) GFP expression of *Tg(flh:GFP)*, marking the pineal gland anlage, (B,F,J,N) immunofluorescence for isl1, showing the differentiated pineal cells, (C,G,K,O) immunofluorescence for sox2, (D,H,L,P) merged images with *Tg(flh:GFP)* in green, isl1 in blue and sox2 in red, dorsal views with anterior to the top, developmental stages are shown at the beginning of each row, scale bars = 25 μm.

4.3 sox2 is required for the development of the pineal gland

In order to dissect the roles of sox2 in the development of the zebrafish epithalamus, we began our investigation by analyzing the development of the pineal gland in embryos with compromised *sox2* expression. Previous studies showed that the Notch signaling pathway, as well as the BMP pathway, are important for proper neurogenesis and cell-fate determination within the zebrafish pineal gland (Cau et al., 2008; Quillien et al., 2011). We hypothesized that sox2 may have similar functions during pineal gland development either by working in the same pathway(s) as Notch and/or BMP or through parallel ones.

4.3.1 sox2 inhibits neurogenesis within the pineal anlage

Correct levels of Sox2 are crucial during neurogenesis. In particular, constitutive expression of SOX2 in chick embryos results in reduced neuronal differentiation and maintenance of progenitor characteristics, such as proliferative capacity. In contrast, inhibition of SOX2 leads to premature cell-cycle exit of progenitor cells and the early onset of neuronal differentiation (Graham et al., 2003). We therefore hypothesized that downregulation of sox2 in zebrafish may result in defective neurogenesis within the pineal anlage.

To test our hypothesis, we investigated the expression profile of *isl1*, a marker for pineal cells (both photoreceptors and projection neurons). By whole mount *in situ* hybridization experiments, we showed that *isl1* is upregulated in *sox2* morphants when compared to control siblings, at all stages analyzed (28, 32 and 48 hpf) (**Figure 4.2**). We also examined *otx5* (*orthodenticle homolog 5*), which is normally expressed in the pineal gland and also in the developing parapineal organ. Similarly to *isl1*, *otx5* is expressed in a broader domain in *sox2* morphants when compared to control siblings (**Figure 4.2**). In order to quantitatively characterize the increase in neurogenesis observed in *sox2* morphants, we performed whole mount immunofluorescence against isl1, combined with confocal microscopy. By counting the number of isl1-positive cells in *sox2* morphants and control siblings, we showed that downregulation of sox2 results in a highly significant increase in the number of epiphysial neuronal cells at 24 hpf (Mann-

Whitney U test (MWU test); p-value <0.001) and 28 hpf (MWU test; p-value <0.001) (**Figure 4.2**). Particularly, control embryos have on average 38 isl1-positive cells at 24 hpf (n= 41) and 40 cells at 28 hpf (n = 48), whereas downregulation of sox2 results in approximately 50% increase in the number of cells expressing isl1: 59 cells at 24 hpf (n = 24) and 60 cells at 28 hpf (n = 44).

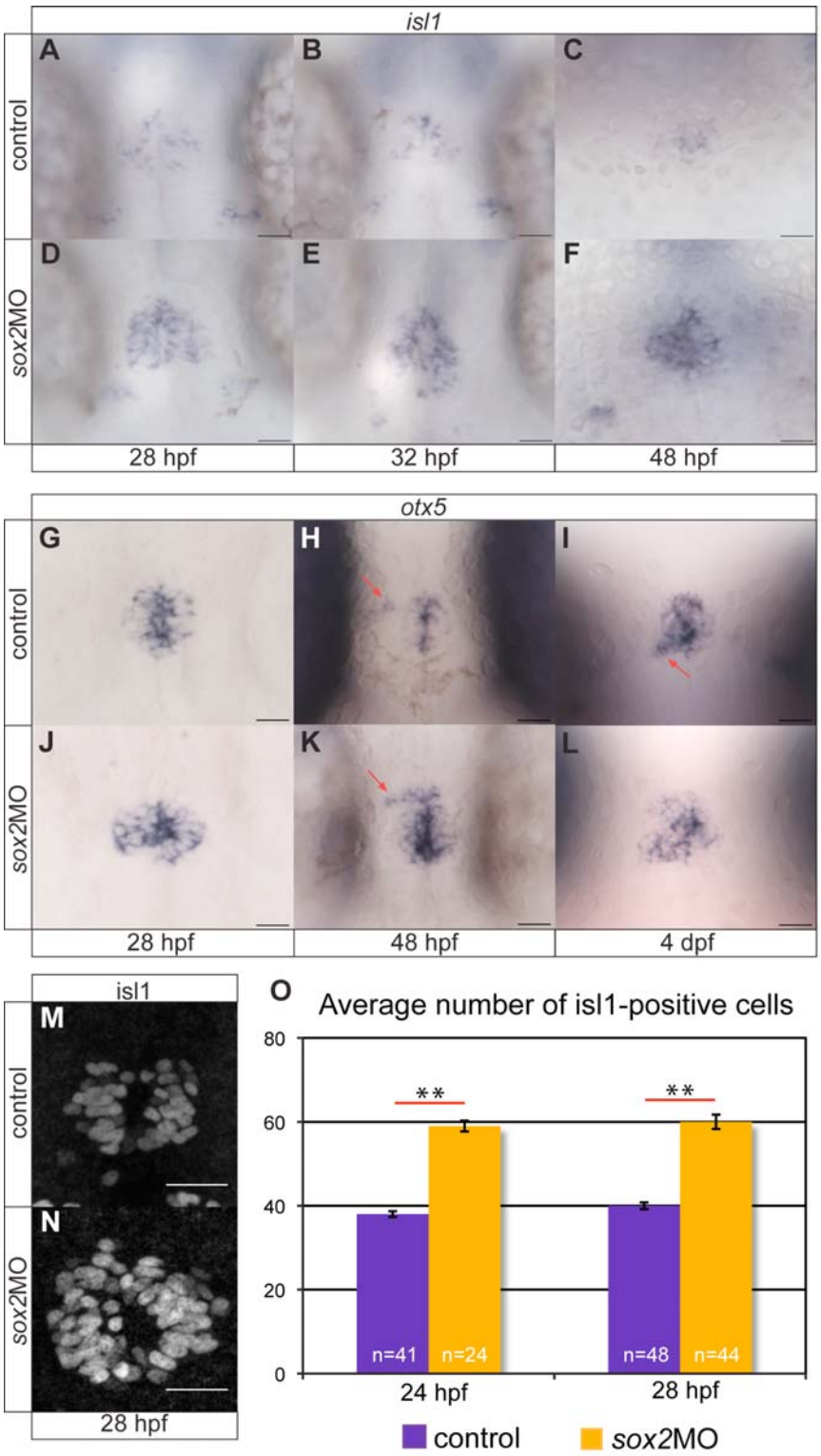

Figure 4.2 sox2 modulates neurogenesis within the pineal gland. (**A-C**) *isl1* is expressed in epiphysial neuronal cells at 28, 32 and 48 hpf. (**D-F**) Downregulation of

sox2 results in increased *isl1* expression, suggesting an increase in neurogenesis. (**G-I**) *otx5* is expressed within the pineal gland at 28 hpf. At 48 hpf and 4 dpf, parapineal cells (red arrow) are also visible as a group of *otx5*-positive cells on the left side of the pineal. (**J-L**) In *sox2* morphants, *otx5* is expressed in a broader domain within the pineal gland when compared to the control embryos. (**M-N**) Whole mount immunofluorescence using isl1 antibody confirms the increase in neurogenesis observed in *sox2* morphants. (**O**) Average number of isl1-positive cells in control (purple bar) and *sox2* morphants (orange bar), at 24 and 28 hpf. Dorsal views with anterior to the top, developmental stages are shown at the bottom of each column, (M-N) confocal maximum projections, scale bars = 25 μm, error bars represent ± standard error, ** = highly significant; MWU test; p-value <0.001.

4.3.2 sox2 controls *flh* expression at early stages

The presumptive pineal gland can be identified very early during development by the expression of *flh*. *flh* is a homeodomain-containing transcription factor that controls neurogenesis within the pineal gland by modulating the expression of two proneural genes: *ascl1a* and *neurog1* (Masai et al., 1997). In order to test whether the increase in neurogenesis observed in *sox2* morphants reflects an increase in the size of the pineal anlage, we analyzed the expression of *flh*. At early stages (3-4 ss), *flh* is detected in two domains on each side of the neural plate. As neurulation proceeds (at approximately 7-8 ss), the two *flh*-positive domains fuse to form the presumptive pineal gland (Masai et al., 1997) (**Figure 4.3**). A small delay in the fusion of the *flh*-domains is observed in *sox2* morphants, possibly due to a general delay in development: *sox2* morphants also show delayed arborization of the optic tectum (discussed in section **3.3**) and delayed parapineal and habenular formation (discussed in section **5.2.1** and **5.3**, respectively). Nevertheless, at 3-4 ss and 7-8 ss, the pineal anlage is enlarged in *sox2* morphants when compared to control siblings (**Figure 4.3**). This demonstrates that more pineal precursors are present at these stages, which in turn can explain the increase in neurogenesis observed in *sox2* morphants (as judged by the increase in isl1-positive cells). Interestingly, at 24, 28 and 32 hpf, there is no difference in the expression of *flh* between the control and *sox2* morphant siblings, as assessed by whole mount *in situ* hybridization for *flh* and GFP expression in the *Tg(flh:GFP)* transgenic embryos (**Figure 4.3**). Therefore, a second sox2-independent mechanism may exist to control *flh* expression.

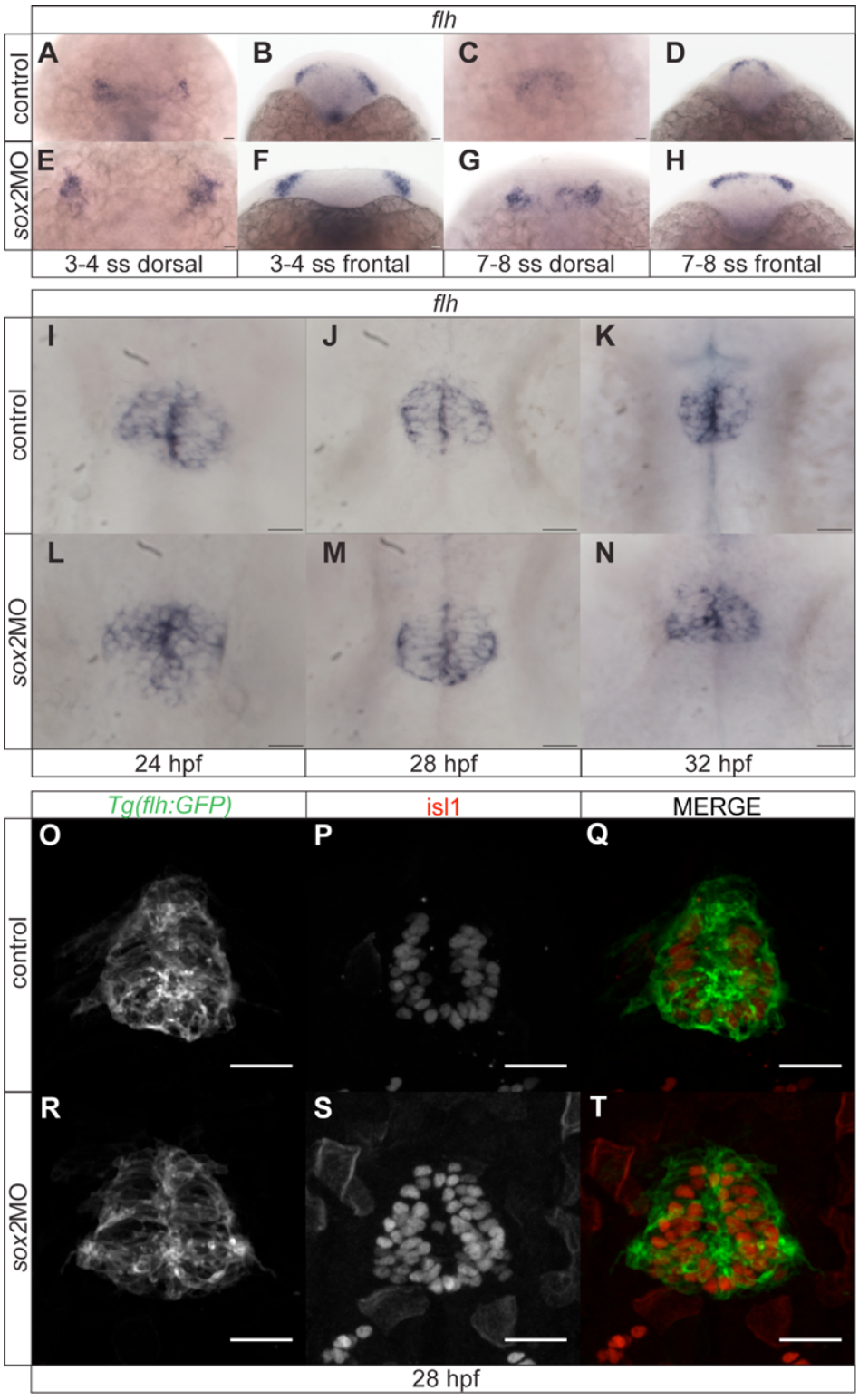

Figure 4.3 Downregulation of sox2 leads to upregulation of *flh* expression at early somite stages. (**A-D**) Whole mount *in situ* hybridization for *flh*, a marker for the

presumptive pineal gland. At 3-4 ss, two *flh*-domains are observed on either side of the neural plate (A-B). By 7-8 ss, the two domains fuse to form the presumptive pineal gland (C-D). (**E-F**) In *sox2* morphants, *flh* is expressed in broader domains in relation to control siblings at 3-4 and 7-8 ss. (**I-K**) *flh* expression persists within the pineal gland during neurogenesis. (L-M) Between 24 and 32 hpf, *flh* expression is indistinguishable between *sox2* morphant and control siblings. (**O-T**) Similarly, no difference was observed in GFP expression of the *Tg(flh:GFP)* between control and *sox2* morphant embryos at 28 hpf. isl1 was used to mark the pineal gland. (A,C,E,G,I-T) dorsal views with anterior to the top, (B,D,F,H) frontal views, developmental stages are shown at the bottom of each column, (G-L) confocal maximum projections, scale bars = 25 μm.

As mentioned above, *flh* is essential for the expression of the proneural genes *ascl1a* and *neurog1*, which in turn are important for the proper neurogenesis within the pineal anlage (Masai et al., 1997; Cau and Wilson, 2003). Since *flh* expression is abnormal at early stages in *sox2* morphants, we investigated whether *ascl1a* is also affected.

Downregulation of *ascl1a* (via morpholino injections) results in a small reduction, but not complete loss, of *isl1*-positive cells (Cau and Wilson, 2003). In contrast, *neurog1* morphants and mutants have normal *isl1* expression in the pineal gland, suggesting that loss of *neurog1* expression alone does not affect neurogenesis. Simultaneous downregulation of both *ascl1a* and *neurog1* results in severely reduced or absent *isl1* expression in the pineal gland (Cau and Wilson, 2003). Since downregulation of *ascl1a* has a greater effect on neurogenesis, we examined its expression profile in embryos with compromised *sox2* expression. At early stages (20 ss and 24 hpf), *ascl1a* expression is normal in *sox2* morphants (**Figure 4.4**). A small but robust increase in *ascl1a* expression is observed in *sox2* morphants at 28 hpf, suggesting that sox2 normally inhibits *ascl1a* expression (**Figure 4.4**). However, the number of isl1-positive cells is greatly increased in *sox2* morphants from 24 hpf (when *ascl1a* expression is normal) (**Figure 4.2**), suggesting that sox2 controls neurogenesis, at least in part, through a different pathway.

Cau and Wilson (2003) demonstrated that *flh* controls the expression of other genes involved in neurogenesis and/or cell-fate determination (such as the *delta* genes, *otx5* and *flh* itself), independently of *ascl1a*. It is therefore likely that sox2 modulates

pineal neurogenesis by controlling the expression of *flh* and therefore the expression of at least some downstream genes. In agreement with this hypothesis, we showed that *otx5* is upregulated in *sox2* morphants (**Figure 4.2**). Downregulation of *otx5* results in a decreased number of photoreceptors, but further studies are required to determine whether this decrease reflects a decrease in neurogenesis or whether it reflects a defect in cell-fate determination (Gamse et al., 2002; Appelbaum et al., 2005; Pierce et al., 2008). Therefore, further investigation is required to elucidate the complete pathway(s) modulating pineal neurogenesis.

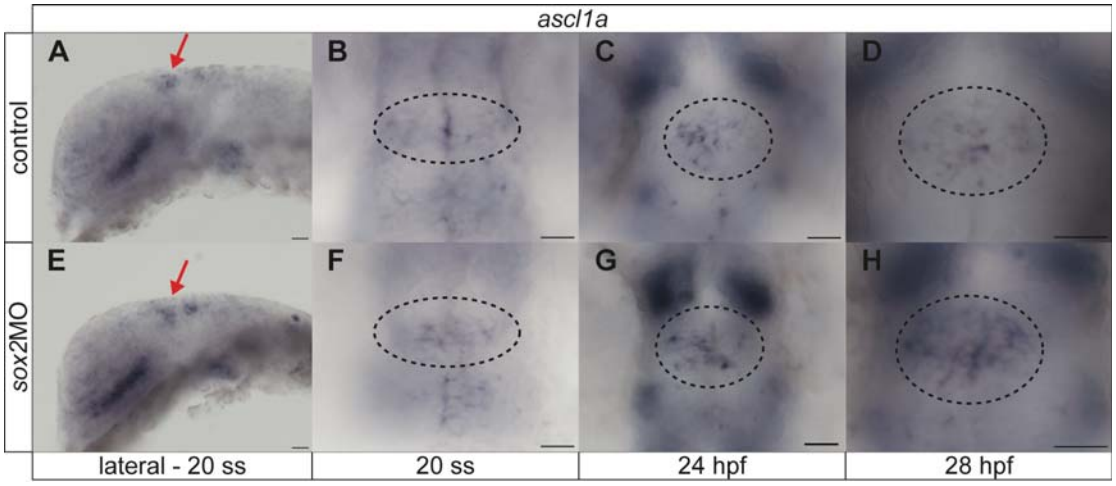

Figure 4.4 sox2 downregulation results in normal expression of *ascl1a* at early stages and slight upregulation at 28 hpf. (**A-D**) *ascl1a* is expressed within the presumptive pineal gland (red arrows and circles) from approximately 20 ss. (**E-H**) *sox2* morphants have normal *ascl1a* expression at 20 ss and 24 hpf. *ascl1a* expression is upregulated at 28 hpf. (A, E) Lateral views with anterior to the left, (B-D, F-H) dorsal views with anterior to the top, developmental stages are shown at the bottom of each column, scale bars = 25 μm.

4.3.3 sox2 controls the specification of pineal photoreceptors

The pineal gland consists of only two cell types: the photoreceptors and the projection neurons (Masai et al., 1997) (**Figure 1.1**). Since downregulation of sox2 results in increased neurogenesis, we questioned whether both cell types are affected.

aanat2 is specifically expressed in the pineal photoreceptors (Gothilf et al., 2002). Whole mount *in situ* hybridization experiments show that the expression of

aanat2 is highly increased in *sox2* morphants in relation to control siblings, at 24, 28, 32 and 48 hpf (**Figure 4.5**). In order to quantitatively characterize this defect, we used the transgenic line *Tg(aanat2:GFP)* that expresses GFP in the pineal photoreceptors (Gothilf et al., 2002; Cau et al., 2008). The transgenic embryos were counterstained using isl1 antibody, to confirm that the GFP-positive cells are within the pineal gland. Moreover, GFP expression of the *Tg(aanat2:GFP)* embryos is both nuclear and cytoplasmic and thus it is very difficult to distinguish and count single cells. Therefore for the quantifications, the cells expressing both isl1 and GFP were counted as photoreceptors. In control embryos, there are on average 16 photoreceptors at 28 hpf (n=41). However, downregulation of sox2 results in almost 2 fold increase in the number of photoreceptors (29 photoreceptors, n=28) (**Figure 4.5**). The difference in the number of photoreceptors between the control and *sox2* morphants is highly significant (MWU test; p-value <0.001), suggesting that sox2 normally inhibits the photoreceptor identity.

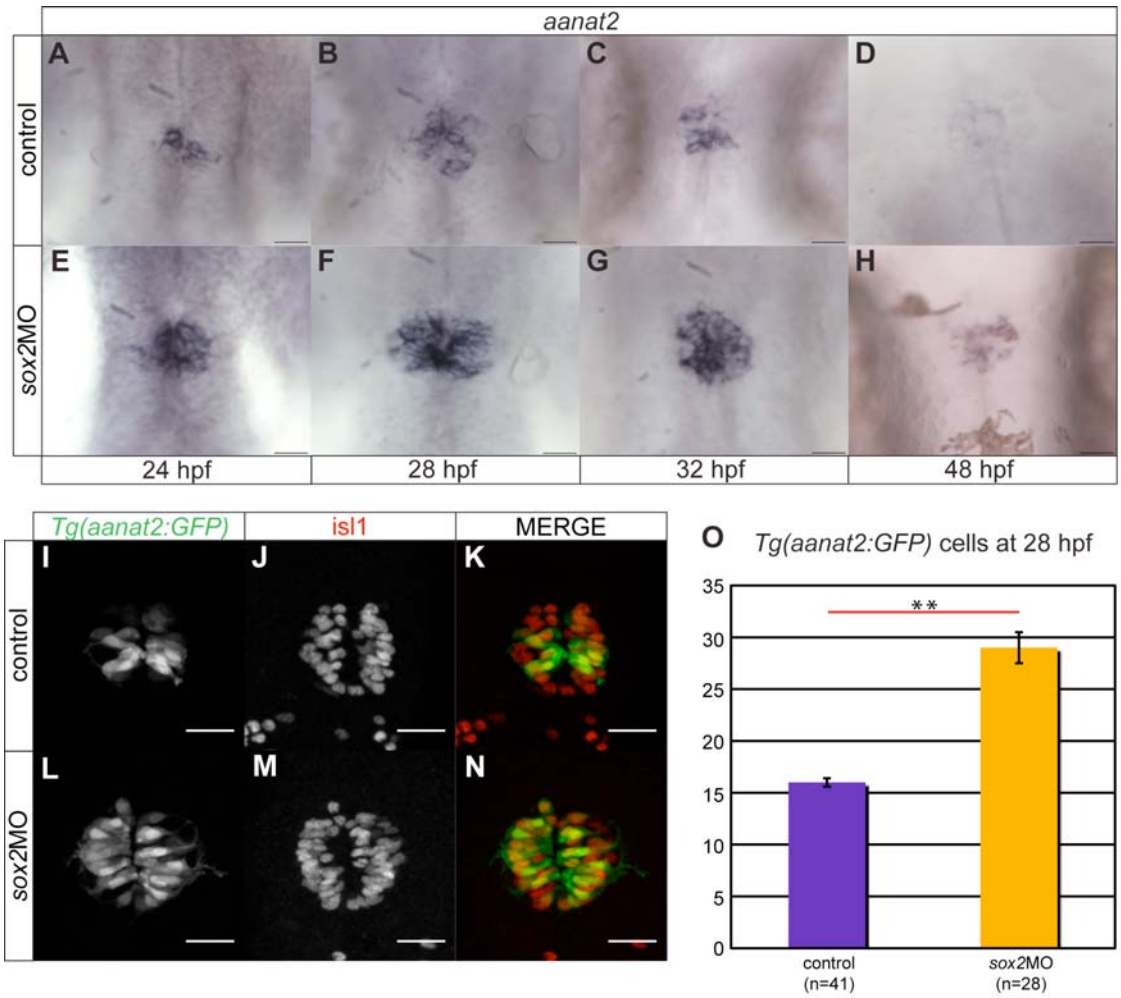

Figure 4.5 sox2 negatively regulates the photoreceptor cell fate. (**A-D**) *aanat2* is expressed in the photoreceptors between 24 and 48 hpf, as detected by whole mount *in situ* hybridization. (**E-H**) At all stages analyzed, an upregulation of *aanat2* expression is observed in *sox2* morphants when compared to control siblings. (**I-K**) *Tg(aanat2:GFP)* drives GFP expression in the pineal photoreceptors. Whole mount immunofluorescence for isl1 was performed to confirm the localization of the signal. (**L-N**) Downregulation results in increased number of cells expressing GFP. (**O**) Average number of GFP-positive cells (that are also isl1-positive) in control (purple bar) and *sox2* morphants (orange bar). Dorsal views with anterior to the top, (I-N) confocal maximum projections, scale bars = 25 μm, error bars represent ± standard error, ** = highly significant; MWU test; p-value <0.001.

Downregulation of sox2 results in increased neurogenesis and increased number of photoreceptors. Are the projection neurons also affected in *sox2* morphants? To address this question, we analyzed the expression pattern of *pax6*, a gene expressed in

the projection neurons (Masai et al., 1997). In zebrafish, there are two known *pax6* paralogs: *pax6a* and *pax6b* (Kleinjan et al., 2008). The two genes have overlapping but divergent expression profiles. Within the brain, *pax6a* is expressed in a broad domain including the diencephalon, whereas *pax6b* expression is restricted to the pineal gland (Kleinjan et al., 2008). *pax6b* was therefore selected for whole mount *in situ* hybridization and as shown in **Figure 4.6** there is no difference in the number of *pax6b*-positive cells between the control and *sox2* morphant embryos, at all stages analyzed. Notably, *pax6b*-positive cells are more dispersed in *sox2* morphants when compared to control siblings at 48 hpf. We hypothesize that this is a secondary result of the increase in the size of the pineal gland. The projection neurons are found lateral to the medially located photoreceptors. Since downregulation of sox2 results in an increased number of photoreceptors in the middle of the pineal gland, we hypothesize that the projection neurons are forced to move more laterally.

In addition to the projection neurons, *pax6* is expressed in a number of pineal progenitor cells (Cau et al., 2008; Quillien et al., 2011) and thus it is not a suitable marker for projection neurons. The transgenic line *Tg(elavl3:GFP)* was therefore used to confirm the previous findings (**Figure 4.6**). As with the photoreceptors, the transgenic embryos were counterstained with isl1 as a marker for the pineal cells and also to facilitate counting of single cells. The average number of projection neurons in controls is 13 (n=23) and in *sox2* morphants is 14 (n=23), at 28 hpf. This difference is not statistically significant (MWU test; p-value = 0.058), suggesting that sox2 does not control the projection neuron identity.

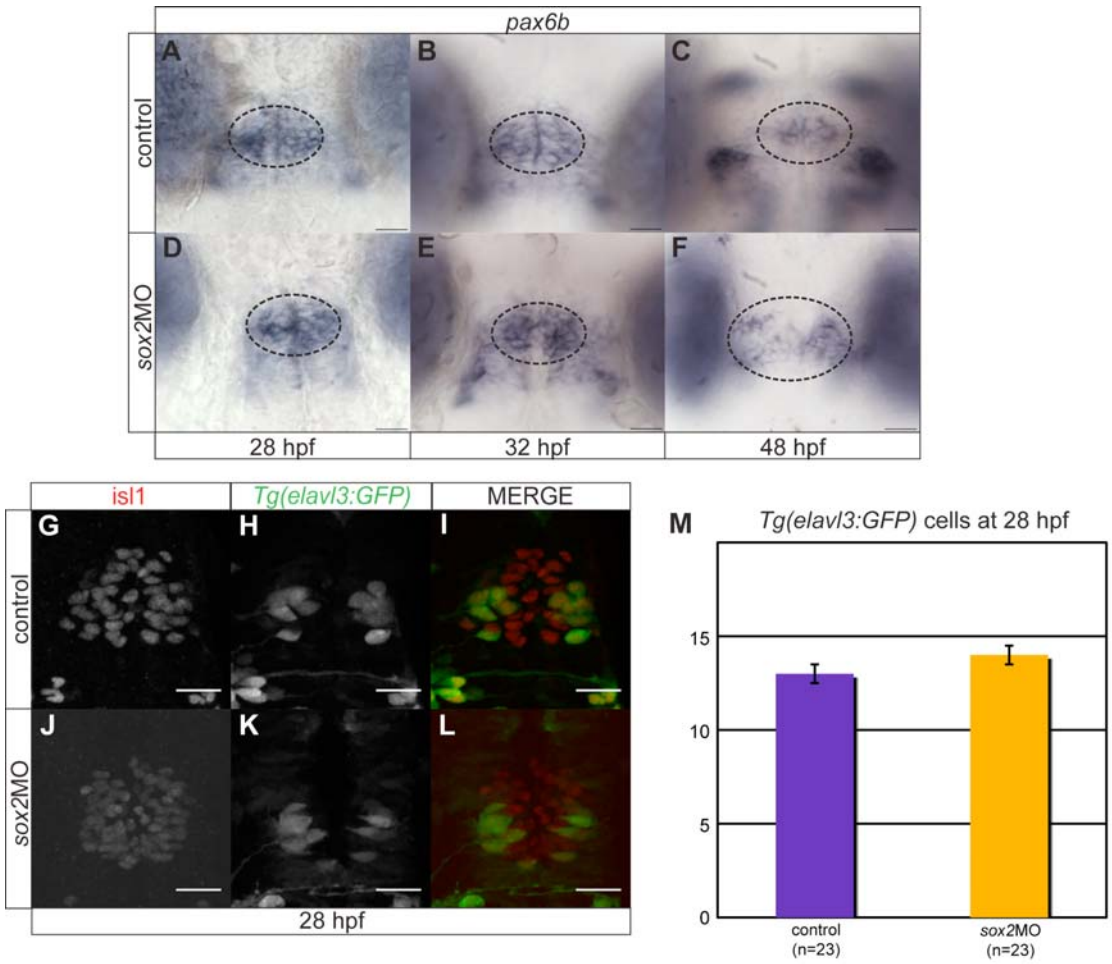

Figure 4.6 sox2 does not control the number of projection neurons within the pineal gland. (**A-C**) *pax6b* is expressed in the projection neurons and a subset of pineal precursors from 28 hpf to 48 hpf. (**D-F**) Downregulation of sox2 does not affect the number of *pax6b*-positive cells. However, at 48 hpf, *pax6b* is expressed in a broader domain in *sox2* morphants when compared to control siblings. (**G-L**) *Tg(elavl3:GFP)* drive GFP expression specifically in the projection neurons, at 28 hpf. Embryos were counterstained with isl1 antibody to confirm the pineal localization. (**M**) The average number of projection neurons in controls (purple bar) and *sox2* morphants (orange bar) does not significantly differ. Dorsal views with anterior to the top, (G-L) confocal maximum projections, scale bars = 25 μm, error bars represent ± standard error, MWU test; p-value = 0.058.

4.3.4 sox2 works in parallel with Notch in regulating neurogenesis and cell-fate determination within the pineal gland

Previous studies suggest that the Notch pathway is essential for the proper development of the pineal gland. In particular, Cau et al. (2008) showed that Notch

normally inhibits neurogenesis within the pineal anlage by downregulating the proneural genes *ascl1a* and *neurog1*. They also showed that downregulation of Notch results in increased number of projection neurons, whereas the number of photoreceptors remains unaffected. We showed that sox2 also negatively regulates neurogenesis, raising the question whether sox2 works in the same pathway as Notch. We also showed that sox2 specifically controls the number of photoreceptors and therefore complements Notch function in cell-fate specification.

To test whether sox2 and Notch work in the same pathway, we checked Notch activity when sox2 was compromised and *vice versa*. For this, we used a transgenic reporter line for Notch activity: *Tg(csl:venus)* (unpublished line, obtained from Dr. Gering, Nottingham). *Tg(csl:venus)* drives venus expression within a subset of isl1-positive pineal cells (**Figure 4.7**). Notably, only about 50% of venus-positive cells are also isl1-positive. In order to confirm the specificity of the transgenic line, embryos were treated with DAPT, a γ-secretase inhibitor known to inhibit Notch activity (Geling et al., 2002), at 9 hpf. Since DAPT is dissolved in DMSO, DMSO-treated embryos were used as controls. As shown in **Figure 4.7**, DAPT treatment results in fewer venus-positive cells, suggesting that venus expression in these transgenics reflects Notch activity.

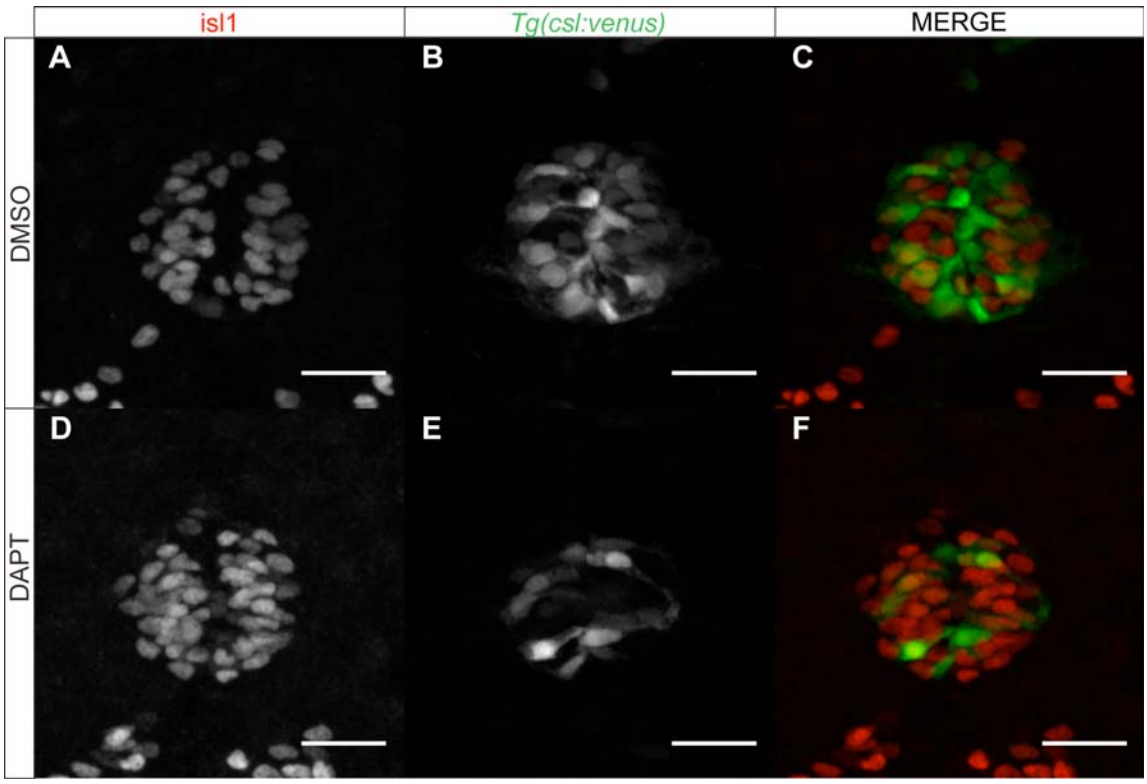

Figure 4.7 *Tg(csl:venus)* is a Notch-activity reporter transgenic line. (**A-C**) *Tg(csl:venus)* drives venus expression within the pineal gland anlage, as marked by isl1 antibody staining, at 28 hpf. Control embryos were treated with DMSO. (**D-F**) Treatment with DAPT, a γ-secretase inhibitor known to inhibit Notch activity, significantly reduces venus expression within the pineal gland. Confocal maximum projections of dorsal views with anterior to the top, 28 hpf embryos, scale bars = 25 μm.

To test the hypothesis that sox2 and Notch work in the same pathway in regulating neurogenesis, we assessed the number of venus-positive cells in control and morpholino injected *Tg(csl:venus)* embryos. We found that downregulation of sox2 does not affect the number of venus-positive cells within the pineal gland (**Figure 4.8**). Particularly, we quantified the total number of venus-positive cells, as well as the number of cells expressing both venus and isl1 ($venus^{+}/isl1^{+}$) and the cells that express only venus ($venus^{+}/isl1^{-}$). At 24 hpf, there is no significant difference between the control and morphant embryos in any of the three categories (MWU test; p-value = 1). At 28 hpf, although the total number of venus-positive cells is unaffected (MWU test; p-value = 1), there is a small but significant decrease in the number of $venus^{+}/isl1^{-}$ cells

(MWU test; p-value = 0.035). As shown previously, downregulation of sox2 results in increased isl1-positive cells (**Figure 4.2**). We therefore hypothesize that there are fewer venus^{+}/isl1^{-} cells because there are fewer isl1-negative cells in *sox2* morphants.

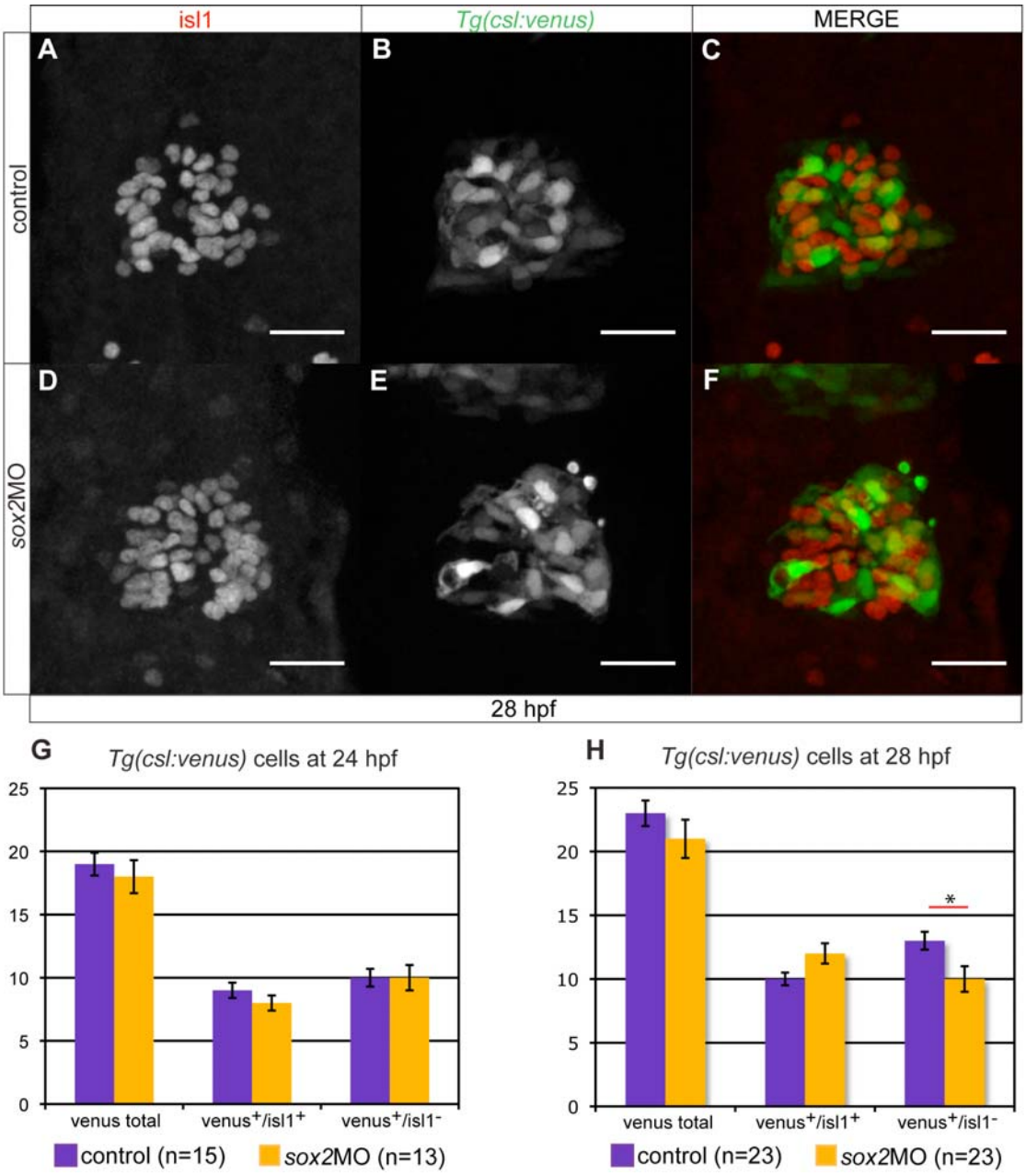

Figure 4.8 Downregulation of sox2 does not affect Notch activity within the pineal gland. (**A-C**) *Tg(csl:venus)* is a Notch reporter line and drives venus expression within the pineal gland, which is marked by isl1 antibody staining. Only about 50% of venus-expressing cells are positive for isl1. (**D-F**) Microinjections with *sox2* morpholinos have

no effect on Notch activity, as shown by venus expression. (**G**) The average number of venus-positive cells in control and *sox2* morphant *Tg(csl:venus)* embryos at 24 hpf. The average number of cells that express both venus and isl1 ($venus^{+}/isl1^{+}$) or venus only ($venus^{+}/isl1^{-}$), as well as the total number of venus-positive cells (venus total) was calculated in control and *sox2* morphants. There is no significant difference in any of the three categories. (**H**) The average number of venus-positive cells (venus total, $venus^{+}/isl1^{+}$, $venus^{+}/isl^{-}$) in control and *sox2* morphants at 28 hpf. Downregulation of sox2 results in a small but significant decrease in the number of $venus^{+}/isl1^{-}$ cells. However, the overall number of venus cells is unaffected. Confocal maximum projections, dorsal views with anterior to the top, scale bars = 25 μm, error bars represent ± standard error, * = significant; MWU test; p-value < 0.05.

Since downregulation of sox2 does not affect the total number of Notch-positive cells, we can conclude that sox2 does not function upstream of Notch in regulating neurogenesis within the pineal gland. However, in order to better understand the relationship between sox2 and Notch, we analyzed *sox2* expression in embryos with disrupted Notch activity.

Downregulation of Notch was achieved via DAPT treatments at 9 hpf. Whole mount *in situ* hybridizations for *sox2* in DMSO-treated control and DAPT-treated embryos showed that the overall sox2 expression in the neural tube and CNS is reduced when Notch is compromised (**Figure 4.9**).

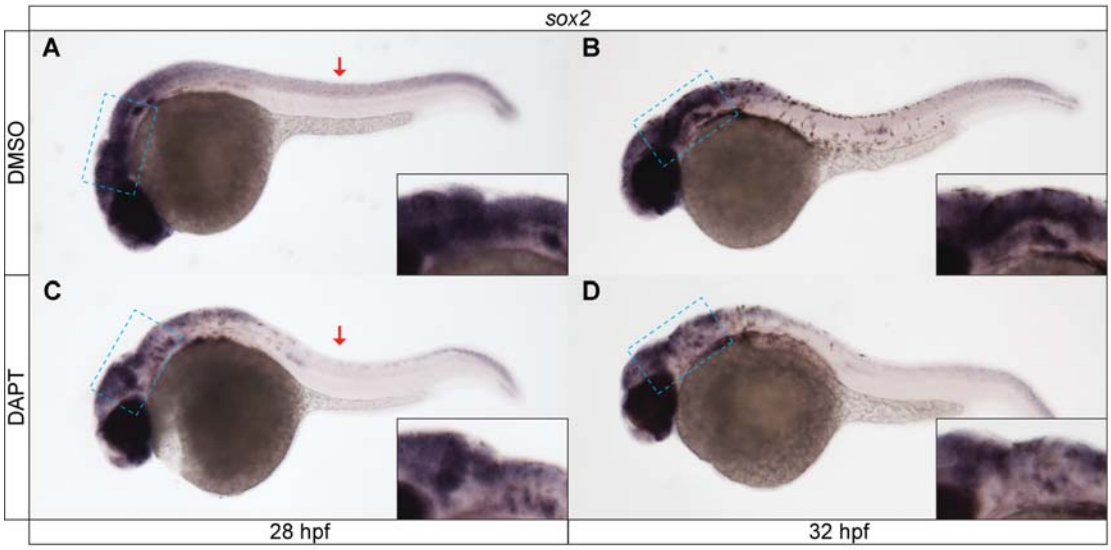

Figure 4.9 Inhibition of Notch activity leads to downregulation of *sox2*. (**A-B**) *sox2* is highly expressed in the brain (blue rectangles) and neural tube (red arrow) at 28 hpf.

Neural tube expression is downregulated at 32 hpf. (**C-D**) DAPT-treatment leads to downregulation of *sox2* expression. Lateral views, developmental stages are shown in the bottom of each column, rectangles in the right corner show the brain in higher magnification.

In order to get a better insight into the relationship of Notch and sox2 within the developing epithalamus, *Tg(flh:GFP)* embryos were used since they drive GFP expression in the presumptive pineal gland allowing visualization of the structure. The embryos were also labelled with isl1, a marker for post-mitotic pineal cells. Control embryos were treated with DMSO. In agreement with previous findings (Cau et al., 2008), DAPT-treated embryos have more isl1-positive cells when compared to control embryos at 15 ss (**Figure 4.10**), confirming that correct levels of Notch activity are crucial for proper neurogenesis. Similar to control embryos, in DAPT-treated embryos sox2 is expressed throughout the presumptive pineal gland but is downregulated in cells expressing isl1 (differentiated cells) (**Figure 4.10** and **Movie S7** in supplementary material). Since there are more isl1-positive cells when Notch is compromised, sox2 is downregulated in a broader domain in relation to controls.

Upregulation of Notch was achieved using the double transgenics: *Tg(hs:Gal4)*; *Tg(UAS:Notch-intra)*. The embryos were heat-shocked at 10 ss to activate the transgene that results in ectopic expression of the *Notch1a* intracellular domain fused with six myc epitopes (Scheer and Campos-Ortega, 1999; Scheer et al., 2001). Whole mount immunofluorescence using an antibody against myc was then performed at 20 ss to confirm the activation of the transgene and thus the upregulation of Notch activity. As previously shown (Cau et al., 2008), ectopic expression of Notch results in decreased neurogenesis, as judged by the decreased number of isl1-positive cells. When Notch is upregulated, sox2 is still expressed in the precursor cells but not in the isl1 differentiated cells (**Figure 4.11** and **Movie S8** in supplementary material). Since there are fewer isl1 cells, sox2 is expressed in a broader domain when compared to control siblings.

To conclude, both downregulation and upregulation of Notch affects the expression of sox2 in the epithalamus. At this stage, we cannot conclude whether the differences in sox2 expression are a direct effect of the compromised Notch pathway. Nevertheless, the data suggest that sox2 expression is tightly linked with differentiation:

sox2 is always expressed in the pineal progenitor cells, but not in the isl1-differentiated pineal cells.

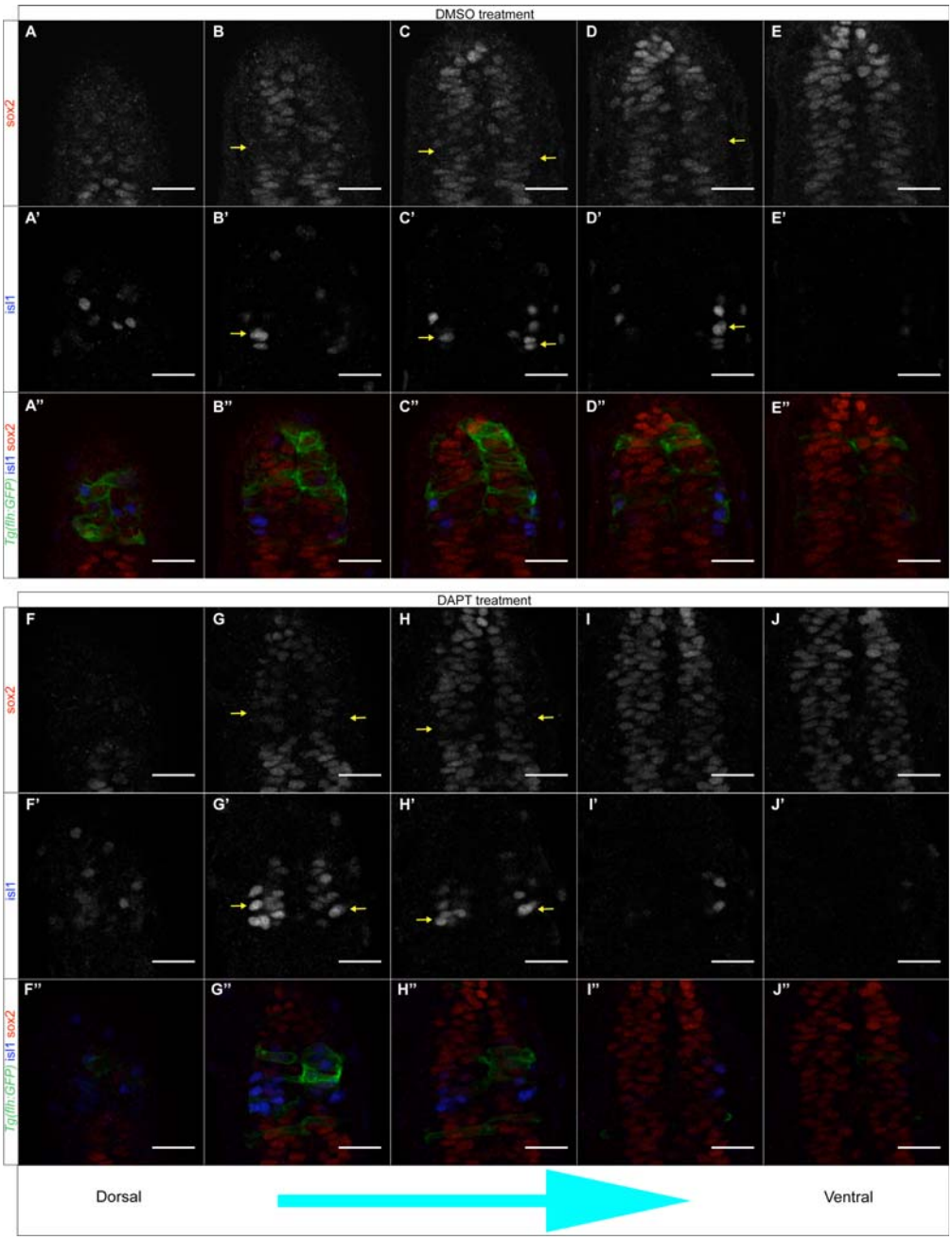

Figure 4.10 Downregulation of Notch results in more isl1^{+}/sox2^{-} cells in relation to controls. (**A-E''**) sox2 is expressed throughout the pineal anlage and is downregulated in isl1-positive cells, in DMSO-treated control embryos at 15 ss. (A-E) sox2 expression, (A'-E') isl1 expression, (A''-E'') merged images of sox2, isl1 and *Tg(flh:GFP)* that

marks the pineal anlage. (**F-J''**) DAPT treatment results in increased number of cells expressing isl1 (F'-J'). sox2 (F-J) is still expressed in the undifferentiated pineal precursor cells (green in F''-J'') but not in the differentiated isl1-positive cells (F'-J'). Since there are more isl1-positive cells, sox2 is downregulated in a broader domain in relation to controls. Series of optical sections from dorsal (first column) to ventral (5th column) obtained using confocal microscope (**Movie S7** in supplementary data show all the optical sections acquired). Anterior to the top, scale bars = 25 μm, yellow arrows show cells, in which sox2 is downregulated and isl1 is upregulated.

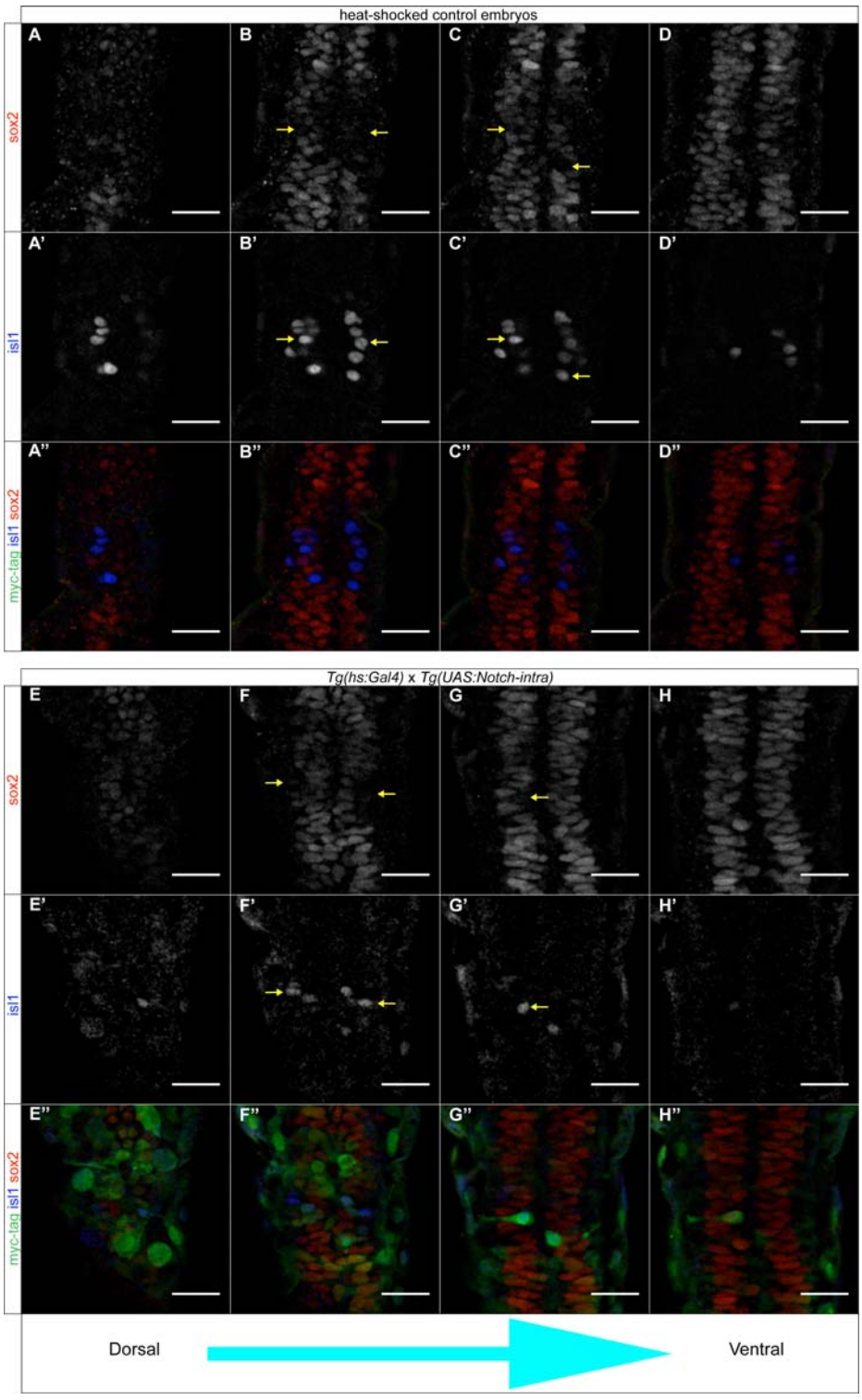

Figure 4.11 Upregulation of Notch results in a broader domain of sox2 expression at 20 ss. (**A-D''**) sox2 is expressed throughout the pineal anlage and is downregulated in isl1-positive cells, in heat-shocked control embryos, at 20 ss. (A-D) sox2 expression,

(A'-D') isl1 expression, (A''-D'') merged images of sox2, isl1 and myc-tag, showing that heat-shock did not activate the *Notch1a* intracellular domain. (**E-H''**) Heat-shock of the double transgenics *Tg(hs:Gal4)*; *Tg(UAS:Notch-intra)* results in fewer isl1-positive cells (E'-H') and therefore sox2 is expressed in a broader domain (E-H). (E''-H'') Merged images of sox2, isl1 and myc-tag, showing the activation of the transgene and thus the upregulation of Notch. Series of optical sections from dorsal (first column) to ventral (4th column) obtained using confocal microscope (**Movie S8** in supplementary data show all the optical sections acquired). Anterior to the top, scale bars = 25 μm, yellow arrows show cells, in which sox2 is downregulated and isl1 is upregulated.

The data suggest that Notch and sox2 have complementary roles in cell-fate specification, by specifically inhibiting the projection neuron and photoreceptor identity, respectively. To get a better understanding, we decided to downregulate both simultaneously and examine their effect on the two cell types within the pineal gland. We first analyzed the phenotypes by whole mount *in sit*u hybridization for *isl1* (all neurons within the epiphysis), *aanat2* (photoreceptors) and *pax6b* (projection neurons and progenitor cells) (**Figure 4.12**). Downregulation of either Notch or sox2 results in an increase in neurogenesis, as marked by the number of *isl1*-positive cells. Downregulation of both simultaneously results in a greater increase in the number of *isl1* cells than downregulation of Notch or sox2 separately, suggesting that they control neurogenesis (at least partly) through different pathways. In contrast, the number of photoreceptors is increased only when sox2 is downregulated, whereas the number of projection neurons is increased only when Notch is compromised. This suggests that sox2 and Notch have complementary roles in controlling cell-fate determination within the pineal gland.

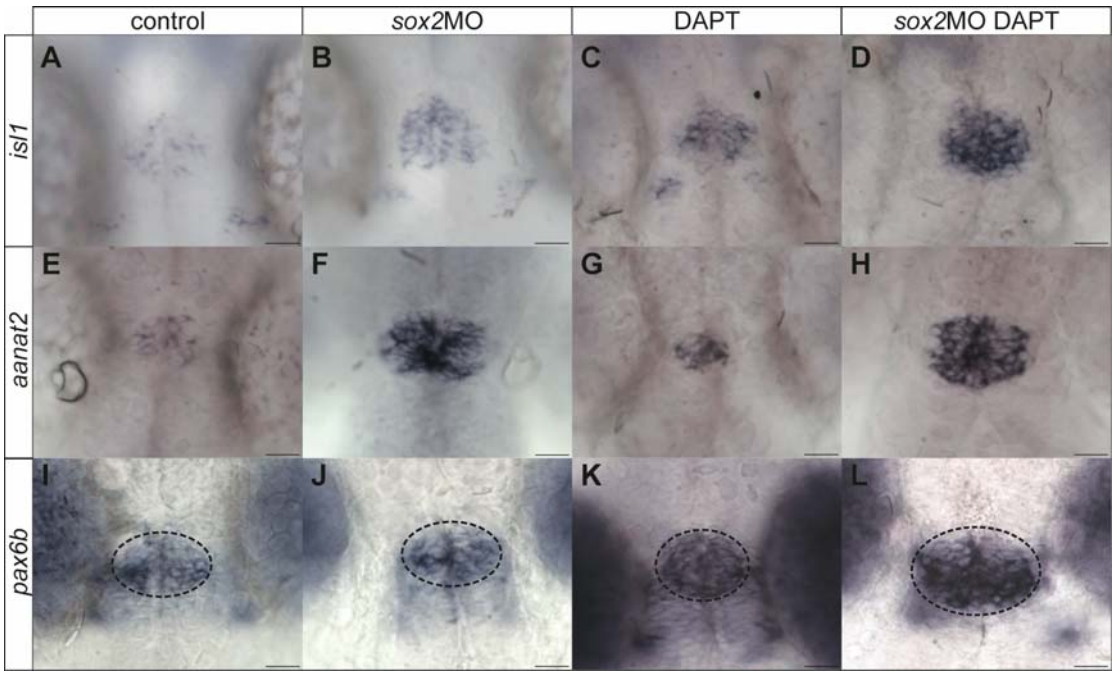

Figure 4.12 sox2 and Notch work in parallel to control neurogenesis and have complementary roles in cell-fate determination within the pineal gland. (**A-D**) The number of pineal cells (*isl1*-positive cells) is increased in *sox2* morphants (B) and in DAPT-treated (Notch inhibitor) embryos (C) in relation to controls (A). A greater increase is observed when both sox2 and Notch are downregulated (D). (**E-H**) Expression of *aanat2* in the photoreceptors is upregulated in *sox2* morphants (F), but remains unaffected in DAPT-treated embryos (G). Downregulation of both sox2 and Notch (H) results in an upregulation of *aanat2* expression, comparable to the one observed in *sox2* morphants. (**I-L**) The expression of the projection neuron marker *pax6b* is unaffected in *sox2* morphants (J), but increased in DAPT-treated embryos (K) and in embryos where both Notch and sox2 are downregulated (L). Dorsal views of 28 hpf embryos, with anterior to the top, scale bars = 25 μm.

In order to quantitatively characterize our previous findings, we repeated the experiment using the transgenic lines *Tg(elavl3:GFP)* and *Tg(aanat2:GFP)*, in combination with whole mount immunofluorescence for isl1. Since DAPT is dissolved in DMSO, we first examined whether DMSO affects neurogenesis. As shown in **Figure 4.13**, the average number of isl1-positive cells in control and *sox2* morphants is not affected by DMSO treatment (MWU test; p-value = 1). However, the average number of isl1-positive cells in *sox2* morphants at 28 hpf (60 isl1 cells) is significantly increased when compared to control embryos (40 isl1 cells), according to MWU test (p-value <

0.001). DAPT treatment also significantly increases neurogenesis (55 isl1 cells, MWU test; p-value < 0.001). Notably, there is a small, but significant difference in the number of isl1 cells between the *sox2* morphants treated with DMSO and DAPT-treated embryos (MWU test; p-value = 0.0035). Interestingly, simultaneous downregulation of sox2 and Notch has a synergistic effect on neurogenesis. In particular, the number of isl1-positive cells in *sox2* morphants treated with DAPT (84 cells) is greater than the one expected from the sum of the individual downregulations (expected number of cells: 75 when calculated based on untreated controls or 74 when calculated based on the DMSO-treated controls; calculations are discussed in section **2.16.4**). According to the chi-square test and the absolute standardized residual values, the difference between observed and expected values of *sox2*MO/DAPT embryos is statistically significant (based on untreated controls: p-value = 1.14e-07; absolute standardized residual = 7.3, whereas based on DMSO-treated controls: p-value = 9.815e-10; absolute standardized residual = 8.19).

As discussed above, sox2 and Notch also regulate cell-fate determination within the pineal gland, where sox2 specifically controls the number of photoreceptors and Notch controls the number of projection neurons. We confirmed these results by analyzing GFP-positive cells in *Tg(aanat2:GFP)* and *Tg(elavl3:GFP)* embryos. As before, embryos were counterstained with isl1 to facilitate counting of single cells and only cells that were positive for both GFP and isl1 were counted.

sox2 morphants treated with DMSO have fewer photoreceptors when compared to untreated morphant embryos; 23 photoreceptors in *sox2*MO/DMSO and 29 cells in untreated *sox2*MO (MWU test; p-value = 0.01). Nevertheless, DMSO treated *sox2* morphants have significantly more photoreceptors than control DMSO-treated embryos (23 cells in *sox2*MO/DMSO and 14 cells in DMSO control embryos, MWU test; p-value < 0.001). In contrast, treatment with DAPT does not alter the number of photoreceptors in relation to DMSO-treated (14 photoreceptors in both DAPT and DMSO control embryos, MWU test; p-value = 1) or untreated controls (16 photoreceptors in untreated embryos, MWU test; p-value = 0.35). Simultaneous downregulation of Notch and sox2, results in an increased number of GFP embryos at levels similar to downregulation of

sox2 alone (23 cells in *sox2*MO/DMSO and 26 in *sox2*MO/DAPT, MWU test; p-value = 0.82) (**Figure 4.13**). These results show that sox2, but not Notch, is involved in the specification of pineal photoreceptors.

sox2 morphants have on average 14 projection neurons, which is similar to control embryos (13 neurons). DMSO treatment results in a small, but significant increase in the number of projection neurons in *sox2* morphants (17 neurons in *sox2*MO/DMSO and 14 in *sox2*MO, MWU test; p-value = 0.02). In contrast, downregulation of Notch results in almost 2 fold increase in the projection neurons (24 neurons in DAPT-treated and 14 neurons in DMSO-treated embryos, MWU test; p-value < 0.001). Downregulation of both sox2 and Notch results in increased projection neurons, at level comparable to DAPT treatment alone (27 neurons in *sox2*MO/DAPT and 24 neurons in DAPT-treated embryos, MWU test; p-value = 0.087) (**Figure 4.13**).

As discussed above, simultaneous downregulation of sox2 and Notch has a synergistic effect on neurogenesis, as judged by the number of isl1-positive cells. To test whether sox2 and Notch also act synergistically in controlling cell-fate determination, we performed a chi-square test using the observed and expected numbers of *aanat2*- and *elavl3*- positive cells (photoreceptors and projection neurons respectively, calculations are discussed in section **2.16.4**). We found that there is no statistically significant difference between the observed and expected number of photoreceptors (chi-square test; p-value = 0.81 based on untreated controls and p-value = 0.2 based on DMSO-treated controls) or projection neurons (chi-square test; p-value = 0.39 based on untreated controls and p-value = 0.99 based on DMSO-treated controls).

In conclusion, the data suggest that sox2 and Notch synergize for the regulation of pineal neurogenesis. Also, they complement each other in cell-fate determination of the pineal photoreceptors and projection neurons.

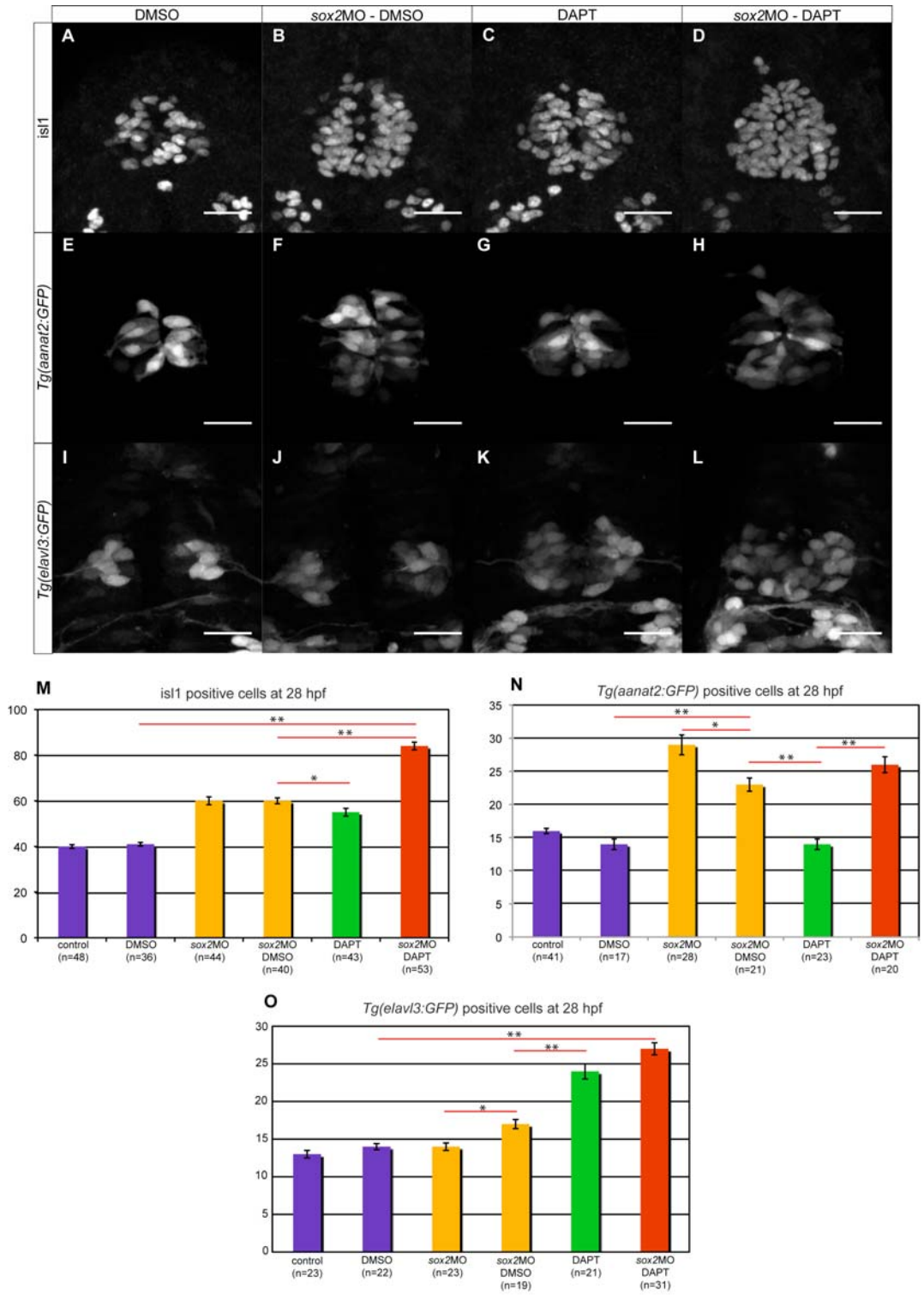

Figure 4.13 sox2 complements Notch in modulating neurogenesis and cell-fate determination within the pineal gland. (**A-D**) The number of epiphysial neuronal cells (isl1-positive cells) is increased in *sox2* morphants (B) and in DAPT-treated embryos

(C), when compared to DMSO-treated controls (A). A synergistic effect is observed when both sox2 and Notch are downregulated (D). (**E-H**) *Tg(aanat2:GFP)* transgene drives GFP expression in the pineal photoreceptors, in DMSO-treated controls (E). The number of GFP-positive cells is increased in *sox2* morphants (F), but remains unaffected in DAPT-treated embryos (G). Downregulation of both sox2 and Notch results in an upregulation of GFP expression (H), comparable to the one observed in *sox2* morphants. (**I-L**) *Tg(elavl3:GFP)* expresses GFP in projection neurons. There is no difference in the number of GFP-positive cells in *sox2* morphants (J) when compared to DMSO-treated controls (I). Downregulation of Notch alone (K) or simultaneously with sox2 (L) results in a similar increase in GFP expression. (**M-O**) The average number of isl1-positive cells (M), photoreceptors (N) and projection neurons (O) in untreated controls, DMSO-treated controls, untreated *sox2* morphants, DMSO-treated *sox2* morphants, DAPT-treated embryos and DAPT-treated *sox2* morphants. Confocal maximum projections of dorsal views with anterior to the top, 28 hpf embryos, scale bars = 25 μm, error bars represent ± standard error, * = significant; MWU test; p-value < 0.05, ** = highly significant; MWU test; p-value < 0.001.

4.3.5 sox2 controls the photoreceptor identity independently of BMP signaling

The zebrafish pineal gland has two cell types: the photoreceptors and the projection neurons. Before the start of this project, Cau et al. (2008) showed that Notch negatively regulates the specification of projection neurons and they suggested that a second mechanism must exist to control the photoreceptor cell fate. Our data suggests that sox2 is part of this second mechanism, since downregulation of sox2 results in increased number of photoreceptors. However, Quillien and colleagues (2011) showed that BMP promotes photoreceptor specification. We therefore decided to investigate the possible interaction(s) between sox2 and BMP signaling.

Three possibilities can explain the defects observed when either sox2 or BMP signaling are compromised: a) sox2 normally inhibits BMP activity that in turn promotes photoreceptors specification and/or b) BMP negatively regulates sox2 that inhibits the photoreceptors identity or c) sox2 and BMP work in two independent pathways in which sox2 inhibits, whereas BMP promotes the photoreceptors identity. To address these, we analyzed sox2 expression within the epithalamus when BMP activity was compromised and *vice versa*.

Dorsomorphin, a drug known to inhibit BMP activity (Yu et al., 2007), was used in order to investigate whether sox2 expression is controlled by BMP. Embryos were

treated with three different concentrations of dorsomorphin (30 μM, 40 μM and 50 μM) at 6 hpf and allowed to develop to the desired stage. As shown in **Figure 4.14**, treatment with any of the three dosages of dorsomorphin results in similar dorsalization phenotypes.

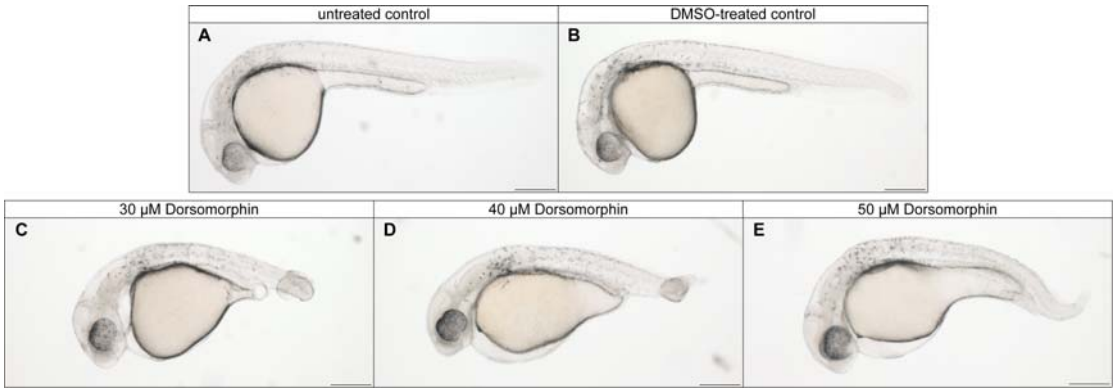

Figure 4.14 Dorsomorphin treatment leads to dorsalization phenotype. (**A**) Control embryos at 30 hpf. (**B**) DMSO-treatment has no phenotypic effects. (**C-E**) Treatment with 30 μM (C), 40 μM (D) and 50 μM (E) dorsomorphin reasults in similar phenotypes, which include tail abnormalities. Lateral views of 30 hpf embryos with anterior to the left, scale bars = 250 μm.

In order to test our hypothesis that sox2 and BMP may work in the same pathway, we performed whole mount immunofluorescence for sox2 and isl1, in DMSO-treated and dorsomorphin-treated embryos (**Figure 4.15** and **Movie S9** in supplementary material). No difference in the expression of sox2 was detected between the control and 40 μM dorsomorphin-treated embryos at 15 ss: sox2 is expressed in the pineal precursors and is downregulated with differentiation. All three concentrations of dorsomorphin (30 μM, 40 μM and 50 μM) give the same results (data not shown).

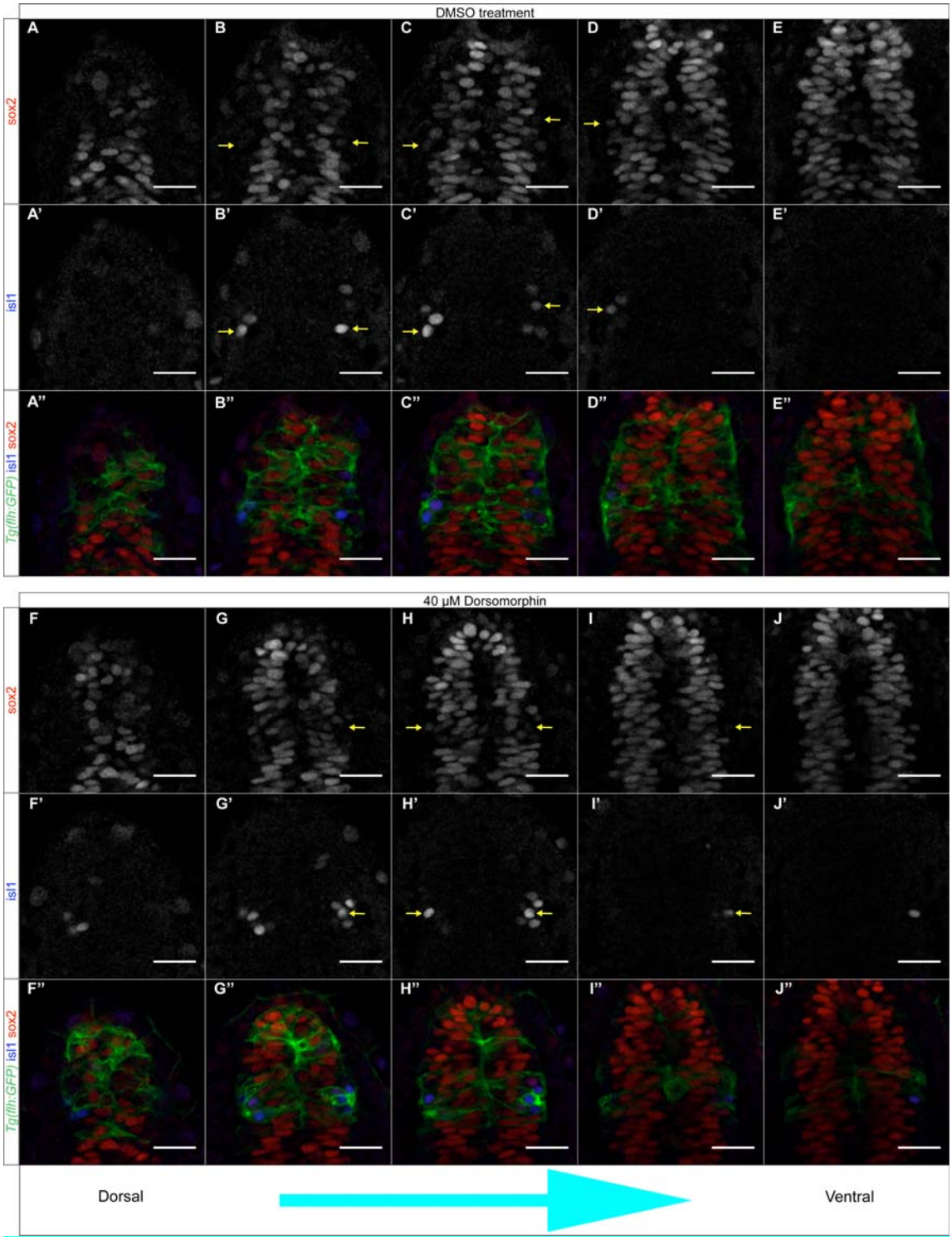

Figure 4.15 Downregulation of BMP does not affect sox2 expression at 15 ss. (**A-E’’**) sox2 is expressed throughout the pineal anlage and is downregulated in isl1-positive cells, in DMSO-treated control embryos. (A-E) sox2 expression, (A’-E’) isl1 expression,

(A''-E'') merged images of sox2, isl1 and *Tg(flh:GFP)*, showing the presumptive pineal gland. (**F-J''**) Dorsomorphin treatment (40 μM) does not affect sox2 expression at 15 ss. sox2 is expressed in the pineal precursors and is downregulated with differentiation (as shown by isl1-positive cells). (F-J) sox2 expression, (F'-J') isl1 expression, (F''-J'') merged images of sox2, isl1 and *Tg(flh:GFP)*. Series of optical sections from dorsal (first column) to ventral (5th column) obtained using confocal microscope (**Movie S9** in supplementary data show all the optical sections acquired). Anterior to the top, scale bars = 25 μm, yellow arrows show cells, in which sox2 is downregulated and isl1 is upregulated.

In order to investigate whether BMP activity is disrupted in *sox2* morphants, we used a BMP reporter line: *Tg(BRE:GFP)* (Collery and Link, 2011). We microinjected *sox2* morpholinos into *Tg(BRE:GFP)* embryos and counted the number of GFP-positive cells at 24 and 28 hpf (**Figure 4.16**). There was no significant difference in the number of GFP-positive cells between control and *sox2* morphant siblings, at 24 hpf (MWU test; p-value = 0.597). However, later in development (at 28 hpf), a small but significant increase in the cells expressing GFP was observed when sox2 was downregulated (MWU test; p-value < 0.001). This suggests that BMP activity is disrupted in *sox2* morphants.

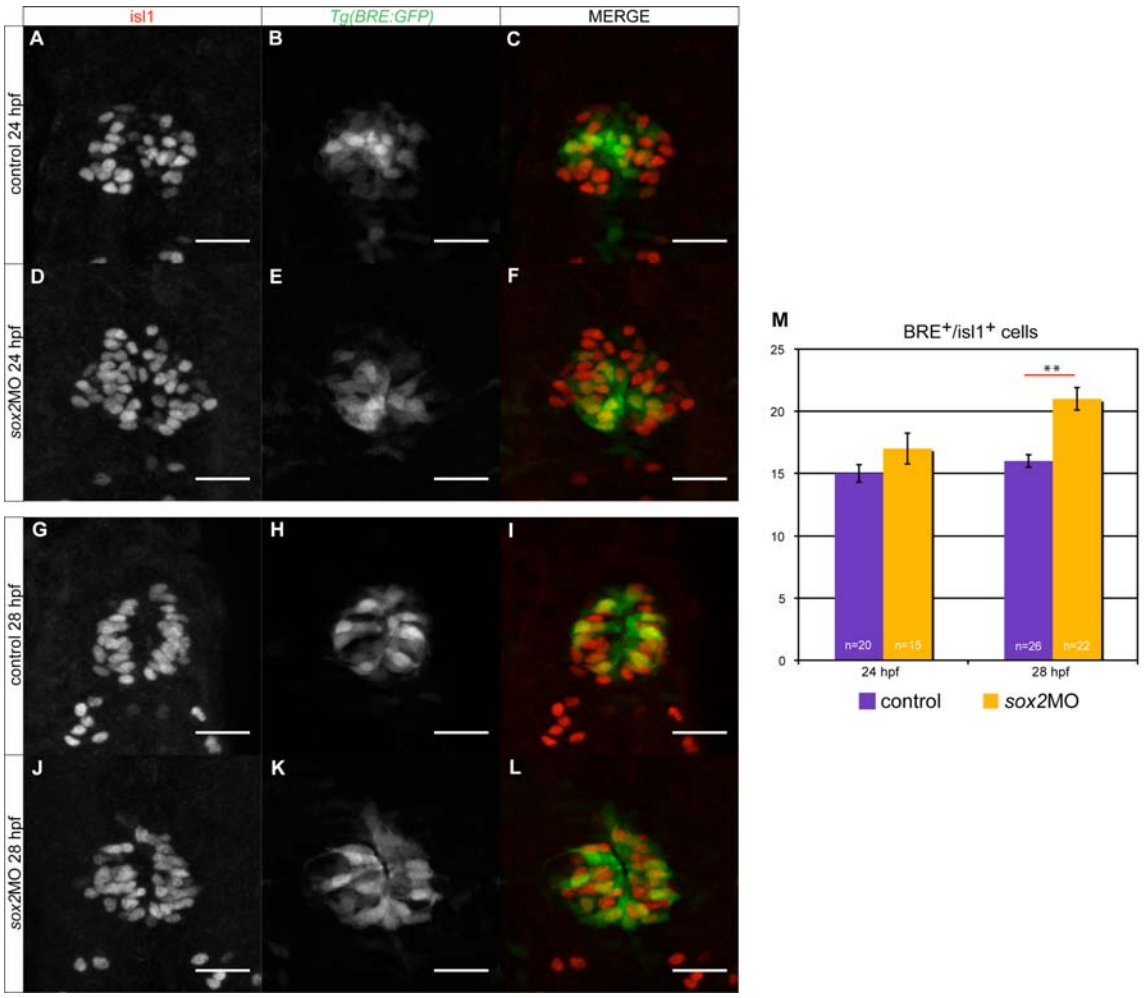

Figure 4.16 Downregulation of sox2 results in increased BMP activity at 28 hpf. (**A-F**) *Tg(BRE:GFP)* is a BMP reporter line. At 24 hpf, there is no difference in the number of cells expressing GFP in control and *sox2* morphant siblings. isl1 was used as a marker for the pineal gland. (**G-L**) At 28 hpf, GFP expression is upregulated in *sox2* morphants when compared to control siblings. (**M**) Average number of cells expressing both GFP and isl1, in *Tg(BRE:GFP)* control (purple bar) and *sox2* morphants (orange bar). Confocal maximum projections of dorsal views with anterior to the top, scale bars = 25 μm, error bars represent ± standard error, ** = highly significant; MWU test; p-value < 0.001.

Quillien et al. (2011) showed that BMP is active within the pineal anlage, by both whole mount *in situ* hybridization for *bmp2a* and immunofluorescence for Psmad1/5/8, from about 14 hpf. Moreover, we showed that *Tg(BRE:GFP)* transgenics express GFP in pineal cells, as marked by isl1 antibody staining. The position of cells positive for BMP suggests that BMP is active within (at least) a subset of photoreceptors

(**Figure 4.17**), although no double staining has been performed to date to confirm the localization of BMP. In agreement with this, BMP is cell-autonomously required to promote photoreceptors identity (Quillien et al., 2011). As discussed previously, downregulation of sox2 results in an increase in the number of photoreceptors. Therefore, these data give rise to a critical question: is the increased in photoreceptors observed in *sox2* morphants due to upregulation of BMP or is the increased number of photoreceptors responsible for the increased number of cells expressing BMP? In order to answer this, we investigated whether at 24 hpf (when the number of BMP-positive cells is unaffected) the number of photoreceptors is increased in *sox2* morphants. Interestingly, the number of GFP-positive cells in *Tg(aanat2:GFP)* is higher in *sox2* morphants (26 photoreceptors, n = 25) when compared to control siblings (14 photoreceptors, n = 26) (MWU test; p-value < 0.001) (**Figure 4.17**). Since the increase in the number of photoreceptors occurs before the upregulation of BMP in the pineal gland of *sox2* morphants, we conclude that sox2 inhibits the photoreceptors identity independently of BMP. In addition, the increase in the number of photoreceptors observed in *sox2* morphants is higher than the increase in BMP-positive cells. The small increase in the number of BMP-positive cells in *sox2* morphants may be a consequence of the overall increase in the number of photoreceptors, which are cells competent to express BMP.

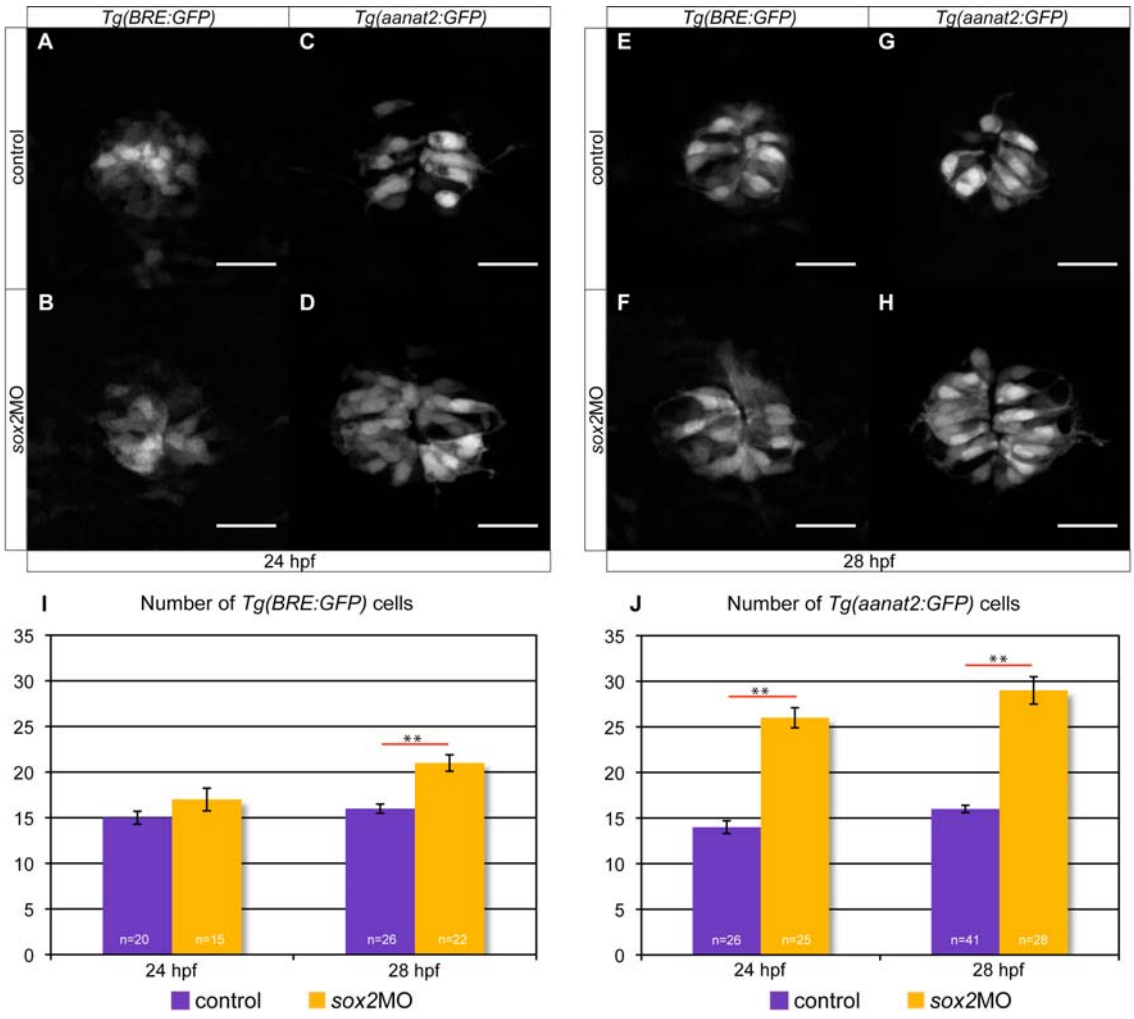

Figure 4.17 sox2 controls the photoreceptor identity independently of BMP. (**A-B**) Downregulation of sox2 does not affect the number of GFP-expressing cells in *Tg(BRE:GFP)* embryos at 24 hpf. (**C-D**) In contrast, GFP-positive cells in *Tg(aanat2:GFP) sox2* morphants are highly increased in relation to control siblings, at 24 hpf. (**E-H**) At 28 hpf, downregulation of *sox2* results in increased GFP-positive cells in both *Tg(BRE:GFP)* (E-F) and *Tg(aanat2:GFP)* (G-H). (**I**) The average number of GFP/isl1-positive cells in *Tg(BRE:GFP)* embryos that reflects the average number of epiphysial cells with BMP activity. There is no significant difference at 24 hpf, but a small and significant increase is observed at 28 hpf between the controls (purple bars) and *sox2* morphants (orange bars). (**J**) The average number of GFP/isl1-positive cells in *Tg(aanat2:GFP)* embryos that represents the average number of photoreceptors. *sox2* morphants show a highly significant increase in the number of photoreceptors in relation to controls, at both 24 and 28 hpf. Confocal maximum projections of dorsal views with anterior to the top, scale bars = 25 µm, error bars represent ± standard error, ** = highly significant; MWU test; p-value < 0.001.

4.4 Conclusion

sox2 is expressed in pineal precursors and is downregulated with differentiation. Downregulation of sox2 results in increased pineal neurogenesis, possibly due to the abnormal expression of *flh* and its downstream genes. We also demonstrated that sox2 and Notch act synergistically in modulating neurogenesis. In addition, sox2 is important for the proper cell-fate determination within the pineal gland, where it specifically inhibits the photoreceptor fate, independently of the BMP pathway.

Chapter 5. Correct levels of sox2 are required for proper establishment of epithalamic asymmetries

“Πάθει μάθος”

“[There is] learning in suffering/experience”

Aeschylus, 525-456 BC

5.1 Introduction

We showed that neurogenesis and cell-fate determination within the pineal gland are controlled by sox2. Since sox2 is expressed throughout the presumptive epithalamus, we hypothesized that disruption of its expression may also affect parapineal organ and habenular development.

5.2 sox2 is important for the proper specification and migration of parapineal cells

5.2.1 Downregulation of sox2 leads to aberrantly positioned parapineal cells

In order to investigate our hypothesis that sox2 may be involved in the development of the parapineal organ, we analyzed the expression profile of *otx5*, a gene expressed in both the pineal and the parapineal. During early development of the pineal complex, *otx5* is expressed only within the pineal gland in control and *sox2* morphant embryos (**Figure 5.1**). At 48 hpf, a group of *otx5*-positive cells (the parapineal cells) start migrating from the anterior part of the pineal gland towards the left. At 4 dpf, the parapineal organ is apparent on the left and posterior side of the brain in control embryos. In a subset of *sox2* morphants, the parapineal cells are abnormally located on the right side, suggesting that downregulation of sox2 affects the placement of the parapineal organ.

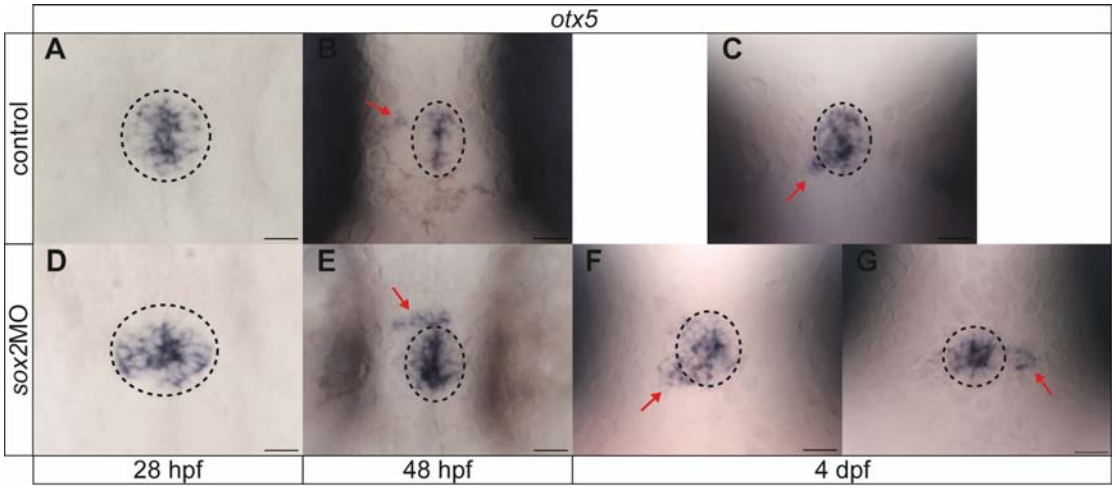

Figure 5.1 A subset of *sox2* morphants have abnormally positioned parapineal organs. (**A-C**) In control embryos, *otx5* is expressed within the pineal gland (circles) at 28 hpf. At 48 hpf, parapineal cells (red arrows) emerge and start migrating towards the left. By 4 dpf, the parapineal organ is at its final position on the left, posterior side of the pineal gland. (**D-G**) A subset of *sox2* morphants have right-sided parapineal organs (G). Dorsal views with anterior to the top, circles = pineal gland, red arrows = parapineal cells, scale bars = 25 μm.

To obtain a better understanding of the phenotype, we performed whole mount *in situ* hybridizations for *gfi1ab*, which is specifically expressed in parapineal cells (**Figure 5.2**). In control embryos, *gfi1ab* is detectable from 48 hpf in a group of cells on the left side of the brain. In *sox2* morphants, a delay in the onset of *gfi1ab* expression is observed with no staining at 48 hpf (data not shown). At 4 dpf, *gfi1ab* was always on the left side of the brain in control embryos (total n=56 from 3 replicates). In contrast, *sox2* morphants were categorized into three groups according to the position of the *gfi1ab*-positive cells (total n=54 from 3 replicates):

1) Left, where a single group of *gfi1ab*-expressing cells was detected on the left side of the brain, similar to control embryos (52%).
2) Right, where a single group of *gfi1ab*-positive cells were located on the right side of the pineal gland, the reverse phenotype (12%).
3) Scattered, where *gfi1ab*-positive cells failed to group with each other and were scattered around the pineal gland (35%).

Whole mount *in situ* hybridizations for *gfi1ab* were performed in triplicate. For each experiment, the percentage of embryos falling into each category was calculated. The average percentage of embryos from the three replicates is shown in **Figure 3.34**.

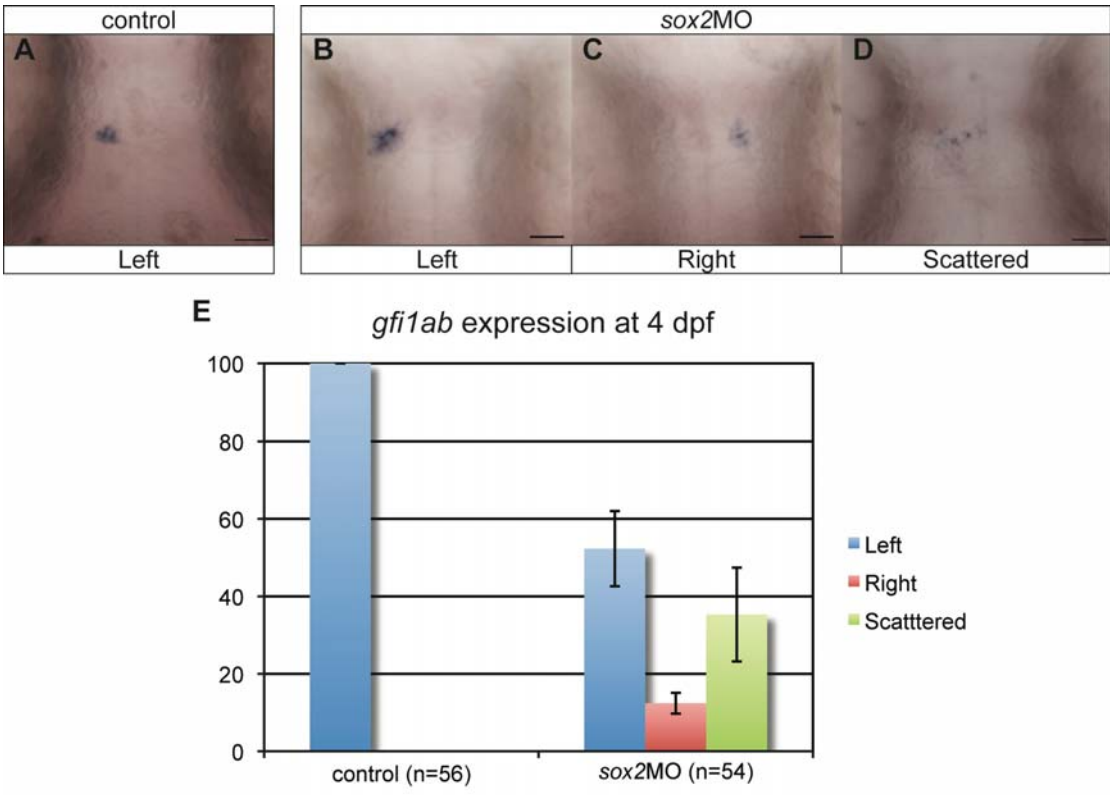

Figure 5.2 Parapineal organ development is abnormal in *sox2* morphants. (**A**) *gfi1ab*, a marker for parapineal cells, is expressed in a group of cells on the left side of the brain in control embryos. (**B-D**) *sox2* morphants are categorized into three groups according to *gfi1ab* expression. Aprroximately 50% of embryos have normal left-sided *gfi1ab* expression (B), 12% have right-sided parapineal organs (C) and in 35% of sox2 morphants, *gfi1ab* cells are scattered (D). (**E**) The average percentage of embryos falling into the three categories in control and *sox2* morphants. Dorsal views with anterior to the top of 4 dpf embryos, scale bars = 25 μm, error bars represent ± standard error.

In addition to *gfi1ab*, the transgenic line *Tg(foxd3:GFP)* is often used to study parapineal development. These embryos express GFP in both pineal and parapineal cells. In control embryos (at 4 dpf) the parapineal organ was found in the left-side of the brain, projecting towards the left habenula, in about 95% of *Tg(foxd3:GFP)* embryos (total n = 19 from two replicates) (**Figure 5.3**). Particularly, only one embryo (out of 19)

had a right-sided parapineal organ, which is consistent with previous studies suggesting that about 5% of wildtype embryos have reverse parapineals (Concha et al., 2000). In contrast, closer examination of GFP expression in *Tg(foxd3:GFP) sox2* morphants (total n = 41 from two replicates), led to the classification of embryos into three groups (**Figure 5.3**):

1) Left, where parapineal cells project towards the left habenula, although a left-sided parapineal organ is not always apparent (average percentage 27%).
2) Right, where a right-sided parapineal is present that projects to the right side (average percentage 22%).
3) Bilateral, where parapineal cells are scattered, a coherent parapineal organ is not always detected and in all cases projections towards both habenulae are observed (average percentage 51%).

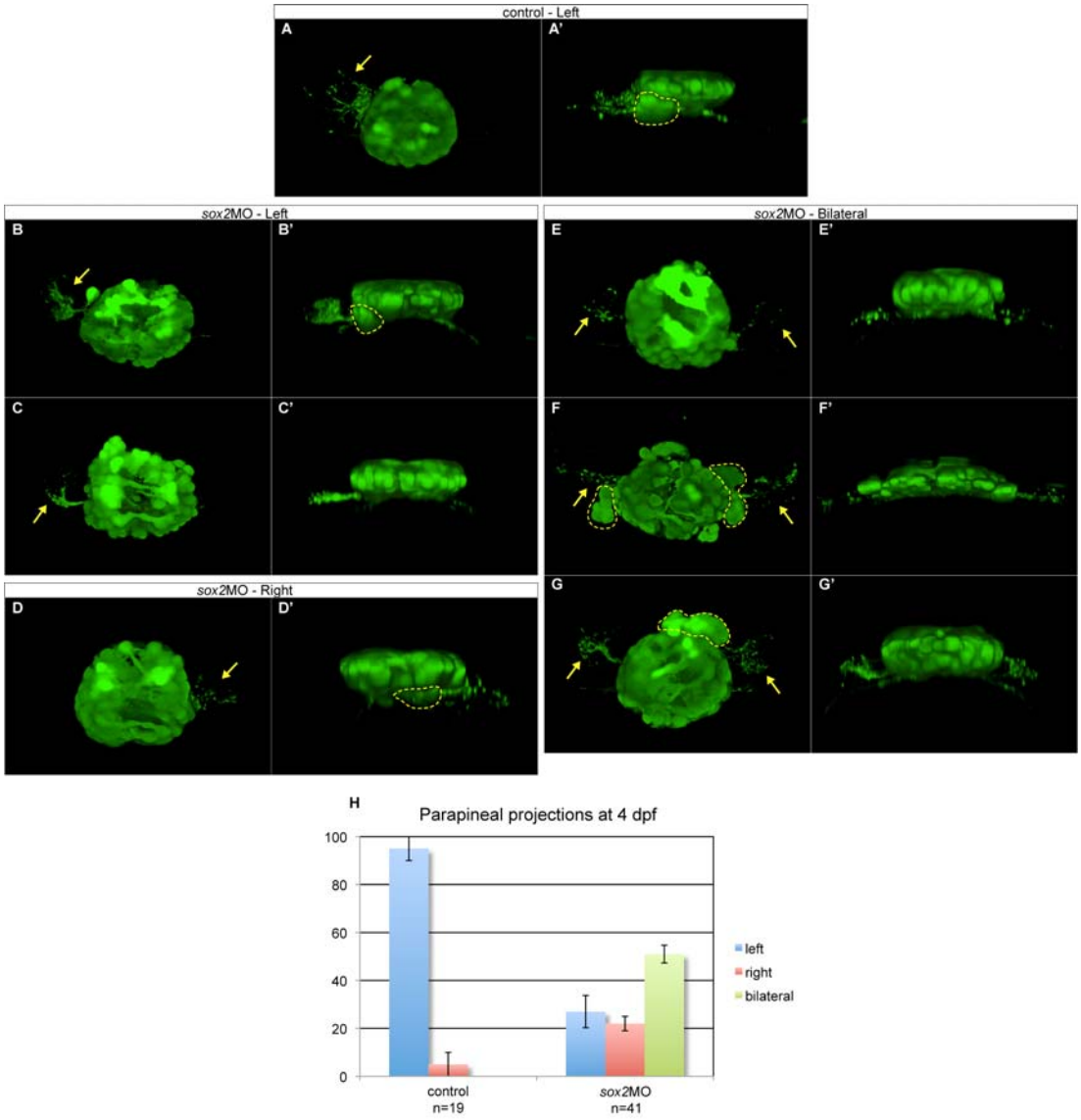

Figure 5.3 Downregulation of sox2 results in bilateral parapineal projections towards both the left and right habenulae. (**A-A'**) In control embryos, the left-sided parapineal projects to the left habenula. (**B-C'**) In a subset of *sox2* morphants, the parapineal cells project to the left habenula. An apparent parapineal organ is not always visible (C-C'). (**D**) Approximately 22% of *sox2* morphants have right-sided parapineal organs that project to the right habenula. (**E-G'**) The majority of *sox2* morphants has abnormally located parapineal cells, projecting to both the left and right habenulae. (**H**) Percentage of embryos with left (blue bars), right (red bars) and bilateral (green bars) parapineal projections at 4 dpf. 3D reconstructions of confocal images, (A-G) dorsal views with anterior to the top, (A'-G') posterior views with left to the left, arrows show the parapineal projections, apparent parapineal cells are surrounded with yellow lines, error bars represent ± standard error.

Notably, depending on the staining method some variability in the percentages of embryos falling in each category is observed (**Table 5.1**). Since scattered GFP-positive cells of *Tg(foxd3:GFP)* embryos are able to project to both sides of the brain, we hypothesize that *gfi1ab*-scattered cells will also project bilaterally and therefore the two categories are the same (refer to as bilateral parapineals). However, according to *gfi1ab* staining, approximately half of *sox2* morphants have normal left-sided parapineals, whereas only about 35% of embryos have scattered (and thus bilateral) parapineal cells. In contrast, GFP in *Tg(foxd3:GFP)* embryos suggests that only ~30% of embryos have normal parapineal organs and approximately 50% have bilateral parapineal organs. GFP expression is in agreement with *kctd12.1* staining that highlights the habenular asymmetries (discussed in section **5.3**). We suspect that the GFP expression of *Tg(foxd3:GFP)* embryos is more representative. In particular, we assume that a subset of embryos with normal left-sided *gfi1ab* expression, do have a few scattered cells that, although not detectable by whole mount *in situ* hybridization, may be sufficient to project towards the right habenula and result in left isomerism. In the case of reversal, we speculate that the variation observed (10-20% of embryos) reflects differences in the background of embryos or is due to the small number of embryos analyzed.

Table 5.1 Percentage of embryos with normal, reversed or bilateral parapineal organs using different staining methods.

Parapineal	***gfi1ab*** [1]	***kctd12.1*** [2]	***Tg(foxd3:GFP)*** [3]
Left-sided	52%	35%	27%
Right-sided	12%	10%	22%
Bilateral	35%	55%	51%

[1] *gfi1ab* is a gene specifically expressed in parapineal cells. Detection was achieved by whole mount *in situ* hybridization.

[2] *kctd12.1* is asymmetrically expressed within the habenulae. Since habenular defects observed in *sox2* morphants are due to parapineal organ abnormalities (discussed in section **3.6**), *kctd12.1* can be used to predict parapineal organ position. In particular, higher *kctd12.1* expression in the left than the right habenula correlates with a left-sided parapineal, reversal of *kctd12.1* expression pattern reflects reversal of the parapineal organ and symmetric expression (upregulation of the right expression) reflects bilateral parapineal organs. Detection was performed by whole mount *in situ* hybridization.

[3] *Tg(foxd3:GFP)* transgenics express GFP in the pineal gland, the parapineal organ and the parapineal projections towards the habenulae.

5.2.2 Abnormal bilateral activation of the Nodal pathway accounts for the reverse-parapineal phenotype observed in a subset of *sox2* morphants

The parapineal organ has a bilateral origin from the anterior part of the pineal anlage (Concha et al., 2003). At about 28 hpf, parapineal cells form a coherent structure and migrate towards the left side of the brain. The migration of parapineal cells requires two known signals: fgf8a and Nodal. fgf8a is important for the migration of parapineal cells *per se*. In mutant embryos, in which there is no fgf8a activity in the epithalamus, parapineal cells differentiate normally, as shown by *gfi1ab* expression, but they fail to migrate (Regan et al., 2009). In contrast, Nodal is required for the proper laterality of the migration. That is, in mutants where Nodal is bilateral or absent, the parapineal position becomes random, with 50% of embryos carrying a normal left-sided parapineal and 50% a right-sided parapineal (**Table 1.2**). Since a fraction of *sox2* morphants has right-sided parapineal organs and others have scattered parapineal cells, we analyzed *fgf8a* and Nodal activity in the dorsal diencephalon.

fgf8a is normally expressed bilaterally in the epithalamus before the migration of parapineal cells. Subtle differences in its expression are, however, observed between the left and right side. At the 22 ss, *fgf8a* expression on the right is higher than the expression on the left (Regan et al., 2009). Interestingly, during the migration of the parapineal cells (from about 28 hpf until at least 4 dpf) most embryos have higher *fgf8a* expression on the left (**Figure 5.4** and Regan et al., 2009). In addition, *fgf8a* expression becomes restricted to the medial part of the diencephalon as development proceeds. Not surprisingly, *sox2* morphants have normal bilaterally expressed *fgf8a* with higher levels on the left side, as shown by whole mount *in situ* hybridization (**Figure 5.4**). However, *fgf8a* is expressed in a broader domain even at later stages. Since fgf8a acts as a chemoattractant, the broader *fgf8a*-domain may account for the scattering effect observed in 50% of *sox2* morphants.

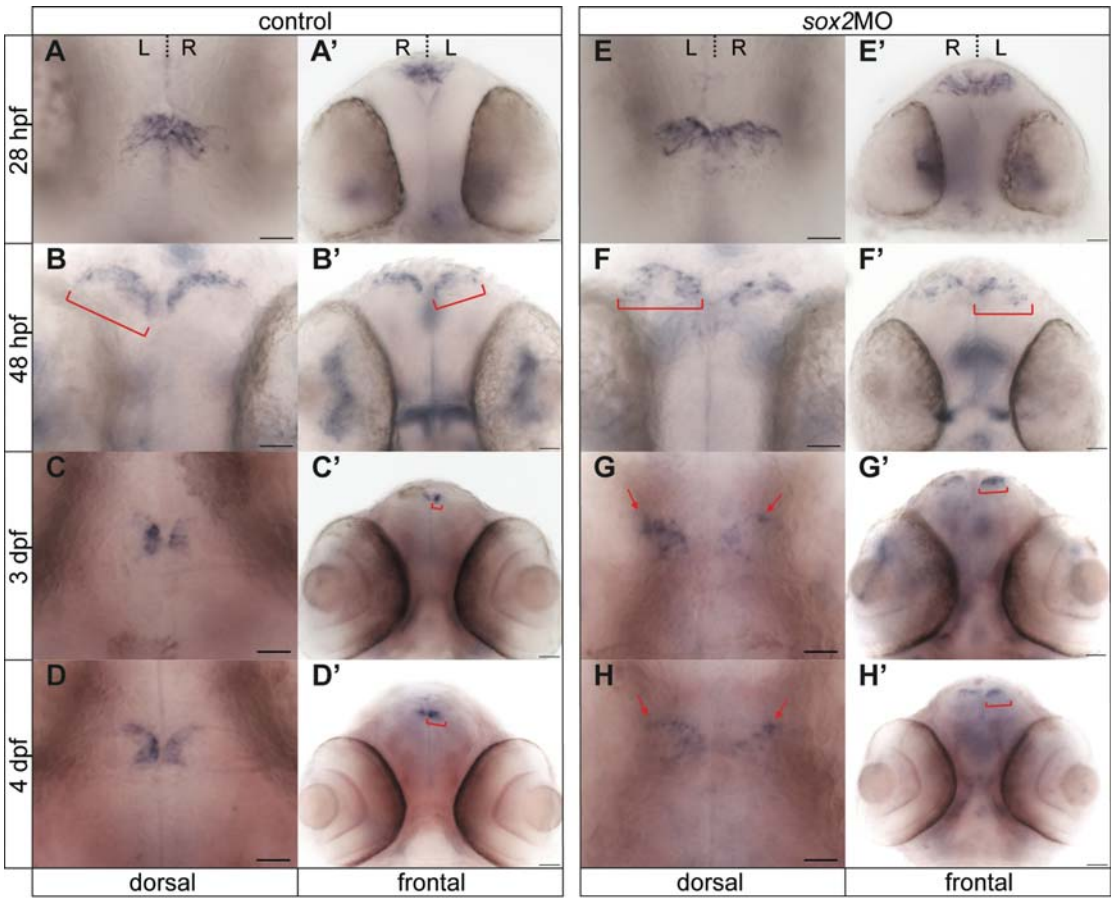

Figure 5.4 *fgf8a* is expressed in a broader domain in *sox2* morphants when compared to control siblings. (**A-D'**) *fgf8a* is normally expressed bilaterally in the epithalamus, in control embryos. From 48 hpf, expression on the left side is higher than the right. As development proceeds, *fgf8a* expression becomes restricted to the medial part of the diencephalon. (**E-H'**) *fgf8a* is expressed bilaterally, with higher expression on the left than the right side, in *sox2* morphants. However, *fgf8a*-positive cells are found in a broader domain when compared to control siblings (red brackets and arrows). (A-H) Dorsal views with anterior to the top. (A'-H') Frontal views of the same embryos. Developmental stages are shown at the side of each row, scale bars = 25 μm.

Although *fgf8a* expression is necessary for the initiation of migration, correct expression of Nodal genes in the diencephalon is vital for the proper laterality of the parapineal organ. The Nodal-signaling pathway is transiently active within the epithalamus from about the 18 ss to 28 hpf. In particular, the Nodal ligand *ndr2*, the antagonist *lft1* and the downstream effector *pitx2* are expressed unilaterally in control embryos. To assess Nodal activity in *sox2* morphants, whole mount *in situ*

hybridizations were performed for *pitx2*, at 28 hpf (**Figure 5.5**). *pitx2* is expressed in the left-side of the epithalamus in 95% of control embryos and bilaterally in 5% (average percentage from 3 replicates, total n=117). In contrast, only 60% of *sox2* morphants have normal unilateral *pitx2* expression, while 40% have bilateral expression (average percentage from 3 replicates, total n=85).

As discussed earlier, bilateral expression of Nodal genes in the diencephalon leads to randomization of the parapineal organ. We therefore conclude that the right-sided parapineal organ observed in 10-20% of *sox2* morphants is due to the bilateral activation of the Nodal pathway in 40% of *sox2* morphants.

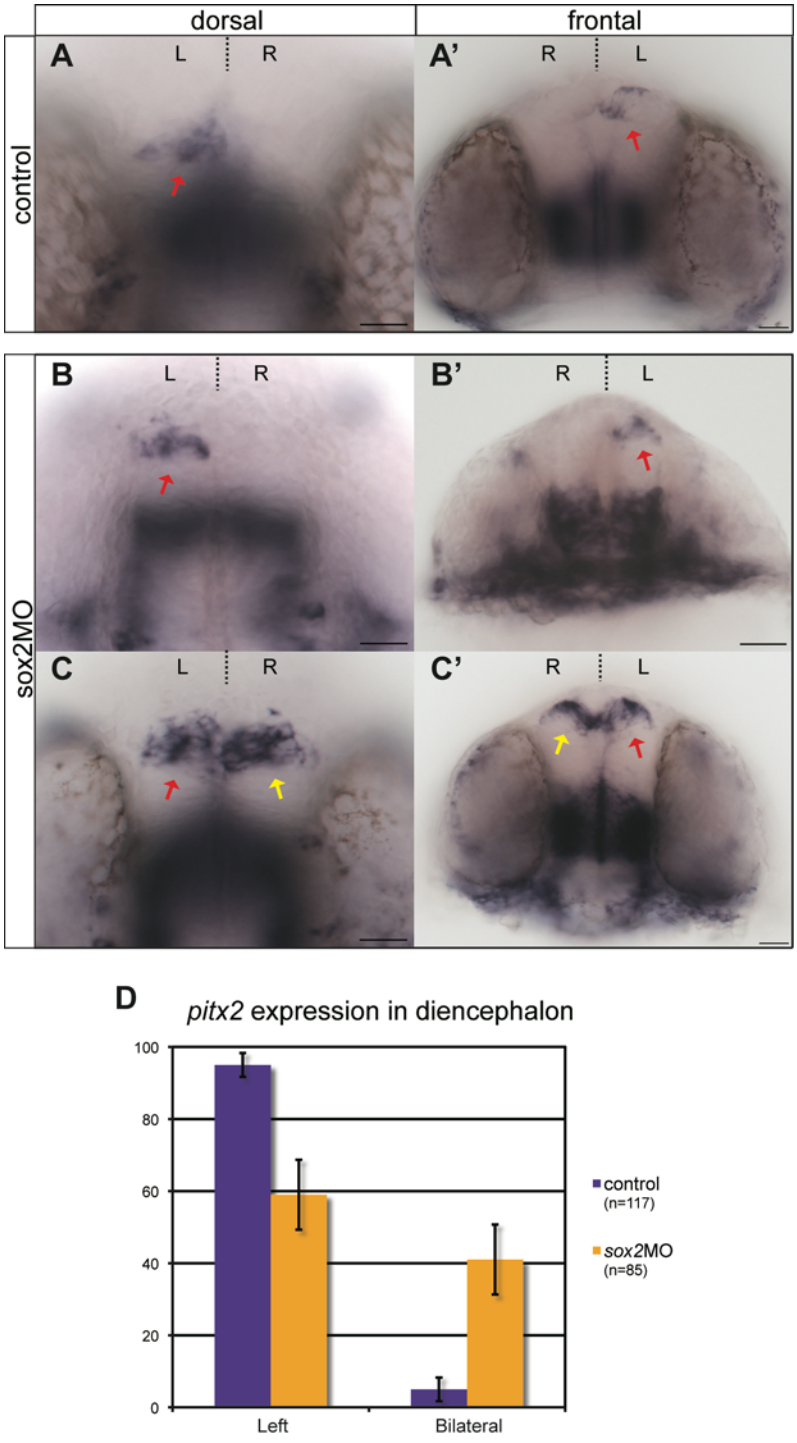

Figure 5.5 A subset of *sox2* morphants has bilateral *pitx2* expression in the diencephalon. (**A-A'**) *pitx2* is normally expressed in the left side of zebrafish diencephalon (red arrow). (**B-B'**) Approximately 60% of *sox2* morphants have normal left-sided *pitx2* expression. (**C-C'**) *pitx2* is abnormally expressed in both the left (red

arrow) and right side (yellow arrow), in 40% of morphant embryos. (**D**) Average percentage of embryos with left or bilateral *pitx2* expression in controls (purple bars) and *sox2* morphants (orange bars). (A-C) Dorsal views of 28 hpf embryos, with anterior to the top. (A'-C') Frontal views of the same embryos, scale bars = 25 μm, error bars represent ± standard error.

5.2.3 Downregulation of sox2 results in bilateral activation of the Nodal pathway in the lateral plate mesoderm (LPM)

Brain laterality defects, such as right-sided parapineal organs, are often associated with reversal of the viscera (**Table 1.2**). Previous studies showed that Nodal pathway is one of the key components controlling lateralization in both the brain and the body. Since a subset of *sox2* morphants has right-sided parapineal organs and abnormal bilateral activation of Nodal pathway in the diencephalon, we decided to investigate if laterality defects are also apparent in the body.

Similar to the diencephalon, Nodal genes (*ndr2*, *lft1*, *lft2* and *pitx2*) are transiently expressed in the left lateral plate mesoderm (LPM) in control embryos between 17 ss and 24 hpf (**Figure 5.6**) (total n = 40 from two replicates). Whole mount *in situ* hybridization for *pitx2* in 20 ss-24 hpf embryos, showed that downregulation of sox2 disrupts Nodal activity in the LPM. Particularly, only 30% of *sox2* morphants have normal left-sided *pitx2* expression, whereas the majority of morphants (60%) has bilateral *pitx2* expression in the LPM (total n = 107 from three replicates).

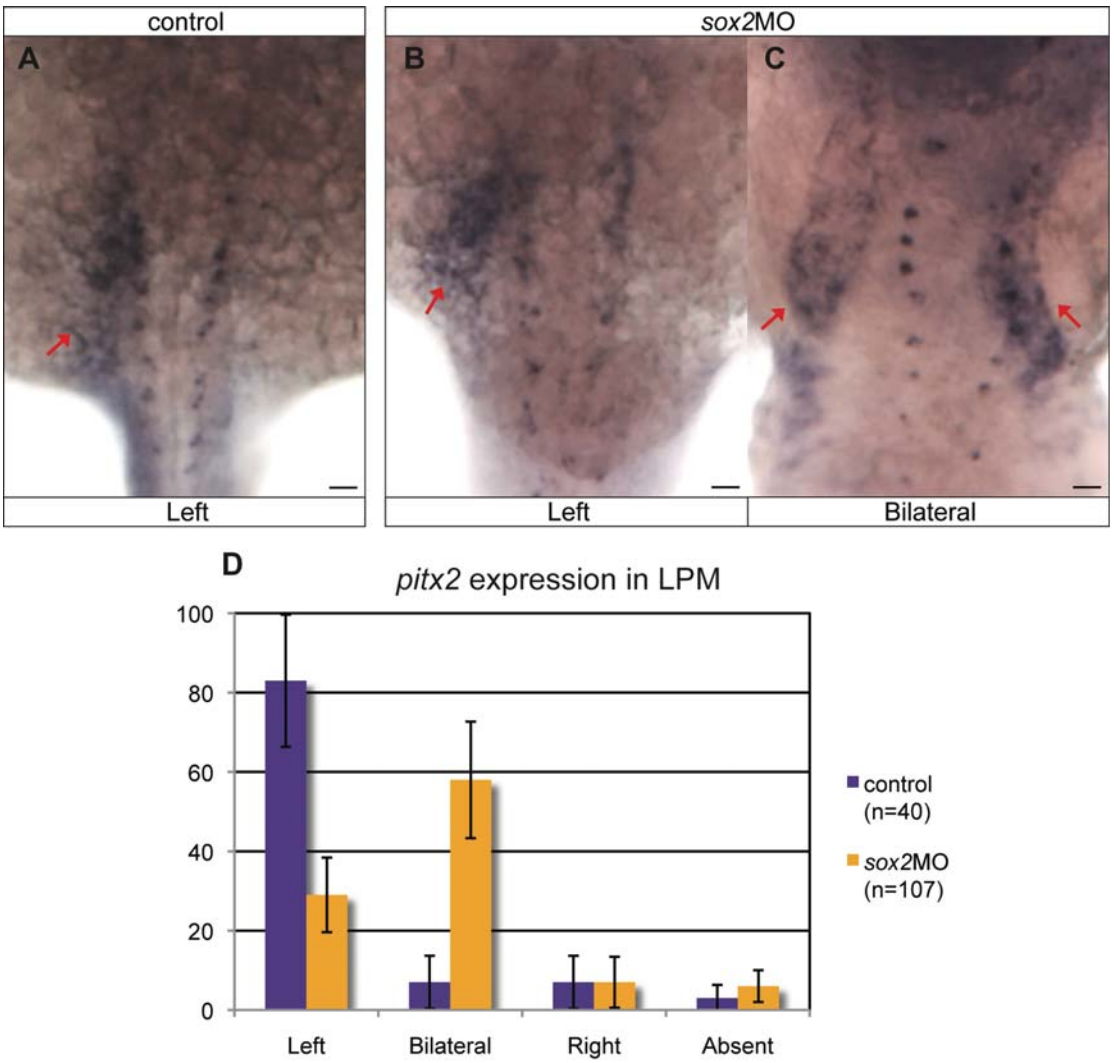

Figure 5.6 Downregulation of sox2 leads to bilateral activation of the Nodal pathway in the lateral plate mesoderm (LPM). (**A**) *pitx2*, a Nodal downstream effector, is unilaterally expressed in the left LPM (red arrow) in control embryos. (**B,C**) In *sox2* morphants, *pitx2* expression is normal only in 30% of the embryos and bilateral in about 60%. (**D**) Average percentage of embryos with left, bilateral, right or absent *pitx2* expression in the LPM in control (purple bars) and *sox2* morphants (orange bars). Dorsal views with anterior to the top, scale bars = 25 μm, error bars represent ± standard error.

Due to the difference in timing between the peak of *pitx2* expression in the diencephalon (expression was scored at 28 hpf) and LPM (expression was scored between 20 ss-24 hpf), we were unable to investigate whether the abnormal bilateral expression of *pitx2* in the diencephalon and LPM are coupled in *sox2* morphants. However, in a subset of embryos, where both the diencephalic and LPM expression were

apparent, we found that the two are often uncoupled (**Figure 5.7**). Particularly, some embryos with bilaterally expressed *pitx2* in the LPM had normal left-sided expression in the diencephalon. This is also illustrated by the different percentages of embryos with bilateral expression in LPM (60%) and diencephalon (40%).

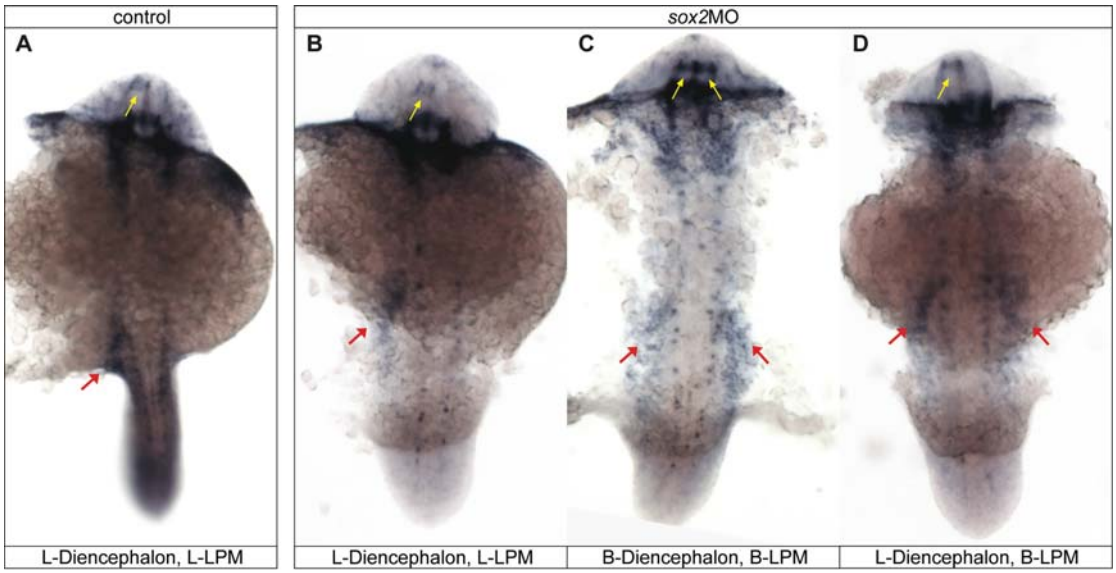

Figure 5.7 Expression of *pitx2* in the diencephalon and LPM are uncoupled in a subset of *sox2* morphants. (**A**) *pitx2* is expressed in the left diencephalon (yellow arrow) and left LPM (red arrow) in control embryos. (**B-D**) Downregulation of sox2 often results in abnormal *pitx2* expression. Particularly, a subset of embryos show normal left-sided expression in the diencephalon and LPM (B), whereas some embryos have bilateral expression (C). Often diencephalic and LPM expression are uncoupled in *sox2* morphants (D). Dorsal views with anterior to the top of 22 ss embryos.

Since downregulation of sox2 results in bilateral expression of *pitx2* in the LPM in approximately 60% of embryos, we would expect randomization of the visceral asymmetries in these embryos. To test this hypothesis, we scored heart looping in control and *sox2* morphant embryos at 2 dpf (three replicates, control total n=154, *sox2*MO total n=123) (**Figure 5.8**). Interestingly, *sox2* morphants do not exhibit a reversal phenotype. Instead, in approximately 35% of *sox2* morphants the heart tube fails to loop. Although the majority of Nodal mutants and morphants exhibit randomization of heart looping, most *spaw* morphants have no-looping phenotype (Long

et al., 2003), similar to *sox2* morphants. Our data suggest that sox2 is involved in the regulation of heart looping, possibly through a *spaw*-mediated pathway.

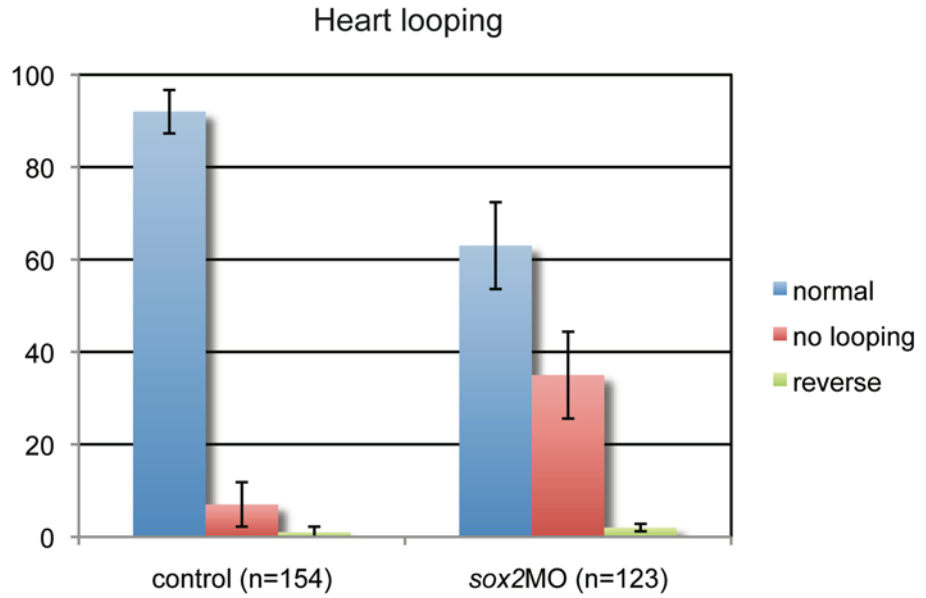

Figure 5.8 Correct levels of sox2 expression are required for the proper looping of the heart tube. Average percentage of embryos with normal looping (blue bars), no looping (red bars) or reverse looping (green bars) of the heart tube at 2 dpf. In approximately 35% of *sox2* morphants, the heart tube fails to loop. Error bars represent ± standard error.

5.2.4 Downregulation of sox2 results in reduced expression of *tbx2b*, which is important for the proper specification of parapineal cells

As discussed above, downregulation of sox2 results in two distinct phenotypes: right-sided parapineal organ, which is a consequence of the bilateral activation of Nodal, and scattered parapineal cells. We hypothesize that the scattered phenotype may result from defects in the specification and/or migration properties of parapineal cells. Previous studies suggest that *tbx2b* activity is important for the proper specification of parapineal cells. The *from beyond* (*fby*) mutation results in a premature stop codon in *tbx2b*, leading to complete loss of the protein. As a result, embryos have fewer parapineal cells that fail to form a coherent structure and do not migrate properly to the left side of the brain. By whole mount *in situ* hybridizations, we showed that *tbx2b* expression is reduced in *sox2* morphants (**Figure 5.9**). Since the number of *gfi1ab*-

positive cells is relatively normal, we hypothesise that the reduced *tbx2b* expression may result in loss of some properties of the parapineal cells that are necessary for their proper migration.

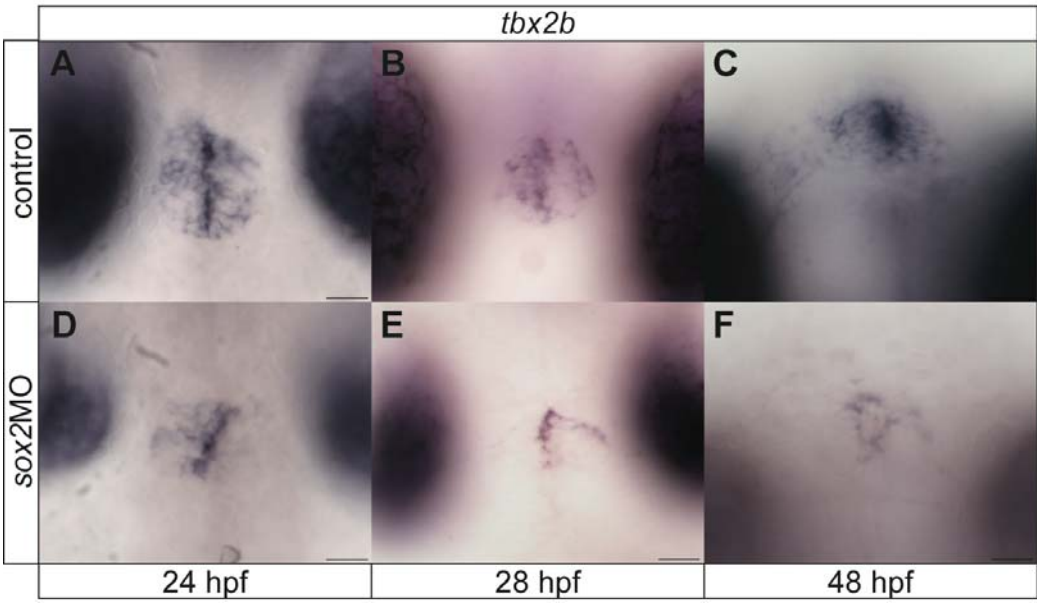

Figure 5.9 *tbx2b* is downregulated in *sox2* morphants. (**A-C**) *tbx2b* is expressed within the pineal gland anlage and is important for the proper specification of parapineal cells. (**D-F**) Downregulation of sox2 results in reduced *tbx2b* expression at all stages analyzed. Dorsal views with anterior to the top. Developmental stages are shown at the bottom of each column, scale bars = 25 μm.

5.2.5 Migration of parapineal cells is defective in *sox2* morphants

In order to obtain a better insight into the scattered (bilateral) parapineal phenotype, we performed timelapse experiments that enabled us to observe migration of parapineal cells in live embryos. For these experiments we used the transgenic line *Tg(foxd3:GFP)* that expresses GFP in both the pineal and the parapineal organ. In these transgenic embryos, GFP is expressed within the pineal gland before 24 hpf and at about 40 hpf GFP is visible within the migrating parapineal cells. The migration of the parapineal cells start at about 28-32 hpf and therefore the first steps of migration are not detectable using the *Tg(foxd3:GFP)* line. Nevertheless, from about 40 hpf we can clearly see parapineal cells migrating towards the left side in control embryos (**Figure 5.10** and

Movie S10 in supplementary material), as previously described (Snelson et al., 2008a). In a subset of *sox2* morphants, parapineal migration is normal (**Figure 5.11** and **Movie S11** in supplementary material). However, in some *sox2* morphants parapineal cells migrate towards the right (**Figure 5.11** and **Movie S12** in supplementary material) or parapineal cells are misguided and disconnected from the group resulting in scattered (bilateral) parapineals (**Figure 5.12** and **Movie S13-S14** in supplementary material).

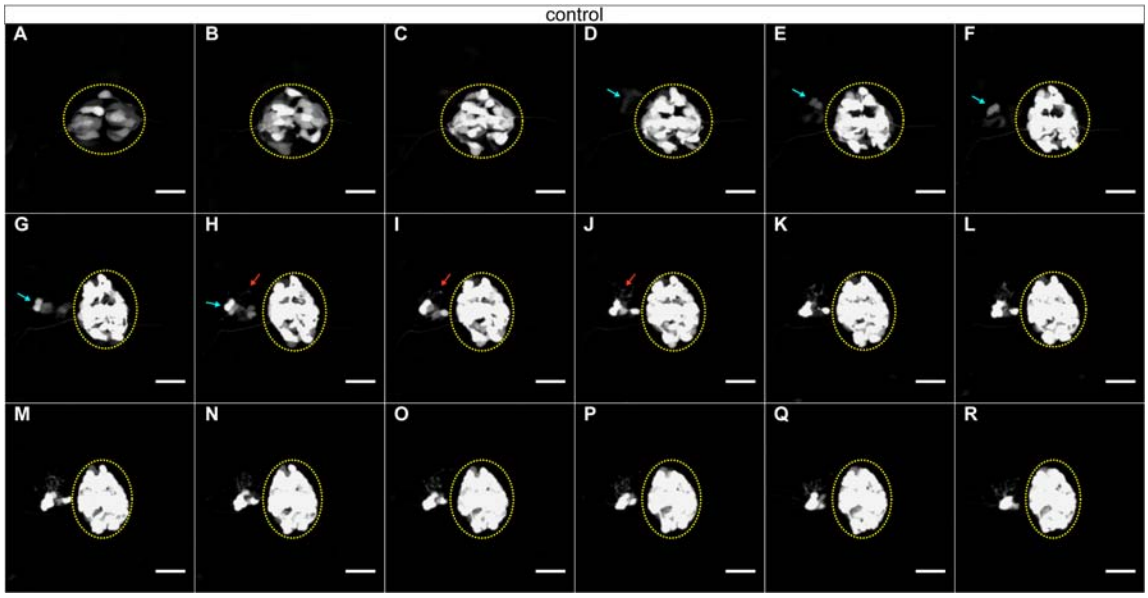

Figure 5.10 Parapineal cells migrate leftwards in control embryos. Snapshots of timelapse confocal microscopy from approximately 30 hpf to 90 hpf (**Movie S10** in supplementary materials). Images were acquired every 40 minutes, but here snapshots represent 200-minutes intervals. (**A-R**) *Tg(foxd3:GFP)* control embryo, expressing GFP within the pineal gland (yellow circle) and the migrating parapineal cells (blue arrows). Parapineal cells migrate as a group of GFP-positive cells from 40 hpf (D). At approximately 50 hpf, parapineal cells send projections (red arrows) towards the left habenula (H). Dorsal views with anterior to the top, scale bars = 25 μm.

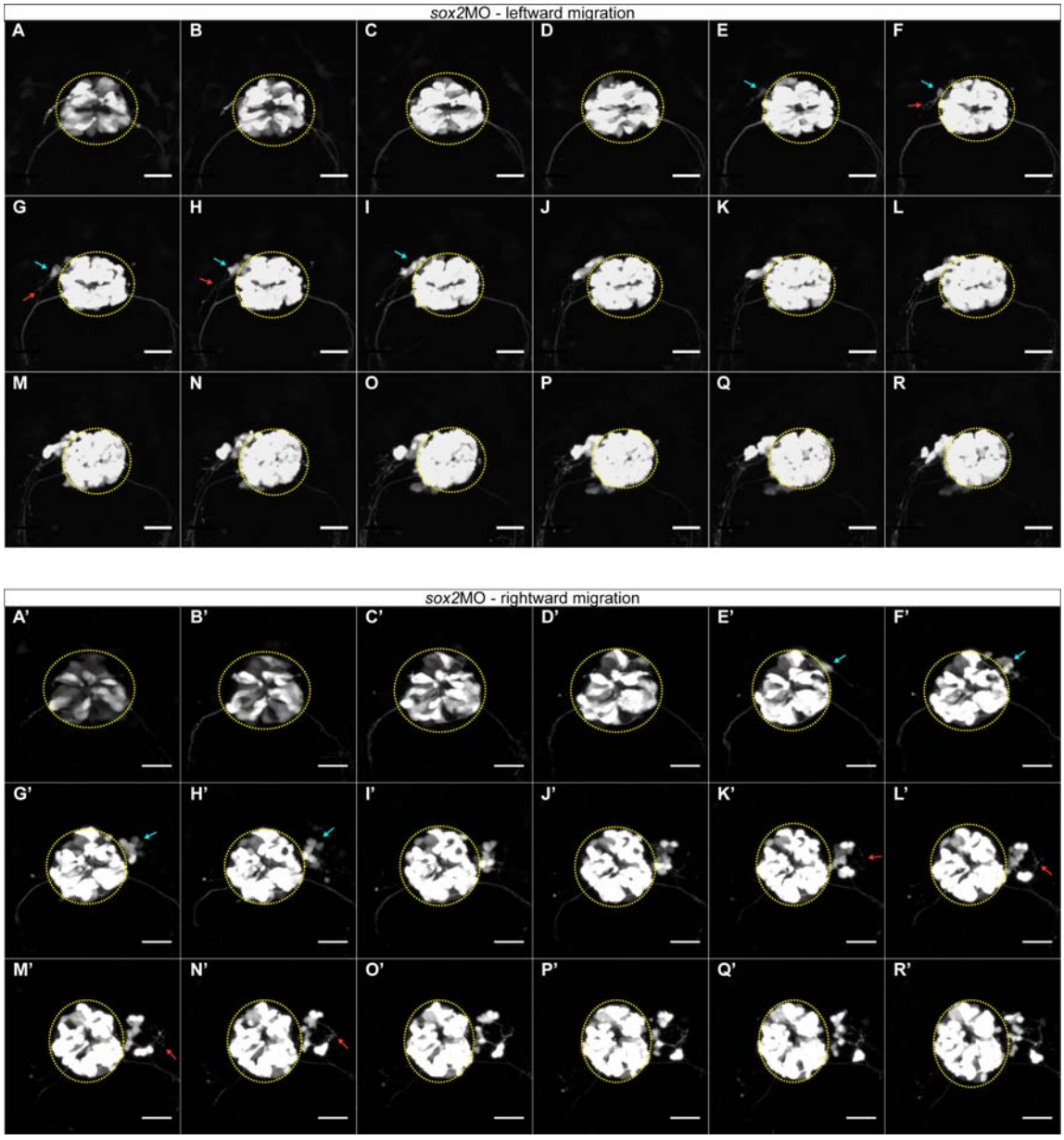

Figure 5.11 In a subset of *sox2* morphants, parapineal cells migrate towards the right. Snapshots of timelapse confocal microscopy from approximately 30 hpf to 90 hpf. Images were acquired every 40 minutes, but here snapshots represent 200-minutes intervals. (**A-R**) One example of *Tg(foxd3:GFP) sox2* morphant embryo, expressing GFP within the pineal gland (yellow circle), the migrating parapineal cells (blue arrows) and the parapineal projections towards the habenulae (red arrows). In this example, parapineal cells migrate towards the left side, similar to control embryos (**Movie S11** in supplementary materials). (**A'-R'**) A *sox2* morphant embryo in which parapineal cells migrate towards the right (**Movie S12** in supplementary materials). Dorsal views with anterior to the top, scale bars = 25 μm.

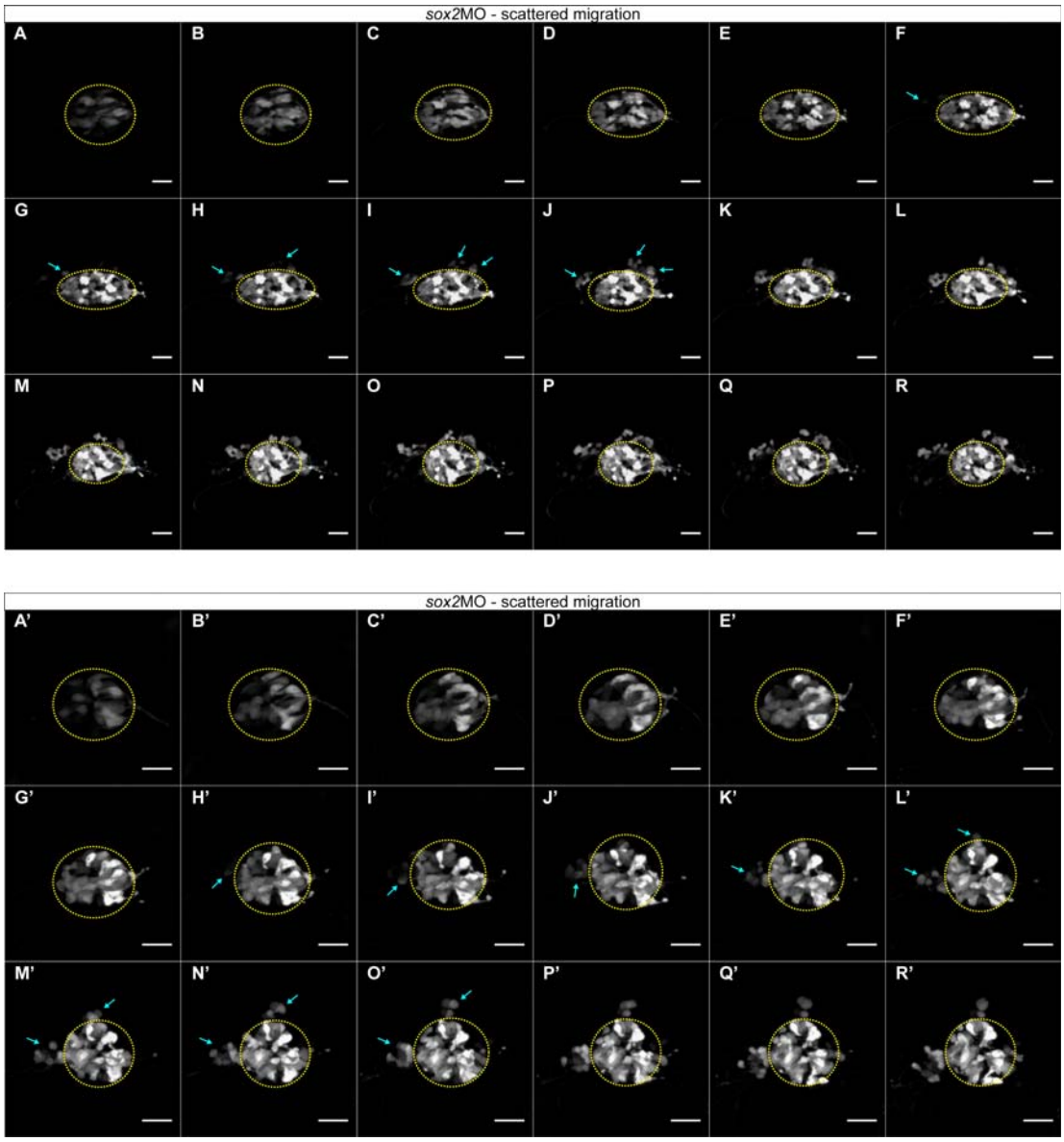

Figure 5.12 In some *sox2* morphants, parapineal cells are scattered. Snapshots of timelapse confocal microscopy from approximately 30 hpf to 90 hpf (**Movie S13-S14** in supplementary materials). Images were acquired every 40 minutes, but here snapshots represent 200-minutes intervals. (**A-R**) One example of *Tg(foxd3:GFP)* control embryo, expressing GFP within the pineal gland (yellow circle) and the migrating parapineal cells (blue arrows). Parapineal cells fail to form a coherent structure. Instead they migrate as groups of 2-3 cells towards multiple sites. (**A'-R'**) A second example of a *sox2* morphant embryo. In this case, parapineal migration initiates normally with cells migrating towards the left as a group, but at approximately 64 hpf (L') a few cells appear at the anterior part of the pineal gland. Dorsal views with anterior to the top, scale bars = 25 μm.

5.3 The asymmetric architecture of the habenular nuclei is disrupted when sox2 is downregulated

We showed that downregulation of sox2 results in defective pineal and parapineal organs. Since a normal parapineal organ is crucial for the proper development of the habenular nuclei, we hypothesize that the latter may be defective in *sox2* morphants.

The habenular nuclei are bilateral structures, adjacent to the pineal complex, that show left-right differences in size, number of neuropil and gene expression. To test our hypothesis, we analyzed the expression profile of the asymmetrically expressed marker: *kctd12.1*.

kctd12.1 is predominantly expressed in the left habenula with fewer positive cells in the right habenula, from about 48 hpf. In *sox2* morphants, no *kctd12.1* expression was detected at 48 hpf, confirming a delay in development (data not shown). However, by 4 dpf, *sox2* morphants were grouped into three categories according to their *kctd12.1* expression (total n=51 from 3 replicates) (**Figure 5.13**):

1) Left, where *kctd12.1* is expressed in a broader domain in the left habenula in relation to the right, like the control embryos (average percentage from 3 replicates = 35%).
2) Right, where *kctd12.1* expression is reversed, with more positive cells in the right habenula (average percentage from 3 replicates = 10%).
3) Symmetric, where both habenulae had approximately the same number of *kctd12.1* expressing cells. The expression was comparable to the normal left habenula, suggesting that both habenulae adopted a left-side character (average percentage from 3 replicates = 55%).

Whole mount *in situ* hybridizations for *kctd12.1* were performed in triplicate. For each experiment the percentage of embryos falling into each category was calculated. The average percentage of embryos from the three replicates is shown in **Figure 3.45**.

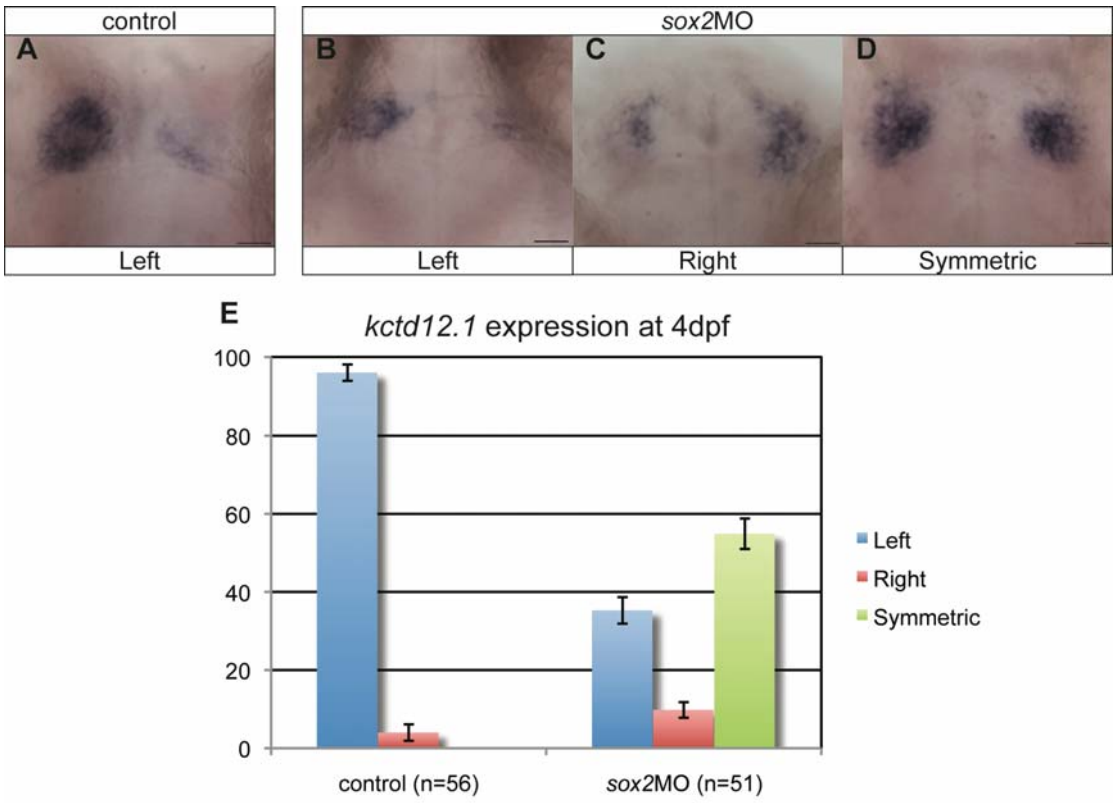

Figure 5.13 The asymmetric architecture of the habenular nuclei is disrupted in *sox2* morphants. (**A**) *kctd12.1* is asymmetrically expressed in the habenulae, with a broader expression domain in the left than the right habenula, at 4 dpf. (**B-D**) In *sox2* morphants, *kctd12.1* expression can be: asymmetric with more on the left side like the control embryos (B), asymmetric with more on the right side (C) or symmetric (D). (**E**) Average percentage of embryos falling into the three categories in control and *sox2* morphants. Dorsal views with anterior to the top of 4 dpf embryos, scale bars = 25 μm, error bars represent ± standard error.

5.4 The habenular defects observed in *sox2* morphants are associated with the abnormal parapineal development

Previous studies suggested that abnormal parapineal development is associated with abnormal habenular development. In particular, laser ablation of parapineal cells, prior to their migration to the left side, results in two right-character habenulae (Concha et al., 2003; Gamse et al., 2003; Bianco et al., 2008). Similarly, in *fby* mutants in which parapineal cells fail to migrate, the habenulae are symmetric (Snelson et al., 2008a). In addition, embryos with right-sided parapineals show reversal of the habenular

architecture (**Table 1.2**). Since *sox2* morphants display abnormalities in both the parapineal and the habenulae, we hypothesized that the two phenotypes are coupled.

To test our hypothesis, we used the transgenic line *Tg(foxd3:GFP)* that marks both the pineal gland and the parapineal organ, in combination with phalloidin staining. Phalloidin is a peptide isolated from the *Amanita phalloides* (commonly known as death cap mushroom) and is widely used to label filamentous actin (F-actin). F-actin is enriched in synaptic neuropil (Rössler et al., 2002; Frambach et al., 2004) and therefore phalloidin staining enables the visualization of the habenular neuropil.

The zebrafish habenulae consist of neuropil-rich areas in the middle surrounded by neuron bodies (Doll et al., 2011; Taylor et al., 2011). To confirm the specificity of phalloidin staining in labelling the habenular neuropil, embryos were counterstained with DAPI. As expected, phalloidin-positive areas within the middle of the habenulae were DAPI-negative in both control and *sox2* morphant embryos (**Figure 5.14**).

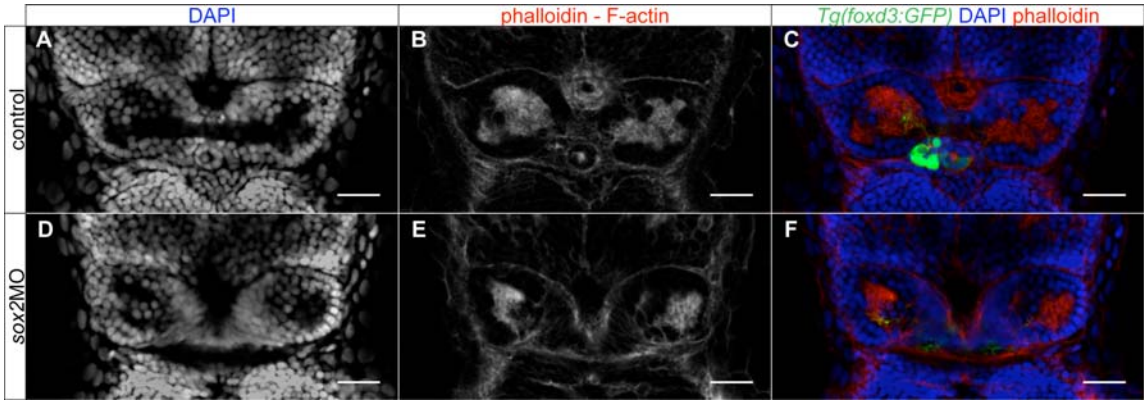

Figure 5.14 Phalloidin can be used to visualize habenular neuropils. (**A-C**) *Tg(foxd3:GFP)* embryos were labelled with phalloidin (F-actin) and DAPI to visualize the habenulae. DAPI (A) labels the nuclei of the neurons at the edge of the habenulae, whereas phalloidin (B) labels the neuropil-rich areas in the middle of each habenula. Parapineal projections (C) end in the neuropil-rich (phalloidin positive) area of the left habenula. (**D-F**) DAPI and phalloidin staining also marks the habenulae of *sox2* morphants. Optical sections of confocal microscopy, dorsal views with anterior to the top, scale bars = 25 μm.

Tg(foxd3:GFP) embryos labelled with phalloidin and DAPI were imaged using confocal microscopy and 3D reconstructions were generated using Volocity

(PerkinElmer). The volume of neuropils within the left and right habenulae was determined by calculating the volume of phalloidin-positive areas. These data were then used to calculate the asymmetry index (AI) between the left and right neuropils for each embryo (Roussigné et al., 2009). By definition, AI values between -1 and 0 correspond to a larger left side and values between 0 and 1 indicate a larger right side.

As shown in **Figure 5.15**, in 4 dpf control embryos, the left neuropils are almost double in volume in relation to the ones found in the right habenula (average volume of the left is 8276 μm^3 compared to 4824 μm^3 for the right), with average AI of -0.26. The difference in volume between the left and right neuropils is highly significant according to Wilcoxon paired signed rank test (Wilcoxon), with p-value < 0.001 (n=11).

The volume of left and right habenular neuropils in *sox2* morphants, as well as the AI, was calculated as above. In all cases, downregulation of sox2 results in smaller neuropils when compared to control embryos (**Figure 5.15**). We hypothesize that smaller volume of the habenular neuropils reflects a general developmental delay. Staining at later stages is, therefore, necessary to confirm this hypothesis.

More interestingly, the data suggest that in *sox2* morphants the volume of habenular neuropils is associated with parapineal projections (**Figure 5.15**). Even though the difference is smaller in relation to controls, the habenula that receives parapineal projections is always larger than the other one. Particularly, in embryos with left-sided parapineal cells that project towards the left, the left neuropils are larger in volume than the right ones (AI = -0.2, average volume of left is 2791 μm^3 compared to 1828 μm^3 in right, Wilcoxon; p-value < 0.05, n=7). Embryos with right-sided parapineals display reversal of the asymmetries (AI = 0.31, average volume of left is 1439 μm^3 compared to 2680 μm^3 in right, Wilcoxon; p-value < 0.05, n=6). Finally, *sox2* morphants that exhibit bilateral projections from the parapineal towards the habenulae have symmetric neuropils (AI = -0.05, average volume of left is 2408 μm^3 compared to 2335 μm^3 in right, Wilcoxon; p-value > 0.05, n=11).

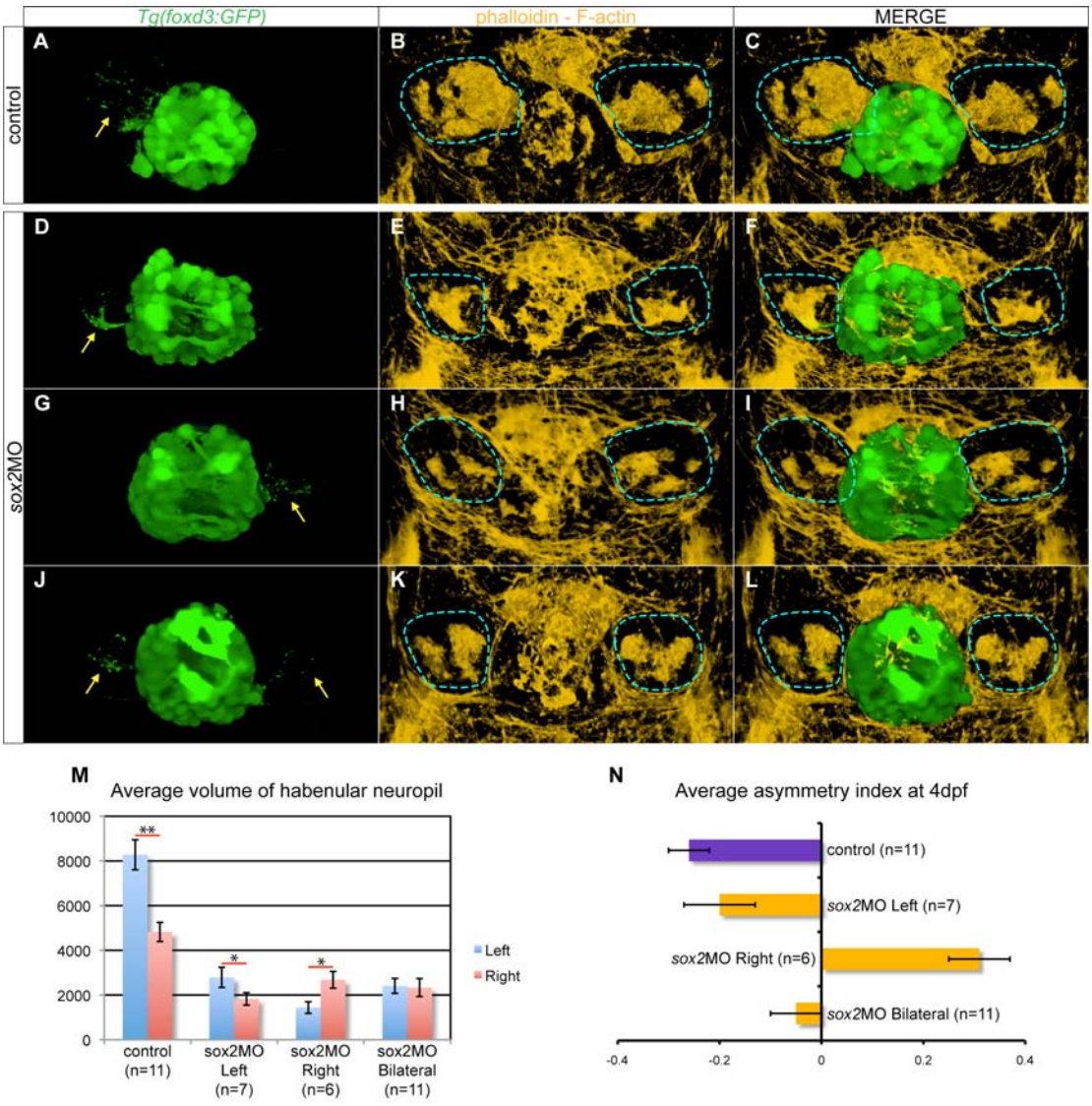

Figure 5.15 The disruption of habenular asymmetries observed in *sox2* morphants is associated with parapineal abnormalities. (**A-C**) In control embryos, the left-sided parapineal projects towards the left habenula. As a result the left habenula has denser neuropils than the right, as determined by phalloidin staining. (**D-F**) In *sox2* morphants with left-sided parapineal projections, the left habenula is larger than the right. (**G-I**) Morphants with right-sided parapineal organs display reverse habenular asymmetries, whereas (**J-L**) morphants with bilateral parapineal projections have symmetric habenulae. (**M**) The average volume of the left (blue bars) and right (red bars) habenular neuropils, as determined by the volume of phalloidin-positive areas within the habenulae. y-axis show volume in μm^3. (**N**) The average asymmetry index in control (purple bar) and *sox2* morphants (orange bars). 3D reconstructions of confocal images at 4 dpf, dorsal views with anterior to the top, arrows show parapineal projections and blue lines surround the habenular neuropils, error bars represent ± standard error, (M) * = significant; Wilcoxon test; p-value < 0.05 and ** = highly significant; Wilcoxon test; p-value < 0.001.

5.5 Conclusion

Downregulation of sox2 disrupts the asymmetric architecture of the epithalamus. In particular, a subset of *sox2* morphants have right-sided parapineal organs and reversed habenular asymmetries, possibly due to abnormal bilateral activation of the Nodal pathway. In addition, some *sox2* morphants have scattered parapineal cells that project to both the left and right habenulae and as a result the two habenulae develop symmetrically.

Chapter 6. Discussion and Future directions

“Χαλεπά τα καλά”

“The good/beautiful things (are) difficult (to attain)”

Plato, 428-348 BC

In this study, we established and characterized an animal model (*sox2* morphant zebrafish embryos) to study the functions of *sox2* during vertebrate development. Using this model, we identified and characterized novel roles for *sox2* during the development of the zebrafish epithalamus. By understanding the molecular pathways modulated by *sox2* during the development of the epithalamus, we aim to obtain a better insight into how *sox2* controls such a plethora of developmental processes during ontogenesis.

6.1 *sox2* morphants resemble the phenotypes observed in human patients and mutant mice

Sox2 is a key regulator during embryogenesis in a dose-dependent manner. In particular, depending on the level of protein present, mice exhibit more or less severe symptoms ranging from early lethality shortly after the implantation stage (*Sox2*-null mice) to viable mice with ocular and brain defects (hypomorphic mice) (Avilion et al., 2003; Ferri et al., 2004; Taranova et al., 2006). Zebrafish are an excellent model to study *sox2*, since downregulation of the gene can easily be achieved by morpholino microinjections. An advantage of this is that depending on the concentration of morpholino injected, different levels of downregulation can be achieved. In addition, the efficiency of different morpholinos targeting the same gene can vary, possibly due to differences in the binding affinity of the molecules. Notably, different *sox2* morpholinos or different dosages of the same morpholinos have been shown to result in different levels of *sox2* downregulation (Kamachi et al., 2008). In agreement with this, we showed that two different morpholinos, injected at the same concentration, result in different levels of sox2 downregulation and as a consequence in different severities of the phenotypes.

In our model, *sox2* morpholinos result in approximately 80% reduction in the protein levels (as judged by western blot analysis from whole embryo extracts). Also, immunofluorescent staining for sox2 showed that morphant embryos have almost no staining within the developing brain and eyes. Altogether, the data suggest that although the protein is not completely lost, the downregulation is very effective. In addition, the

morphological defects of *sox2* morphants can be rescued by co-injecting human *SOX2* mRNA, suggesting that the phenotypes are specific to downregulation of *sox2*.

Interestingly, we found that *sox2* morphants exhibit ocular phenotypes similar to the ones observed in human patients and other animal models. Particularly, downregulation of *sox2* leads to smaller eyes in a dose-dependent manner. This is analogous to anophthalmia/microphthalmia observed in human patients (summarized in http://lsdb.hgu.mrc.ac.uk/variants.php?action=view_all) and the small-eye phenotype observed in hypomorphic mice (Taranova et al., 2006). Also, we showed that *sox2* morphants have fewer RGCs (similar to hypomorphic mice) and fewer amacrine cells (similar to previously published *sox2* morphant zebrafish) in relation to control siblings (Taranova et al., 2006; Pujic et al., 2006). We also found that RGC axons and in particular their arborization at the optic tectum is affected in *sox2* morphants. Further investigation is required to determine whether this defect is cell-autonomous and/or whether axon guidance is abnormal in embryos with compromised *sox2* expression.

In addition to the ocular phenotypes, *sox2* morphants have proliferation defects and an increased number of apoptotic cells. Similar phenotypes have also been observed in the eyes of *Sox2*-hypomorphic mice and inner ears of *sox2* morphant zebrafish embryos (Taranova et al., 2006; Millimaki et al., 2010).

The similar phenotypes observed between different species suggest that *sox2* functions are evolutionarily conserved. Therefore, zebrafish (with their numerous advantages) provide invaluable tools that will allow us to dissect the roles of *sox2* during vertebrate embryogenesis and in particular the development of the brain. Since *sox2* mutant zebrafish are not available yet, morpholinos are the only tool to study *sox2* loss-of-function in zebrafish. However, the generation of *sox2* mutants will help answer a number of questions. For example, it will be interesting to test whether heterozygous *sox2* mutants have any phenotype or whether (like mice) a phenotype is observed only with more than 50% reduction in the protein level.

6.2 sox2 is necessary for the development of the pineal gland

The roles of *Sox2* in the developing retina, as well as in neural progenitor cells, have been well studied in mice. However, very little is known about the molecular networks controlled by *Sox2* during the development of specific structures within the brain. Here, we identified and characterized novel roles for *sox2* in the development of the zebrafish epithalamus, aiming to obtain a better understanding on how *sox2* controls similar biological processes elsewhere in the brain.

Within the presumptive pineal gland, we showed that *sox2* is expressed in progenitor cells (*flh* positive) but is downregulated following differentiation (in isl1-positive cells). This is in agreement with previous finding suggesting that *Sox2* is a marker for proliferating neural progenitor cells (Ellis et al., 2004).

6.2.1 *sox2* inhibits neurogenesis

Our data suggest that *sox2* modulates neurogenesis within the pineal anlage. In particular, *sox2* morphants exhibit increased neurogenesis, as judged by the increased number of isl1-positive cells and the increased expression of *otx5* within the pineal anlage. Interestingly, we found that downregulation of *sox2* leads to a moderate, but significant enlargement of the presumptive pineal gland, as judged by the expression of *flh*. We therefore hypothesize that sox2 controls neurogenesis by inhibiting the expression of *flh*. However, by 24 hpf, *flh* expression is indistinguishable between morphant and control siblings, suggesting that a different gene/pathway is involved that provides a second/independent mechanism of regulation (**Figure 6.1**).

flh modulates neurogenesis by controlling the expression of the proneural genes, *ascl1a* and *neurog1* (Masai et al., 1997; Cau and Wilson, 2003). Expression of *ascl1a* is normal at early stages, but upregulated at 28 hpf when sox2 is downregulated. Notably, we found that neurogenesis is increased in *sox2* morphants even at 24 hpf, when *ascl1a* expression is relatively normal. Therefore, *ascl1a* upregulation cannot alone explain the increased number of neurons observed in *sox2* morphants. However, Cau and Wilson (2003) demonstrated that *flh* controls the expression of other genes also involved in neurogenesis and/or cell-fate determination, such as *otx5*, *delta* and *flh* itself. Therefore,

further investigation is required to fully elucidate the mechanisms that control pineal neurogenesis.

The Notch pathway also negatively regulates neurogenesis, but downregulation of Notch does not affect the number of progenitor cells (*flh* expression is normal). In contrast, Notch controls neurogenesis by inhibiting the expression of the proneural genes *ascl1a* and *neurog1* (Cau et al., 2008). Our data demonstrate that simultaneous downregulation of both *sox2* and Notch leads to a synergistic effect (the total number of isl-positive neurons is greater than the sum of individual downregulations). Although it is well accepted that the additive effect of phenotypes upon downregulation of two genes/pathways means that the two genes/pathways work independently of each other, the interpretation of synergistic effects is controversial (reviewed in Pérez-Pérez et al., 2009). At least three models have been proposed to explain how synergy arises:

a) Mutation of paralogs with functional redundancy.

b) Disruption of two at least partially independent pathways that have a common node.

c) Mutation of one gene increases the sensitivity to the phenotype of a second mutation.

However, all three explanations are based on the assumption that mutation results in complete loss of the protein. In the case of downregulation, two genes may interact synergistically even if they work in a linear pathway (reviewed in Pérez-Pérez et al., 2009).

In the case of the zebrafish epithalamus, *sox2* and Notch are not homologous, thereby ruling out the first explanation. Since, downregulation of one does not affect the expression of the other, we hypothesize that the two do not work through the same linear pathway. It is likely that downregulation of *sox2* makes the embryos more sensitive to drug treatments (*sox2* morphants are smaller and thus DAPT-treatment may be more effective than in control embryos). However, as discussed in section **6.2.2**, simultaneous downregulation of *sox2* and Notch results in an additive effect (not synergistic effect) in cell-type specification, suggesting that *sox2* morphants are not more sensitive to DAPT-treatment than control siblings. Instead, the most attractive explanation is that *sox2* and

Notch work through two different pathways that converge at a common node. In particular, we showed that *sox2* controls neurogenesis by modulating the expression of *flh* and as a consequence the expression of downstream genes, such as *ascl1a* and *otx5* (**Figure 6.1**). In contrast, Notch controls neurogenesis by inhibiting *ascl1a* expression. It is unknown whether downregulation of Notch affects other genes involved in neurogenesis and/or cell fate determination, such as *otx5*. Therefore, further studies are required in order to fully understand the mechanism(s) that control pineal neurogenesis. Also, it will be interesting to investigate whether *sox2* affects other members of the pathway, such as *neurog1*, *neurod* and *delta* genes. Alternatively, sox2 may control neurogenesis by modulating the timing of cell-cycle exit and differentiation of the pineal progenitor cells, similar to the BMP pathway (Quillien et al., 2011). Birthdating experiments are necessary to test whether proliferation and cell-cycle exit are affected in *sox2* morphants. In addition, although downregulation of *otx5* leads to decreased number of photoreceptors, it is unknown whether this is due to a defect in neurogenesis and/or in cell-fate determination (Gamse et al., 2002; Appelbaum et al., 2005; Pierce et al., 2008).

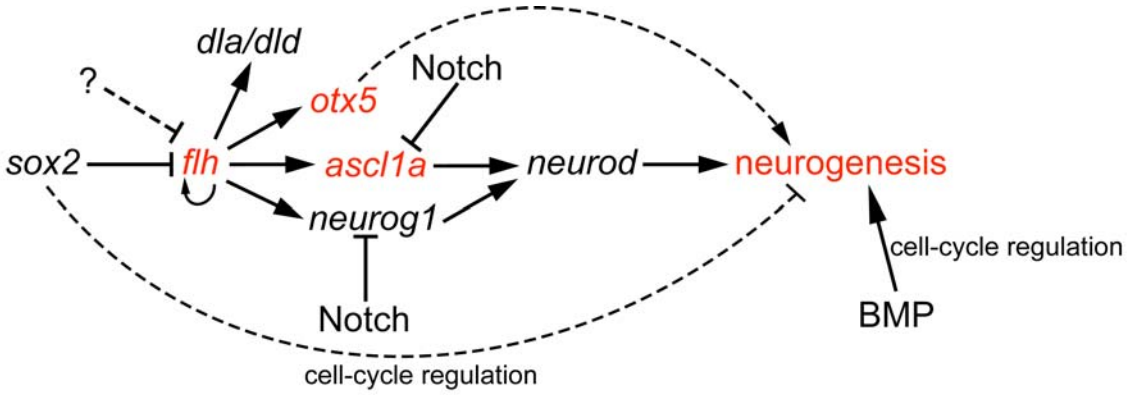

Figure 6.1 sox2 controls neurogenesis by inhibiting the expression of *flh*. *sox2* negatively regulates *flh*, which in turn promotes neurogenesis by modulating the expression of the proneural genes *ascl1a* and *neurog1*. *flh* also controls the expression of *dla*, *dld*, *otx5* and *flh* itself through an *ascl1a*/*neurog*-independent pathway. In contrast to *sox2*, the Notch pathway controls neurogenesis by inhibiting the expression of the proneural genes *ascl1a* and *neurog1*, without affecting the expression of *flh*. BMP also modulates neurogenesis by controlling the timing of cell-cycle exit and differentiation of progenitor cells (cell-cycle regulation). sox2 may act (at least in part) through a similar mechanism. Dashed lines represent possible interactions, ? represents a possible second

mechanism important for *flh* modulation, red represents genes and process (neurogenesis) affected in *sox2* morphants.

6.2.2 Cell-fate determination: *sox2*, BMP and Notch

In addition to its role in modulating neurogenesis, *sox2* is involved in cell-fate determination within the pineal anlage. In particular, we showed that downregulation of *sox2* results in an increased number of photoreceptors, while the number of projection neurons is unaffected. Currently, two other pathways are known to control the specification of pineal cells: Notch and BMP pathway. Notch negatively regulates projection neuron fate (Cau et al., 2008), while BMP promotes photoreceptor fate (Quillien et al., 2011). We found that downregulation of both *sox2* and Notch results in additive effects: *sox2* morphants have an increased number of photoreceptors, downregulation of Notch (via DAPT treatment) leads to an increased number of projection neurons, downregulation of both sox2 and Notch simultaneously results in increases in both cell types at levels comparable to the single downregulations. Therefore, *sox2* and Notch work through two different and independent pathways in controlling cell-fate determination. This is also supported by the fact that downregulation of one gene does not affect the expression of the other within the pineal anlage.

In contrast to *sox2* and Notch, which negatively regulate photoreceptor and projection neuron identity respectively, the BMP pathway promotes the photoreceptor fate. Therefore, downregulation of BMP results in fewer photoreceptors, whereas upregulation of the pathway leads to excess photoreceptors (Quillien et al., 2011). These data raise the question whether *sox2* and BMP work in the same or parallel pathways in modulating photoreceptor identity. Interestingly, although at 24 hpf the number of BMP-positive cells is similar between *sox2* morphants and control siblings, a small increased in the number of BMP-positive cells is observed at 28 hpf in *sox2* morphants. Since BMP is expressed (at least in part) in the photoreceptors, it is unclear whether:

a) *sox2* negatively regulates BMP which in turn promotes photoreceptor identity.

b) *sox2* negatively regulates photoreceptors independent of BMP. In this case, downregulation of *sox2* leads to an increased number of photoreceptors (which are cells competent to express BMP) and as a result an increased number of BMP-positive cells.

The fact that we observed an increased number of photoreceptors in *sox2* morphants at 24 hpf (when BMP expression is normal) suggests that *sox2* controls photoreceptor identity independently of BMP. It will be interesting to test whether simultaneous overexpression of BMP and downregulation of *sox2* leads to additive effect on the number of photoreceptors.

Notably, *sox2* is expressed in all progenitor cells. Therefore, how does *sox2* inhibit the photoreceptor program only in a subset of them? Two possible explanations can be envisioned. Firstly, previous studies demonstrated that *sox2* is a dose-dependent regulator during development (Avilion et al., 2003; Ferri et al., 2004; Taranova et al., 2006). Thus, subtle differences in the expression levels of *sox2* may provide specificity to its function (i.e. cells that express higher levels of *sox2* are more prone to *sox2*-mediated photoreceptor-inhibition). Alternatively, a sox2 partner protein (expressed only in a subset of progenitors) may provide specificity to its function. This is in agreement with previous studies demonstrating that in order to properly function, sox2 requires a partner protein that stabilizes its DNA binding and also provides specificity. Particularly, depending on the developmental time and/or cell type, different partner proteins are available and therefore different *sox2* targets are modulated (reviewed in Kamachi et al., 2000; Hever et al., 2006; Lefebvre et al., 2007). A good candidate to act as a sox2 partner within the developing pineal gland is pax6. Pax6 is a known Sox2 partner and co-binding of the two proteins is required for lens induction (Kondoh et al., 2004). Interestingly, within the developing pineal gland, *pax6* is expressed in projection neurons and in a subset of progenitor cells (Cau et al., 2008; Quillien et al., 2011). Therefore, one possibility is that although sox2 is expressed in all progenitor cells, only cells that express both *sox2* and *pax6* (or some other partner protein) are affected by its function and therefore become projection neurons.

One interesting characteristic of cell-fate determination within the pineal gland is that disruption of a specific modulator (BMP, Notch or *sox2*) only affects one of the two

cell-types. This is different from previous models for Notch-mediated cell-fate determination elsewhere in the brain, where Notch is responsible for binary decisions and thus in the absence of Notch one cell type is increased at the expense of the other (reviewed in Cau and Blader, 2009). Based on this striking difference, Quillien et al. (2011) proposed a number of models that can explain (at least in part) how cell fate is determined within the pineal gland. Below we describe two possible models (adapted from Quillien et al., 2011) and discuss how *sox2*, BMP and Notch functions can be incorporated into them.

6.2.2.1 Model I: One inhibiting and one inducing modulator for each cell type

According to this model, two modulators control the fate of a single cell: one modulator induces a specific fate, whereas the other inhibits the opposite fate (**Figure 6.2**). However, it should be noted that the proposed mechanism is dose-dependent. Therefore, lower levels of the inducing modulator will result in fewer cells adopting that specific fate. Similarly, if neurogenesis is increased, the wildtype levels of modulators are not sufficient to determine the fate of these extra neurons. Also, although the inhibiting modulators negatively regulate a cell fate, they are not sufficient to specify a cell. As a consequence, in the absence of an inducing modulator some cells will be unspecified as the inhibiting modulator inhibits them from adopting the opposite fate.

In particular, BMP cell-autonomously promotes photoreceptor identity. Within the same cells, Notch is activated, which inhibits the cells from becoming projection neurons. Therefore, BMP is the photoreceptor-inducing modulator, whereas Notch is the projection-neuron-inhibiting modulator. However, if these were the only cell-fate determinants, simultaneous downregulation of both BMP and Notch would result in a projection-neurons-only pineal gland. Since this is not the case (unpublished data discussed in Quillien et al., 2011), the authors proposed that a projection-neuron-inducing (PN-inducing) signal (yet to be identified) is required for cells to become projection neurons. Therefore, in the case of simultaneous downregulation of BMP and Notch, not enough PN-inducing signal is present and thus not all cells become projection neurons.

In this model, we hypothesize that *sox2* will function within the presumptive projection neurons to inhibit them from becoming photoreceptors (photoreceptor-inhibiting modulator). Therefore, in *sox2* morphants, the BMP/Notch/PN-inducing signals are still able to specify the normal number of photoreceptors and projection neurons (even in the absence of *sox2*). However, the extra neurons generated (downregulation of *sox2* leads to increased neurogenesis) are not inhibited by *sox2* and thus are more competent to become photoreceptors.

Although this model can explain most of the defects observed in mutants/morphants, it has some limitations. For example, downregulation of Notch leads to increased number of projection neurons. But if the levels of the PN-inducing signal are normal, how are these extra neurons specified? One possibility is that Notch negatively regulates the PN-inducing signal, i.e. downregulation of Notch leads to increased PN-inducing signal and subsequently increased projection neurons. Further studies are required to identify this PN-inducing signal and characterize its molecular interactions. Similarly, downregulation of *sox2* results in an increased number of photoreceptors. However, since BMP levels are normal, at least at early stages, in *sox2* morphants, how are these extra photoreceptors induced? In addition, as discussed above, simultaneous downregulation of BMP and Notch does not result in projection-neurons-only pineal glands. Even if the PN-inducing signal is not sufficient to specify all neurons toward the projection neurons fate, what induces some of these cells to become photoreceptors? All these limitations suggest an alternative model.

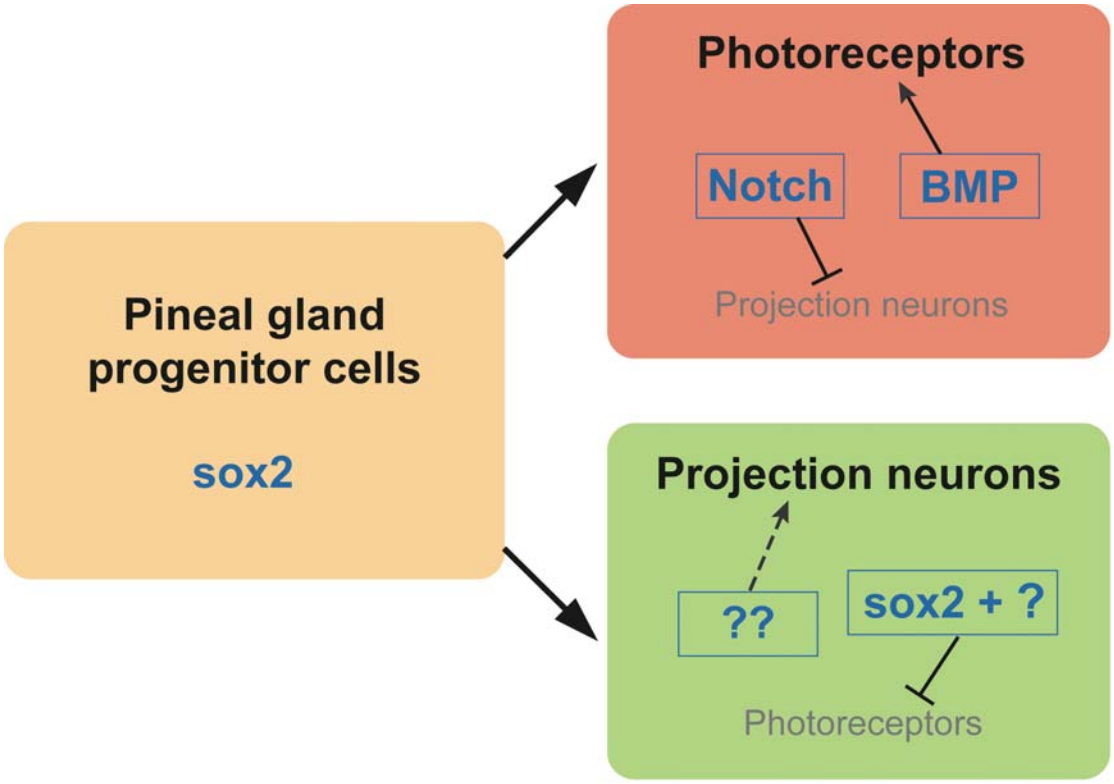

Figure 6.2 Model I: One inhibiting and one inducing modulator for each cell type. Pineal gland progenitor cells (orange) can give rise to both photoreceptors (red) and projection neurons (green). According to this model, each cell type is defined by the activity of an inducing and an inhibiting modulator. In particular, within the presumptive photoreceptors, the activity of BMP promotes the photoreceptor fate, while Notch inhibits the projection neuron fate. In contrast, within the presumptive projection neurons, a yet-to-be-identified modulator (??) promotes the projection neuron fate, whereas the function of sox2 (differential levels of sox2 or sox2 along with a partner protein(?)) inhibits cells from becoming photoreceptors.

6.2.2.2 Model II: Prepatterning of the pineal cells

Our second model is based on the proposal from Quillien et al. (2011) that pineal gland progenitor cells are prepatterned towards a specific cell fate (**Figure 6.3**). According to this model, a subset of pineal gland progenitor cells is more primed to become photoreceptors, while others are more primed to become projection neurons. However, this first step of regulation (prepatterning) is not sufficient to determine correct numbers of both cell types. Instead, a second level of regulation (BMP, Notch

and the PN-inducing signal) is required to fine-tune this initial prepatterning, by a mechanism similar to the one described for Model I (discussed in section **6.2.2.1**).

Based on our data, we hypothesize that *sox2* is important for this prepatterning of the pineal gland progenitors. In particular, levels of sox2 and/or partner protein(s) (discussed above) provide specificity to its function, so that some cells are inhibited from becoming prepatterned towards the photoreceptor program.

This model can explain the questions arising from the first model. For example, simultaneous downregulation of BMP and Notch does not result in a projection-neuron-only pineal gland, because prepatterning towards the photoreceptor program is able to guide at least some cells to adopt photoreceptor fate, even in the absence of BMP. Moreover, downregulation of sox2 results in all or more progenitor cells becoming prepatterned towards a photoreceptor fate. Since BMP, Notch and the PN-inducing signal are intact, normal numbers of photoreceptors and projection neurons are generated, as these modulators are able to overcome the prepatterning. However, the extra neurons generated as a consequence of the *sox2* downregulation become photoreceptors, because not enough PN-inducing signal is available to change their prepatterning. Interestingly, a significant increased in the number of cells expressing BMP is observed in *sox2* morphants, following the increase in the number of photoreceptors (as judged by *aanat2* expression). These data suggest that prepatterning towards the photoreceptor fate may be necessary for the activation of the BMP pathway in the cells that will become photoreceptors. Therefore, in the case of *sox2* morphants, more cells initiate the photoreceptor program and thus BMP activity is upregulated in order to properly specify these cells.

Although during the last few years our knowledge regarding the mechanism(s) that controls cell-fate determination within the pineal gland has increased dramatically, several aspects remain elusive. For example, what is the PN-inducing signal and does it interact with other modulators? Also, if sox2 function is necessary for inhibiting prepatterning towards the photoreceptor program, is there another signal(s) that inhibits prepatterning towards the projection neuron program? Or perhaps, is there a signal to promote prepatterning towards the photoreceptor and/or projection neuron fate?

Alternatively, is photoreceptor prepatterning the default state? In addition, what provides specificity to *sox2* function? Is pax6 a sox2-partner protein necessary for prepatterning? Finally, during normal pineal gland development, how are these modulators (*sox2*, BMP and Notch) controlled and what are their downstream targets?

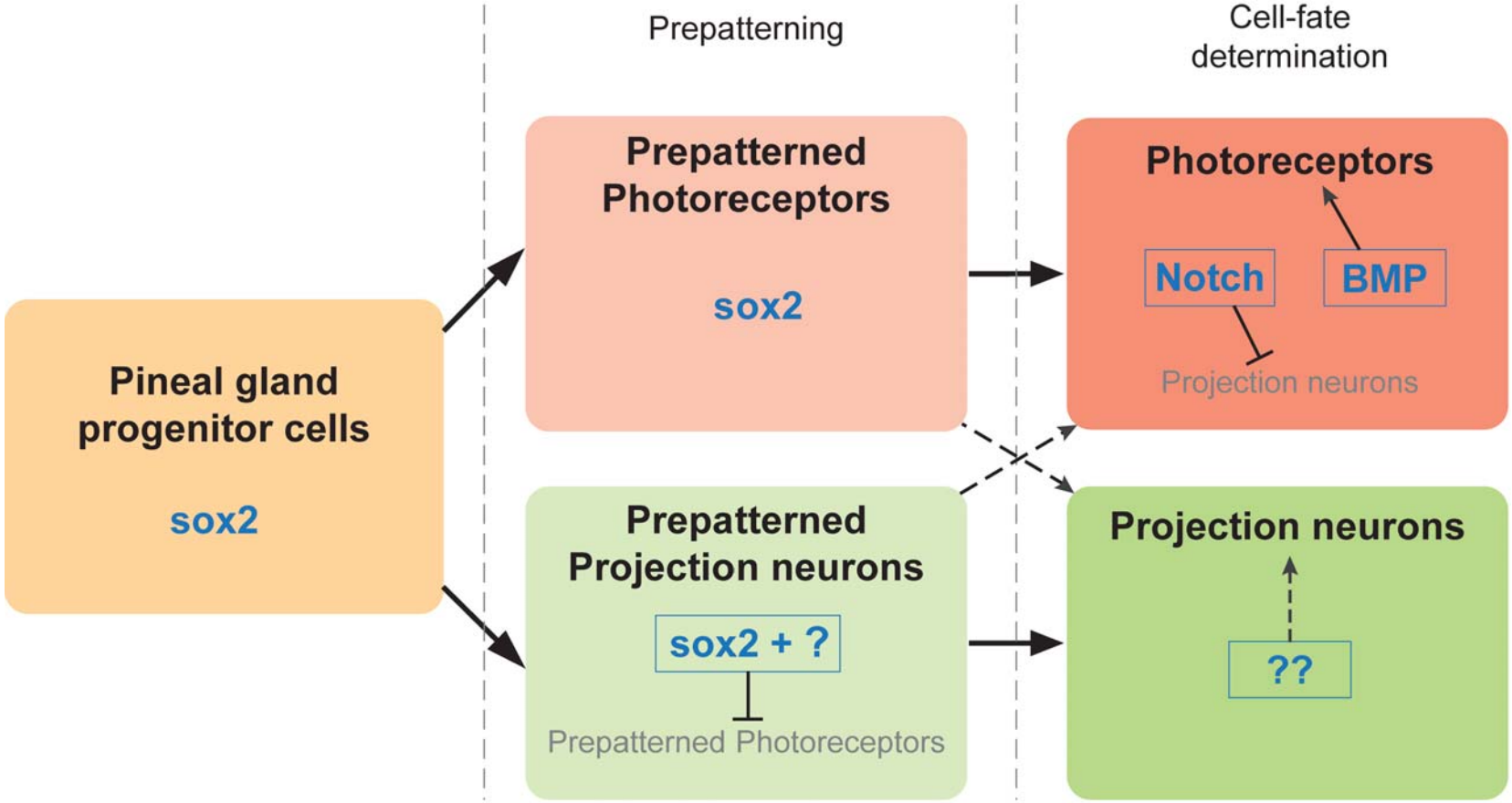
Prepatterning
Cell-fate determination
Pineal gland progenitor cells
sox2
Prepatterned Photoreceptors
sox2
Prepatterned Projection neurons
sox2 + ?
Prepatterned Photoreceptors
Photoreceptors
Notch
BMP
Projection neurons
Projection neurons
??

Figure 6.3 Model II: sox2 is important for the prepatterning of pineal progenitor cells. According to this model, pineal progenitor cells (orange) are prepatterned towards a photoreceptor (light red) or projection neuron (light green) fate. sox2, along with its partner protein or high levels of sox2 (?), inhibits prepatterning towards the photoreceptor program in a subset of progenitor cells. As a result, these cells are prepatterned to become projection neurons. However, this prepatterning is not sufficient for proper cell-fate determination. Instead, a second level of regulation controlled by Notch, BMP and the PN-inducing modulator (??) is required to fine-tune the number of photoreceptors (red) and projection neurons (green) generated.

6.3 sox2 is required for the proper specification/migration of parapineal cells and consequently for the proper establishment of habenular asymmetries

In addition to the role of *sox2* in neurogenesis and cell-fate determination within the pineal anlage, we have demonstrated that *sox2* morphants have abnormal parapineal organs and consequently disrupted habenular architecture. In particular, *sox2* morphants have either normal left-sided or reversed right-sided or bilateral/scattered parapineal organs. The number of parapineal cells appears normal in *sox2* morphants, but quantitative analysis is necessary to confirm this.

The abnormal placement of the parapineal organ observed in *sox2* morphants leads to disruption of the asymmetric architecture of the habenulae. In particular:

a) Embryos with normal left-sided parapineal organs have more intense neuropil staining in the left than the right habenula, similar to controls.
b) Embryos with right-sided parapineal organ exhibit reversal of the habenular asymmetries.
c) In embryos with scattered parapineal cells that result in bilateral parapineal projections, the left and right habenulae appear symmetric.

These results are in agreement with previous studies suggesting that the parapineal organ is important for the proper elaboration of habenular asymmetries (**Table 1.2**). However, it should be noted that the asymmetric architecture of the habenulae was determined only by analyzing the expression of the *kctd12.1* marker that labels the majority of lateral habenular neurons and the volume of neuropils was analyzed using phalloidin staining. Therefore, further investigation (e.g. markers for the other subtypes of neurons) is required to confirm the asymmetric defects. In addition,

although the habenular asymmetry correlates with the position of the parapineal in *sox2* morphants, the neuropil volume is smaller in all morphants when compared to control siblings. Since *sox2* morphants show a general growth delay, as well as a delay in the expression of parapineal (*gfi1ab*) and habenular (*kctd12.1*) markers, we hypothesize that the smaller volume of the habenular neuropils reflects a delay in development. Staining at later stages is necessary to confirm this hypothesis.

6.3.1 Randomization of parapineal organ and habenular asymmetries

As discussed above, we found that 10-20% of embryos exhibit reversal of parapineal positioning, coupled with reversal of the habenular asymmetries. In addition, about 30% of embryos have normal parapineal and habenular development. Disruption of Nodal signaling within the diencephalon results in randomization of asymmetries: 50% of embryos develop normal parapineal organs and habenulae, while 50% of embryos exhibit right-sided parapineal organs and reversal of habenular asymmetries (**Table 1.2**). Approximately 40% of *sox2* morphants have abnormal bilateral expression of *pitx2*, a downstream effector of Nodal normally expressed only in the left diencephalon. Therefore, the data suggest that parapineal and habenular reversal (10-20%) is due to disruption of the Nodal pathway. To confirm this hypothesis, we need to sort embryos according to their Nodal expression at early stages and check parapineal and habenular development at later stages.

However, based on the hypothesis that disruption of Nodal is responsible for randomization of epithalamic asymmetries in *sox2* morphants, we would expect normal parapineal positioning and habenular asymmetries in about 20% of embryos (instead of the observed 30%). This difference probably reflects a limitation of the morpholinos. Previous studies showed that *Sox2* is a dose-dependent regulator during development (Ferri et al., 2004; Taranova et al., 2006). Therefore, subtle differences in the levels of downregulation may lead to the variability observed.

Further investigation is required to understand how *sox2* controls the expression of Nodal genes both in the LPM and the diencephalon. For example, it will be interesting to test whether expression of *spaw* (the first asymmetrically expressed Nodal

gene) is disrupted in *sox2* morphants. Moreover, the asymmetric activation of Nodal is controlled by cilia movements in the Kupffer's vesicle. Therefore, does downregulation of *sox2* result in abnormal formation/function of the Kupffer's vesicle? In addition, heart looping is defecting in *sox2* morphants and therefore cannot be used to study visceral laterality. But is laterality of other visceral organs (such as liver and pancreas) affected in *sox2* morphants? This could be determined by carrying out optical projection tomography (OPT) analysis on morphants to visualize the viscera. Finally, why does only a subset (about 40%) of *sox2* morphants have disrupted Nodal expression in the diencephalon?

6.3.2 Bilateral parapineal organs and left isomerism of the habenulae

In addition to the randomization of the parapineal organ, about 50% of *sox2* morphants exhibit a rare defect: scattered parapineal cells that project towards both the left and right habenulae, resulting in symmetric development of the habenulae (left isomerism). Bilateral parapineal organs coupled with symmetric habenulae are only observed in about 0.3% of wildtype embryos (Gamse et al., 2003). This phenotype is also observed in some mutants, but at much lower frequency (between 1-6%) (Gamse et al., 2003) than in *sox2* morphants (50%). Therefore, the high frequency of this phenotype in *sox2* morphants makes them an attractive model to study the mechanisms that control migration of the parapineal organ as a coherent structure rather than individual cells. In addition, *sox2* morphants can be used to test whether left isomerism of the habenulae affects innervation of the IPN. Moreover, although a number of studies demonstrated that reversal of the epithalamic asymmetries affects some behavioral functions, nothing is known about the behavior of animals with bilateral parapineals and symmetric habenulae. Unfortunately, *sox2* morphants die around at 6 dpf, at a stage where behavioral test are difficult to perform.

Notably, recent data suggest that failure of the anterior neural tube to close also leads to bilateral parapineal organs and left isomerism of the habenulae (Lu et al., 2012). In particular, embryos with disrupted Nodal signaling, as well as disrupted *cadherin 2, neuronal* (*cdh2*, previously known as *n-cadherin*) expression, have bilateral parapineal

organs that lead to symmetric habenular development (Lu et al., 2012, 2012). However, in contrast to *sox2* morphants, in these embryos the pineal gland is also divided as the two *flh*-positive domains fail to fuse at the midline. Therefore, these embryos cannot be used to study the mechanism that controls the migration of parapineal cells as a coherent group.

Why does the downregulation of *sox2* result in bilateral parapineal organs? To answer this question, we first need to understand how parapineal migration is achieved. Two major types of migration exist: single-cell migration and collective-cell migration. In single-cell migration, cells move individually and independently of other migrating cells. In contrast, collective-cell migration is observed when a loosely- or closely-associated group of cells moves together. These cells affect each other's migration through either direct cell-cell interactions (adhesion) or signaling. Another feature of collective migration is that cells within the group have different properties: leaders/followers, front/back, tip/stalk (reviewed in Rørth, 2009, 2012). The current data suggest that parapineal cells migrate collectively:

a) They all tend to migrate towards the same direction at the same developmental stage.
b) Timelapse experiments revealed that a few cells start migrating towards the left (leader cells) and are followed by the remaining cells (followers), suggesting the leader-follower mechanism often seen in collective migration.
c) Parapineal cells appear to contact each other (as judged by timelapse) at least at some points during their migration.

Collective-cell migration is a very dynamic process that requires proper polarization of cells, use of the cytoskeleton, establishment of different cell states (leader/follower), interactions between the migrating cells, as well as interactions between the migrating cells and their environment (reviewed in Rørth, 2009, 2012). In the case of parapineal organ, previous studies demonstrated that parapineal cells required Fgf and Nodal signaling for their proper migration towards the left. These signals reflect "interactions" between parapineal cells and their environment. In addition, Snelson et al. (2008a) suggested that *tbx2b* is required for the specification

and/or maintenance of leader cells. Therefore, in the absence of *tbx2b* leader cells are missing/defective, they cannot initiate migration and as a consequence parapineal cells remain at the midline. Interestingly, *sox2* morphants have reduced levels of *tbx2b* expression, suggesting that specification of leader cells may be defective. Since, parapineal cells manage to migrate (albeit abnormally), reduction of *tbx2b* cannot solely explain the defects observed. Instead, we hypothesize that downregulation of *sox2* disrupts the communication between parapineal cells and as a consequence parapineal cells migrate individually. In particular, we propose that *sox2* is important for cell adhesion between parapineal cells by directly or indirectly modulating the levels and/or intracellular localization of adhesion molecules, such as cadherins. *cdh2* is a good candidate for this since it is expressed in the epithalamus at the appropriate stage and modulates the adhesion properties of the pineal complex: *cdh2* mutants and morphants have divided pineal and parapineal organs (Lu et al., 2012, 2012). However, *sox2* morphants only have bilateral parapineal organs (not pineal glands) suggesting that downregulation of sox2 specifically affects the adhesion properties of parapineal cells (not pineal cells).

In agreement with our hypothesis, Parrinelo and colleagues (2010) demonstrated a role for *Sox2* in the coordination of cell migration and tissue patterning following injury of the peripheral nervous system in rodents. In particular, the authors showed that ephrin/Eph signaling modifies and/or stabilizes Sox2 in dedifferentiated Schwann cells (glial cells found in the peripheral nervous system) during nerve regeneration. Sox2 is then necessary and sufficient to relocalize Cdh2 at the junctions of Schwann cells. This relocalization of Cdh2 promotes direct cell-cell interactions, which are important for nerve regeneration. Notably, overexpression of Sox2 in cultured Schwann cells increases both the levels of junctional Cdh2 and the clustering behavior of cells. In contrast, downregulation of *Sox2* using small interfering RNA greatly reduced cell clustering (Parrinello et al., 2010). In addition, SOX2 controls CDH2 levels in the developing neural tube in chick embryos: downregulation of SOX2 leads to decreased expression of CDH2 in neural progenitor cells and as a consequence some cells migrate abnormally away from the ventricular zone (Graham et al., 2003). Finally, Matsuma et al. (2005)

suggested that SOXB1 genes (SOX1-3) directly control the expression of CDH2 in developing chicks. In particular, they showed that *CDH2* enhancers contain SOX-binding sites and that *SOX2* expression always precedes *CDH2* expression in developing sensory placodes, suggesting that SOX2 (and/or SOX1-3) modulates *CDH2* expression. Moreover, misexpression of *SOXB1* genes in the head ectoderm results in ectopic activation of CDH2 and abnormal clustering of cells (Matsumata et al., 2005). All these suggest that sox2 may control parapineal migration by modulating the levels and/or localization of cdh2 in parapineal cells. However, further investigation is necessary to confirm this hypothesis.

6.4 Concluding remarks

In this study, we established and characterized an animal model that enables us to dissect the functions of *sox2* during vertebrate development and disease. In particular, downregulation of *sox2* (using morpholino microinjections) in zebrafish recapitulates many of the phenotypic defects observed in human patients with heterozygous mutations in *SOX2* and in *Sox2*-hypomorphic mice. This, along with the numerous advantages of zebrafish, makes *sox2* morphants an excellent model to study embryogenesis and in particular brain development.

In addition, the data presented here demonstrate novel roles for *sox2* during the development of the zebrafish epithalamus. Specifically, we showed that *sox2* controls both neurogenesis and cell-fate determination within the pineal gland. In addition, *sox2* is important for the proper specification and migration of parapineal cells towards the left side of the brain and as a consequence for the proper establishment of habenular asymmetries.

References

Abulafia, R., Zalkind, V., and Devor, M. (2009). Cerebral activity during the anesthesia-like state induced by mesopontine microinjection of pentobarbital. *J. Neurosci.*, **29**, 7053–7064.

Agetsuma, M., Aizawa, H., Aoki, T., Nakayama, R., Takahoko, M., Goto, M., Sassa, T., Amo, R., Shiraki, T., Kawakami, K., et al. (2010). The habenula is crucial for experience-dependent modification of fear responses in zebrafish. *Nat. Neurosci.*, **13**, 1354–1356.

Aghajanian, G. K. and Wang, R. Y. (1977). Habenular and other midbrain raphe afferents demonstrated by a modified retrograde tracing technique. *Brain Res.*, **122**, 229–242.

Aizawa, H., Bianco, I. H., Hamaoka, T., Miyashita, T., Uemura, O., Concha, M. L., Russell, C., Wilson, S. W., and Okamoto, H. (2005). Laterotopic representation of left-right information onto the dorso-ventral axis of a zebrafish midbrain target nucleus. *Curr. Biol.*, **15**, 238–243.

Aizawa, H., Goto, M., Sato, T., and Okamoto, H. (2007). Temporally regulated asymmetric neurogenesis causes left-right difference in the zebrafish habenular structures. *Dev. Cell*, **12**, 87–98.

Albertson, R. C. and Yelick, P. C. (2005). Roles for fgf8 signaling in left-right patterning of the visceral organs and craniofacial skeleton. *Dev. Biol.*, **283**, 310–321.

Alexander, J., Rothenberg, M., Henry, G. L., and Stainier, D. Y. (1999). casanova Plays an Early and Essential Role in Endoderm Formation in Zebrafish. *Developmental Biology*, **215**, 343–357.

Amo, R., Aizawa, H., Takahoko, M., Kobayashi, M., Takahashi, R., Aoki, T., and Okamoto, H. (2010). Identification of the zebrafish ventral habenula as a homolog of the mammalian lateral habenula. *J. Neurosci.*, **30**, 1566–1574.

Appelbaum, L., Anzulovich, A., Baler, R., and Gothilf, Y. (2005). Homeobox-clock protein interaction in zebrafish. A shared mechanism for pineal-specific and circadian gene expression. *J. Biol. Chem.*, **280**, 11544–11551.

Araki, M., McGeer, P. L., and Kimura, H. (1988). The efferent projections of the rat lateral habenular nucleus revealed by the PHA-L anterograde tracing method. *Brain Res.*, **441**, 319–330.

Araki, M., McGeer, P. L., and McGeer, E. G. (1984). Retrograde HRP tracing combined with a pharmacohistochemical method for GABA transaminase for the

identification of presumptive GABAergic projections to the habenula. *Brain Res.*, **304**, 271–277.

Archer, S. N., Robilliard, D. L., Skene, Debra J, Smits, M., Williams, A., Arendt, Josephine, and Von Schantz, M. (2003). A length polymorphism in the circadian clock gene Per3 is linked to delayed sleep phase syndrome and extreme diurnal preference. *Sleep*, **26**, 413–415.

Avilion, A. A., Nicolis, S. K., Pevny, L. H., Perez, L., Vivian, N., and Lovell-Badge, R. (2003). Multipotent cell lineages in early mouse development depend on SOX2 function. *Genes Dev*, **17**, 126–140.

Bakrania, P., Robinson, D. O., Bunyan, D. J., Salt, A, Martin, A., Crolla, J. A., Wyatt, A., Fielder, A., Ainsworth, J., Moore, A., et al. (2007). SOX2 anophthalmia syndrome: 12 new cases demonstrating broader phenotype and high frequency of large gene deletions. *Br J Ophthalmol*, **91**, 1471–1476.

Barth, K. A., Kishimoto, Y., Rohr, K. B., Seydler, C., Schulte-Merker, S., and Wilson, S. W. (1999). Bmp activity establishes a gradient of positional information throughout the entire neural plate. *Development*, **126**, 4977–4987.

Barth, K. A., Miklosi, A., Watkins, J., Bianco, I. H., Wilson, S. W., and Andrew, R. J. (2005). fsi zebrafish show concordant reversal of laterality of viscera, neuroanatomy, and a subset of behavioral responses. *Curr. Biol.*, **15**, 844–850.

Bartsch, C., Bartsch, H., Flüchter, S. H., Attanasio, A., and Gupta, D. (1985). Evidence for modulation of melatonin secretion in men with benign and malignant tumors of the prostate: relationship with the pituitary hormones. *J. Pineal Res.*, **2**, 121–132.

Bartsch, C., Bartsch, H., Jain, A. K., Laumas, K. R., and Wetterberg, L. (1981). Urinary melatonin levels in human breast cancer patients. *J. Neural Transm.*, **52**, 281–294.

Bedell, V. M., Wang, Y., Campbell, J. M., Poshusta, T. L., Starker, C. G., Krug Ii, R. G., Tan, W., Penheiter, S. G., Ma, A. C., Leung, A. Y. H., et al. (2012). In vivo genome editing using a high-efficiency TALEN system. *Nature*.

Benabid, A. L. and Jeaugey, L. (1989). Cells of the rat lateral habenula respond to high-threshold somatosensory inputs. *Neurosci. Lett.*, **96**, 289–294.

Beretta, C. A., Dross, N., Guiterrez-Triana, J. A., Ryu, S., and Carl, M. (2012). Habenula circuit development: past, present, and future. *Front Neurosci*, **6**, 51.

Bertrand, N., Castro, D. S., and Guillemot, F. (2002). Proneural genes and the specification of neural cell types. *Nat. Rev. Neurosci.*, **3**, 517–530.

Bianco, I. H. and Wilson, S. W. (2009). The habenular nuclei: a conserved asymmetric relay station in the vertebrate brain. *Philos. Trans. R. Soc. Lond., B, Biol. Sci*, **364**, 1005–1020.

Bianco, I. H., Carl, M., Russell, C., Clarke, J. D. W., and Wilson, S. W. (2008). Brain asymmetry is encoded at the level of axon terminal morphology. *Neural Dev*, **3**, 9.

Binkley, S. A., Riebman, J. B., and Reilly, K. B. (1978). The pineal gland: a biological clock in vitro. *Science*, **202**, 1198–1120.

Bisgrove, B. W., Essner, J. J., and Yost, H. J. (2000). Multiple pathways in the midline regulate concordant brain, heart and gut left-right asymmetry. *Development*, **127**, 3567–3579.

Blake, M. J., Nowak, T. S., J., and Holbrook, N. J. (1990). In vivo hyperthermia induces expression of HSP70 mRNA in brain regions controlling the neuroendocrine response to stress. *Brain Res. Mol. Brain Res.*, **8**, 89–92.

Boyer, L. A., Lee, T. I., Cole, M. F., Johnstone, S. E., Levine, S. S., Zucker, J. P., Guenther, M. G., Kumar, R. M., Murray, H. L., Jenner, R. G., et al. (2005). Core transcriptional regulatory circuitry in human embryonic stem cells. *Cell*, **122**, 947–956.

Bray, S. J. (2006). Notch signalling: a simple pathway becomes complex. *Nat. Rev. Mol. Cell Biol.*, **7**, 678–689.

Buijs, R. M. (1978). Intra- and extrahypothalamic vasopressin and oxytocin pathways in the rat. Pathways to the limbic system, medulla oblongata and spinal cord. *Cell Tissue Res.*, **192**, 423–435.

Cade, L., Reyon, D., Hwang, W. Y., Tsai, S. Q., Patel, S., Khayter, C., Joung, J. K., Sander, J. D., Peterson, R. T., and Yeh, J. R. J. (2012). Highly efficient generation of heritable zebrafish gene mutations using homo- and heterodimeric TALENs. *Nucleic Acids Res.*, **40**, 8001–8010.

Cagnacci, A., Soldani, R., and Yen, S. S. (1993). The effect of light on core body temperature is mediated by melatonin in women. *J. Clin. Endocrinol. Metab.*, **76**, 1036–1038.

Cahill, G. M. (1996). Circadian regulation of melatonin production in cultured zebrafish pineal and retina. *Brain Res.*, **708**, 177–181.

Caldecott-Hazard, S., Mazziotta, J., and Phelps, M. (1988). Cerebral correlates of depressed behavior in rats, visualized using 14C-2-deoxyglucose autoradiography. *J. Neurosci.*, **8**, 1951–1961.

Caputo, A., Ghiringhelli, L., Dieci, M., Giobbio, G. M., Tenconi, F., Ferrari, L., Gimosti, E., Prato, K., and Vita, A. (1998). Epithalamus calcifications in schizophrenia. *Eur Arch Psychiatry Clin Neurosci*, **248**, 272–276.

Carl, M., Bianco, I. H., Bajoghli, B., Aghaallaei, N., Czerny, T., and Wilson, S. W. (2007). Wnt/Axin1/beta-catenin signaling regulates asymmetric nodal activation, elaboration, and concordance of CNS asymmetries. *Neuron*, **55**, 393–405.

Carlson, J., Armstrong, B., Switzer, R. C., 3rd, and Ellison, G. (2000). Selective neurotoxic effects of nicotine on axons in fasciculus retroflexus further support evidence that this a weak link in brain across multiple drugs of abuse. *Neuropharmacology*, **39**, 2792–2798.

Carlson, J., Noguchi, K., and Ellison, G. (2001). Nicotine produces selective degeneration in the medial habenula and fasciculus retroflexus. *Brain Res.*, **906**, 127–134.

Cau, E. and Blader, P. (2009). Notch activity in the nervous system: to switch or not switch? *Neural Dev*, **4**, 36.

Cau, E., Quillien, A., and Blader, P. (2008). Notch resolves mixed neural identities in the zebrafish epiphysis. *Development*, **135**, 2391–2401.

Cau, E. and Wilson, Stephen W (2003). Ash1a and Neurogenin1 function downstream of Floating head to regulate epiphysial neurogenesis. *Development*, **130**, 2455–2466.

Cavallaro, M., Mariani, J., Lancini, C., Latorre, E., Caccia, R., Gullo, F., Valotta, M., DeBiasi, S., Spinardi, L., Ronchi, A., et al. (2008). Impaired generation of mature neurons by neural stem cells from hypomorphic Sox2 mutants. *Development*, **135**, 541–557.

Cenci, M. A., Kalén, P., Mandel, R. J., and Björklund, A. (1992). Regional differences in the regulation of dopamine and noradrenaline release in medial frontal cortex, nucleus accumbens and caudate-putamen: a microdialysis study in the rat. *Brain Res.*, **581**, 217–228.

Cernysiov, V., Gerasimcik, N., Mauricas, M., and Girkontaite, I. (2010). Regulation of T-cell-independent and T-cell-dependent antibody production by circadian rhythm and melatonin. *Int. Immunol.*, **22**, 25–34.

Chambers, I. and Tomlinson, S. R. (2009). The transcriptional foundation of pluripotency. *Development*, **136**, 2311–2322.

Chassaing, N., Gilbert-Dussardier, B., Nicot, F., Fermeaux, V., Encha-Razavi, F., Fiorenza, M., Toutain, A., and Calvas, P. (2007). Germinal mosaicism and

familial recurrence of a SOX2 mutation with highly variable phenotypic expression extending from AEG syndrome to absence of ocular involvement. *Am. J. Med. Genet. A*, **143**, 289–291.

Chen, X., Xu, H., Yuan, P., Fang, F., Huss, M., Vega, V. B., Wong, E., Orlov, Y. L., Zhang, W., Jiang, J., et al. (2008). Integration of external signaling pathways with the core transcriptional network in embryonic stem cells. *Cell*, **133**, 1106–1117.

Choo, B. G. H., Kondrichin, I., Parinov, S., Emelyanov, A., Go, W., Toh, W., and Korzh, V. (2006). Zebrafish transgenic Enhancer TRAP line database (ZETRAP). *BMC Dev. Biol.*, **6**, 5.

Christoph, G. R., Leonzio, R. J., and Wilcox, K. S. (1986). Stimulation of the lateral habenula inhibits dopamine-containing neurons in the substantia nigra and ventral tegmental area of the rat. *J. Neurosci.*, **6**, 613–619.

Chung, W. S., Andersson, O., Row, R., Kimelman, D., and Stainier, D. Y. R. (2010). Suppression of Alk8-mediated Bmp signaling cell-autonomously induces pancreatic β-cells in zebrafish. *PNAS*, **107**, 1142–1147.

Cohen, S. R. and Melzack, R. (1986). Habenular stimulation produces analgesia in the formalin test. *Neurosci. Lett.*, **70**, 165–169.

Cohen, S. R. and Melzack, R. (1985). Morphine injected into the habenula and dorsal posteromedial thalamus produces analgesia in the formalin test. *Brain Res.*, **359**, 131–139.

Collery, R. F. and Link, B. A. (2011). Dynamic smad-mediated BMP signaling revealed through transgenic zebrafish. *Dev. Dyn.*, **240**, 712–722.

Concha, M L, Burdine, R. D., Russell, C, Schier, A. F., and Wilson, S W (2000). A nodal signaling pathway regulates the laterality of neuroanatomical asymmetries in the zebrafish forebrain. *Neuron*, **28**, 399–409.

Concha, M. L. and Wilson, S. W. (2001). Asymmetry in the epithalamus of vertebrates. *J. Anat.*, **199**, 63–84.

Concha, Miguel L, Russell, Claire, Regan, J. C., Tawk, M., Sidi, S., Gilmour, D. T., Kapsimali, M., Sumoy, L., Goldstone, K., Amaya, E., et al. (2003). Local tissue interactions across the dorsal midline of the forebrain establish CNS laterality. *Neuron*, **39**, 423–438.

Concha, M. L., Signore, I. A., and Colombo, A. (2009). Mechanisms of directional asymmetry in the zebrafish epithalamus. *Semin. Cell Dev. Biol.*, **20**, 498–509.

Covassin, L., Amigo, J. D., Suzuki, K., Teplyuk, V., Straubhaar, J., and Lawson, N. D. (2006). Global analysis of hematopoietic and vascular endothelial gene expression by tissue specific microarray profiling in zebrafish. *Dev. Biol*, **299**, 551–562.

Dadda, M., Domenichini, A., Piffer, L., Argenton, F., and Bisazza, A. (2010). Early differences in epithalamic left-right asymmetry influence lateralization and personality of adult zebrafish. *Behav. Brain Res.*, **206**, 208–215.

Dahlitz, M., Alvarez, B., Vignau, J., English, J., Arendt, J, and Parkes, J. D. (1991). Delayed sleep phase syndrome response to melatonin. *Lancet*, **337**, 1121–1124.

Deacon, S. and Arendt, J (1995). Melatonin-induced temperature suppression and its acute phase-shifting effects correlate in a dose-dependent manner in humans. *Brain Res.*, **688**, 77–85.

Deguchi, T. (1979). A circadian oscillator in cultured cells of chicken pineal gland. *Nature*, **282**, 94–96.

Doll, C. A., Burkart, J. T., Hope, K. D., Halpern, M. E., and Gamse, J. T. (2011). Subnuclear development of the zebrafish habenular nuclei requires ER translocon function. *Dev. Biol.*, **360**, 44–57.

Dollins, A. B., Lynch, H. J., Wurtman, R. J., Deng, M. H., Kischka, K. U., Gleason, R. E., and Lieberman, H. R. (1993). Effect of pharmacological daytime doses of melatonin on human mood and performance. *Psychopharmacology (Berl.)*, **112**, 490–496.

Ducy, P. and Karsenty, G. (2000). The family of bone morphogenetic proteins. *Kidney Int.*, **57**, 2207–2214.

Dufourcq, P., Rastegar, S., Strähle, U., and Blader, P. (2004). Parapineal specific expression of gfi1 in the zebrafish epithalamus. *Gene Expr. Patterns*, **4**, 53–57.

Ebisawa, T., Uchiyama, M., Kajimura, N., Mishima, K., Kamei, Y., Katoh, M., Watanabe, T., Sekimoto, M., Shibui, K., Kim, K., et al. (2001). Association of structural polymorphisms in the human period3 gene with delayed sleep phase syndrome. *EMBO Rep.*, **2**, 342–346.

Ellis, P., Fagan, B. M., Magness, S. T., Hutton, S., Taranova, O., Hayashi, S., McMahon, A., Rao, M., and Pevny, L. (2004). SOX2, a persistent marker for multipotential neural stem cells derived from embryonic stem cells, the embryo or the adult. *Dev. Neurosci.*, **26**, 148–165.

Ellison, G. (1992). Continuous amphetamine and cocaine have similar neurotoxic effects in lateral habenular nucleus and fasciculus retroflexus. *Brain Res.*, **598**, 353–356.

Ericson, J., Thor, S., Edlund, T., Jessell, T. M., and Yamada, T. (1992). Early stages of motor neuron differentiation revealed by expression of homeobox gene Islet-1. *Science*, **256**, 1555–1560.

Essner, J. J., Amack, J. D., Nyholm, M. K., Harris, E. B., and Yost, H. J. (2005). Kupffer's vesicle is a ciliated organ of asymmetry in the zebrafish embryo that initiates left-right development of the brain, heart and gut. *Development*, **132**, 1247–1260.

Etzioni, A., Luboshitzky, R., Tiosano, D., Ben-Harush, M., Goldsher, D., and Lavie, P. (1996). Melatonin replacement corrects sleep disturbances in a child with pineal tumor. *Neurology*, **46**, 261–263.

Facchin, L., Burgess, H. A., Siddiqi, M., Granato, M., and Halpern, M. E. (2009). Determining the function of zebrafish epithalamic asymmetry. *Philos. Trans. R. Soc. Lond., B, Biol. Sci.*, **364**, 1021–1032.

Faivre, L., Williamson, K. A., Faber, V., Laurent, N., Grimaldi, M., Thauvin-Robinet, C., Durand, C., Mugneret, F., Gouyon, J.-B., Bron, A., et al. (2006). Recurrence of SOX2 anophthalmia syndrome with gonosomal mosaicism in a phenotypically normal mother. *Am. J. Med. Genet. A*, **140**, 636–639.

Falcón, J., Migaud, H., Muñoz-Cueto, J. A., and Carrillo, M. (2010). Current knowledge on the melatonin system in teleost fish. *Gen. Comp. Endocrinol.*, **165**, 469–482.

Fantes, J., Ragge, N. K., Lynch, S. A., McGill, N. I., Collin, J. R. O., Howard-Peebles, P. N., Hayward, C., Vivian, A. J., Williamson, K., Van Heyningen, V., et al. (2003). Mutations in SOX2 cause anophthalmia. *Nat. Genet.*, **33**, 461–463.

Ferri, A. L. M., Cavallaro, M., Braida, D., Di Cristofano, A., Canta, A., Vezzani, A., Ottolenghi, S., Pandolfi, P. P., Sala, M., DeBiasi, S., et al. (2004). Sox2 deficiency causes neurodegeneration and impaired neurogenesis in the adult mouse brain. *Development*, **131**, 3805–3819.

Frambach, I., Rössler, W., Winkler, M., and Schürmann, F. W. (2004). F-actin at identified synapses in the mushroom body neuropil of the insect brain. *J. Comp. Neurol.*, **475**, 303–314.

Gamse, J. T., Kuan, Y. S., Macurak, M., Brösamle, C., Thisse, B., Thisse, C., and Halpern, M. E. (2005). Directional asymmetry of the zebrafish epithalamus

guides dorsoventral innervation of the midbrain target. *Development*, **132**, 4869–4881.

Gamse, J. T., Shen, Y.-C., Thisse, Christine, Thisse, Bernard, Raymond, P. A., Halpern, Marnie E, and Liang, Jennifer O (2002). Otx5 regulates genes that show circadian expression in the zebrafish pineal complex. *Nat. Genet.*, **30**, 117–121.

Gamse, J. T., Thisse, C., Thisse, B., and Halpern, M. E. (2003). The parapineal mediates left-right asymmetry in the zebrafish diencephalon. *Development*, **130**, 1059–1068.

Garcia-Mauriño, S., Gonzalez-Haba, M. G., Calvo, J. R., Rafii-El-Idrissi, M., Sanchez-Margalet, V., Goberna, R., and Guerrero, J. M. (1997). Melatonin enhances IL-2, IL-6, and IFN-gamma production by human circulating CD4+ cells: a possible nuclear receptor-mediated mechanism involving T helper type 1 lymphocytes and monocytes. *J. Immunol.*, **159**, 574–581.

Gavrieli, Y., Sherman, Y., and Ben-Sasson, S. A. (1992). Identification of programmed cell death in situ via specific labeling of nuclear DNA fragmentation. *J. Cell Biol.*, **119**, 493–501.

Geling, A., Steiner, H., Willem, M., Bally-Cuif, L., and Haass, C. (2002). A gamma-secretase inhibitor blocks Notch signaling in vivo and causes a severe neurogenic phenotype in zebrafish. *EMBO Rep*, **3**, 688–694.

Germanà, A., Montalbano, G., Guerrera, M. C., Amato, V., Laurà, R., Magnoli, D., Campo, S., Suarez-Fernandez, E., Ciriaco, E., and Vega, J. A. (2010). Developmental changes in the expression of sox2 in the zebrafish brain. *Microsc. Res. Tech.*

Gilmour, D. T., Maischein, H. M., and Nüsslein-Volhard, C. (2002). Migration and function of a glial subtype in the vertebrate peripheral nervous system. *Neuron*, **34**, 577–588.

Glasgow, E., Karavanov, A. A., and Dawid, I. B. (1997). Neuronal and neuroendocrine expression of lim3, a LIM class homeobox gene, is altered in mutant zebrafish with axial signaling defects. *Dev. Biol.*, **192**, 405–419.

Goldstein, R. (1983). A GABAergic habenulo-raphe pathway mediation of the hypnogenic effects of vasotocin in cat. *Neuroscience*, **10**, 941–945.

Gómez-Skarmeta, J. L., Campuzano, S., and Modolell, J. (2003). Half a century of neural prepatterning: the story of a few bristles and many genes. *Nat. Rev. Neurosci.*, **4**, 587–598.

Gonzalez, R., Sanchez, A., Ferguson, J. A., Balmer, C., Daniel, C., Cohn, A., and Robinson, W. A. (1991). Melatonin therapy of advanced human malignant melanoma. *Melanoma Res.*, **1**, 237–243.

Gothilf, Y., Toyama, R., Coon, S. L., Du, S.-J., Dawid, I. B., and Klein, D. C. (2002). Pineal-specific expression of green fluorescent protein under the control of the serotonin-N-acetyltransferase gene regulatory regions in transgenic zebrafish. *Dev. Dyn*, **225**, 241–249.

Graham, V., Khudyakov, J., Ellis, P., and Pevny, L. (2003). SOX2 functions to maintain neural progenitor identity. *Neuron*, **39**, 749–765.

Greatrex, R. M. and Phillipson, O. T. (1982). Demonstration of synaptic input from prefrontal cortex to the habenula i the rat. *Brain Res.*, **238**, 192–197.

Groenewegen, H. J., Ahlenius, S., Haber, S. N., Kowall, N. W., and Nauta, W. J. (1986). Cytoarchitecture, fiber connections, and some histochemical aspects of the interpeduncular nucleus in the rat. *J. Comp. Neurol.*, **249**, 65–102.

Hagstrom, S. A., Pauer, G. J. T., Reid, J., Simpson, E., Crowe, S., Maumenee, I. H., and Traboulsi, E. I. (2005). SOX2 mutation causes anophthalmia, hearing loss, and brain anomalies. *Am. J. Med. Genet. A*, **138A**, 95–98.

Hardeland, R., Balzer, I., Poeggeler, B., Fuhrberg, B., Uría, H., Behrmann, G., Wolf, R., Meyer, T. J., and Reiter, R. J. (1995). On the primary functions of melatonin in evolution: mediation of photoperiodic signals in a unicell, photooxidation, and scavenging of free radicals. *J. Pineal Res.*, **18**, 104–111.

Harman, D. (1956). Aging: a theory based on free radical and radiation chemistry. *J Gerontol*, **11**, 298–300.

Harris, J. A., Guglielmotti, V., and Bentivoglio, M. (1996). Diencephalic asymmetries. *Neurosci Biobehav Rev*, **20**, 637–643.

Hattar, S., Kumar, M., Park, A., Tong, P., Tung, J., Yau, K.-W., and Berson, D. M. (2006). Central projections of melanopsin-expressing retinal ganglion cells in the mouse. *J. Comp. Neurol.*, **497**, 326–349.

Haun, F., Eckenrode, T. C., and Murray, M. (1992). Habenula and thalamus cell transplants restore normal sleep behaviors disrupted by denervation of the interpeduncular nucleus. *J. Neurosci.*, **12**, 3282–3290.

Heisenberg, C. P., Brand, M., Jiang, Y. J., Warga, R. M., Beuchle, D., Van Eeden, F. J., Furutani-Seiki, M., Granato, M., Haffter, P., Hammerschmidt, M., et al. (1996). Genes involved in forebrain development in the zebrafish, Danio rerio. *Development*, **123**, 191–203.

Heisenberg, C. P., Houart, C., Take-Uchi, M., Rauch, G. J., Young, N., Coutinho, P., Masai, I., Caneparo, L., Concha, M. L., Geisler, R., et al. (2001). A mutation in the Gsk3-binding domain of zebrafish Masterblind/Axin1 leads to a fate transformation of telencephalon and eyes to diencephalon. *Genes Dev.*, **15**, 1427–1434.

Hendricks, M. and Jesuthasan, S. (2007). Asymmetric innervation of the habenula in zebrafish. *J. Comp. Neurol.*, **502**, 611–619.

Herkenham, M. (1981). Anesthetics and the habenulo-interpeduncular system: selective sparing of metabolic activity. *Brain Res.*, **210**, 461–466.

Herkenham, M. and Nauta, W. J. (1977). Afferent connections of the habenular nuclei in the rat. A horseradish peroxidase study, with a note on the fiber-of-passage problem. *J. Comp. Neurol.*, **173**, 123–146.

Herkenham, M. and Nauta, W. J. (1979). Efferent connections of the habenular nuclei in the rat. *J. Comp. Neurol.*, **187**, 19–47.

Herxheimer, A. and Petrie, K. J. (2002). Melatonin for the prevention and treatment of jet lag. *Cochrane Database Syst Rev*, CD001520.

Hever, A. M., Williamson, K. A., and Van Heyningen, V. (2006). Developmental malformations of the eye: the role of PAX6, SOX2 and OTX2. *Clin. Genet*, **69**, 459–470.

Hikosaka, O. (2010). The habenula: from stress evasion to value-based decision-making. *Nat. Rev. Neurosci.*, **11**, 503–513.

Hill, S. M., Spriggs, L. L., Simon, M. A., Muraoka, H., and Blask, D. E. (1992). The growth inhibitory action of melatonin on human breast cancer cells is linked to the estrogen response system. *Cancer Lett.*, **64**, 249–256.

Hohjoh, H., Takasu, M., Shishikura, K., Takahashi, Y., Honda, Y., and Tokunaga, K. (2003). Significant association of the arylalkylamine N-acetyltransferase (AA-NAT) gene with delayed sleep phase syndrome. *Neurogenetics*, **4**, 151–153.

Hughes, R. J. and Badia, P. (1997). Sleep-promoting and hypothermic effects of daytime melatonin administration in humans. *Sleep*, **20**, 124–131.

Inatani, M. (2005). Molecular mechanisms of optic axon guidance. *Naturwissenschaften*, **92**, 549–561.

Inbal, A., Kim, S. H., Shin, J., and Solnica-Krezel, L. (2007). Six3 represses nodal activity to establish early brain asymmetry in zebrafish. *Neuron*, **55**, 407–415.

Itoh, M., Kim, C. H., Palardy, G., Oda, T., Jiang, Y. J., Maust, D., Yeo, S. Y., Lorick, K., Wright, G. J., Ariza-McNaughton, L., et al. (2003). Mind bomb is a ubiquitin ligase that is essential for efficient activation of Notch signaling by Delta. *Dev. Cell*, **4**, 67–82.

James, S. P., Mendelson, W. B., Sack, D. A., Rosenthal, N. E., and Wehr, T. A. (1987). The effect of melatonin on normal sleep. *Neuropsychopharmacology*, **1**, 41–44.

Jan, J. E., Tai, J., Hahn, G., and Rothstein, R. R. (2001). Melatonin replacement therapy in a child with a pineal tumor. *J. Child Neurol.*, **16**, 139–140.

Jesuthasan, S. (2012). Fear, anxiety, and control in the zebrafish. *Dev Neurobiol*, **72**, 395–403.

Ji, H. and Shepard, P. D. (2007). Lateral habenula stimulation inhibits rat midbrain dopamine neurons through a GABA(A) receptor-mediated mechanism. *J. Neurosci.*, **27**, 6923–6930.

Kalén, P., Lindvall, O., and Björklund, A. (1989). Electrical stimulation of the lateral habenula increases hippocampal noradrenaline release as monitored by in vivo microdialysis. *Exp Brain Res*, **76**, 239–245.

Kamachi, Y., Uchikawa, M., and Kondoh, H. (2000). Pairing SOX off: with partners in the regulation of embryonic development. *Trends Genet.*, **16**, 182–187.

Kamachi, Y., Okuda, Y., and Kondoh, H. (2008). Quantitative assessment of the knockdown efficiency of morpholino antisense oligonucleotides in zebrafish embryos using a luciferase assay. *Genesis*, **46**, 1–7.

Kamachi, Yusuke, Uchikawa, Masanori, Tanouchi, A., Sekido, R., and Kondoh, Hisato (2001). Pax6 and SOX2 form a co-DNA-binding partner complex that regulates initiation of lens development. *Genes & Development*, **15**, 1272–1286.

Karasek, M. (2007). Does melatonin play a role in aging processes? *J. Physiol. Pharmacol.*, **58 Suppl 6**, 105–113.

Karlsson, J., Von Hofsten, J., and Olsson, P. E. (2001). Generating Transparent Zebrafish: A Refined Method to Improve Detection of Gene Expression During Embryonic Development. *Marine Biotechnology*, **3**, 0522–0527.

Kelberman, D., De Castro, S. C. P., Huang, S., Crolla, J. A., Palmer, R., Gregory, J. W., Taylor, D., Cavallo, L., Faienza, M. F., Fischetto, R., et al. (2008). SOX2 plays a critical role in the pituitary, forebrain, and eye during human embryonic development. *J. Clin. Endocrinol. Metab.*, **93**, 1865–1873.

Kelberman, D., Rizzoti, K., Avilion, A., Bitner-Glindzicz, M., Cianfarani, S., Collins, J., Chong, W. K., Kirk, J. M. W., Achermann, J. C., Ross, R., et al. (2006). Mutations within Sox2/SOX2 are associated with abnormalities in the hypothalamo-pituitary-gonadal axis in mice and humans. *J. Clin. Invest*, **116**, 2442–2455.

Khoory, R. and Stemme, D. (1988). Plasma melatonin levels in patients suffering from colorectal carcinoma. *J. Pineal Res.*, **5**, 251–258.

Kiefer, J. C. (2007). Back to basics: Sox genes. *Dev. Dyn.*, **236**, 2356–2366.

Kilduff, T. S., Miller, J. D., Radeke, C. M., Sharp, F. R., and Heller, H. C. (1990). 14C-2-deoxyglucose uptake in the ground squirrel brain during entrance to and arousal from hibernation. *J. Neurosci.*, **10**, 2463–2475.

Kimber, S. J., Sneddon, S. F., Bloor, D. J., El-Bareg, A. M., Hawkhead, J. A., Metcalfe, A. D., Houghton, F. D., Leese, H. J., Rutherford, A., Lieberman, B. A., et al. (2008). Expression of genes involved in early cell fate decisions in human embryos and their regulation by growth factors. *Reproduction*, **135**, 635–647.

Kimmel, C. B., Ballard, W. W., Kimmel, S. R., Ullmann, B., and Schilling, T. F. (1995). Stages of embryonic development of the zebrafish. *Dev. Dyn*, **203**, 253–310.

Kleinjan, D. A., Bancewicz, R. M., Gautier, P., Dahm, R., Schonthaler, H. B., Damante, G., Seawright, A., Hever, A. M., Yeyati, P. L., Van Heyningen, V., et al. (2008). Subfunctionalization of duplicated zebrafish pax6 genes by cis-regulatory divergence. *PLoS Genet.*, **4**, e29.

Klemm, W. R. (2004). Habenular and interpeduncularis nuclei: shared components in multiple-function networks. *Med. Sci. Monit.*, **10**, RA261–273.

Kondo, M. (2007). Bone morphogenetic proteins in the early development of zebrafish. *FEBS J.*, **274**, 2960–2967.

Kondoh, H., Uchikawa, M., and Kamachi, Y. (2004). Interplay of Pax6 and SOX2 in lens development as a paradigm of genetic switch mechanisms for cell differentiation. *Int. J. Dev. Biol.*, **48**, 819–827.

Kovall, R. A. (2008). More complicated than it looks: assembly of Notch pathway transcription complexes. *Oncogene*, **27**, 5099–5109.

Kräuchi, K., Cajochen, C., and Wirz-Justice, A. (1997). A relationship between heat loss and sleepiness: effects of postural change and melatonin administration. *J. Appl. Physiol.*, **83**, 134–139.

Kringelbach, M. L., Green, A. L., Owen, S. L. F., Schweder, P. M., and Aziz, T. Z. (2010). Sing the mind electric - principles of deep brain stimulation. *Eur. J. Neurosci.*, **32**, 1070–1079.

Kuan, Y. S., Yu, H. H., Moens, C. B., and Halpern, M. E. (2007). Neuropilin asymmetry mediates a left-right difference in habenular connectivity. *Development*, **134**, 857–865.

Lapin, V. and Frowein, A. (1981). Effects of growing tumours on pineal melatonin levels in male rats. *J. Neural Transm.*, **52**, 123–136.

Larison, K. D. and Bremiller, R. (1990). Early onset of phenotype and cell patterning in the embryonic zebrafish retina. *Development*, **109**, 567–576.

Lavie, P. (1997). Melatonin: role in gating nocturnal rise in sleep propensity. *J. Biol. Rhythms*, **12**, 657–665.

Lecourtier, L. and Kelly, P. H. (2007). A conductor hidden in the orchestra? Role of the habenular complex in monoamine transmission and cognition. *Neurosci Biobehav Rev*, **31**, 658–672.

Lecourtier, L. and Kelly, P. H. (2005). Bilateral lesions of the habenula induce attentional disturbances in rats. *Neuropsychopharmacology*, **30**, 484–496.

Lecourtier, L., Neijt, H. C., and Kelly, P. H. (2004). Habenula lesions cause impaired cognitive performance in rats: implications for schizophrenia. *Eur. J. Neurosci.*, **19**, 2551–2560.

Lee, A., Mathuru, A. S., Teh, C., Kibat, C., Korzh, V., Penney, T. B., and Jesuthasan, S. (2010). The habenula prevents helpless behavior in larval zebrafish. *Curr. Biol.*, **20**, 2211–2216.

Lee, E. H. and Huang, S. L. (1988). Role of lateral habenula in the regulation of exploratory behavior and its relationship to stress in rats. *Behav. Brain Res.*, **30**, 265–271.

Lefebvre, V., Dumitriu, B., Penzo-Méndez, A., Han, Y., and Pallavi, B. (2007). Control of cell fate and differentiation by Sry-related high-mobility-group box (Sox) transcription factors. *Int. J. Biochem. Cell Biol.*, **39**, 2195–2214.

Lehmann, E. D., Cockerell, O. C., and Rudge, P. (1996). Somnolence associated with melatonin deficiency after pinealectomy. *Lancet*, **347**, 323.

Lehner, M., Taracha, E., Skórzewska, A., Wisłowska, A., Zienowicz, M., Maciejak, P., Szyndler, J., Bidziński, A., and Płaźnik, A. (2004). Sensitivity to pain and c-Fos expression in brain structures in rats. *Neurosci. Lett.*, **370**, 74–79.

Li, Y., Chopp, M., Yoshida, Y., and Levine, S. R. (1992). Distribution of 72-kDa heat-shock protein in rat brain after hyperthermia. *Acta Neuropathol.*, **84**, 94–99.

Liang, J. O., Etheridge, A., Hantsoo, L., Rubinstein, A. L., Nowak, S. J., Izpisúa Belmonte, J. C., and Halpern, M. E. (2000). Asymmetric nodal signaling in the zebrafish diencephalon positions the pineal organ. *Development*, **127**, 5101–5112.

Lincoln, G. A., Almeida, O. F., and Arendt, J (1981). Role of melatonin and circadian rhythms in seasonal reproduction in rams. *J. Reprod. Fertil. Suppl.*, **30**, 23–31.

Lissoni, P., Barni, S., Ardizzoia, A., Paolorossi, F., Crispino, S., Tancini, G., Tisi, E., Archili, C., De Toma, D., and Pipino, G. (1992). Randomized study with the pineal hormone melatonin versus supportive care alone in advanced nonsmall cell lung cancer resistant to a first-line chemotherapy containing cisplatin. *Oncology*, **49**, 336–339.

Lissoni, P., Viviani, S., Bajetta, E., Buzzoni, R., Barreca, A., Mauri, R., Resentini, M., Morabito, F., Esposti, D., and Esposti, G. (1986). A clinical study of the pineal gland activity in oncologic patients. *Cancer*, **57**, 837–842.

Liu, A. and Niswander, L. A. (2005). Bone morphogenetic protein signalling and vertebrate nervous system development. *Nat. Rev. Neurosci.*, **6**, 945–954.

Lockley, S. W., Skene, D J, James, K., Thapan, K., Wright, J., and Arendt, J (2000). Melatonin administration can entrain the free-running circadian system of blind subjects. *J. Endocrinol.*, **164**, R1–6.

Long, S., Ahmad, N., and Rebagliati, M. (2003). The zebrafish nodal-related gene southpaw is required for visceral and diencephalic left-right asymmetry. *Development*, **130**, 2303–2316.

Loots, G. G. (2008). Genomic identification of regulatory elements by evolutionary sequence comparison and functional analysis. *Adv. Genet.*, **61**, 269–293.

Lopez-Gonzalez, M. A., Calvo, J. R., Osuna, C., and Guerrero, J. M. (1992). Interaction of melatonin with human lymphocytes: evidence for binding sites coupled to potentiation of cyclic AMP stimulated by vasoactive intestinal peptide and activation of cyclic GMP. *J. Pineal Res.*, **12**, 97–104.

Lu, P. N., Lund, C., Khuansuwan, S., Schumann, A., Harney-Tolo, M., Gamse, J. T., and Liang, J. O. (2012). Failure in closure of the anterior neural tube causes left isomerization of the zebrafish epithalamus. *Dev. Biol.*

Lydic, R., Baghdoyan, H. A., Hibbard, L., Bonyak, E. V., DeJoseph, M. R., and Hawkins, R. A. (1991). Regional brain glucose metabolism is altered during

rapid eye movement sleep in the cat: a preliminary study. *J. Comp. Neurol.*, **304**, 517–529.

Lyseng-Williamson, K. A. (2012). Melatonin prolonged release: in the treatment of insomnia in patients aged ≥55 years. *Drugs Aging*, **29**, 911–923.

Macchi, M. M. and Bruce, J. N. (2004). Human pineal physiology and functional significance of melatonin. *Front Neuroendocrinol*, **25**, 177–195.

Maestroni, G. J., Conti, A., and Pierpaoli, W. (1986). Role of the pineal gland in immunity. Circadian synthesis and release of melatonin modulates the antibody response and antagonizes the immunosuppressive effect of corticosterone. *J. Neuroimmunol.*, **13**, 19–30.

Magri, F., Locatelli, M., Balza, G., Molla, G., Cuzzoni, G., Fioravanti, M., Solerte, S. B., and Ferrari, E. (1997). Changes in endocrine circadian rhythms as markers of physiological and pathological brain aging. *Chronobiol. Int.*, **14**, 385–396.

Mano, H. and Fukada, Y. (2007). A median third eye: pineal gland retraces evolution of vertebrate photoreceptive organs. *Photochem. Photobiol.*, **83**, 11–18.

Masai, I., Heisenberg, C. P., Barth, K. A., Macdonald, R., Adamek, S., and Wilson, S. W. (1997). floating head and masterblind regulate neuronal patterning in the roof of the forebrain. *Neuron*, **18**, 43–57.

Matsumata, M., Uchikawa, M., Kamachi, Y., and Kondoh, H. (2005). Multiple N-cadherin enhancers identified by systematic functional screening indicate its Group B1 SOX-dependent regulation in neural and placodal development. *Dev. Biol.*, **286**, 601–617.

Matsumoto, M. and Hikosaka, O. (2009). Representation of negative motivational value in the primate lateral habenula. *Nat. Neurosci.*, **12**, 77–84.

McConnell, S. J. (1986). Seasonal changes in the circadian plasma melatonin profile of the tammar, Macropus eugenii. *J. Pineal Res.*, **3**, 119–125.

Meng, H., Wang, Y., Huang, M., Lin, W., Wang, S., and Zhang, B. (2011). Chronic deep brain stimulation of the lateral habenula nucleus in a rat model of depression. *Brain Res.*, **1422**, 32–38.

Millimaki, B. B., Sweet, E. M., and Riley, B. B. (2010). Sox2 is required for maintenance and regeneration, but not initial development, of hair cells in the zebrafish inner ear. *Dev. Biol.*, **338**, 262–269.

Mitchell, T. N., Free, S. L., Williamson, K. A., Stevens, J. M., Churchill, A. J., Hanson, I. M., Shorvon, S. D., Moore, A. T., Van Heyningen, V., and Sisodiya, S. M. (2003). Polymicrogyria and absence of pineal gland due to PAX6 mutation. *Ann. Neurol*, **53**, 658–663.

Mori, I., Diehl, A. D., Chauhan, A., Ljunggren, H. G., and Kristensson, K. (1999). Selective targeting of habenular, thalamic midline and monoaminergic brainstem neurons by neurotropic influenza A virus in mice. *J. Neurovirol.*, **5**, 355–362.

Morrey, K. M., McLachlan, J. A., Serkin, C. D., and Bakouche, O. (1994). Activation of human monocytes by the pineal hormone melatonin. *J. Immunol.*, **153**, 2671–2680.

Morris, J. S., Smith, K. A., Cowen, P. J., Friston, K. J., and Dolan, R. J. (1999). Covariation of activity in habenula and dorsal raphé nuclei following tryptophan depletion. *Neuroimage*, **10**, 163–172.

Murphy, C. A., DiCamillo, A. M., Haun, F., and Murray, M. (1996). Lesion of the habenular efferent pathway produces anxiety and locomotor hyperactivity in rats: a comparison of the effects of neonatal and adult lesions. *Behav. Brain Res.*, **81**, 43–52.

Nagtegaal, J. E., Kerkhof, G. A., Smits, M. G., Swart, A. C., and Van Der Meer, Y. G. (1998). Delayed sleep phase syndrome: A placebo-controlled cross-over study on the effects of melatonin administered five hours before the individual dim light melatonin onset. *J Sleep Res*, **7**, 135–143.

Nasevicius, A. and Ekker, S. C. (2000). Effective targeted gene “knockdown” in zebrafish. *Nat. Genet.*, **26**, 216–220.

Nave, R., Herer, P., Haimov, I., Shlitner, A., and Lavie, P. (1996). Hypnotic and hypothermic effects of melatonin on daytime sleep in humans: lack of antagonism by flumazenil. *Neurosci. Lett.*, **214**, 123–126.

Nilsson, O. G., Kalén, P., Rosengren, E., and Björklund, A. (1990). Acetylcholine release in the rat hippocampus as studied by microdialysis is dependent on axonal impulse flow and increases during behavioural activation. *Neuroscience*, **36**, 325–338.

Nowling, T. K., Johnson, L. R., Wiebe, M. S., and Rizzino, A. (2000). Identification of the transactivation domain of the transcription factor Sox-2 and an associated co-activator. *J. Biol. Chem.*, **275**, 3810–3818.

Okamoto, H., Agetsuma, M., and Aizawa, H. (2012). Genetic dissection of the zebrafish habenula, a possible switching board for selection of behavioral strategy to cope with fear and anxiety. *Dev Neurobiol*, **72**, 386–394.

Okuda, Y., Yoda, H., Uchikawa, M., Furutani-Seiki, M., Takeda, H., Kondoh, H., and Kamachi, Y. (2006). Comparative genomic and expression analysis of group B1 sox genes in zebrafish indicates their diversification during vertebrate evolution. *Dev. Dyn.*, **235**, 811–825.

Parent, M., Lévesque, M., and Parent, A. (2001). Two types of projection neurons in the internal pallidum of primates: single-axon tracing and three-dimensional reconstruction. *J. Comp. Neurol.*, **439**, 162–175.

Park, H. C., Kim, C. H., Bae, Y. K., Yeo, S. Y., Kim, S. H., Hong, S. K., Shin, J., Yoo, K. W., Hibi, M., Hirano, T., et al. (2000). Analysis of upstream elements in the HuC promoter leads to the establishment of transgenic zebrafish with fluorescent neurons. *Dev. Biol*, **227**, 279–293.

Parrinello, S., Napoli, I., Ribeiro, S., Digby, P. W., Fedorova, M., Parkinson, D. B., Doddrell, R. D. S., Nakayama, M., Adams, R. H., and Lloyd, A. C. (2010). EphB signaling directs peripheral nerve regeneration through Sox2-dependent Schwann cell sorting. *Cell*, **143**, 145–155.

Pavlou, S. (2009). A systems biology approach to decipher the role of sox2 in development.

Paydar-Ravandi, F. and Meier, A. H. (1989). Melatonin mediates alternation of seasonality in Syrian hamsters. *Biol. Reprod.*, **40**, 475–480.

Pedace, L., Castori, M., Binni, F., Pingi, A., Grammatico, B., Scommegna, S., Majore, S., and Grammatico, P. (2009). A novel heterozygous SOX2 mutation causing anophthalmia/microphthalmia with genital anomalies. *European Journal of Medical Genetics*, **52**, 273–276.

Pérez-Pérez, J. M., Candela, H., and Micol, J. L. (2009). Understanding synergy in genetic interactions. *Trends Genet.*, **25**, 368–376.

Perkins, B. D., Nicholas, C. S., Baye, L. M., Link, B. A., and Dowling, J. E. (2005). dazed gene is necessary for late cell type development and retinal cell maintenance in the zebrafish retina. *Dev. Dyn.*, **233**, 680–694.

Pevny, L. and Placzek, M. (2005). SOX genes and neural progenitor identity. *Curr. Opin. Neurobiol.*, **15**, 7–13.

Pierce, L. X., Noche, R. R., Ponomareva, O., Chang, C., and Liang, J. O. (2008). Novel functions for Period 3 and Exo-rhodopsin in rhythmic transcription and melatonin biosynthesis within the zebrafish pineal organ. *Brain Res.*, **1223**, 11–24.

Piezzi, R. S., Guzmán, J. A., Pelzer, L. E., Scardapane, L., and Domínguez, S. (1984). Biological role of the pineal. Responses to the environmental photoperiod. *Arch. Biol. Med. Exp.*, **17**, 273–282.

Pujic, Z., Omori, Y., Tsujikawa, M., Thisse, B., Thisse, C., and Malicki, J. (2006). Reverse genetic analysis of neurogenesis in the zebrafish retina. *Dev. Biol.*, **293**, 330–347.

Qu, T., Dong, K., Sugioka, K., and Yamadori, T. (1996). Demonstration of direct input from the retina to the lateral habenular nucleus in the albino rat. *Brain Res.*, **709**, 251–258.

Quillien, A., Blanco-Sanchez, B., Halluin, C., Moore, J. C., Lawson, N. D., Blader, P., and Cau, E. (2011). BMP signaling orchestrates photoreceptor specification in the zebrafish pineal gland in collaboration with Notch. *Development*, **138**, 2293 –2302.

Ragge, N. K., Lorenz, B., Schneider, A., Bushby, K., De Sanctis, L., De Sanctis, U., Salt, A., Collin, J. R. O., Vivian, A. J., Free, S. L., et al. (2005). SOX2 anophthalmia syndrome. *Am. J. Med. Genet. A*, **135**, 1–7; discussion 8.

Rauch, G. J., Lyons, D. A., Middendorf, I., Friedlander, B., Arana, N., Reyes, T., and Talbot, W. S. (2003). Submission and Curation of Gene Expression Data.

Ravichandran, K. S. (2011). Beginnings of a Good Apoptotic Meal: The Find-Me and Eat-Me Signaling Pathways. *Immunity*, **35**, 445–455.

Regan, J. C., Concha, M. L., Roussigne, M., Russell, C., and Wilson, S. W. (2009). An Fgf8-dependent bistable cell migratory event establishes CNS asymmetry. *Neuron*, **61**, 27–34.

Reis, L. M., Tyler, R. C., Schneider, A., Bardakjian, T., and Semina, E. V. (2010). Examination of SOX2 in variable ocular conditions identifies a recurrent deletion in microphthalmia and lack of mutations in other phenotypes. *Mol Vis*, **16**, 768–773.

Renninger, S. L., Schonthaler, H. B., Neuhauss, S. C. F., and Dahm, R. (2011). Investigating the genetics of visual processing, function and behaviour in zebrafish. *Neurogenetics*, **12**, 97–116.

Revel, F. G., Masson-Pévet, M., Pévet, P., Mikkelsen, J. D., and Simonneaux, V. (2009). Melatonin controls seasonal breeding by a network of hypothalamic targets. *Neuroendocrinology*, **90**, 1–14.

Rinkwitz, S., Mourrain, P., and Becker, T. S. (2011). Zebrafish: an integrative system for neurogenomics and neurosciences. *Prog. Neurobiol.*, **93**, 231–243.

Rodin, A. E. (1963). The growth and spread of walker 256 carcinoma in pinealectomized rats. *Cancer Res.*, **23**, 1545–1548.

Rørth, P. (2009). Collective cell migration. *Annu. Rev. Cell Dev. Biol.*, **25**, 407–429.

Rørth, P. (2012). Fellow travellers: emergent properties of collective cell migration. *EMBO Rep.*, **13**, 984–991.

Rosenthal, N. E., Sack, D. A., Gillin, J. C., Lewy, A. J., Goodwin, F. K., Davenport, Y., Mueller, P. S., Newsome, D. A., and Wehr, T. A. (1984). Seasonal affective disorder. A description of the syndrome and preliminary findings with light therapy. *Arch. Gen. Psychiatry*, **41**, 72–80.

Rössler, W., Kuduz, J., Schürmann, F. W., and Schild, D. (2002). Aggregation of f-actin in olfactory glomeruli: a common feature of glomeruli across phyla. *Chem. Senses*, **27**, 803–810.

Roussigné, M., Bianco, Isaac H, Wilson, Stephen W, and Blader, P. (2009). Nodal signalling imposes left-right asymmetry upon neurogenesis in the habenular nuclei. *Development*, **136**, 1549–1557.

Roussigné, M. and Blader, P. (2006). Divergence in regulation of the PEA3 family of ETS transcription factors. *Gene Expr. Patterns*, **6**, 777–782.

Sack, R. L., Brandes, R. W., Kendall, A. R., and Lewy, A. J. (2000). Entrainment of free-running circadian rhythms by melatonin in blind people. *N. Engl. J. Med.*, **343**, 1070–1077.

Salas, R., Sturm, R., Boulter, J., and De Biasi, M. (2009). Nicotinic receptors in the habenulo-interpeduncular system are necessary for nicotine withdrawal in mice. *J. Neurosci.*, **29**, 3014–3018.

Sanes, D. H., Reh, T. A., and Harris, W. A. (2011). Development of the Nervous System 3rd ed. Academic Press, Elsevier.

Sartorius, A., Kiening, K. L., Kirsch, P., Von Gall, C. C., Haberkorn, U., Unterberg, A. W., Henn, F. A., and Meyer-Lindenberg, A. (2010). Remission of major depression under deep brain stimulation of the lateral habenula in a therapy-refractory patient. *Biol. Psychiatry*, **67**, e9–e11.

Sato, T, Deguchi, T., Ichikawa, T., Fujieda, H., and Wake, K. (1991). Localization of hydroxyindole O-methyltransferase-synthesizing cells in bovine epithalamus: immunocytochemistry and in-situ hybridization. *Cell Tissue Res.*, **263**, 413–418.

Savitz, J. B., Nugent, A. C., Bogers, W., Roiser, J. P., Bain, E. E., Neumeister, A., Zarate, C. A. J., Manji, H. K., Cannon, D. M., Marrett, S., et al. (2011).

Habenula volume in bipolar disorder and major depressive disorder: a high-resolution magnetic resonance imaging study. *Biol. Psychiatry*, **69**, 336–343.

Scalabrino, G., Ferioli, M. E., Basagni, M., Nebuloni, R., and Fraschini, F. (1979). Endocrine regulation of thymic biosynthetic polyamine decarboxylases in adult rat. *Am. J. Physiol.*, **237**, E6–10.

Scheer, N, Groth, A., Hans, S., and Campos-Ortega, J A (2001). An instructive function for Notch in promoting gliogenesis in the zebrafish retina. *Development*, **128**, 1099–1107.

Scheer, N. and Campos-Ortega, J. A. (1999). Use of the Gal4-UAS technique for targeted gene expression in the zebrafish. *Mechanisms of Development*, **80**, 153–158.

Schneider, A., Bardakjian, T., Reis, L. M., Tyler, R. C., and Semina, E. V. (2009). Novel SOX2 mutations and genotype-phenotype correlation in anophthalmia and microphthalmia. *Am. J. Med. Genet. A*, **149A**, 2706–2715.

Shah, P. N., Mhatre, M. C., and Kothari, L. S. (1984). Effect of melatonin on mammary carcinogenesis in intact and pinealectomized rats in varying photoperiods. *Cancer Res.*, **44**, 3403–3407.

Shaw, L., Sneddon, S. F., Brison, D. R., and Kimber, S. J. (2012). Comparison of gene expression in fresh and frozen-thawed human preimplantation embryos. *Reproduction*, **144**, 569–582.

Shelton, L., Becerra, L., and Borsook, D. (2012). Unmasking the mysteries of the habenula in pain and analgesia. *Prog. Neurobiol.*, **96**, 208–219.

Shepard, P. D., Holcomb, H. H., and Gold, J. M. (2006). Schizophrenia in translation: the presence of absence: habenular regulation of dopamine neurons and the encoding of negative outcomes. *Schizophr Bull*, **32**, 417–421.

Shumake, J., Edwards, E., and Gonzalez-Lima, F. (2003). Opposite metabolic changes in the habenula and ventral tegmental area of a genetic model of helpless behavior. *Brain Res.*, **963**, 274–281.

Sisodiya, S. M., Ragge, N. K., Cavalleri, G. L., Hever, A., Lorenz, B., Schneider, A., Williamson, K. A., Stevens, J. M., Free, S. L., Thompson, P. J., et al. (2006). Role of SOX2 mutations in human hippocampal malformations and epilepsy. *Epilepsia*, **47**, 534–542.

Smith, W. J., Stewart, J., and Pfaus, J. G. (1997). Tail pinch induces fos immunoreactivity within several regions of the male rat brain: effects of age. *Physiol. Behav.*, **61**, 717–723.

Snelson, C. D., Burkart, J. T., and Gamse, J. T. (2008b). Formation of the Asymmetric Pineal Complex in Zebrafish Requires Two Independently Acting Transcription Factors. *Dev Dyn*, **237**, 3538–3544.

Snelson, C. D. and Gamse, J. T. (2009). Building an asymmetric brain: development of the zebrafish epithalamus. *Semin Cell Dev Biol*, **20**, 491–497.

Snelson, C. D., Santhakumar, K., Halpern, M. E., and Gamse, J. T. (2008a). Tbx2b is required for the development of the parapineal organ. *Development*, **135**, 1693–1702.

Spence, R., Gerlach, G., Lawrence, C., and Smith, C. (2008). The behaviour and ecology of the zebrafish, Danio rerio. *Biol Rev Camb Philos Soc*, **83**, 13–34.

Stehle, J. H., Saade, A., Rawashdeh, O., Ackermann, K., Jilg, A., Sebestény, T., and Maronde, E. (2011). A survey of molecular details in the human pineal gland in the light of phylogeny, structure, function and chronobiological diseases. *J. Pineal Res.*, **51**, 17–43.

Stern, W. C., Johnson, A., Bronzino, J. D., and Morgane, P. J. (1979). Effects of electrical stimulation of the lateral habenula on single-unit activity of raphe neurons. *Exp. Neurol.*, **65**, 326–342.

Stone, B. M., Turner, C., Mills, S. L., and Nicholson, A. N. (2000). Hypnotic activity of melatonin. *Sleep*, **23**, 663–669.

Strassman, R. J., Qualls, C. R., Lisansky, E. J., and Peake, G. T. (1991). Elevated rectal temperature produced by all-night bright light is reversed by melatonin infusion in men. *J. Appl. Physiol.*, **71**, 2178–2182.

Sugama, S., Cho, B. P., Baker, H., Joh, T. H., Lucero, J., and Conti, B. (2002). Neurons of the superior nucleus of the medial habenula and ependymal cells express IL-18 in rat CNS. *Brain Res.*, **958**, 1–9.

Takahashi, Kazutoshi and Yamanaka, S. (2006). Induction of pluripotent stem cells from mouse embryonic and adult fibroblast cultures by defined factors. *Cell*, **126**, 663–676.

Tamarkin, L., Cohen, M., Roselle, D., Reichert, C., Lippman, M., and Chabner, B. (1981). Melatonin inhibition and pinealectomy enhancement of 7,12-dimethylbenz(a)anthracene-induced mammary tumors in the rat. *Cancer Res.*, **41**, 4432–4436.

Taranova, O. V., Magness, S. T., Fagan, B. M., Wu, Y., Surzenko, N., Hutton, S. R., and Pevny, L. H. (2006). SOX2 is a dose-dependent regulator of retinal neural progenitor competence. *Genes Dev*, **20**, 1187–1202.

Taylor, R. W., Qi, J. Y., Talaga, A. K., Ma, T. P., Pan, L., Bartholomew, C. R., Klionsky, D. J., Moens, C. B., and Gamse, J. T. (2011). Asymmetric inhibition of Ulk2 causes left-right differences in habenular neuropil formation. *J. Neurosci.*, **31**, 9869–9878.

Teh, C., Parinov, S., and Korzh, V. (2005). New ways to admire zebrafish: progress in functional genomics research methodology. *BioTechniques*, **38**, 897–906.

Thisse, C., Thisse, B., Schilling, T. F., and Postlethwait, J. H. (1993). Structure of the zebrafish snail1 gene and its expression in wild-type, spadetail and no tail mutant embryos. *Development*, **119**, 1203–1215.

Thornton, E. W. and Bradbury, G. E. (1989). Effort and stress influence the effect of lesion of the habenula complex in one-way active avoidance learning. *Physiol. Behav.*, **45**, 929–935.

Thornton, E. W. and Evans, J. C. (1982). The role of habenular nuclei in the selection of behavioral strategies. *Physiological Psychology*, **10**, 361–367.

Tomioka, M., Nishimoto, M., Miyagi, S., Katayanagi, T., Fukui, N., Niwa, H., Muramatsu, M., and Okuda, A. (2002). Identification of Sox-2 regulatory region which is under the control of Oct-3/4–Sox-2 complex. *Nucleic Acids Research*, **30**, 3202.

Touitou, Y., Fèvre, M., Bogdan, A., Reinberg, A., De Prins, J., Beck, H., and Touitou, C. (1984). Patterns of plasma melatonin with ageing and mental condition: stability of nyctohemeral rhythms and differences in seasonal variations. *Acta Endocrinol.*, **106**, 145–151.

Touitou, Y., Fèvre, M., Lagoguey, M., Carayon, A., Bogdan, A., Reinberg, A., Beck, H., Cesselin, F., and Touitou, C. (1981). Age- and mental health-related circadian rhythms of plasma levels of melatonin, prolactin, luteinizing hormone and follicle-stimulating hormone in man. *J. Endocrinol.*, **91**, 467–475.

Tziaferi, V., Kelberman, D., and Dattani, M. T. (2008). The role of SOX2 in hypogonadotropic hypogonadism. *Sex Dev*, **2**, 194–199.

Ullsperger, M. and Von Cramon, D. Y. (2003). Error monitoring using external feedback: specific roles of the habenular complex, the reward system, and the cingulate motor area revealed by functional magnetic resonance imaging. *J. Neurosci.*, **23**, 4308–4314.

Urist, M. R. (1965). Bone: formation by autoinduction. *Science*, **150**, 893–899.

Valjakka, A., Vartiainen, J., Tuomisto, L., Tuomisto, J. T., Olkkonen, H., and Airaksinen, M. M. (1998). The fasciculus retroflexus controls the integrity of

REM sleep by supporting the generation of hippocampal theta rhythm and rapid eye movements in rats. *Brain Res. Bull.*, **47**, 171–184.

Villarreal, J. S., Gonzalez-Lima, F., Berndt, J., and Barea-Rodriguez, E. J. (2002). Water maze training in aged rats: effects on brain metabolic capacity and behavior. *Brain Res.*, **939**, 43–51.

Waldhauser, F., Weiszenbacher, G., Tatzer, E., Gisinger, B., Waldhauser, M., Schemper, M., and Frisch, H. (1988). Alterations in nocturnal serum melatonin levels in humans with growth and aging. *J. Clin. Endocrinol. Metab.*, **66**, 648–652.

Wang, R. Y. and Aghajanian, G. K. (1977). Physiological evidence for habenula as major link between forebrain and midbrain raphe. *Science*, **197**, 89–91.

Wang, X. and Yost, H. J. (2008). Initiation and propagation of posterior to anterior (PA) waves in zebrafish left-right development. *Dev. Dyn.*, **237**, 3640–3647.

Westerfield, M. (2000). The zebrafish book. A guide for the laboratory use of zebrafish (Danio rerio). 4th ed. University of Oregon Press, Eugene, Oregon, USA.

Wickman, G., Julian, L., and Olson, M. F. (2012). How apoptotic cells aid in the removal of their own cold dead bodies. *Cell Death Differ.*, **19**, 735–742.

Williamson, K. A., Hever, A. M., Rainger, J., Rogers, R. C., Magee, A., Fiedler, Z., Keng, W. T., Sharkey, F. H., McGill, N., Hill, C. J., et al. (2006). Mutations in SOX2 cause anophthalmia-esophageal-genital (AEG) syndrome. *Hum. Mol. Genet*, **15**, 1413–1422.

Wolpert, L., Beddington, R., Jessell, T., Lawrence, P., Meyerowitz, E., and Smith, J. (2002). Principles of Development 2nd ed. Oxford University Press, New York.

Wood, H. B. and Episkopou, V. (1999). Comparative expression of the mouse Sox1, Sox2 and Sox3 genes from pre-gastrulation to early somite stages. *Mech. Dev.*, **86**, 197–201.

Xiao, T., Roeser, T., Staub, W., and Baier, H. (2005). A GFP-based genetic screen reveals mutations that disrupt the architecture of the zebrafish retinotectal projection. *Development*, **132**, 2955–2967.

Yang, L.-M., Hu, B., Xia, Y.-H., Zhang, B.-L., and Zhao, Hua (2008). Lateral habenula lesions improve the behavioral response in depressed rats via increasing the serotonin level in dorsal raphe nucleus. *Behav. Brain Res.*, **188**, 84–90.

Yu, P. B., Hong, C. C., Sachidanandan, C., Babitt, J. L., Deng, D. Y., Hoyng, S. A., Lin, H. Y., Bloch, K. D., and Peterson, R. T. (2007). Dorsomorphin inhibits BMP signals required for embryogenesis and iron metabolism. *Nature Chemical Biology*, **4**, 33–41.

Yuan, H., Corbi, N., Basilico, C., and Dailey, L. (1995). Developmental-specific activity of the FGF-4 enhancer requires the synergistic action of Sox2 and Oct-3. *Genes Dev.*, **9**, 2635–2645.

Zappone, M. V., Galli, R., Catena, R., Meani, N., De Biasi, S., Mattei, E., Tiveron, C., Vescovi, A. L., Lovell-Badge, R., Ottolenghi, S., et al. (2000). Sox2 regulatory sequences direct expression of a (beta)-geo transgene to telencephalic neural stem cells and precursors of the mouse embryo, revealing regionalization of gene expression in CNS stem cells. *Development*, **127**, 2367–2382.

Zenteno, J. C., Gascon-Guzman, G., and Tovilla-Canales, J. L. (2005). Bilateral anophthalmia and brain malformations caused by a 20-bp deletion in the SOX2 gene. *Clin. Genet.*, **68**, 564–566.

Zhao, H and Rusak, B. (2005). Circadian firing-rate rhythms and light responses of rat habenular nucleus neurons in vivo and in vitro. *Neuroscience*, **132**, 519–528.

Supplementary materials

Movie S1. Arborization of RGC axons at the optic tectum in control embryos. Timelapse of *Tg(pou4f3:GFP)* embryos from 50 hpf until 110 hpf, showing the arborization of RGC axons at the optic tectum. Images were acquired every 40 minutes. Dorsal view with anterior to the top.

Movie S2. Arborization of RGC axons at the optic tectum is abnormal in *sox2* morphants. Timelapse of *Tg(pou4f3:GFP) sox2* morphants from 50 hpf until 110 hpf, showing the arborization of RGC axons at the optic tectum. Some axons are misguided and travel outside the optic tectum. Images were acquired every 40 minutes. Dorsal view with anterior to the top.

Movie S3. sox2 expression at the 8 ss. During early stages, sox2 (red) is expressed throughout the pineal anlage, as marked by GFP expression in *Tg(flh:GFP)* embryos (green). At the 8 ss, there are no isl1-positive cells (blue). Navigation through the optical stacks, starting with the dorsal-most optical section of the pineal anlage and moving ventrally.

Movie S4. sox2 expression at the 10 ss. At the 10 ss, sox2 (red) is expressed is co-expressed with GFP in *Tg(flh:GFP)* embryos (green). However, sox2 expression is downregulated as cells start to express isl1 (blue). Navigation through the optical stacks, starting with the dorsal-most optical section of the pineal anlage and moving ventrally.

Movie S5. sox2 expression at the 15 ss. At the 15 ss, sox2 (red) is not expressed in isl1-positive cells (blue), but some expression is detected in undifferentiated *flh*-positive cells (green). Navigation through the optical stacks, starting with the dorsal-most optical section of the pineal anlage and moving ventrally.

Movie S6. sox2 expression at 28 hpf. sox2 expression (red) is excluded from the fully differentiated pineal gland (isl1-positive cells shown in blue, GFP of *Tg(flh:GFP)* embryos is shown in green). Navigation through the optical stacks, starting with the dorsal-most optical section of the pineal anlage and moving ventrally.

Movie S7. sox2 expression in DMSO- and DAPT-treated embryos at the 15 ss. DMSO (**left panel**) and DAPT (**right panel**) treatments do not qualitatively affect sox2 expression: sox2 is expressed in undifferentiated GFP-positive (green) pineal cells of *Tg(flh:GFP)* embryos, but it is downregulated in post-mitotic isl1-expressing cells (blue). Navigation through the optical stacks, starting with the dorsal-most optical section of the pineal anlage and moving ventrally.

Movie S8. sox2 expression in control and *Tg(hs:Gal4);Tg(UAS:Notch-intra)* embryos at the 20 ss. Heat-shock (**left panel**) does not affect sox2 expression: sox2 (red) is expressed in undifferentiated pineal cells, but it is downregulated in post-mitotic isl1-expressing cells (blue). Heat-shock of *Tg(hs:Gal4);Tg(UAS:Notch-intra)* embryos (**right panel**) results in upregulation of Notch signaling. This does not qualitatively

affect sox2 expression. Embryos were stained using an antibody against the myc-tag (green) to demonstrate the absence (in controls) or presence of the *Tg(UAS:Notch-intra)* transgene. Navigation through the optical stacks, starting with the dorsal-most optical section of the pineal anlage and moving ventrally.

Movie S9. sox2 expression in DMSO- and dorsomorphin-treated embryos at the 15 ss. DMSO (**left panel**) or dorsomorphin (**right panel**) treatments do not affect sox2 expression: sox2 (red) is expressed in undifferentiated GFP-positive (green) pineal cells of *Tg(flh:GFP)* embryos, but it is downregulated in post-mitotic isl1-expressing cells (blue). Navigation through the optical stacks, starting with the dorsal-most optical section of the pineal anlage and moving ventrally.

Movie S10. Parapineal migration in control embryos. Timelapse of *Tg(foxd3:GFP)* embryos from 30 hpf until 90 hpf, showing the migration of parapineal cells (as a group) towards the left, in control embryos. Images were acquired every 40 minutes. Dorsal view with anterior to the top.

Movie S11. Example of parapineal migration towards the left in sox2 morphants. Timelapse of *Tg(foxd3:GFP)* embryos from 30 hpf until 90 hpf, showing the migration of parapineal cells (as a group) towards the left in some *sox2* morphants. Images were acquired every 40 minutes. Dorsal view with anterior to the top.

Movie S12. Example of reverse parapineal migration in sox2 morphants. Timelapse of *Tg(foxd3:GFP)* embryos from 30 hpf until 90 hpf, showing the migration of parapineal cells (as a group) towards the right, in a subset of sox2 morphants. Images were acquired every 40 minutes. Dorsal view with anterior to the top.

Movie S13. Example of abnormal parapineal migration in *sox2* morphants, resulting in scattered parapineal cells around the pineal gland. Timelapse of *Tg(foxd3:GFP)* embryos from 30 hpf until 90 hpf, showing the migration of parapineal cells in *sox2* morphants. Notably, in this example, some parapineal cells are disconnected from the group and are abnormally placed around the pineal gland. Images were acquired every 40 minutes. Dorsal view with anterior to the top.

Movie S14. Example of abnormal parapineal migration in *sox2* morphants, resulting in scattered parapineal cells around the pineal gland. Timelapse of *Tg(foxd3:GFP)* embryos from 30 hpf until 90 hpf, showing the migration of parapineal cells in *sox2* morphants. Notably, in this example, some parapineal cells are disconnected from the group and are abnormally placed around the pineal gland. Images were acquired every 40 minutes. Dorsal view with anterior to the top.